

THE INTERNATIONAL FOOD OPERATIONS & PROCESSING SIMULATION WORKSHOP

SEPTEMBER 18 - 20, 2017
BARCELONA, SPAIN



EDITED BY
AGOSTINO BRUZZONE
FRANCESCO LONGO
MIQUEL ANGEL PIERA
GIUSEPPE VIGNALI

PRINTED IN RENDE (CS), ITALY, SEPTEMBER 2017

ISBN 978-88-97999-94-2 (Paperback)
ISBN 978-88-97999-86-7 (PDF)

© 2017 DIME UNIVERSITÀ DI GENOVA

RESPONSIBILITY FOR THE ACCURACY OF ALL STATEMENTS IN EACH PAPER RESTS SOLELY WITH THE AUTHOR(S). STATEMENTS ARE NOT NECESSARILY REPRESENTATIVE OF NOR ENDORSED BY THE DIME, UNIVERSITY OF GENOVA. PERMISSION IS GRANTED TO PHOTOCOPY PORTIONS OF THE PUBLICATION FOR PERSONAL USE AND FOR THE USE OF STUDENTS PROVIDING CREDIT IS GIVEN TO THE CONFERENCES AND PUBLICATION. PERMISSION DOES NOT EXTEND TO OTHER TYPES OF REPRODUCTION NOR TO COPYING FOR INCORPORATION INTO COMMERCIAL ADVERTISING NOR FOR ANY OTHER PROFIT - MAKING PURPOSE. OTHER PUBLICATIONS ARE ENCOURAGED TO INCLUDE 300 TO 500 WORD ABSTRACTS OR EXCERPTS FROM ANY PAPER CONTAINED IN THIS BOOK, PROVIDED CREDITS ARE GIVEN TO THE AUTHOR(S) AND THE CONFERENCE.

FOR PERMISSION TO PUBLISH A COMPLETE PAPER WRITE TO: DIME UNIVERSITY OF GENOVA, PROF. AGOSTINO BRUZZONE, VIA OPERA PIA 15, 16145 GENOVA, ITALY. ADDITIONAL COPIES OF THE PROCEEDINGS OF THE FOODOPS ARE AVAILABLE FROM DIME UNIVERSITY OF GENOVA, PROF. AGOSTINO BRUZZONE, VIA OPERA PIA 15, 16145 GENOVA, ITALY.

ISBN 978-88-97999-94-2 (Paperback)
ISBN 978-88-97999-86-7 (PDF)

THE INTERNATIONAL FOOD OPERATIONS & PROCESSING
SIMULATION WORKSHOP, FOODOPS 2017
SEPTEMBER 18 - 20, 2017
BARCELONA, SPAIN

ORGANIZED BY



DIME - UNIVERSITY OF GENOA



LIOPHANT SIMULATION



SIMULATION TEAM



IMCS - INTERNATIONAL MEDITERRANEAN & LATIN AMERICAN COUNCIL OF
SIMULATION



DIMEG, UNIVERSITY OF CALABRIA



MSC-LES, MODELING & SIMULATION CENTER, LABORATORY OF ENTERPRISE
SOLUTIONS



AUTONOMOUS UNIVERSITY OF BARCELONA



UNIVERSITY OF PARMA



MODELING AND SIMULATION CENTER OF EXCELLENCE (MSCOE)



LATVIAN SIMULATION CENTER - RIGA TECHNICAL UNIVERSITY



LOGISIM



LSIS - LABORATOIRE DES SCIENCES DE L'INFORMATION ET DES SYSTEMES



MIMOS - MOVIMENTO ITALIANO MODELLAZIONE E SIMULAZIONE



MITIM PERUGIA CENTER - UNIVERSITY OF PERUGIA



BRASILIAN SIMULATION CENTER, LAMCE-COPPE-UFRJ



MITIM - MCLEOD INSTITUTE OF TECHNOLOGY AND INTEROPERABLE MODELING AND SIMULATION - GENOA CENTER



M&SNET - MCLEOD MODELING AND SIMULATION NETWORK



LATVIAN SIMULATION SOCIETY



ECOLE SUPERIEURE D'INGENIERIE EN SCIENCES APPLIQUEES



FACULTAD DE CIENCIAS EXACTAS. INGENIERIA Y AGRIMENSURA



UNIVERSITY OF LA LAGUNA



CIFASIS: CONICET-UNR-UPCAM



INSTICC - INSTITUTE FOR SYSTEMS AND TECHNOLOGIES OF INFORMATION, CONTROL AND COMMUNICATION



NATIONAL RUSSIAN SIMULATION SOCIETY



CEA - IFAC



UNIVERSITY OF BORDEAUX



UNIVERSITY OF CYPRUS



DUTCH BENELUX SIMULATION SOCIETY

I3M 2017 INDUSTRIAL SPONSORS



CAL-TEK SRL



LIOTECH LTD



MAST SRL



SIM-4-FUTURE

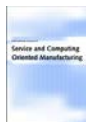
I3M 2017 MEDIA PARTNERS



INDERSCIENCE PUBLISHERS – INTERNATIONAL JOURNAL OF SIMULATION AND PROCESS MODELING



INDERSCIENCE PUBLISHERS – INTERNATIONAL JOURNAL OF OIL, GAS AND COAL TECHNOLOGY



INDERSCIENCE PUBLISHERS – INTERNATIONAL JOURNAL OF SERVICE AND COMPUTING ORIENTED MANUFACTURING



IGI GLOBAL – INTERNATIONAL JOURNAL OF PRIVACY AND HEALTH INFORMATION MANAGEMENT



HalldaleGroup



HALLDALE MEDIA GROUP: MILITARY SIMULATION AND TRAINING MAGAZINE



HALLDALE MEDIA GROUP: THE JOURNAL FOR HEALTHCARE EDUCATION, SIMULATION AND TRAINING



SAGE
SIMULATION TRANSACTION OF SCS



DE GRUYTER
INTERNATIONAL JOURNAL OF FOOD ENGINEERING

EDITORS

AGOSTINO BRUZZONE

MITIM-DIME, UNIVERSITY OF GENOA, ITALY
agostino@itim.unige.it

FRANCESCO LONGO

DIMEG, UNIVERSITY OF CALABRIA, ITALY
f.longo@unical.it

MIQUEL ANGEL PIERA

AUTONOMOUS UNIVERSITY OF BARCELONA, SPAIN
MIQUELANGEL.PIERA@UAB.CAT

GIUSEPPE VIGNALI

UNIVERSITY OF PARMA, ITALY
giusppe.vignali@unipr.it

THE INTERNATIONAL MULTIDISCIPLINARY MODELING AND SIMULATION MULTICONFERENCE, I3M 2017

GENERAL CO-CHAIRS

AGOSTINO BRUZZONE, *MITIM DIME, UNIVERSITY OF GENOA, ITALY*

MIQUEL ANGEL PIERA, *AUTONOMOUS UNIVERSITY OF BARCELONA, SPAIN*

PROGRAM CO-CHAIRS

FRANCESCO LONGO, *DIMEG, UNIVERSITY OF CALABRIA, ITALY*

YURY MERKURYEV, *RIGA TECHNICAL UNIVERSITY, LATVIA*

THE INTERNATIONAL FOOD OPERATIONS & PROCESSING SIMULATION WORKSHOP, FOODOPS 2017

GENERAL CHAIR

GIUSEPPE VIGNALI, *UNIVERSITY OF PARMA ITALY*

PROGRAM CO-CHAIRS

FRANCESCO LONGO, *DIMEG, UNIVERSITY OF CALABRIA, ITALY*

MIQUEL ANGEL PIERA, *AUTONOMOUS UNIVERSITY OF BARCELONA, SPAIN*

FoodOPS 2017 INTERNATIONAL PROGRAM COMMITTEE

MATTEO AGRESTA, *UNIVERSITY OF GENOA, ITALY*
MARCO BETTER, *OPTTEK SYSTEMS, USA*
ELEONORA BOTTANI, *UNIVERSITY OF PARMA, ITALY*
AGOSTINO BRUZZONE, *DIME, UNIVERSITY OF GENOA, ITALY*
GERSON GOMES CUNHA, *COPPE UFRJ, BRAZIL*
RICCARDO DI MATTEO, *UNIVERSITY OF GENOA, ITALY*
MICHEL HAVET, *GEPEA RESEARCH UNIT, FRANCE*
FRANCESCO LONGO, *MSC-LES, UNIVERSITY OF CALABRIA, ITALY*
GIANLUCA MAGLIONE, *UNIVERSITY OF GENOA, ITALY*
FRANCESCO MARRA, *UNIVERSITY OF SALERNO, ITALY*
MARINA MASSEI, *LIOPHANT SIMULATION, ITALY*
RUBEN MERCADE PRIETO, *SOOCHOW UNIVERSITY, CHINA*
YURI MERKURYEV, *RIGA TECHNICAL UNIVERSITY, LATVIA*
ROBERTO MONTANARI, *UNIVERSITY OF PARMA, ITALY*
LETIZIA NICOLETTI, *CAL-TEK SRL, ITALY*
ANTONIO PADOVANO, *UNIVERSITY OF CALABRIA, ITALY*
MIQUEL ANGEL PIERA, *UNIVERSITY OF BARCELONA, SPAIN*
OLIVIER ROUAUD, *GEPEA RESEARCH UNIT, FRANCE*
STEFANO SAETTA, *UNIVERSITY OF PERUGIA, ITALY*
FEDERICO SOLARI, *UNIVERSITY OF PARMA, ITALY*
TOMAS SKOGLUND, *TETRAPAK, SWEDEN*
JACK VANDER VORST, *ORL GROUP - WAGENINGEN UNIVERSITEIT, NL*
GIUSEPPE VIGNALI, *UNIVERSITY OF PARMA, ITALY*
MUSTAFA TAHSIN YILMAZ, *YILDIZ TEKNİK ÜNİVERSİTESİ, TURKEY*

TRACKS AND WORKSHOP CHAIRS

LIQUID FOOD PROCESSING

CHAIRS: TOMAS SKOGLUND, SWEDEN, TETRAPAK, SWEDEN; MARCO BETTER, OPTTEK SYSTEMS, USA

SIMULATION OF FOOD SUPPLY CHAIN

CHAIR: JACK VANDER VORST, ORL GROUP - WAGENINGEN UNIVERSITEIT, NETHERLANDS

MODELLING AND SIMULATION OF FOOD PROCESSING

CHAIR: MICHEL HAVET, GEPEA RESEARCH UNIT, FRANCE

MODELLING AND SIMULATION OF FOOD PROPERTIES

CHAIR: MUSTAFA TAHSIN YILMAZ, YILDIZ TEKNİK ÜNİVERSİTESİ, TURKEY

SUSTAINABILITY OF FOOD PROCESSES

CHAIR: GIUSEPPE VIGNALI, UNIVERSITY OF PARMA, ITALY

MODELLING AND SIMULATION OF FOOD FOULING AND CLEANING TECHNIQUES

CHAIR: RUBEN MERCADE PRIETO, SOOCHOW UNIVERSITY, CHINA

MODELING OF TRANSPORT PHENOMENA IN FOOD PROCESSES ASSISTED BY MICROWAVES AND RADIO-FREQUENCIES

CHAIR: FRANCESCO MARRA, UNIVERSITY OF SALERNO, ITALY

CHAIRS' MESSAGE

WELCOME TO FOODOPS 2017!

Dear Attendees,

It is a great pleasure for us to welcome you to the third edition of "The international Food Operations & Processing Simulation Workshop" (FoodOPS 2017) that this year is held in the vibrant, rich and fascinating Barcelona, the capital city of Catalonia.

FoodOPS has renewed the opportunity for academics, professionals, researchers and subject matter experts to share results and critical issues in the fields of Food Engineering, Food Production and Process Simulation, Simulation for Food Supply Chain, Sustainability of Food Processes, Modelling and Simulation of Food Properties, and many others.

In the past recent years, food engineering has expanded enormously in terms of issues addressed, theories and tools deployed to improve food operations and processing. This widening domain along with the dynamism in the M&S technologies and approaches is revealing many challenges for researchers and practitioners seeking to come to terms with the scope and diversity of the field. As a matter of fact the food sector has its own particular nature that makes it quite different from other industrial sectors. Among others the need to ensure quality standards against time and environmental conditions, to guarantee the traceability along the whole supply chain, to meet customers' needs with costs and energy savings are merely a few of all the hallmarks of food engineering. Therefore FoodOPS has the potential to make an important contribution to the literature both in appraising the current state of research and in providing advanced approaches for the future development of the field. The topics of the papers submitted this year include M&S of food production and processes, optimization of emerging food technologies, numerical analysis of food properties, analysis and modeling of food packaging, food processing sustainability, production planning and scheduling, supply chain design and management, plant management, market analysis etc.

On behalf of the Organization Committee, we also would like to express our gratitude to the International Program Committee and the reviewers. Their invaluable work allowed us to increase the scientific relevance of this workshop and receive very high-quality contributions as confirmed by the renovated opportunity for the authors of the best papers of this workshop to extend their work and publish in a Special Issue of the ISI indexed Journal "International Journal of Food Engineering", and many other Special Issues in the field of Modeling & Simulation.

We finally hope for a seamless growth of the FoodOPS workshop towards the delineation of new paths for future research and wish all the attendees a fruitful conference and wonderful stay in Barcelona.



Giuseppe Vignali
University of Parma
Italy



Francesco Longo
University of Calabria
Italy



MIQUEL ANGEL PIERA,
*Autonomous University of
Barcelona, Spain*

ACKNOWLEDGEMENTS

The FoodOPS 2017 International Program Committee (IPC) has selected the papers for the Conference among many submissions; therefore, based on this effort, a very successful event is expected. The FoodOPS 2017 IPC would like to thank all the authors as well as the reviewers for their invaluable work.

A special thank goes to Prof. Miquel Angel Piera from Universitat Autònoma de Barcelona as local organizer and to all the organizations, institutions and societies that have supported and technically sponsored the event.

I3M 2017 INTERNAL STAFF

MATTEO AGRESTA, *SIMULATION TEAM, ITALY*

MARGARITA BAGAMANOVA, *AUTONOMOUS UNIVERSITY OF BARCELONA, SPAIN*

LUIGI BRUNO, *DIMEG, UNIVERSITY OF CALABRIA, ITALY*

AGOSTINO G. BRUZZONE, *DIME, UNIVERSITY OF GENOA, ITALY*

ALESSANDRO CHIURCO, *DIMEG, UNIVERSITY OF CALABRIA, ITALY*

RICCARDO DI MATTEO, *SIMULATION TEAM, ITALY*

CATERINA FUSTO, *CAL-TEK SRL, ITALY*

THIMJO KOÇA, *AUTONOMOUS UNIVERSITY OF BARCELONA, SPAIN*

FRANCESCO LONGO, *DIMEG, UNIVERSITY OF CALABRIA, ITALY*

GIANLUCA MAGLIONE, *SIMULATION TEAM, ITALY*

MARINA MASSEI, *DIME, UNIVERSITY OF GENOA, ITALY*

ROMUALDO MORENO, *AUTONOMOUS UNIVERSITY OF BARCELONA, SPAIN*

MERCEDES NARCISO, *AUTONOMOUS UNIVERSITY OF BARCELONA, SPAIN*

LETIZIA NICOLETTI, *CAL-TEK SRL, ITALY*

ANTONIO PADOVANO, *DIMEG, UNIVERSITY OF CALABRIA, ITALY*

MIQUEL ANGEL PIERA, *AUTONOMOUS UNIVERSITY OF BARCELONA, SPAIN*

MARKO RADANOVIC, *AUTONOMOUS UNIVERSITY OF BARCELONA, SPAIN*

JUAN JOSE RAMOS, *AUTONOMOUS UNIVERSITY OF BARCELONA, SPAIN*

CATALDO RUSSO, *CAL-TEK SRL, ITALY*

NINA SCHEFERS, *AUTONOMOUS UNIVERSITY OF BARCELONA, SPAIN*

MARCO VETRANO, *CAL-TEK SRL, ITALY*



This International Workshop is part of the I3M Multiconference: the Congress leading Simulation around the World and Along the Years



INDEX

Computational Fluid Dynamics (CFD) simulation of hot-air flow profile and temperature distribution in a CECH dryer	1
A. M. Olaniyan, S. K. Oyeniyi, A. O. Oloye, O. I. Ogunniyi, E. W. Igwegbe	
Drying characteristics of soybean (glycine max) using continuous drying and intermittent drying	8
H. W. Park, W. Y. Han, H.-W. Kang, W. B. Yoon	
Developing a linearization method to determine an optimum formulation in surimi blend with varied moisture content using linear programming	16
H. W. Park, J. W. Park, W. B. Yoon	
Accurate prediction of heat penetration of a surimi paste with various salt and moisture contents using numerical simulation with temperature dependent thermal property functions	25
H. W. Park, M.-G. Lee, J. W. Park, W. B. Yoon	
Effect of inulin in Jerusalem Artichoke (<i>Helianthus Tuberosus</i> L.) flour on the viscoelastic behavior of cookie dough and quality of cookies	35
Y. J. Lee, O.-H. Lee, W. B. Yoon	
Sustainable distribution system in food retail sector - a simulation modelling approach	45
S. Saad, R. Bahadori, J. Ravisankar	
Drying process simulation in food industry using lattice Boltzmann method	51
M. Mobarak, M. Hussein, A. Delgado	
Advanced approaches to solving critical and complex production scheduling problems	59
M. Better, J. P. Kelly, M. Laguna, R. Palmer	
Discrete event simulation of a pigmeat packing plant	68
L. M. Plà-Aragones, A. Pagès-Bernaus, E. Novoa-Tufet, J. Mateo-Fornés, P. Terrafeta, D. Mendiroiz, L. Pérez-Cànovas, S. López-Nogales	
CFD model validation of a bag filter for air filtration in a milling plant	73
F. Solari, G. Tagliavini, R. Montanari, E. Bottani, N. Malagoli, M. Armenzoni	
Market analysis of dairy products produced in the Parmigiano-Reggiano area	82
R. Mantione, G. Vignali	
Author's Index	93

COMPUTATIONAL FLUID DYNAMICS (CFD) SIMULATION OF HOT-AIR FLOW PROFILE AND TEMPERATURE DISTRIBUTION IN A CECH DRYER

Adesoji Matthew Olaniyan^(a), Samuel Kehinde Oyeniyi^(b), Abraham Olusola Oloye^(c), Oluwole Idowu Ogunniyi^(d), Ezinne Winnifred Igwegbe^(e)

^{(a),(c)}Department of Agricultural and Bioresources Engineering, Faculty of Engineering, Federal University Oye-Ekiti, Ikole-Ekiti Campus, Nigeria

^{(b),(d)}Department of Agricultural and Environmental Engineering, Faculty of Technology, University of Ibadan, Ibadan, Nigeria

^(e)Union Bank of Nigeria Plc, Plot 36, Marina, Lagos, Nigeria

^(a)amol397@hotmail.com, adesoji.olaniyan@fuoye.edu.ng

ABSTRACT

This paper presents the computational fluid dynamics simulation of air flow and temperature distribution in a CECH dryer. The CAD model of the dryer was done using Solidworks 2014 software. The discretization process was done in ANSYS ICEM in order to cope-up with the thermal and velocity layers formation. ANSYS FLUENT 14.5, a Computational Fluid Dynamic (CFD) software in which flow fields and other physics are calculated in detail for various engineering applications, was used as the CFD solver. The analysis was done to characterize velocity vectors, temperature distribution, pressure, air flow pattern and turbulence intensity. Experimental data was used for the boundary conditions. Standard k-ε turbulence model was allowed to predict the three-dimensional flow and the conjugate various profiles of the air parameters. Simulation results revealed air temperature profile to be 365.56K, 368.93K, 376.14K, 373.53K and 383.12K on trays 1, 2, 3, 4 and 5 respectively. Taking tray 5 as a reference point, air temperature decreased from 383.12K at the reference point (0) along the distance of travel of heated air to 363.54K at the end point 0.65 m. Air density profile shows $9.74 \times 10^{-1} \text{ kg/m}^3$, $9.65 \times 10^{-1} \text{ kg/m}^3$, $9.46 \times 10^{-1} \text{ kg/m}^3$, $9.53 \times 10^{-1} \text{ kg/m}^3$ and $9.29 \times 10^{-1} \text{ kg/m}^3$ on trays 1, 2, 3, 4 and 5 respectively. From the results, it is noted that the heated air was not flowing well to tray 1 and 2 and this is due to the configuration of the dryer. It is therefore suggested that during drying operation, the trays should be inter-changed intermittently in order to achieve uniform distribution of the heated air in the drying chamber. It can be inferred from the study that the drying rate of the product would be significantly influenced by the air velocity, the drying air temperatures and the arrangement of the trays.

Key words: CECH dryer, CFD simulation, food processing, heat transfer, SWFS software

1. INTRODUCTION

One of the easiest and oldest methods of food processing which can contribute to a reduction in postharvest losses and promote food security is drying. This operation is energy consuming, so there is need for an actual optimization based on dynamic mathematical models, analysis and numerical simulations. The system behaviour and performance of a dryer is directly influenced by the air flow pattern and temperature distribution in the drying chamber. A thorough understanding of the fundamental principles of this system behaviour is highly essential for the optimization of the drying process.

Olaniyan and Alabi (2014) designed and fabricated a prototype dryer for paddy rice using locally-available construction materials. A preliminary test carried out on the dryer revealed that it was able to dry paddy rice from a moisture content of 22.36% to 13.37% and this shows that the dryer performed satisfactorily. Olaniyan and Omoleiyomi (2014) designed, built and tested a hot-air dryer for small scale drying of tomato taking into consideration the techno-economic status of small holder farmers and tomato processors. Testing the dryer with 840g samples of sliced tomato at 55°C for 6h showed that it was able to dry the tomato samples from a moisture content of 89% (wb) to 21.8% (wb). Olaniyan et al (2017) conducted experiments to determine the effects of foaming agent, foam stabilizer and whipping time on the drying process of tomato paste under different drying equipment. Result showed that showed that an optimum drying rate of 11.36 g/h could be achieved using a mechanical dryer if tomato paste is pretreated with foaming agent, foam stabilizer and whipping time of 14.0 %EW, 0.48 %CMC and 9 min respectively.

An understanding of temperature distribution at any point in the drying chamber is important because spoilage can start from regions with poor temperature distribution and caking of the products

can occur at the region with undesirable level of temperature. Therefore, the objective of this study is to investigate the air flow profile and temperature distribution in a CECH dryer using Solidworks 2014 SP4.0 software. The work presents the computational fluid dynamics simulation of air flow and temperature distribution in the CECH dryer.

2. MATERIALS AND METHODS

2.1. Description of the CECH Dryer

The CECH dryer was designed and constructed as part of a project on drying of agricultural products. As shown in Figure 1 below, the dryer has three major functioning units, which are the inlet air diverging unit, heating (plenum) chamber and the drying chamber (having five drying trays numbered upwards from the bottom). The major components of the dryer are the blower, heating elements, diverging unit to direct the flow of air, and drying trays which are stacked vertically in the drying unit. The mesh analysis of the geometry of the dryer is shown in Figure 2.

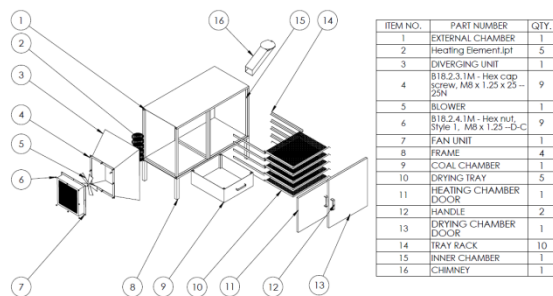


Figure 1: Exploded View of the CECH Dryer

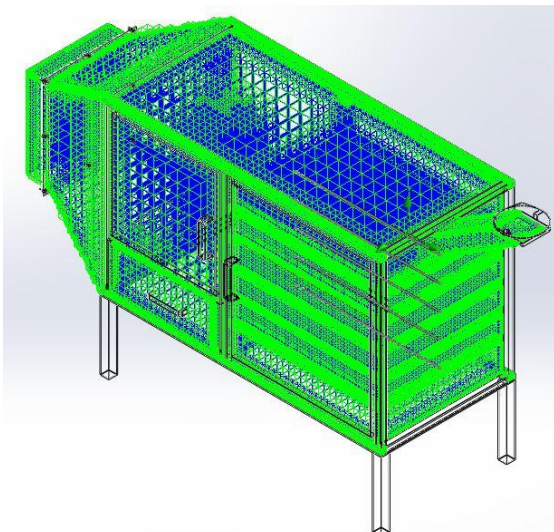


Figure 2: Mesh Analysis of the Geometry of the CECH Dryer

2.2. Simulation Model

The CAD model of the dryer was done using Solidworks 2014 software as used by Oyeniyi *et al.* (2016). The discretization process was done in

ANSYS ICEM in order to cope-up with the thermal and velocity layers formation. Thereafter, ANSYS FLUENT 14.5, a Computational Fluid Dynamic (CFD) software in which flow fields and other physics are calculated in detail for various engineering applications, was used as the CFD solver. The analysis was done to characterize velocity vectors, temperature distribution, pressure, air flow pattern and turbulence intensity. The experimental data was used for the boundary conditions. Standard k-ε turbulence model was allowed to predict the three-dimensional flow and the conjugate various profiles of the air parameters.

2.3. Boundary Conditions

The boundary conditions considered are as shown in Tables 1 and 2 and illustrated by Figure 3 below. This takes into consideration x-axis as the reference axis with global coordinate system.

Table 1: Boundary Conditions for Inlet Velocity

Type	Boundary Conditions
Flow parameters	Flow vectors direction: Normal to face Velocity normal to face: 2.000 m/s
Thermodynamic parameters	Fully developed flow: Yes Approximate pressure: 101325.00 Pa Temperature: 363.20 K

Table 2: Boundary Conditions for Environment Pressure

Type	Boundary Conditions
Thermodynamic parameters	Environment pressure: 101325.00 Pa Temperature: 273.20 K
Turbulence parameters	Turbulence energy and dissipation Energy: 1.000 J/kg Dissipation: 1.00 W/kg
Boundary layer parameters	Boundary layer type: Turbulent

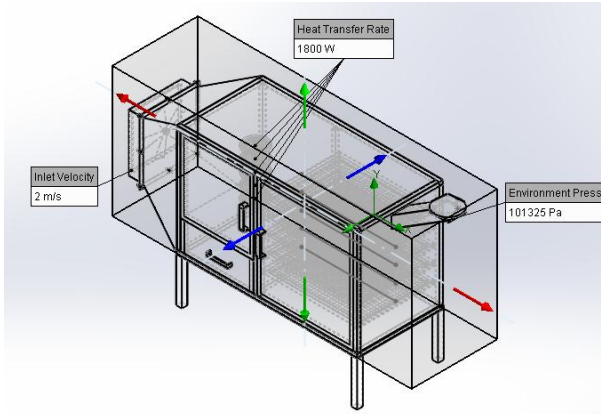


Figure 3: Boundary Conditions and the Computational Domain of the CECH Dryer

2.4. CFD Governing Equations

The basic governing equations of CFD analysis is the Navier-Stokes equations which is the conservation laws for mass, momentum and energy in the Cartesian coordinate (x,y,z) system rotating with angular velocity about an axis passing through the coordinate system's origin. These equations can be written as follows (Solidworks, 2012, Oyeniyi *et al.*, 2016):

Mass Equation:

$$\frac{\rho}{t} + \frac{\partial(\rho u_i)}{\partial x_i} = 0 \quad (1)$$

Momentum Equation:

$$\begin{aligned} \frac{\partial(\rho u_i)}{\partial t} + \frac{\partial(\rho u_i u_j)}{\partial x_j} + \frac{\partial p}{\partial x_i} \\ = \frac{\partial(\tau_{ij} + \tau_{ij}^R)}{\partial x_j} + S_i \quad i \\ = 1,2,3 \end{aligned} \quad (2)$$

Energy Equation:

$$\begin{aligned} \frac{\rho H}{t} + \frac{\partial(\rho u_i H)}{\partial x_i} = \frac{\partial}{\partial x_i} (u_j (\tau_{ij} + \tau_{ij}^R) + q_i) + \frac{\partial p}{\partial t} \\ - \tau_{ij}^R \frac{u_i}{x_j} + \rho \epsilon + S_i u_i \\ + Q_H \end{aligned} \quad (3)$$

Where: u is the fluid velocity (m/s), ρ is the fluid density (kg/m^3), S_i is a mass-distributed external force per unit mass (N), h is the thermal enthalpy, Q is a heat source per unit volume, τ_{ij} is the viscous shear stress tensor, q_i is the diffusive heat flux. The subscripts are used to denote summation over the three coordinate directions. P is pressure (Pa),

$\frac{\partial \tau_{ij}}{\partial x_i}$ is the body forces (N), and t is time (s), (i, j, k) depicts the three main coordinates which the mass force depends on, c_μ is the fourth-order tensor representing the constant of proportionality, λ is the viscosity tensor, μ the dynamic viscosity (Ns/m^3) and δ_{ij} is the Kronecker delta.

3. RESULTS AND DISCUSSION

3.1. CFD Post Process of the Air Flow Profile Cut Plots in the CECH Dryer

As shown in Figures 4 and 5 below, the temperature contours grew from the heating element to the drying chamber. It is also noted the heated air was not flowing well to trays 1 and 2 due to the configuration of the dryer. Hence, it is suggested that during drying operation, the trays should be inter-changed intermittently in order to achieve uniform distribution of the heated air in the drying chamber. In another sense, another fan to cause more turbulence in the drying chamber should be placed therein. It can also be suggested that the fan should be closer to the heating source. It is highly essential to note that the walls of the drying chamber are well insulated in order to minimize heat transfer through the dryer walls

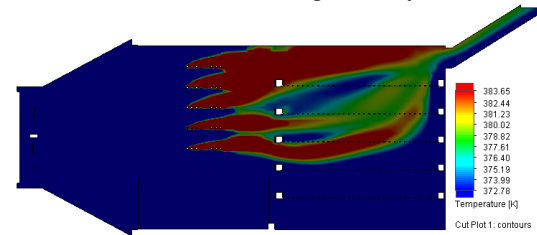


Figure 4: Temperature Field Pattern of the Hot Air in the CECH Dryer



Figure 5: Pressure Profile of the Hot Air in the CECH Dryer

3.2. Variation of Drying Parameters in respect to the Arrangement of the Trays

As illustrated in Figures 6-12 below, simulation results revealed air temperature profile to be 365.56K, 368.93K, 376.14K, 373.53K and 383.12K on trays 1, 2, 3, 4 and 5 respectively. Considering tray 5 as a reference point, air temperature decreased from 383.12K at the reference point (0) along the distance of travel of

heated air to 363.54K at the end point 0.65 m. Air density profile shows $9.74 \times 10^{-1} \text{ kg/m}^3$, $9.65 \times 10^{-1} \text{ kg/m}^3$, $9.46 \times 10^{-1} \text{ kg/m}^3$, $9.53 \times 10^{-1} \text{ kg/m}^3$ and $9.29 \times 10^{-1} \text{ kg/m}^3$ on trays 1, 2, 3, 4 and 5 respectively. On tray 5, air density decreased $9.29 \times 10^{-1} \text{ kg/m}^3$ at the reference point to $9.78 \times 10^{-1} \text{ kg/m}^3$ at the end point 0.65 m. Air velocity profile indicates $5.08 \times 10^{-1} \text{ m/s}$, $7.79 \times 10^{-1} \text{ m/s}$, $4.75 \times 10^{-1} \text{ m/s}$, $2.14 \times 10^{-1} \text{ m/s}$ and $1.36 \times 10^{-1} \text{ m/s}$ on trays 1, 2, 3, 4, and 5 respectively. On tray 5, air velocity increased from 0.14 m/s at the reference point to 2.56 m/s at the end point. The total enthalpy were 371.00, 374.43kJ/kg, 381.71 kJ/kg, 379.07 kJ/kg and 388.78 kJ/kg on trays 1, 2, 3, 4 and 5 respectively. On tray 5, the total enthalpy 388.78 kJ/kg at the reference point to 369.06 kJ/kg at the end point.

It is obvious from the results that the heated air was not flowing well to tray 1 and 2 and this can be added to the configuration of the dryer. It is therefore suggested that during drying operation, the trays should be inter-changed intermittently in order to achieve uniform distribution of the heated air in the drying chamber. Alternatively, another fan to cause more turbulence in the drying chamber should be placed installed closer to the heating chamber.

Tray 3 has the highest range of air temperature with the peak being at 0.4 m along distance of travel of the heated air on the drying tray while tray 1 has the least temperature profile due to its location in the drying chamber. This trend shows that the temperature of the fluid varies with the distance of travel best along tray 4 and the percentage of hot air it contributed to at this level is greater than others. It was observed that there are peak periods at the distance between 0.25-0.4 m along the trays and the temperature later drops towards the end of the trays due to the collision of a boundary (dryer door).

Turner and Jolly (1991) and Zhang and Mujumdar (1992) in microwave convective drying and Golestani *et al.* (2013) in convective drying simulations also reported a decreasing temperature profile near the wall of the drying chamber door due to the fact that in simulation, heat loss due to conduction is considered negligible. There was a surge in temperature level at a distance 0.3 m from the rare end of the dryer wall on tray 3 and this might be due to the flow trajectory of the hot air as a result of the upward direction of the flow.

It can be inferred from the study that the drying rate of the product would be significantly influenced by the air velocity, the drying air temperatures and the arrangement of the trays. The study revealed that it is possible to determine the effective length of the

drying chamber and recirculation points which is in agreement with the study conducted by Karim and Hawlader, (2005).

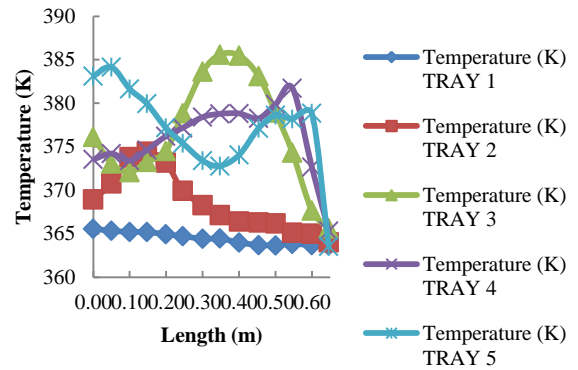


Figure 6: Temperature Profile at Various Points on the Tray with respect to Length

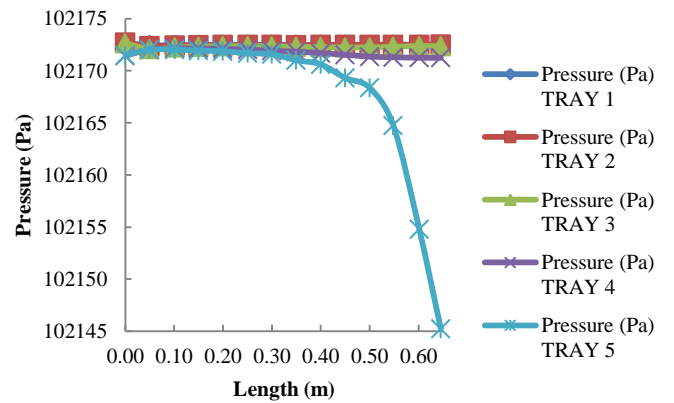


Figure 7: Air Pressure Profile at Various Points on the Tray with respect to Length

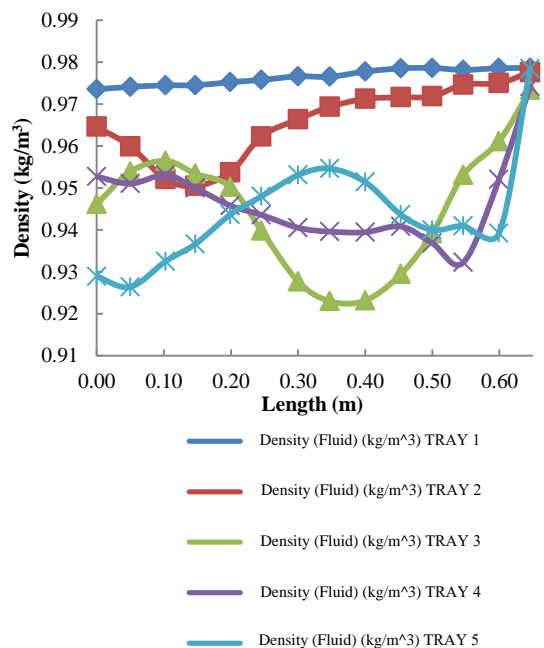


Figure 8: Fluid Density Profile at Various points on the tray with respect to length

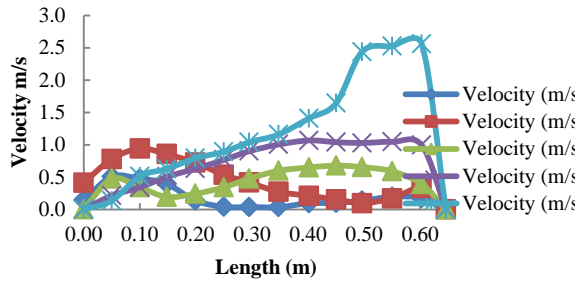


Figure 9: Air Velocity Profile at Various points on the tray with respect to length

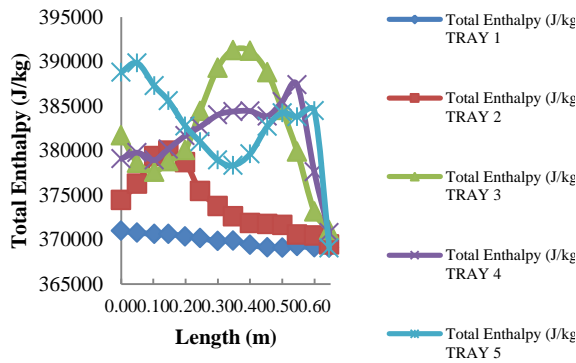


Figure 10: Total Enthalpy Profile at Various points on the tray with respect to length

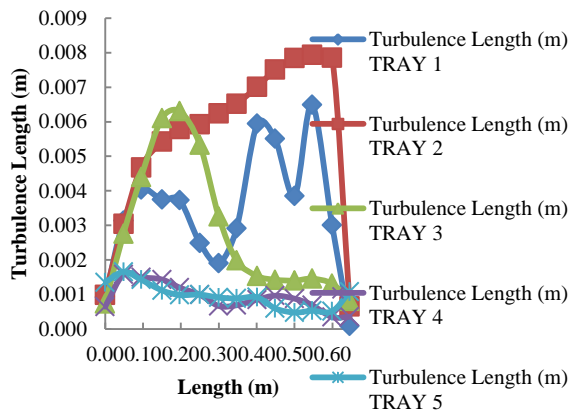


Figure 11: Turbulence Length with respect to the length of trays

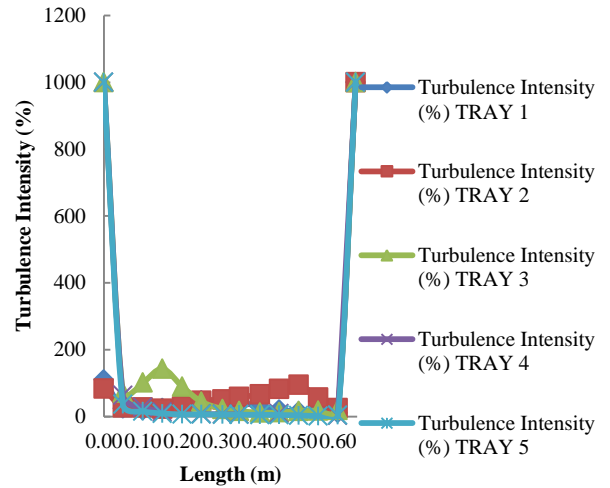


Figure 12: Variation of Turbulence Intensity along the Length of Trays

4. CONCLUSION

The computational fluid dynamic (CFD) simulation was used to predict the temperature distribution, velocity profile and pressure fields in the drying chamber of a CECH dryer. The air flow properties in terms of temperature distribution, velocity field profiles, pressure, fluid density, total enthalpy and turbulence effect of the air were also analyzed to predict the efficiency of the CECH dryer. From the study, it can be inferred that the drying rate of the product would be significantly influenced by air velocity, air temperatures and the arrangement of the trays. It can be concluded that the turbulence model used for the CFD simulation is capable of predicting the dynamic behaviour of the dryer. Thus, CFD is highly efficient in predicting airflow pattern and analysis of drying parameters. Its application to dryer design is capable of solving the problems of uneven drying of products.

REFERENCES

- Golestani, R., Raisi, A., Aroujalian, A. (2013). Mathematical modeling on air drying of apples considering shrinkage and variable diffusion coefficient. *Drying Technology*, 31 (1): 40–51.
- Karim, M.A., Hawlader, M.N.A. (2005). Mathematical modeling and experimental investigation of tropical fruits drying. *International Journal of Heat and Mass Transfer*, 48: 4914-4925.
- Olaniyan, A.M. and Alabi, A.A. (2014). Conceptual Design of Column Dryer for Paddy Rice including Fabrication and Testing of Prototype. *International Journal of Basic and Applied Sciences*, 2 (3): 11-20.

Olaniyan, A.M. and Omoleiyomi, B.D. (2014). Conceptual Design of Tomato Dryer: Fabrication and Testing of Prototype. *International Journal of Postharvest Technology and Innovation*, 4 (2): 114-124.

Olaniyan, A.M., Adeoti, J.A. and Sunmonu, M.O. (2017). Effect of Foaming Agent, Foam Stabilizer and Whipping Time on the Drying Process of Tomato Paste under Different Drying Equipment. *International Journal of Modelling, Simulation and Scientific Computing*, 8 (2).

Oyeniyi, S.K., Aviara, N.A. and Aremu, A.K. (2016). *Computational Fluid Dynamics Modelling of a CSRTC Dryer*. LAP LAMBERT Academic Publishing.

Turner, I.W. and Jolly, P.C. (1991). Combined microwave and convective drying of a porous material. *Drying Technology*, 9 (5): 1209–1269.

Zhang, W., Mujumdar, A.S. (1992). Deformation and stress analysis of porous capillary bodies during intermittent volumetric thermal drying. *Drying Technology*, 10 (2): 421–443.

BIOGRAPHY OF THE AUTHORS

1. Adesoji Matthew Olaniyan graduated with BEng, MEng and PhD in Agricultural Engineering from University of Ilorin, Nigeria in 1991, 1998 and 2006 respectively. Since 1998, he has been working on techniques, processes and equipment for processing agricultural and bioresources materials to food, fibre and industrial raw materials. Dr. Olaniyan's principal area of research is on Bioproduct Processing and Food Process Engineering, where he has carried out a number of projects and published a number of papers in local and international journals. He joined the service of the University of Ilorin in 1998 as an Assistant Lecturer in the Department of Agricultural and Biosystems Engineering and rose to the position of a Senior Lecturer in 2009. Currently, he is an Associate Professor at the Department of Agricultural and Bio-resources Engineering, Federal University Oye-Ekiti, Nigeria. Dr. Olaniyan has bagged several awards including the Award for the Best Paper (2007) in the *Journal of Food Science and Technology*, Mysore, India; Chinese Government Sponsorship (2008) for International Training Programme in Protected Agriculture at International Exchange Centre, Yangling, China; Netherlands Fellowship Programme (2009) for International Training Programme in Milk Processing at Practical Training Centre, Onkerk, the Netherlands; and Postdoctoral Fellowship (2011) of the Academy of Sciences of Developing Countries.

2. Samuel Kehinde Oyeniyi is currently an Agricultural Engineer at OFN-San Carlos Nigeria Limited, he had a BEng degree in Agricultural and Biosystems Engineering at University of Ilorin and MSc degree in Agricultural and Environmental Engineering from University of Ibadan. His research interests are majorly in machine design and computational fluid dynamics analysis. He has published over fifteen (15) scholarly papers in reputable journals, and he is a member of the following professional bodies Nigerian Institute of Agricultural Engineers (NIAE), Nigerian Society of Engineers (NSE), World Association of Scientific Research and Technical Innovation (WASRTI).

3. Abraham Olusola Oloye bagged a National Diploma in Agricultural Engineering from the Federal Polytechnic, Ado-Ekiti and proceeded to the Federal University of Technology, Akure where he obtained his BEng and MEng degrees in Agricultural Engineering. He is a Corporate Member of the Nigerian Institution of Agricultural Engineers (MNIAE), Nigerian Society of Engineers (MNSE) and a Registered Engineer with the Council for the Regulation of Engineering in Nigeria (COREN). He joined the service of the Federal University, Oye-Ekiti as a Lecturer II in the Department of Agricultural and Bioresources Engineering specializing in Processing and Storage Engineering. He is a Member of the University COREN and NUC Accreditation Committee and has jointly published in a scientific research.

4. Oluwole Idowu Ogunniyi is the CEO/Customer Support Officer of Hithe Technologies Nigeria (an ICT/Web Development Company). Born in the South-West part of Nigeria, Oluwole attended the University of Ilorin where he was awarded BEng degree in Agricultural Engineering. He received his MSc degree in Agricultural and Environmental Engineering from the University of Ibadan. Oluwole has always enjoyed starting and running businesses, some of which includes Nairashopping.com Data Transfer Service and Hithe Technologies Nigeria. At Hithe Technologies Nigeria, Oluwole has worked with and served several individual and many Corporate Organizations on various projects.

5. Ezinne Winnifred Igwegbe hails from Ideato North Local Government Area of Imo State but was born in Zaria, Kaduna State. She obtained her primary and secondary school education in NEPA Senior Staff School, Kanji, Niger State and Federal Government Girls' College Owerri, Imo

State respectively. She attended the University of Ilorin, between 2005-2009 and graduated with BEng degree in Agricultural Engineering with Second Class Honours (Upper Division). She had her 1-year mandatory National Youth Service with Power Holding Company of Nigeria, Benin, Edo State in 2009/2010 as Human Resource personnel and Neboosh Certificate in Occupational Health and Safety in 2014. Currently, she works with Union Bank of Nigeria Plc as a Relationship Manager.

DRYING CHARACTERISTICS OF SOYBEAN (*GLYCINE MAX*) USING CONTINUOUS DRYING AND INTERMITTENT DRYING

Hyeon Woo Park^(a), Won Young Han^(b), Hang-Won Kang^(c)
Won Byong Yoon^(d)

^{(a),(d)}Department of Food Science and Biotechnology, College of Agricultural and Life Science, Kangwon National University, Chuncheon 200-701, Korea

^{(b),(c)}Department of Functional crop, National Institute of Crop Science Milyang, 627-803, Korea

^(a)hwpark0978@gmail.com, ^(b)hanwy@korea.kr, ^(c)kanghw@korea.kr
^(d)wbyoon@kangwon.ac.kr

ABSTRACT

The effects of drying temperature by continuous and intermittent drying on the drying characteristics of soybean was determined in this study. Among the thin layer drying models, the Midilli-Kucuk model showed the best fit ($R^2 > 0.99$) to describe the drying of soybean. At 300 min of the effective drying time, the moisture content of continuous drying at 35, 40, and 45°C were 9.38 (± 0.00), 8.69 (± 0.17), and 7.70% (± 0.48), respectively; while the moisture content of intermittent drying at 35, 40, and 45°C were 8.28 (± 0.21), 7.31 (± 0.41), and 6.97% (± 0.07), respectively. The image analysis method for detection of the crack in soybean demonstrated that at the target moisture content (7.7%), cracked grain ratios with intermittent drying at 35, 40, and 45°C were reduced by 52.08, 27.59, and 18.24%, respectively. With the effective drying time, the activation energy for intermittent drying (9.33kJ/mol) was significantly lower than that value for continuous drying (21.23kJ/mol).

Keywords: intermittent drying, image analysis, thin-layer drying models, soybean

1. INTRODUCTION

Soybean (*Glycine max*) is one of the most important food resources in Asian countries, due to high protein and oil content. Traditionally, soybeans are processed and served in many ways including tofu, soybean paste, and soybean sauce (Kwon 1972). The moisture content of soybean is an important factor for controlling the quality during storage and processing. Since the 20 to 25% post-harvest moisture content is unsuitable for long term storage, solar or hot air drying is used to reduce the moisture content in soybeans (Rafiee 2009, Soponronnarit et al. 2001). Solar drying is traditionally used due to its low cost of energy consumption. However, solar drying has several drawbacks including weather dependence that makes it difficult to control the soybean quality; low heat and mass transfer rate that causes a longer drying time and outdoor conditions that carry a risk of contamination by microorganisms and

insects (Doymaz 2006). The hot air drying method has advantages of short drying time and low labor cost. However, hot air drying has a fast drying rate due to high heat and mass transfer rate, which causes thermal damage to the soybeans. The best-known thermal damages include cracking or breaking of soybeans (Soponronnarit et al. 2001, Wiriyumpaiwong et al. 2003). Cracking or breaking of soybean is mainly due to the tension on the skin of soybeans associated with an abrupt or a steep moisture gradient from the surface to the center of beans (Hirunlabh et al. 1992). Therefore, it is necessary to develop a drying method to minimize the amount of thermal damage to soybeans by controlling the moisture gradient associated with a hot air drying. A few studies have focused on minimizing the thermal degradation of soybeans during hot air drying (Lee and Lee 2009, Niamnuy et al. 2012); however, an alternate drying method for reducing the amount of thermal damage in soybeans has not been proposed to data.

Intermittent drying (ID), also called cyclic drying, is a novel method to minimize the moisture gradient of the product during drying (Kumar et al. 2014). In ID, samples are removed from the dryer for a certain time interval to allow central to peripheral diffusion of moisture; subsequently, the samples are returned to the dryer. The repeated periodic drying process reduces thermal damage by controlling the products' diffusion rate and producing a less steep moisture gradient. ID is commercially applied to several agricultural products, including soybeans. Few studies have been reported to demonstrate the effect of drying air condition and intermittency on the moisture changes of soybean during intermittent drying (Defendi et al. 2017, Zhu et al. 2016). However, the thermal degradation of soybeans during ID remain still unknown. Most commercial scale ID processes are based on trial-and-error or operators' experience.

Drying process is one of the most complex unit operation, because in most, heat, mass, and momentum transfer phenomena are simultaneously connected (Kudra and Mujumdar 2002, Yilbas et al. 2003). Due to the complexity of developing an analytical or a numerical

model to interpret the drying process, many empirical models have been developed (Baker 1997, Marinos-Kouris and Maroulis 1995). Thin layer model, a well-known empirical model for drying, has been practically used to design the drying process based on the experimentally-derived drying curves (Moon et al. 2014, Rafiee 2009). Since there are no empirical models to characterize an ID method for soybeans, it is useful to construct a mathematical model to describe the drying behavior of ID for soybeans based on the thin-layer drying model.

The purposes of this study were 1) to analyze the drying characteristics of soybean according to a continuous hot air drying and an intermittent hot air drying method, 2) to compare the change in quality of soybean according to continuous drying (CD) and ID, and 3) to develop a model to describe the drying behavior of ID for soybean based on the thin-layer model.

2. MATERIALS AND METHODS

2.1. Material

Soybeans were donated from National Institute of Crop Science, Department of Functional Crop (Miryang, Kyungsangbuk-do, S. Korea). The initial moisture content of soybeans was adjusted to 22.0% (± 0.8) immediately after harvesting (Overhults et al. 1973, Soponronnarit et al. 2001). All samples were vacuum packed and stored at room temperature during the experiment.

2.2. Drying process

A tray dryer (width \times depth \times height = 550 \times 520 \times 600 mm, Dong Yang Science Co., Seoul, S. Korea) was used for the CD and the ID. The target moisture content for this study was set at 7.7 % because the moisture content measured from the cracked beans was 7.7%. Soybeans (25 g (± 0.7)) were placed in the center of the dryer throughout the drying process to minimize the effect of temperature gradient in the dryer on the drying rate. The drying temperature was varied at 35, 40, and 45 °C, and the inlet air velocity was fixed at 3.0 m/s. Drying time was 600 min, and the weight of the soybean was measured every 30 min. For the CD, the drying time was 600 min (without interruption); and, for the ID, soybean was dried for 30 min in the dryer followed by diffusion of the moisture for 30 min in the desiccator, repeatedly during the 600 min time period.

2.3. Detection of cracked bean with image analysis

The quality of soybean during the drying process was evaluated by the ratio (%) of cracked bean at the target moisture content of 7.7% after continuous and intermittent drying at 35, 40, and 45 °C, respectively. Image analysis was used to detect the cracks of soybeans. The image analysis procedures for this study included (1) image acquisition, (2) image segmentation, (3) thresholding, (4) filtering, and (5) image analysis (Fig. 1).

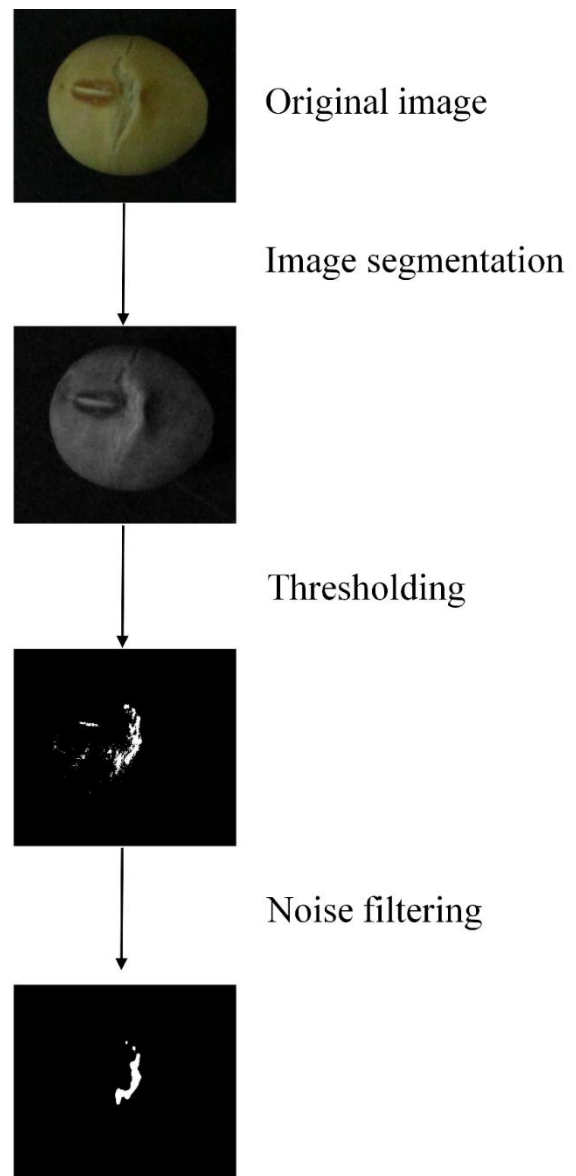


Figure 1: The Overall Procedure for Image Analysis of Soybean.

A digital single-lens reflex camera (DSLR-500D, Canon Inc., Tokyo, Japan) with a lens (EF-S 18-55 mm *f*/3.5-5.6, Canon Inc., Tokyo, Japan) was placed vertically over the sample at a distance of 18 cm. The image of the sample was acquired using a camera with a resolution of 2.1 million pixels. Image acquisition was replicated 10 times with shaking for 3 s. The image processing tool in MATLAB (Mathworks® Inc., Natick, MA, USA) was used for analysis of the structural features of the soybeans. Threshold-based segmentation was a particularly effective technique for imaging solid objects on a contrasting background. After image segmentation, the threshold was obtained from histogram of the image (not shown). With the optimal threshold, all pixels at or above the threshold level were assigned to white color and all pixels below the threshold level were assigned to black color. After applying this process, the hilar fissures and the crack of soybeans were extracted with white

color. A median filter is a non-linear filtering technique that allows the edges to be preserved while filtering out unwanted noise (Du and Sun 2004). It replaces the output pixels with the median of the adjacent pixel values instead of a weighted sum of those values. In this study, the median filter was applied to remove the hilar fissures from the soybean images after applying the thresholding technique. The cracked bean ratio was estimated from the maximum detected edge ratio of 10 replicates.

2.4. Thin-layer drying model and drying rate

Four different thin-layer drying models were applied to evaluate the drying behavior of soybeans. The thin-layer drying models used in this study were presented in Table 1. These drying models have been used in many food products (Herderson and Pabis 1961, Lewis 1921, Midilli et al. 2002, Page 1949).

The moisture ratio and the drying rate were calculated as the follows:

$$MR = \frac{M - M_e}{M_i - M_e} \quad (1)$$

where MR is the moisture content, M is the moisture content according to the drying time (g/g d.b.), M_e is an equilibrium moisture content (g/g d.b.), and M_i is the initial moisture content.

Table 1: Thin Layer Models Used to Describe the Drying Kinetics of Soybean.

Model no.	Model name	Model equation	References
1	Newton	$MR = e^{-kt}$	Lewis (1921)
2	Page	$MR = e^{-kt^n}$	Page (1949)
3	Henderson and Pabis	$MR = ae^{-kt}$	Henderson and Pabis (1961)
4	Midilli-Kucuk equation	$MR = ae^{-kt^n} + bt$	Midilli et al. (2002)

The drying rates at initial stages of drying, during drying, and at the final stage of drying were calculated according to Guine and Fernandes (2006):

$$\text{at } t = t_0, \quad \frac{dM}{dt} = \frac{M_i - M_0}{t_1 - t_0} \quad (2)$$

$$\text{at } t = t_i \ (i = 1, 2, \dots, n - 1), \quad \frac{dM}{dt} = \frac{M_{i+1} - M_{i-1}}{t_{i+1} - t_{i-1}} \quad (3)$$

$$\text{at } t = t_n, \quad \frac{dM}{dt} = \frac{M_n - M_{n-1}}{t_n - t_{n-1}} \quad (4)$$

2.5. Effective moisture diffusivity and activation energy

The effective moisture diffusivity (D_{eff}), which is affected by the porosity, moisture content, composition, temperature a material, provides useful information to

understand the mechanism of moisture movement during drying process. The D_{eff} at given moisture content can be estimated using the “methods of slope” technique from the solution of Fick’s second law equation (Karathanos et al. 1990, Marinos-Kouris and Maroulis 1995, Zogzas et al. 1996). For Fick’s second law of diffusion,

$$\frac{\partial M}{\partial t} = \frac{1}{r} \left[\frac{\partial}{\partial r} \left(D_{eff} r \frac{\partial M}{\partial r} \right) + \frac{\partial}{\partial z} \left(D_{eff} r \frac{\partial M}{\partial z} \right) \right] \quad (5)$$

For a sphere,

$$MR = \frac{M - M_e}{M_i - M_e} = \frac{6}{\pi^2} \sum_{n=1}^{\infty} \frac{1}{n^2} \times \exp \left(-n^2 \frac{\pi^2 D_{eff}}{r^2} t \right) \quad (6)$$

where D_{eff} is the effective moisture diffusivity (m^2/s), and r is the spherical radius (m).

When the drying time is long enough, the solutions are simplified by eliminating the second term:

$$MR = \frac{M - M_e}{M_i - M_e} = \frac{6}{\pi^2} \exp \left(-\frac{\pi^2 D_{eff}}{r^2} t \right) \quad (7)$$

The simplified solution can be written in a logarithmic form as follows:

$$\ln MR = A - B \times t \quad (8)$$

where B is $\pi^2 D_{eff} / r^2$ for a sphere.

The temperature dependence of the D_{eff} is generally expressed as the Arrhenius-type relationship as follows:

$$D_{eff} = D_0 \exp \left(\frac{E_a}{RT} \right) \quad (9)$$

$$\ln D_{eff} = \ln D_0 - \frac{E_a}{RT} \quad (10)$$

where D_0 is the pre-exponential/frequency factor of the Arrhenius equation (m^2/s); E_a is the activation energy (kJ/mol); R is the universal gas constant (kJ/mol K) and T is the absolute temperature (K). In this study, the effective moisture diffusivity and the activation energy for intermittent drying were calculated from the effective drying time (i.e., the time that soybeans are dried in the drying chamber).

3. RESULT AND DISCUSSION

3.1. Drying kinetics

CD and ID were conducted with different drying temperatures (35, 40, and 45 °C) to investigate the effect of drying temperature on the drying kinetics. Drying temperature significantly affected the rate of moisture reduction in both CD (Fig. 2A) and ID (Fig. 2B). The higher drying temperature showed the faster moisture reduction rate for both drying methods. However, the moisture content at the same drying time showed a difference between CD and ID (Table 2). The moisture content of ID after 300 min of the effective drying time (duration within the drying chamber), was lower than that of CD regardless of drying temperatures. The moisture contents of CD at 35, 40, and 45 °C were 9.38

(± 0.00), $8.69 (\pm 0.17)$, and $7.70\% (\pm 0.48)$, respectively; and those of ID were $8.28 (\pm 0.21)$, $7.31 (\pm 0.41)$, and $6.97\% (\pm 0.07)$, respectively. The rates of moisture

reduction from ID were significantly faster than those of CD for all drying temperatures.

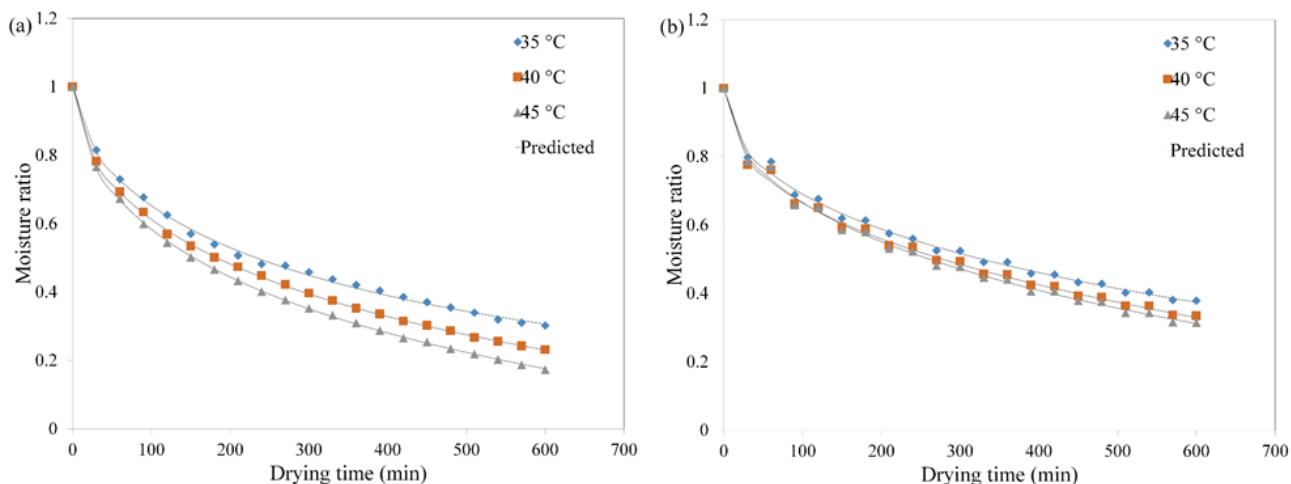


Figure 2: Changes of Moisture Ratio of the Soybean Upon the Drying Temperature Using (a) Continuous Drying and (b) Intermittent Drying.

The faster rate of moisture reduction observed from ID is mainly due to the moisture diffusion from the center to the surface during the rest period. Since the rest period allows moisture transfer solely by concentration difference, the effective drying time applied in the drying chamber was eventually reduced. This result implied that the drying method and the drying temperature

significantly influenced the moisture reduction rate of soybeans. Thus, ID may help reduce the energy consumption required for soybean drying. ID has been applied to the various bio-products because of these advantages (Chua and Chou 2005, Hemati et al. 1992, Putranto et al. 2011b). Putranto et al. (2011a) have described reducing energy consumption in depth.

Table 2: Moisture Content of Soybean at Different Effective Drying Time and Temperature.

Drying method	Temperature (°C)	Effective drying time (min)	Moisture content (%)
Continuous drying	35	90	13.86 \pm 0.09
		180	11.04 \pm 0.11
		300	9.38 \pm 0.00
	40	90	13.88 \pm 0.14
		180	10.98 \pm 0.17
		300	8.69 \pm 0.17
	45	90	13.07 \pm 0.45
		180	10.18 \pm 0.48
		300	7.70 \pm 0.48
Intermittent drying	35	90	13.46 \pm 0.17
		180	10.69 \pm 0.17
		300	8.28 \pm 0.21
	40	90	12.88 \pm 0.31
		180	9.91 \pm 0.38
		300	7.31 \pm 0.41
	45	90	12.88 \pm 0.03
		180	9.81 \pm 0.03
		300	6.97 \pm 0.07

3.2. Thin-layer drying model

Thin-layer drying model is a well-known semi-empirical model to predict the moisture changes during drying. Although many studies have used the thin-layer models to describe the drying behavior of food and biomaterials, the thin-layer model has not been used to characterize the drying behavior of soybean using ID. Four thin-layer models were applied to characterize the drying behavior of soybeans using CD and ID. The Midilli-Kucuk model was the most suitable model among the four models based on the R^2 (> 0.9942), RMSE (< 0.0147), and SSE (< 0.0037); while the minimum R^2 of Newton, Page, and Henderson and Pabis model showed 0.7726, 0.9933, and 0.9251, respectively. The Midilli-Kucuk model well described the moisture changes of soybean during drying for ID and CD (Fig. 2). As energy efficiency is highly dependent on the effective drying time (i.e., the time that soybeans were dried in the drying chamber), the effective drying time to achieve the target moisture content was calculated based on the Midilli-Kucuk equation and the model parameters induced in this study. The effective drying time to achieve the target moisture content for CD and ID were 479 min and 322 min at 35 °C, 358 min and 264 min at 40 °C, and 315 min and 262 at 45 °C, respectively. The effective drying times of ID at different drying temperature were shorter than those of CD due to moisture diffusion during the rest period of ID.

3.3. Drying rate and quality evaluation of soybean

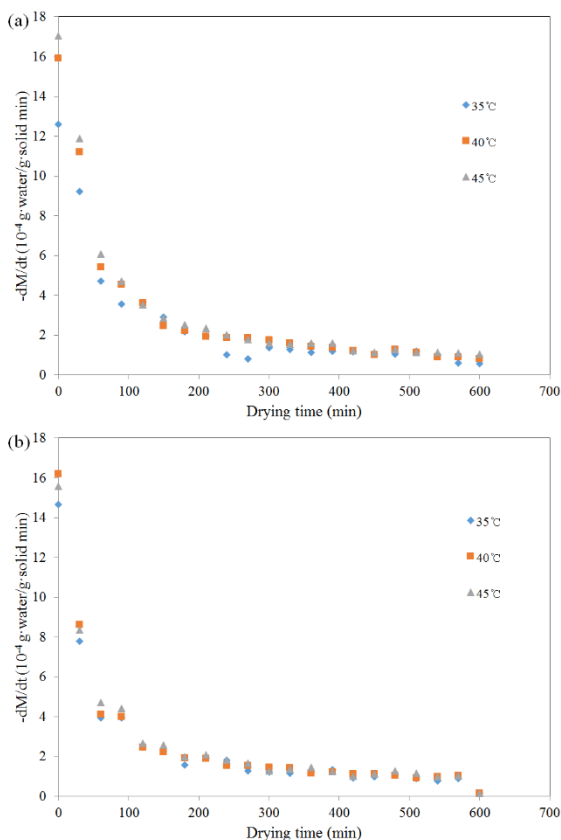


Figure 3: Effect of Drying Temperature on the Changes of Drying Rate Using (a) Continuous Drying and (b) Intermittent Drying.

Changes of the drying rate of soybeans calculated by Eq. 2-4 based on the moisture changes during CD and ID were compared (Fig. 3). Constant rate period was not observed for all drying temperatures in CD and ID, and the drying rate showed continuous decrease as the drying time increased. Because the ratio of the surface area to the volume of soybean is very large, the moisture content on the surface decreases much more rapidly than at the center of a soybean as the drying begins, hence, the falling rate period was presented from the initial stage of drying. The constant rate period may be short or absent in drying of biomaterials, and is dependent on the ratio of surface area to volume or the structure of the biomaterial. Moon et al. (2014) reported that there was no constant rate period in drying sea cucumbers using hot air drying and far infrared drying. The structure of biomaterial is very diverse according to species. Some biomaterials may have a relatively uniform structure, such as a meat, but some biomaterials contain different structure layers for example soybeans or sea cucumbers. When the structure of the dried layers near the surface differs from that near the center, the drying rate may have a gradient in the material. Because the layers near the surface cannot provide a constant supply of water, the drying rate is dominated by the diffusion of moisture from the inside to the outside that consequently causes the drying rate gradient (Chua and Chou 2005, Johnson et al. 1998, Moon et al. 2014, Srikiatden and Roberts 2006).

In the initial stage of drying, the drying rate of ID was lower than that of CD due to the rest period of ID. However, the drying rate of ID was higher than CD with repeated rest and drying periods. Generally, the concentration difference inside a soybean rather than near its surface is the major driving force for the falling rate period. In the early stage, the resistance to drying is predominantly near the surface, but, as the drying time progresses, the moisture diffusion inside of a bean mainly governs the drying rate (Chua and Chou 2005, Hemati et al. 1992, Putranto et al. 2011b). The higher drying rate of ID than CD was due to moisture diffusion in the soy bean during the rest period, which decreased drying resistance near the surface of the bean as the drying time increased. After 360 min of drying, the drying rate of ID showed no significant difference from that of CD at all drying temperatures ($p < 0.05$). The fast drying rate is one of the practical operation conditions of the drying process; however, the fast drying rate obtained from the high drying temperature may cause degradation of soybean quality and thermal damages, such as cracked beans. Therefore, the design of drying process of soybean should consider the effect of drying temperature and drying rate on the quality of soybeans (Karathanos et al. 1990, Sangkram and Noomhorm 2002, Soponronnarit et al. 2001, Wiriyaumpaiwong 2003).

The results of the cracked bean ratio from image analysis were compared with the cracked grain ratio determined manually by the expert group (Fig. 4). No significant differences were observed between two results. Thus, the results demonstrated that the proposed image analysis

method was applicable for high accuracy measures of cracked beans ratio. The quality changes of soybean on CD and ID were evaluated as the ratio of cracked beans at the target moisture content of 7.7% (Fig. 4).

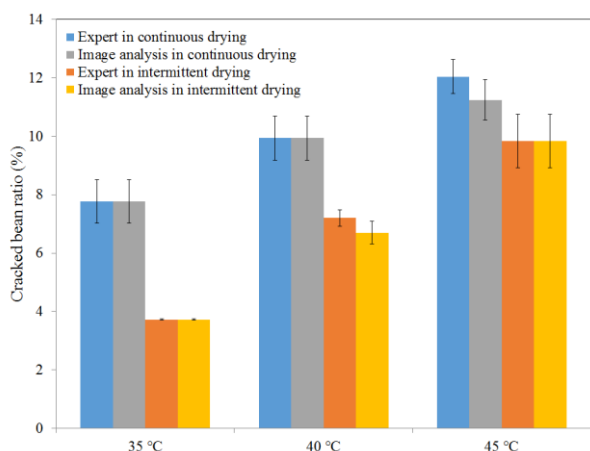


Figure 4: Effect of Drying Temperature on the Cracked Grain Ratio at the Target Moisture Content of 7.7%.

Regardless of drying methods, the cracked bean ratio increased as the drying temperature increased. This is because the high drying temperature has more possibility to cause the moisture gradient in the soybean, creating tension between the surface and the center of the bean that initiates the cracking (Hirunlabh et al. 1992). However, the cracked bean ratios of ID treated samples were much lower, as compared to CD treated samples, possibly due to less abrupt moisture gradient from surface to center, due to diffusion of moisture during the rest period of ID. As the drying temperatures were reduced, the difference of the cracked bean ratios between CD and ID were increased. At 45 °C, the difference was 18.24%, but at 35%, the difference increased to 52.08%, suggestive of a synergistic effect of drying temperature and ID on the thermal damage of soybeans. Our results clearly demonstrated that the drying temperature and the diffusion time, i.e., the time required to move the moisture from around the center to the surface, are important factors to maintain the quality of soybeans after drying.

3.4. Effective moisture diffusivity and activation energy

The values of D_{eff} were calculated by the semi-log relations expressed in Eq. (8). Regardless of the drying methods, the semi-log relation was well fit and showed that the D_{eff} values varied in the range of $3.81 \times 10^{-11} \text{ m}^2/\text{s}$ to $6.10 \times 10^{-11} \text{ m}^2/\text{s}$ and $5.68 \times 10^{-11} \text{ m}^2/\text{s}$ to $6.98 \times 10^{-11} \text{ m}^2/\text{s}$ for CD and ID, respectively (Table 3). These values were in the range of most food or bioproducts (Zogzas et al. 1996). The D_{eff} values for CD were significantly higher than those for ID at the same temperature. Hence, the ID was more efficient drying method for soybean than the CD. The activation energy (E_a) of soybean being dried was estimated using the Arrhenius relation

expressed in Eq. (9) (Fig. 5). The E_a values for CD and ID were 21.23 and 9.33 kJ/mol, respectively.

Table 3: The Effective Moisture Diffusivity Estimated During Continuous Drying and Intermittent Drying of Soybean.

Drying method	Temperature (°C)	Effective moisture diffusivity ($10^{-11} \text{ m}^2/\text{s}$)	R^2
Continuous drying	35	3.81	0.9766
	40	4.75	0.9902
	45	6.10	0.9954
Intermittent drying	35	5.68	0.9922
	40	6.31	0.9959
	45	6.98	0.9963

The physical meaning of the E_a is interpreted as the amount of energy required to transfer moisture through the samples being dried. In this study, the activation energy for ID was significantly lower than that for CD, which indicated that the samples being dried with ID required significantly less energy than those dried with CD.

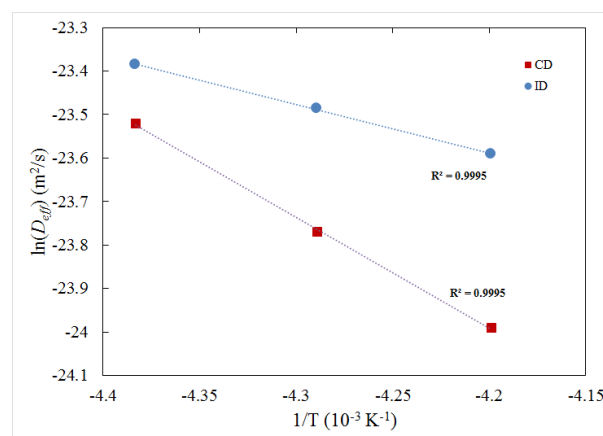


Figure 5: Comparison of the Activation Energy of Samples Dried by Continuous Drying (CD) and Intermittent Drying (ID).

4. CONCLUSION

The continuous drying and intermittent drying were applied to investigate the drying characteristics of soybean with 22.0% (± 0.8) initial moisture content. To describe the drying kinetics of soybean, the Midilli-Kucuk model showed the best fit ($R^2 > 0.99$) among the thin layer models. At 300 min of the effective drying time, the moisture content of continuous drying at 35, 40, and 45°C were 9.38 (± 0.00), 8.69 (± 0.17), and 7.70% (± 0.48), respectively; while the moisture content of intermittent drying at 35, 40, and 45°C were 8.28 (± 0.21), 7.31 (± 0.41), and 6.97% (± 0.07), respectively. The image analysis method for detection of the crack in soybean demonstrated that at the target moisture content of 7.7%, cracked grain ratios with intermittent drying at 35, 40, and 45°C were reduced by 52.08, 27.59, and 18.24%, respectively. Based on the diffusion model, the D_{eff}

values were estimated, and the varied in the range of 3.81×10^{-11} m²/s to 6.10×10^{-11} m²/s and 5.68×10^{-11} m²/s to 6.98×10^{-11} m²/s for CD and ID, respectively. These values were in the range of most food or bioproducts. The activation energy for intermittent drying (9.33 kJ/mol) was significantly lower than that value for continuous drying (21.23kJ/mol), which indicated that the samples being dried with ID required significantly less energy than those dried with CD. The empirical models developed in this study can provide useful information in selecting an optimum condition of intermittent drying to minimize thermal degradation of soybeans.

ACKNOWLEDGMENTS

This work was carried out with the support of “Cooperative Research Program for Agriculture Science & Technology Development (Project Nos. PJ012544022017),” Rural Development Administration, Republic of Korea.

REFERENCES

- Baker C.G.J., 1997. *Industrial Drying of Foods*. London, U.K.: Chapman & Hall.
- Chua K.J., Chou S.K., 2005. A comparative study between intermittent microwave and infrared drying of bioproducts. *International Journal of Food Science & Technology*, 40, 23-39.
- Defendi R.O., Paraíso P.R., Jorge L.M.D.M., 2017. Optimization study of soybean intermittent drying in fixed-bed drying technology. *Drying Technology*, 35(1), 125-137.
- Du C.J., Sun D.W., 2004. Recent developments in the applications of image processing techniques for food quality evaluation. *Trends in Food Science & Technology*, 15, 230-249.
- Doymaz I., 2006. Drying Behavior of Green Beans. *Journal of Food Engineering*, 69, 161-165.
- Guine R.P.F., Fernandes R.M.C., 2006. Analysis of the drying kinetics of chestnuts. *Journal of Food Engineering*, 76, 460-467.
- Hemati M., Mourad M., Steinmetz D., Lagurie C., 1992. Continuous and Intermittent Drying of Maize in a Flotation Fluidized Bed, Fluidization VII. Toulouse Cedex, France: Ensicg Chenmin de la loge, 831-839.
- Henderson S.M., Pabis S., 1961. Grain drying theory. I: Temperature effects on drying coefficients. *Journal of Agricultural Engineering Research*, 6, 169-174.
- Hirunlabh J., Tirawanithakul S., Sophonronarit S., 1992. Strategies for drying soybean: batch process. *Songklanakarin Journal of Science and Technology*, 14, 33-46.
- Johnson P.T., Brennan J.G., Addo-Yobo F.Y., 1998. Air-drying characteristics of plantain (*Musa* AAB). *Journal of Food Engineering*, 37, 233-242.
- Karathanos V.T., Villalobos G., Saravacos G.D., Comparison of two methods of estimation of the effective diffusivity from drying data. *Journal of Food Science*, 55, 218-223.
- Kudra T., Mujumdar A.S., 2002. General discussion: conventional and novel drying concepts. *Advanced Drying Technologies*, 2002, 1-26.
- Kumar C., Karim M.A., Joardder M.U.H., 2014. Intermittent drying of food products: A critical review. *Journal of Food Engineering*, 121, 48-57.
- Kwon S.H., 1972. Origin and importance of protein and oil of Korean soybean. *Korean Journal of Food Science and Technology*, 4, 158-161.
- Lee S.W., Lee J.H., 2009. Effects of oven-drying, roasting, and explosive puffing process on isoflavone distributions in soybeans. *Food Chemistry*, 112, 316-320.
- Lewis W.K., 1921. The rate of drying of solid material. *Journal of Industrial and Engineering*, 13, 427-443.
- Marinos-Kouris D., Maroulis Z.B., 1995. Transfer properties in the drying of solids. In: Mujumdar A.S., ed. *Handbook of Industrial Drying*. New York, NY, USA: Marcel Dekker, 133-155.
- Midilli A., Kucuk H., Yapar Z., 2002. A new model for single layer drying. *Drying Technology*, 20, 1503-1513.
- Moon J.H., Kim M.J., Chung D.H., Pan C., Yoon W.B., 2014. Drying characteristics of sea cucumber (*Stichopus japonicas Selenka*) using far infrared radiation drying and hot air drying. *Journal of Food Processing and Preservation*, 38, 1534-1546.
- Niamnuy C., Nachaisin M., Poomsa-ad N., Devahastin S., 2012. Kinetic modelling of drying and conversion/degradation of isoflavones during infrared drying of soybean. *Food Chemistry*, 133, 946-952.
- Overhults D.G., White G.M., Hamilton H.E., Ross I.J., 1973. Drying soybean with heated air. *Transactions of the American Society of Agricultural Engineers*, 16, 112-113.
- Page G.E., 1949. Factors influencing the maximum rate of air drying shelled corn in thin-layers. MS thesis, Purdue University, West Lafayette, IN, USA.
- Putranto A., Chen X.D., Devahastin S., Xiao Z., Webley P.A., 2011a. Application of the reaction engineering approach (REA) for modelling intermittent drying under time-varying humidity and temperature. *Chemical Engineering Science*, 66, 2149-2156.
- Putranto A., Chen X.D., Xiao Z., Webley P.A., 2011b. Mathematical modeling of intermittent and convective drying of rice and coffee using the reaction engineering approach (REA). *Journal of Food Engineering*, 105, 638-646.
- Rafiee S., 2009. Thin layer drying properties of soybean (*Viliamz* Cultivar). *Journal of Agricultural Science and Technology*, 11, 301-308.
- Sangkram U., Noomhorm A., 2002. The effect of drying and storage of soybean on the quality of bean, oil, and lecithin production. *Drying Technology*, 20, 2014-2054.
- Sophonronarit S., Swasdisevi T., Wetchacama S., Wutiwiwatchai W., 2001. Fluidised bed drying of

- soybeans. *Journal of Stored Products Research*, 37, 133-151.
- Srikiatden J., Roberts J.S., 2006. Measuring moisture diffusivity of potato and carrot (core and cortex) during convective hot air and isothermal drying. *Journal of Food Engineering*, 74, 143-152.
- Wiriyaumpaiwong S., Soponronnarit S., Prachayawarakorn S., 2003. Soybean drying by two dimensional spouted bed. *Drying Technology*, 21, 1735-1757.
- Yilbas B.S., Hussain M.M., Dincer I., 2003. Heat and moisture diffusion in slab products to convective boundary conditions. *Heat and Mass Transfer*, 38, 471-476.
- Zhu Z., Yang Z., Wang F., 2016. Experimental research on intermittent heat pump drying with constant and time-variant intermittency ratio. *Drying Technology*, 34(13), 1630-1640.
- Zogzas N.P., Maroulis Z.B., Marininos-kouris D., 1996. Moisture diffusivity data compilation in foodstuffs. *Drying Technology*, 14, 2225-2253.

AUTHORS BIOGRAPHY

Hyeon Woo Park is a second-year graduate student in Food Science and Biotechnology at Kangwon National University (KNU) in South Korea. He received his Bachelor's Degree in Food Science and Biotechnology from the Kangwon National University in 2015. His research interests include process optimization and new process design, surimi and surimi seafood processing and numerical and CFD simulation.

Dr. Yoon is a professor at Kangwon National University (KNU) since 2008. He has a very unique academic background. He has a B.S. and M.S. in Food Science and Technology, and M.E. in Mechanical Engineering, and a Ph.D. major in Biological Systems Engineering and minor in Chemical Engineering. Before joining KNU, he worked in a processed food industry (associate director in Food R&D Center, CJ CheilJedang, Seoul, S. Korea) and a flavor company (Asia-Pacific regional marketing manager and Seafood specialist, Firmenich-Asia, Singapore). He has been working on food process engineering, food rheology and seafood processing for more than 13 years. His research interest includes gelation characterization of proteins and hydrocolloids, drying and powdering, high viscous fluid mechanics, heat and mass transfer during food processing, least cost formulation development, and computational fluid dynamics. He has so far published more than 80 articles in highly regarded journals in the field of food process engineering. In addition, he has coauthored a chapter of Surimi Paste Preparation, Gel Analysis, and Rheology in the 3rd Edition of Surimi and Surimi Seafood.

DEVELOPING A LINEARIZATION METHOD TO DETERMINE AN OPTIMUM FORMULATION IN SURIMI BLEND WITH VARIED MOISTURE CONTENT USING LINEAR PROGRAMMING

Hyeon Woo Park^(a), Jae W. Park^(b)
Won Byong Yoon^(c)

^{(a),(c)} Department of Food Science and Biotechnology, College of Agricultural and Life Science, Kangwon National University, Chuncheon, Gangwon, 200-701, Republic of Korea

^(b) 2001 Marine Drive, OSU Seafood Research and Education Center, Oregon State University, Astoria, OR 97103, USA

^(a)hwpark0978@gmail.com, ^(b)surimiman1@yahoo.com
^(c)wbyoon@kangwon.ac.kr

ABSTRACT

Novel algorithm to determine the least cost formulation of a surimi blend using linear programming and each surimi properties was developed. Texture properties and the unit cost of surimi blend at the target moisture content were used as constraint functions and the objective function, respectively. The mathematical models to describe the moisture content dependence of the breaking force and the penetration distance were developed using critical moisture content, and the model parameters were used for linearization of moisture content dependence before applying linear programming to determine the optimum formulation. The LCLP model successfully predicted the quality of surimi blend ($p < 0.05$). Sensitivity analysis was used to provide an additional information when the perturbations of design variables are provided. A standard procedure to determine the least cost formulation of surimi blend having varied moisture content was systematically developed.

Keywords: surimi, linear programming, critical moisture content, texture map

1. INTRODUCTION

Surimi, stabilized fish myofibrillar protein, is the major ingredient to produce surimi seafood, such as crab stick, kamaboko, and fish ball. The price of surimi has been unstable because of the limited harvest of valuable species of fish (Guenneugues and Morrisey 2005, Morrisey and Tan 2002, Park 2013) and the increase of oil price. Traditionally, the surimi made from the Alaska pollock has been mainly used to produce the surimi seafood, but the recent development of surimi technology enabled to utilize many other underutilized species from South East Asia and Southern China, such as Threadfin bream (Itoyori) and ribbon fish. It is an essential process for surimi seafood manufacturers to blend various types and grades of surimi lots to develop commercial surimi seafood products, due to the followings: 1) fluctuation of surimi price, 2) unstable supplying of specific species of fish, and 3) maintaining a consistency of quality of surimi seafood.

The myofibrillar protein in surimi is able to form 3 dimensional networks by thermal treatment. The 3 dimensional networks change the rheological properties of surimi paste from liquid-like sol to solid-like gel. The unique texture properties of surimi seafood are mainly from the 3 dimensional networks from myofibrillar proteins and the interaction between protein networks and other ingredients, such as starch, egg white, and soy proteins (Park 2005). Texture properties of surimi seafood are considered as the most important quality characteristics of commercial surimi seafood products. Numerous studies have been conducted to evaluate the texture properties (Park 2005) and to control the texture properties of surimi seafood by formulating the ingredients (Kim et al. 2005, Lanier 1992; Lei-Lei et al. 2014, Yin and Park 2014, Zhang et al. 2015). Punch test is the most widely adopted method to evaluate the texture properties of surimi gels in surimi and surimi seafood industry due to the convenience of the test, although the values obtained from the punch test cannot provide fundamental mechanical properties. Conventionally, the gel strength indicating the texture properties of surimi is defined by a product of the breaking force and penetration distance from the punch test.

Linear programming (LP) is an optimization technique (Eppen et al. 1993, Hiller and Frederick 2012), and has been applied to determine the least cost optimum formula for surimi blending since 1980's (Lanier 1992, Yoon et al. 1997a, Park 2013). The aim of the least cost optimization was to determine the blending ratio of different surimi types to maintain a consistent quality at a least cost. The LP is a simple and useful mathematical tool to determine the optimum formula as long as the functions are expressed in the linear forms (Solow 2014, Ficken 2015, Skau et al. 2014). The simplicity of using LP can be found in that the coefficient of each variable of the linear function is simply determined by measuring the property at 100% of each variable, once the linearity of the function is approved. Yoon et al. (1997a) proposed a systematic procedure to find an optimum formulation for surimi blending using LP. The procedure was widely adopted in the surimi and surimi seafood

industry to find an optimum ratio of surimi blend with different kinds and grades of surimi. However, the method includes limitations of its use: 1) the moisture content of each surimi lot to be blended was assumed to be the same and 2) the moisture content of the blended surimi was assumed to be the same as the each surimi lot used before blending. Such limitations were minor concerns in 1990's, because the moisture content of surimi lots were nearly identical, i.e., 74.5 ~ 75.5%. In addition, the fish species to produce surimi seafood were mainly either Alaska pollock or Pacific whiting. Most of manufacturers which produced surimi with Alaska Pollock or Pacific whiting Surimi well controlled the moisture content of final product and the deviation of moisture content was very little. However, these days many different kinds of fishes are available to produce surimi and also the moisture contents in the surimi are widely varied from 74.5% to 78.0% upon their grades. The LP methods proposed by Yoon et al. (1997a) have caused significant errors to find the least cost formulation using different surimi lots, especially produced in the South East Asia and China, due to the various moisture contents in the surimi. Especially the non-linear characteristics of moisture dependence of texture properties caused a great limitation of using LP to determine the optimum formulation for the final products which might include varied moisture contents.

Regardless of the importance, very few studies on the optimization techniques for surimi seafood were reported and mainly published in late 1990's (Kim et al. 2005, Yoon et al. 1997a, Yoon et al. 1997b, Hsu 1995). Besides Yoon et al. (1997a), most studies focused on describing the non-linear properties due to the interaction between surimi and other ingredients using response surface methodology and mixture design. The non-linear programming approaches provide detailed information to understand the interaction of each ingredient, but they require whole new set of experiments when a new ingredient is introduced to the ingredient system. Due to such complexity, the surimi seafood industry is reluctant to use the non-linear programming method for surimi blending.

In this study, to eliminate the great obstacle for using LP in the surimi and surimi seafood industry, a linearization method was mathematically developed. The objective of this study was to develop a new algorithm and a systematic procedure to use the LP to find a least cost formulation by blending surimi lots with various moisture contents.

2. MATERIALS AND METHODS

2.1. Surimi gel preparation

A high grade (A) and two medium grades (KA1 and KA2) of Threadfin bream (Itoyori) surimi were kindly provided by Pulmuone (Seoul, Korea). The high grade surimi (A) and two medium grades of surimi (KA1 and KA2) were produced from Thailand and Vietnam, respectively. Those surimi contained 4% sugar, 4% sorbitol, and 0.3% sodium tripolyphosphates as

cryoprotectants. Two blocks (10 kg each) of surimi were cut into small pieces (~ 1 kg each) and vacuum packed. Each surimi sample was stored at -18°C. The initial moisture content of each surimi lot was measured according to the AOAC method (1990). A constant level of salt (2%) was applied to the all treatments. The moisture contents of surimi gel were adjusted from 74.5% to 82% to evaluate their texture properties at various moisture contents. The amount of water added to adjust the moisture content in the surimi gel was calculated by solving the material balance (Eq. (1) and (2)):

$$SG = S + W + ST \quad (1)$$

$$MSG = MS + MW + MST \quad (2)$$

where SG is the mass % of the surimi gel, i.e. 100%, S, W, and ST are the mass % of surimi, water, and salt, respectively, and MSG, MS, MW, and MST are the mass % of moisture content of surimi gel, surimi, water and salt, respectively. In order to solve the material balance equation (1) and (2), it is necessary to determine the moisture content of each surimi lot and to decide the target moisture content of surimi gel.

The cost of surimi at target moisture content was calculated according to the material balance (Eq (3)):

$$UCS_{tms} = UCS_{ims} \times (SS_{tms}/SS_{ims}) \quad (3)$$

where UCS is a unit cost of surimi, SS is % of solid content of surimi, subscript tms and ims indicate a target moisture content and an initial moisture content, respectively.

For this study, the unit cost of water and salt were assumed to be zero for simplification. By solving equation (1), (2), and (3), it is possible to calculate the approximate cost of surimi gel at the target moisture content of surimi blend. This provides critical information to apply the LP to find the least cost formulation, because the objective function of the LP must include the cost of surimi blend at the target moisture content. This is one of the major differences from the LP method introduced in Yoon et al. (1997a). Previous approach used a constant moisture content which had to be the moisture content of each surimi lot. Practically the moisture content of surimi gels, i.e. the final product of surimi seafood, could be varied from 75% to 80%. In addition, the moisture content of each surimi lot could be varied as well. The LP must consider the target moisture content of final product and must adjust the cost of each surimi lot based on the target moisture. Consequently, the texture properties of each surimi lot has to be adjusted based on those at the target moisture content. The surimi gel was prepared according to Yoon et al. (1997a). The cooked gels were refrigerated for 12 hrs before the analysis of texture properties.

2.2. Measuring texture properties

To measure texture properties, cooled gels were held at room temperature for 2 hrs. Ten gels were cut into the

cylindrical shape (length = 3 cm, diameter = 1.9 cm), and tested for the breaking force and the penetration distance by punch test (diameter of the probe = 0.5 cm, probe speed = 30 cm/min) using a rheometer (Fudoh, model NOm-3002D rheometer, Tokyo, Japan), according to Hsu (1995).

2.3. Modeling

It has been reported that the failure shear strain or any texture properties related to the deformation ability of surimi gels showed a nonlinear function upon the moisture content, while the failure shear stress or texture properties related to the hardness of surimi gels showed a linear function upon the moisture content (Park 2013, Yoon et al. 1997a). In this study, the critical moisture content (CMC) was empirically defined as the moisture content where the slope of penetration distance function dramatically changed. Based on the observation from Yoon et al. (1997a), the function of the failure shear strain of surimi gels on the moisture contents showed two linear segments upon the moisture content. Empirical equations (Eq. (4), (5a) and (5b)) were developed to describe the moisture content dependence of the breaking force and the penetration distance of each surimi lot, respectively:

$$\text{Breaking force} = F_i \times MC + F_i^0 \quad (4)$$

$$\text{Penetration distance} = D1_i \times MC + D1_i^0, \text{ at } MC \leq CMC \quad (5a)$$

$$\text{Penetration distance} = D2_i \times MC + D2_i^0, \text{ at } MC > CMC \quad (5b)$$

where F_i and F_i^0 are the slope and the intercept of breaking force function of i_{th} surimi lot, respectively; $D1_i$ and $D1_i^0$ are the slope and the intercept of penetration distance of i_{th} surimi lot when the moisture content is lower than CMC, respectively; $D2_i$ and $D2_i^0$ are the slope and the intercept of penetration distance of i_{th} surimi lot when the moisture content is higher than CMC, respectively. If a surimi lot did not show a CMC, the moisture content dependence can be described by eq. (5a). Each empirical model was developed by conducting the linear regression analysis from experimental data averaged from 10 measurements.

2.4. Optimization

Once the breaking force and the penetration distance of each surimi lot at the target moisture content were determined from eq. (4) and equation (5a and 5b) respectively, the breaking force and the penetration distance of a surimi blend at the target moisture content can be expressed as linear canonical models (Yoon et al. 1997a):

$$\text{Breaking force of surimi blend} = \alpha_1 X_1 + \alpha_2 X_2 + \dots + \alpha_n X_n \quad (6)$$

$$\text{Penetration distance of surimi blend} = \beta_1 X_1 + \beta_2 X_2 + \dots + \beta_n X_n \quad (7)$$

where X_n is the ratio of i_{th} of surimi lot adjusted to the target moisture content, α_n is the breaking force of i_{th} surimi lot at the target moisture content which were calculated from equation (4), β_n is the penetration distance of i_{th} surimi lot at the target moisture content which were calculated from equation (5a) and (5b). The equation (6) and (7) can be incorporated into the LP model as constraint functions.

The objective function which represents the cost of surimi blend is expressed by a linear canonical function (Eq. (8)) and the coefficient of each term indicating the unit cost of surimi lot at the target moisture content.

$$\text{Cost of surimi blend} = C_1 X_1 + C_2 X_2 + \dots + C_n X_n \quad (8)$$

where C_n = the unit cost of i_{th} surimi lot at the target moisture content which were determined from equation (3).

The least cost linear programming (LCLP) model for surimi blending includes an objective function (Eq. (8)), decision variables (X_i , the ratio of each surimi lot), and constraint functions (Eq. (6) and (7)). The objective function of LCLP was set to be minimized, while the constraint functions and X_i are greater than constraint values and 0, respectively. In this study, the constraint values of the breaking force and the penetration distance were set at 250 g and 0.5, respectively, according to the target value of commercial surimi seafood product at 78% of target moisture content. The algorithm of the optimization procedure developed in this study was shown in Fig. 1. The optimization procedure of the LCLP for surimi blending was executed using both MS-Excel 2013.

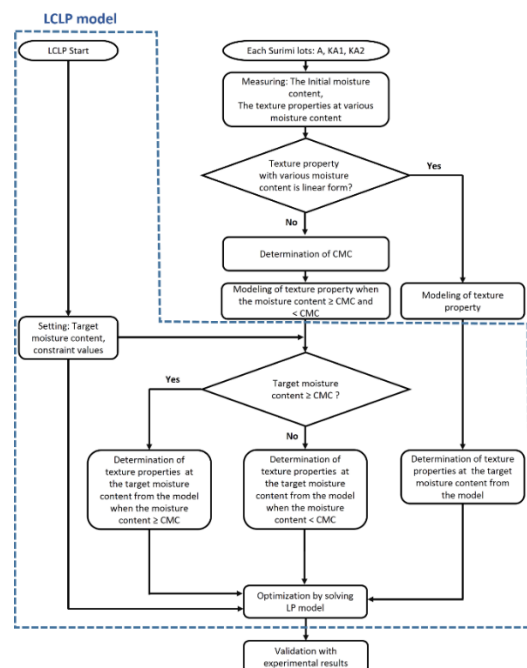


Figure 1: Algorithm of the Optimization Procedure for Surimi Blending Using Least Cost Linear Programming (LCLP).

Experimental values of the breaking force and the penetration distance of a surimi blend formulated based on the LCLP solution were compared with those values predicted from LCLP simulation for validation. In addition, the solutions from two different methods, such as the conventional algorithm and the novel linearization algorithm were compared.

2.5. Sensitivity analysis

Sensitivity analysis is commonly used to compute the sensitivity of performance measures with respect to design variables (Borgonovo and Plischke 2016, Deif, 2014, Sidhu et al. 2014). Sensitivity analysis was conducted according to Saltelli et al. (2008):

$$V = f(X, Y) \quad (9)$$

V is the measure of the value of the decision that is made, X is the variable which are subject to control by X_i , Y is the constraints, which affect the performance but which are not subject to control by X_i within the scope of the problem as defined, and f is the functional relationship between X_i and performance factors, and the dependent variable V . A detailed description of the methods applied to analyze the sensitivity result can be found in Saltelli et al. (2008).

2.6. Statistical analysis

All experiments were triplicated and the ANOVA in MS-Excel-2013 was used for the analysis at the statistical significance of $p < 0.05$.

3. RESULTS AND DISCUSSION

3.1. Effect of moisture on the breaking force of surimi gel

The addition of water to surimi seafood is necessary to maintain acceptable texture and to minimize cost of raw materials. Generally, in surimi seafood industry, the first step to evaluate the quality of surimi lots are 1) to measure the moisture content of surimi lots and 2) to measure the texture properties at various moisture contents. The moisture contents of grade A, KA1, and KA2 used in this study were determined to be 75.0 (± 0.1), 77.1 (± 0.4), and 76.6% (± 0.5), respectively. Changes of breaking force of each surimi lot at varied moisture content (74.4 to 82%) were shown in Fig. 2. The lowest moisture content applied to KA1 and KA2 were 77 and 76%, respectively, since the initial moisture content of KA1 and KA2 were 77.1 and 76.6%, respectively. The highest moisture content applied to KA2 was 81.1%, because gels were not formed when the moisture content was higher than 81.1%. The breaking force of A, KA1, and KA2 linearly decreased from ~503.1 to ~78.9 g ($r^2=0.99$), from ~225.7 to ~59.9 g ($r^2=0.99$), and from ~86.5 to ~33.85 g ($r^2=0.95$), respectively, as moisture content increased. The breaking force or texture properties related to the hardness, such as failure shear stress and failure compressive force,

indicate the quantity of protein networks in the gel. As moisture content increased, the concentration of protein in the gel decreased, so that the probability to form 3 dimensional networks from the myofibrillar protein decreased. Such moisture content dependence of surimi gel can be explained based on the classic rubber elastic theory (Treloar 1975, Yoon et al. 2004a, Yoon et al. 2004b).

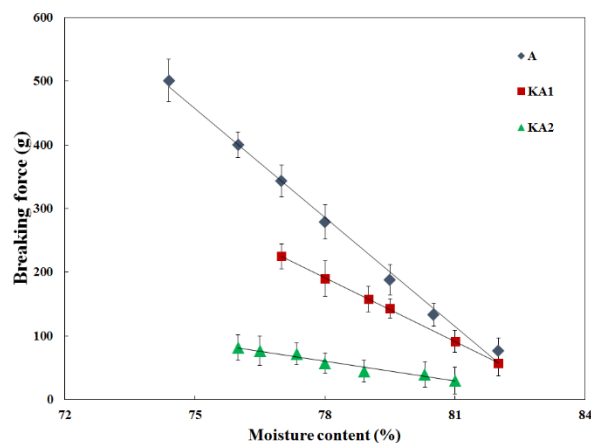


Figure 2: Effect of Moisture Content on the Breaking Force of Threadfin Bream Surimi Gels. Markers Indicate the Experimental Data and the Lines Were Drawn Based on the Values Calculated from the Model Equations Developed by Equation (4).

It is worth to mention that the breaking force values of KA2 were lower than those of KA1 even though the initial moisture content of KA2 was lower than that of KA1. It might be because KA2 included more solid contents, such as sorbitol and sugar, than KA1. It implies that the quality of surimi should be evaluated by measuring not only the moisture content but also the texture properties at varied moisture content. Linear models to describe the moisture content dependence of the breaking force of each surimi lot were developed by linear regression analysis. The coefficients, intercept, and R^2 values of each model were summarized in Table 1, and the lines shown in Fig. 2 were drawn based on the data calculated from model equations. Measuring texture properties at various moisture content is one of the most important procedures to inspect the quality of surimi lots, and the texture behavior and the models might provide useful insights to develop final product formula with surimi lots for the manufacturers.

3.2. Effect of moisture on penetration distance of surimi gel

Penetration distance or texture properties related to the deformation, such as failure shear strain or failure strain, of surimi gels commonly refers to as an indicator of protein quality (Park 2005). In general, such deformation ability was not affected within a certain range of moisture content (Park 2005, Yoon et al. 1997). Changes of penetration distance at varied moisture content were shown in Fig. 3.

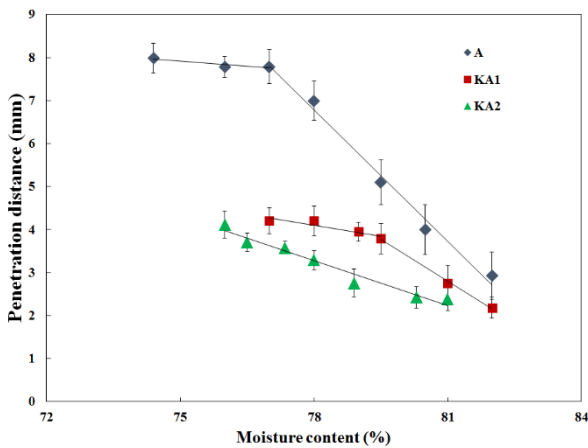


Figure 3: Effect of Moisture Content on the Penetration Distance of Threadfin Bream Surimi Gels. Markers Indicate the Experimental Data and the Lines Were Drawn Based on the Values Calculated from the Model Equations Developed by Equation (5a) and (5b).

As shown in Fig. 3, it is very clear that there were specific moisture contents at which the penetration distance was not affected by increasing moisture content. In this study, the moisture content where the penetration distance begins to decrease as increase of moisture content was defined as the critical moisture content (CMC) of each surimi lot. In this study, the purpose of determining CMC

was to develop empirical models to describe changes of penetration distance on the moisture contents. The penetration distance of A was not affected until the moisture content was 77%, but at 78% of moisture content the breaking force began to decrease dramatically as increase of moisture content. For KA1, the maximum values were maintained up to 79% and, at 79.5% of moisture content, the values dropped as the moisture content increased. However, the KA2 did not show the CMC in the given range of moisture content. To describe the moisture content dependence of penetration distance, eqn. 5a and 5b were applied with CMC of each surimi lot. The unit cost, the initial moisture content, the CMC, the coefficient, and the intercept used in the LCLP model were summarized in Table 1. The lines shown in Fig. 3 were drawn based on the data calculated from eqn. 5a and 5b, and showed good fittings of experimental results. This modeling approach could be the first time ever challenged before. The empirical equations to predict the penetration distance value will greatly contribute to develop surimi seafood products, because the deformation ability is a unique texture property reflecting the protein quality and could not be improved by adding other ingredients, such as wheat flour, unlike the breaking force or texture properties related to the hardness.

Table 1: The Properties of Each Surimi Lot, such as the Unit Cost, Breaking Force, the Penetration Distance, IMC and CMC Used in the LCLP Model.

	A			KA1			KA2		
Unit cost (\$/kg)	2.80			1.30			1.35		
IMC (%)	75.0			77.1			76.6		
CMC (%)	77			79			N.D.		
	Coef.	Int.	R ²	Coef.	Int.	R ²	Coef.	Int.	R ²
B.F. (g)	-55.97	4656.2	0.99	-33.18	2780.9	0.99	-10.52	885.7	0.96
P.D. (mm) (MC ≤ CMC)	-0.24	26.1	0.70	-0.15	15.6	0.82	-0.35	30.5	0.95
P.D. (mm) (MC > CMC)	-1.01	85.9	0.98	-0.63	54.0	0.99	N.D.	N.D.	N.D.

(IMC = initial moisture content, CMC = critical moisture content, MC = moisture content, Coef. = coefficient, Int. = intercept, B.F. = breaking force, P.D. = penetration distance, N.D. = not detected)

3.3. Optimization using LCLP model

The constraint functions and objective function to be incorporated in the LCLP model were developed according to equation (3), (4), (5a) and (5b) (Table 2).

The coefficient of each function indicated the properties, such as the breaking force, the penetration distance, and the cost of surimi gel, at the target moisture content set at 78% for this study.

Table 2: Summary of the Least Cost Linear Programming (LCLP) Model.

LCLP Model					
Surimi type		A	KA1	KA2	
Objective function	Unit price (\$/kg) (adjusted at target moisture content)	2.46	1.25	1.27	Minimizing Σ unit cost
	Constraint function				
	B.F. (g)	290.5	192.9	65.1	≥ 250.0
	P.D. (mm)	7.1	3.9	3.2	≥ 5.0

(B.F. = breaking force, P.D. = penetration distance)

The coefficients of each term used in the constraint function for the breaking force and the penetration distance were calculated from the model equations to describe the changes of breaking force and penetration distance at varied moisture contents (Table 1). Solving the LP model is basically finding a solution of a system of simultaneous of inequality equations (Eppen et al 1993, Hiller and Frederick 2010). In this study, the system of simultaneous inequality equations incorporated in the LCLP model summarized in Table 2 was:

Objective function:

$$\text{Cost of surimi blend} = 2.24 \times (\% \text{ of A}) + 1.13 \times (\% \text{ of KA1}) + 1.15 \times (\% \text{ of KA2}) \quad (10a)$$

Constraint functions:

$$\text{Breaking force} = 290.5 \times (\% \text{ of A}) + 192.9 \times (\% \text{ of KA1}) + 65.1 \times (\% \text{ of KA2}) \geq 250 \quad (10b)$$

$$\text{Penetration distance} = 7.1 \times (\% \text{ of A}) + 3.9 \times (\% \text{ of KA1}) + 3.2 \times (\% \text{ of KA2}) \geq 5 \quad (10c)$$

Nonreactivity constraint:

$$X_A, X_{KA1}, X_{KA2} \geq 0 \quad (10d)$$

where X_i = the ratio of each surimi lot adjusted to the target moisture content.

After solving the system of equation (10a), (10b), (10c) and (10d), the results of simulation of the LCLP model (Table 3) indicated that, when 58.5% of A and 41.5% of KA1 are mixed together, the surimi blend will have the least cost (\$1.96/kg) with 250 g of the breaking force and 5.78 mm of the penetration distance. Because the coefficients of each term in the objective function and the constraint functions were adjusted at the target moisture content, the solution of LCLP model can have more feasibility to be applied in the surimi seafood industry. The long time limit of use of LP model, since proposed by Yoon and et al. (1997a), was overcome and now the LCLP can be practically used in the surimi seafood industry.

Table 3: The Results of LCLP Simulation.

Optimum solution				
Results of simulation	Unit price (\$/kg)	1.96		
	B.F. (g)	250.0		
	P.D. (mm)	5.78		
	Ratio of surimi (%)	Surimi type	A	KA1
			58.5	41.5
				0

(B.F. = breaking force, P.D. = penetration distance)

Conventional simulation, which is a linearization method without CMC, was also conducted to compare with the result of simulation of the LCLP model. The results of conventional simulation indicated the surimi blend will have the least cost (\$1.96/kg) with 250g of the breaking force and 5.40 mm of the penetration distance. The breaking force and the penetration distance values of the

surimi blend formulated according to the simulation result (A = 58.5%, KA1=41.5%, moisture content 78%) were compared with those of simulation results (Fig. 4a & b). The experimental values of breaking force and the penetration distance were 241.8 g (± 9.05) and 6.18 mm (± 0.77), respectively. There were no significant differences between the experimental values and the

results of simulation of the LCLP model ($p < 0.05$), in contrast to the results of conventional simulation.

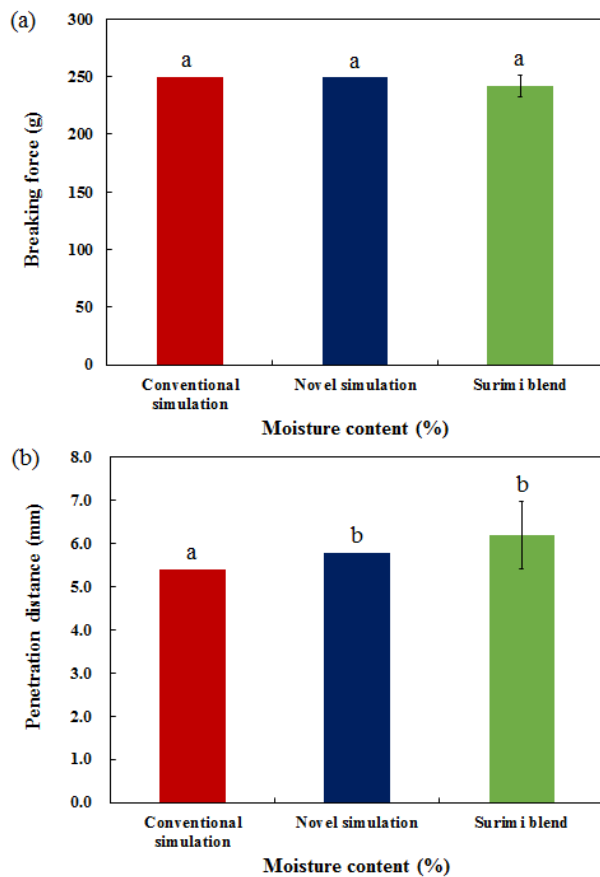


Figure 4: Comparison of the Breaking Force (5a) and the Penetration Distance (5b) Values between Simulation Result and Experimental Results of Surimi Blend. The Surimi Gel Was Blended Based on the Ratio Calculated by the LCLP.

Since the failure shear strain or any texture properties related to the deformation ability of surimi gels showed a nonlinear function upon the moisture content (Park and Yoon 2015, Park 2013, Yoon et al. 1997a), linear programming for surimi gels could not be used with various moisture contents. Novel algorithm was successfully applied to linearize the function of the penetration distance of surimi gels on the moisture contents.

3.4. Sensitivity analysis

Sensitivity analysis based on the simulation results using the LCLP model was conducted to evaluate the optimum solutions (Table 4). Critical price indicated the maximum price of each surimi type to be included in the surimi blend. Surimi lots, such as A and KA1, maintain the ratio of surimi blend within the allowable range of each surimi. In order to include KA2 in surimi blend, the price of KA2 should be lower than \$0.93. To estimate the cost variation of surimi blend depending on the constraints, the sensitivity of constraints was also analyzed as shown in Table 4. As the constraint of breaking force decreases by 1g, the price of surimi blend can decrease by \$0.012 within 226.2 to 290.5 g of breaking force, whereas the price of surimi blend do not depend on the constraint of penetration distance when it is lower than 5.78mm. The information from the sensitivity analysis provides a quantitative estimate for desirable design changes, although a systematic experimental design is not carried out. Based on the sensitivity results, the formula developer can decide the amount of variable changed to improve the performance. In addition, sensitivity information can provide answers to “what if” questions by predicting performance measure perturbations when the perturbations of design variables are provided (Choi and Kim 2006).

Table 4: The Sensitivity Analysis of LCLP Simulation.

Sensitivity analysis			
Surimi type	A	KA1	KA2
Optimized ratio of surimi (%)	58.5	41.5	0
Critical price (\$/kg)	-	-	0.93
Allowable range (\$/kg)	> 1.88	< 1.64	< 0.93
Constraint	B.F. (g)	P.D. (mm)	
Optimized value	250.0	5.78	
Cost variation per unit (\$/g or mm)	0.012	0	
Allowable range (\$/g or mm)	226.2-290.5	< 5.78	

(Critical price = Maximum price of each surimi type to be included in surimi blend)

3.5. Texture map from breaking force and penetration distance

The texture map of surimi gel was first time developed and published by Park (2002), based on the failure shear

stress and failure shear strain values of surimi gels, and widely used for surimi industry and surimi seafood industry to control the quality of surimi lots as well as to develop a new product by blending of surimi lots and

adding ingredients. Fig. 5A was drawn from experimental values used in this study. The size of bubble indicates the unit cost of each surimi gel at various moisture content and optimized surimi blend. The box located at the upper left side referred to the cost of surimi gel in the bubble. As shown in Fig. 5, as the moisture content increased, each surimi gel moved to the south-west direction on the texture map and the bubble size became smaller.

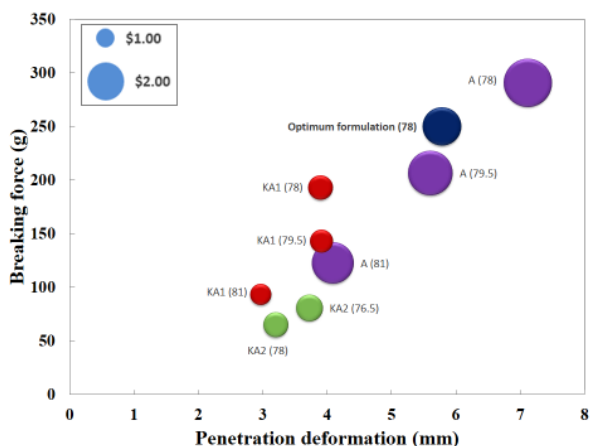


Figure 5: Texture Map Created from the Unit Cost, the Breaking Force and the Penetration Distance. The Location of the Bubbles Indicates the Texture Property of Surimi Gels with Various Moisture Content Described in the Parenthesis. The Size of Bubbles Indicates the Unit Cost of Each Surimi Gel.

The texture map developed in this study is distinguished from that created by Park (2002) in terms of followings: 1) using breaking force and penetration distance instead of failure shear stress and failure shear strain for practical use for surimi and surimi seafood industry, and 2) using a bubble chart which can be created in the commercial spread sheet software to compare the change of cost as well as the texture properties of surimi blend simultaneously. The texture map incorporated with the LCLP developed in this study might provide full of information of using surimi lots at various moisture content to control the texture properties as well as the cost of surimi gels.

4. CONCLUSION

Optimization technique using LCLP model was successfully applied to determine the least cost blending of surimi types. The limit of practical use of LP for surimi blending had existed because the unit cost and texture properties of surimi blend at various moisture contents were unsure to be incorporated into the LP model due to the non-linearity of deformation related property, such as the penetration distance. Empirical models developed in this study showed a good fitness of the changes of texture properties of surimi lot at various moisture content, and these models enabled to use the optimization technique to determine the optimum ratio of surimi blend as well as to predict the texture properties of surimi blend at the

lowest cost. Sensitivity analysis was used to provide an additional information when the perturbations of design variables are provided. The systematic procedure to use LCLP model and the texture map introduced in this study will be very practical tools for surimi seafood industry to maintain the consistency of product quality in fluctuation of surimi price and unstable supplying of specific species of fish at the least cost and to make a decision for surimi purchasing.

ACKNOWLEDGMENTS

This study has been worked with the support of a research grant of Kangwon National University in 2016.

REFERENCES

- AOAC, 1990. Official methods of analysis, 15th ed. Association of Official Analytical Chemists, Washington, D.C., USA.
- Borgonovo E., Elmar P., 2016. Sensitivity analysis: a review of recent advances. *European Journal of Operation Research*, 283(3), 869-887.
- Choi K.K., Kim N.H., 2006. Structural sensitivity analysis and optimization 1: linear systems. New York, NY, USA: Springer Science & Business Media.
- Deif A., 2012. Sensitivity analysis in linear systems. Berlin, Germany: Springer Science & Business Media.
- Eppen G., Gould F., Schmit C., 1993. Management science. Decision modeling with spreadsheets. Upper Saddle River, NJ, USA: Prentice Hall.
- Ficken F., 2015. The simplex method of linear programming. Mineola, NY, USA: Dover Publications.
- Guenneugues P., Morrissey M., 2005. Surimi resources. In: Park J., ed. Surimi and surimi seafood (2nd ed.). New York, NY, USA: CRC Press, 491-582.
- Lanier T., 1992. Measurement of surimi composition and functional properties. In: Lee C., Lee C., eds. Surimi technology. New York, NY, USA: Marcel Dekker Inc., 154-161.
- Lei-Lei Y., Chen-Xi W., Ru L., Juan Y., Yang H., Shan-Bai X., 2014. Effects of types and concentration of cations on surimi gels texture properties. *Journal of Food Safety and Food Quality*, 5(8), 2319-2326.
- Morrissey M., Tan S., 2002. World resources for surimi. In: Park J., ed. Surimi and surimi seafood (1st ed.). New York, NY, USA: CRC Press, 1-21.
- Park J. 2002. Surimi and surimi seafood (1st ed.). New York, NY, USA: CRC Press, 649-707.
- Park H.W., Yoon W.B., 2015. Measuring ring tensile stress and strain of surimi gels using a novel ring tensile test with image analysis. *Journal of Food Engineering*, 163, 9-16.
- Park J., 2005. Ingredient technology for surimi and surimi seafood. In: Park J., ed. Surimi and surimi seafood (2nd ed.). New York, NY, USA: CRC Press, 649-707.
- Park J., 2013. Surimi and surimi seafood (3rd ed.). Boca Raton, FL, USA: CRC Press.

- Saltelli A., Ratto M., Andres T., Campolongo F., Cariboni J., Gatelli D., Tarantola S., 2008. *Global sensitivity analysis: the primer*. Hoboken, NJ, USA: John Wiley & Sons.
- Skau J., Bunthang T., Chamnan C., Wieringa F., Dijkhuizen M., Roos N., Ferguson E., 2014. The use of linear programming to determine whether a formulated complementary food product can ensure adequate nutrients for 6- to 11-month-old Cambodian infants. *The American Journal of Clinical Nutrition*, 99(1), 130-138.
- Solow D., 2014. *Linear programming: an introduction to finite improvement algorithms (2nd ed.)*. Mineola, NY, USA: Dover Publications.
- Sidhu S., Kumar A., Appadoo S., 2014. Mehar methods for fuzzy optimal solution and sensitivity analysis of fuzzy linear programming with symmetric trapezoidal fuzzy numbers. *Mathematical Problems in Engineering* 2014(2014).
- Treloar L., 1975. *The physics of rubber elasticity*. Oxford, UK: Clarendon Press.
- Yin T., Park J., 2014. Effects of nano-scald fish bone on the gelation properties of Alaska Pollock surimi. *Food Chemistry*, 150, 463-468.
- Yoon W.B., Gunasekaran S., Park J., 2004a. Characterization of thermorheological behavior of Alaska Pollock and Pacific whiting surimi. *Journal of Food Science*, 69(7), 338-343.
- Yoon W.B., Gunasekaran S., Park J., 2004b. Evaluating viscosity of surimi paste at different moisture contents. *Applied Rheology*, 14(3), 133-139.
- Yoon W.B., Park J., Kim B., 1997a. Linear programming in blending various components of surimi seafood. *Journal of Food Science*, 62(3), 561-564.
- Yoon W.B., Park J., Kim B., 1997b. Surimi-starch interaction based on mixture design and regression models. *Journal of Food Science*, 62(3), 555-560.
- Zhang L., Zhang F., Wang X., 2015. Effects of hydrolyzed wheat gluten on the properties of high-temperature (≥ 100 °C) treated surimi gels. *Food Hydrocolloids*, 45, 196-202.

AUTHORS BIOGRAPHY

Hyeon Woo Park is a second-year graduate student in Food Science and Biotechnology at Kangwon National University (KNU) in South Korea. He received his Bachelor's Degree in Food Science and Biotechnology from the Kangwon National University in 2015. His research interests include process optimization and new process design, surimi and surimi seafood processing and numerical and CFD simulation.

Dr. Park is a professor of Oregon State University since 1992. He was elected as IFT Fellow in 2007, which is the most prestigious recognition as a food scientist. He published 136 referred journal articles, 41 book chapters, and 3 patents. He offered over 100 invited speeches. Having devoted his entire professional career to fish protein (surimi) research and outstanding outreach in

technology transfer, Dr. Jae Park has distinguished himself as an internationally renowned scientist in surimi research, education, and technology transfer. He received numerous awards to recognize his accomplishment regionally, nationally and internationally. He was recognized by IntraFish as 100 most powerful seafood executives in 2012. His most recent recognition was the 2016 IFT Bor S Luh International Award in Chicago in July, 2016.

Dr. Yoon is a professor at Kangwon National University (KNU) since 2008. He has a very unique academic background. He has a B.S. and M.S. in Food Science and Technology, and M.E. in Mechanical Engineering, and a Ph.D. major in Biological Systems Engineering and minor in Chemical Engineering. Before joining KNU, he worked in a processed food industry (associate director in Food R&D Center, CJ CheilJedang, Seoul, S. Korea) and a flavor company (Asia-Pacific regional marketing manager and Seafood specialist, Firmenich-Asia, Singapore). He has been working on food process engineering, food rheology and seafood processing for more than 13 years. His research interest includes gelation characterization of proteins and hydrocolloids, drying and powdering, high viscous fluid mechanics, heat and mass transfer during food processing, least cost formulation development, and computational fluid dynamics. He has so far published more than 80 articles in highly regarded journals in the field of food process engineering. In addition, he has coauthored a chapter of *Surimi Paste Preparation, Gel Analysis, and Rheology* in the 3rd Edition of *Surimi and Surimi Seafood*.

ACCURATE PREDICTION OF HEAT PENETRATION OF A SURIMI PASTE WITH VARIOUS SALT AND MOISTURE CONTENTS USING NUMERICAL SIMULATION WITH TEMPERATURE DEPENDENT THERMAL PROPERTY FUNCTIONS

Hyeon Woo Park^(a), Myeong-Gi Lee^(b), Jae W. Park^(c)
Won Byong Yoon^(d)

^{(a),(b),(d)} Department of Food Science and Biotechnology, College of Agricultural and Life Science, Kangwon National University, Chuncheon, Gangwon, 200-701, Republic of Korea

^(c) 2001 Marine Drive, OSU Seafood Research and Education Center, Oregon State University, Astoria, OR 97103, USA

^(a)hwpark0978@gmail.com, ^(b)mglee530@gmail.com, ^(c)surimiman1@yahoo.com

^(d)wbyoon@kangwon.ac.kr

ABSTRACT

Alaska pollock surimi paste was prepared (0-3% salt and 76-84% moisture). The density, specific heat, and thermal conductivity have been measured and modelled in the temperature range 20-90°C. The density of AP surimi paste were represented by a multiple linear regression with respect to temperature, moisture and salt content with suitable R² value (0.92). The temperature and moisture and salt content dependence of a specific heat and thermal conductivity of surimi paste was well fitted with a multiple linear regression model with R² value of 0.97 and .087 respectively. The heat penetration curves measured during heating (25 to 90 °C) were compared with the transient temperature profile obtained from simulation models coupled with empirical thermal properties having suitable RMSE (0.43 to 1.22 °C). This study demonstrated that an accurate prediction of the heat transfer of the surimi paste needs to be coupled with the nonlinear thermal property functions.

Keywords: Alaska Pollock, surimi, thermal property, numerical simulation

1. INTRODUCTION

Frozen surimi is a major ingredient to produce surimi seafood products (AbuDagga and Kolbe 1997, Park 2013). The frozen surimi block needs to be thawed, cut, and chopped with salt and water to prepare the surimi paste which may deform to various shapes of surimi seafood products (Fukushima et al. 2007, AbuDagga and Kolbe 2000). Surimi seafood products are conventionally made from heat set gels at high temperatures of approximately 90 °C (Tabilo-Munizaga and Barbosa-Cánovas, 2004). Accurate prediction of the heat transfer profile during processing is necessary to ensure the processing efficiency and the quality of products.

During the last three decades, computer simulation is becoming a powerful tool to interpret complex transport phenomena involved in many unit operations in food processing because of the fast development in the computational technologies as well as in the efficient

numerical algorithms (Pitchai et al. 2014). Particularly, in recent years, many studies demonstrated that the numerical simulation (NS) were practically used in food processing operations, such as thermal processing, drying operation, and freezing (Scott and Richardson, 1997; Anandharamakrishnan 2003 and Norton and Sun 2006). Among many benefits of NS or CFD, the accurate estimation of the transient temperature profiles during thermal treatment would give a great benefit for food processing related to thermal processing. The estimation of transient temperature profile can be used to determine the cold point of food products thermally treated, and consequently the degree of sterilization is appropriately estimated. Including appropriate thermal properties in the heat transfer model is strongly required to obtain suitable transient temperature profiles from the NS (Scott and Richardson 1997, Anandharamakrishnan 2003). Although many advantages of using NS in food industry are found, there is no study related to the application of NS to understand the thermal processing involved in the surimi seafood which requires varied salt and moisture contents for commercial purposes. The NS for surimi paste needs a complicated heat transfer model because the thermal properties of surimi paste at different salt and moisture content could be significantly varied during heating process due to the interaction between compositions and the gelation of myofibrillar protein. Because the thermal processing is the most important process to control the quality of surimi seafood, developing an accurate simulation models for surimi seafood processing may provide many advantages for the process engineers as well as the product developers. In addition, since the thermal process is one of the most costly aspects due to its high energy requirement, the accurately predicted thermal processing conditions will contribute to reduce the processing cost. Thus, it is worth to develop a suitable heat transfer models for surimi seafood with varied compositions such as salt and moisture. However, in order to develop an accurate and suitable model for the thermal process of surimi products, a thorough knowledge of the influence of the

individual component on thermal properties is essentially required. Especially, since the surimi paste inevitably contains salt and water, the thermal properties of surimi paste needs to be determined at various contents of salt and water in the paste. Therefore, the NS application should be accompanied with developing a semi- or empirical model to predict the temperature-dependent thermophysical properties, such as thermal conductivity k , specific heat C_p , and density ρ , of surimi paste at different salt and water levels in the wide range of temperature applied in the thermal processing of surimi seafood (AbuDagga and Kolbe 1997). Thermophysical properties of food are important parameters to determine appropriate operating conditions for various thermal processes including heating, cooking, freezing and cooling systems (Karunakar et al. 1998, Marcotte et al. 2008). In addition, the thermal properties are highly correlated to the degree of pasteurization or sterilization determining the shelf life of final products. Thus, it has been strongly emphasized to measure accurate thermal properties to ensure food safety (Unklesbay et al. 1999). We found no published reports on heat transfer properties of Alaska pollock surimi paste with considering the temperature dependence of thermal properties at various salt and moisture content, despite Alaska pollock still represents the largest fishery biomass used for surimi production (Guenneugues and Morrissey 2004). So far, the only published data on the thermal properties of surimi is limited to pacific whiting surimi of which production amount is only about 10% of Alaska Pollock surimi (AbuDagga and Kolbe 1997, Park 2013). Additionally, only one study on developing the heat transfer simulation model for AP surimi paste was recently reported by Lee and Yoon (2016), however the simulation model developed by Lee and Yoon (2016) was accompanied with constant thermal properties evaluated at a mean temperature during thermal processing. To develop an accurate heat transfer simulation model, thermal properties should be provided according to the temperature distribution of surimi during heating, and also those thermal properties must be evaluated at varied salt and moisture contents. To achieve an accurate heat transfer model to simulate the cooking process of surimi seafood made of AP surimi, the temperature dependent function of thermal properties at varied salt and moisture content must be developed and the functions has to be coupled with a governing equation of heat transfer. The objectives of this study were: (1) to investigate effects of salt and moisture content on thermal properties of AP surimi paste during heating, (2) to develop temperature dependent functions of AP surimi paste at varied salt and moisture content, and (3) to develop an accurate heat transfer simulation model of AP surimi paste coupled with variable thermal property functions to predict the transient temperature profiles in the surimi paste during heating.

2. MATERIALS AND METHODS

2.1. Materials and gel preparation

Alaska pollock (*Theragra chalcogramma*) surimi (A grade, 10 kg blocks), were provided from Trident Seafoods (Seattle, WA, USA) and kept in frozen at -18°C . Surimi pastes with 76, 80 and 84 % moisture content and 0, 1.5 and 3 % salt concentration were prepared as described by Yongsawatdigul et al. (1995). These compositions are mostly used in commercial surimi seafood products beside 0% of salt which was evaluated to characterize thermal properties of surimi itself. Frozen surimi blocks were thawed at room temperature for approximately 1 h and cut into cubes (5 cm). The initial temperature of surimi was about $2-3^{\circ}\text{C}$. Surimi cubes were chopped with temperature control in a Stephan vacuum cutter (UM5, Stephan Machinery Co., Columbus, OH, USA) at low speed for 1 min. Salt content was adjusted to 0, 15, and 30) g kg^{-1} salt of total weight before chopping. Chopping at low speed was continued for 1 min. Ice was added to adjust the moisture concentration to (760, 800, and 840) g kg^{-1} and chopping continued an additional of 1 min on low speed (1800 rpm). Subsequently, samples were chopped at high speed (3600 rpm) for 3 min under vacuum to a final temperature of 4°C . The paste was vacuum-packed in a plastic bag to eliminate air bubbles.

2.2. Thermal properties measurements

2.2.1. Density

Temperature dependence of the density of AP surimi paste was measured at four different temperatures (20, 30, 60, and 90°C), according to AbuDagga and Kolbe (1997) and Lee and Yoon (2016). Surimi paste was extruded into a known size of stainless still tube (length of 17.5 cm; inner diameter of 1.9 cm). Surimi paste in the stainless still tube was placed in a controlled temperature water bath and allowed to expand freely as they gelled. At each heating temperature, the surimi gel expanded to the outside of the cylinder was trimmed off and the weight of the trimmed off part was accurately measured. Then the density was determined by weight of the surimi in the cylinder divided by the volume of the cylinder. Four replicates were used for each sample.

2.2.2. Thermal conductivity, specific heat and thermal diffusivity

Thermal conductivity and the specific heat of surimi pastes and gels were measured using a KD2 Pro Thermal Properties Analyzer (Decagon Devices Inc., Pullman, WA, USA), which is widely used to measure the thermal properties of food materials (Mahapatra et al. 2013). The dual needle SH-1 sensor (30 mm long, 1.28 mm diameter, and 6 mm spacing) measured the thermal conductivity and specific heat (heat capacity) concurrently at 25°C and consequently from 30 to 90°C every 10°C interval. Ten replicates were performed for each sample. Thermal diffusivity of surimi pastes and gels were determined by following equation:

$$\alpha = \frac{k}{\rho C_p} \quad (1)$$

where α = thermal diffusivity (m²/s); k = thermal conductivity (W m⁻¹ °C⁻¹); ρ = density (kg/m³); and C_p = specific heat (J kg⁻¹ °C⁻¹).

2.3. Gelation with conventional water bath cooking

Heat treatment was conducted to the cube shape of surimi paste. The paste was molded into a cube shape molder (5 x 5 x 5 cm³). After removing from the molder, the cube shapes of surimi paste were heated in a water bath (90 °C) for 60min. The temperature at the geometrical center was monitored using a T-type thermocouple probes (diameter 1.02 mm, Omega Engineering, Inc., Stanford, CT, USA) and recorded every 10 s using a Campbell 21X data-logger (Campbell Scientific Inc., Logan, UT, USA). The samples were kept in the water bath until the temperature at the center approached 90 °C. Triplicates were performed for each sample.

2.4. Numerical simulation

The differential equations of transient heat conduction are given by (Mohan and Talukdar 2010):

$$\rho(T, M, S)C_p(T, M, S) \frac{\partial T}{\partial t} = \nabla \cdot [k(T, M, S)\nabla T] \quad (2)$$

where T = product temperature (°C), M = product moisture content (%), S = product salt content (%) and t = time (s).

The initial condition for modeling is as follows:

$$t = 0, T = T_0$$

and the boundary conditions are as follows:

$$x = 0, \frac{\partial T}{\partial x} = 0 \quad (3a)$$

$$y = 0, \frac{\partial T}{\partial y} = 0 \quad (3b)$$

$$z = 0, \frac{\partial T}{\partial z} = 0 \quad (3c)$$

and on the surface as follows:

$$-k(T, M, S) \left(\frac{\partial T}{\partial x} \right) = h(T_s - T_w) \quad (4a)$$

$$-k(T, M, S) \left(\frac{\partial T}{\partial y} \right) = h(T_s - T_w) \quad (4b)$$

$$-k(T, M, S) \left(\frac{\partial T}{\partial z} \right) = h(T_s - T_w) \quad (4c)$$

where T_s = the surface temperature (°C); T_w = the water bath temperature (°C); h = heat transfer coefficient (W m⁻¹ °C⁻¹); x , y and z = distance in x , y and z -directions (m), respectively.

The heat transfer simulation was performed using the ANSYS workbench 16 program (ANSYS Inc., Canonsburg, PA, USA). The finite volume method using Ansys-Fluent module was employed to solve the three-dimensional heat transfer equation. The 4913 of meshes

used in the geometry was determined at the constant RMSE values observed (Fig. 1b).

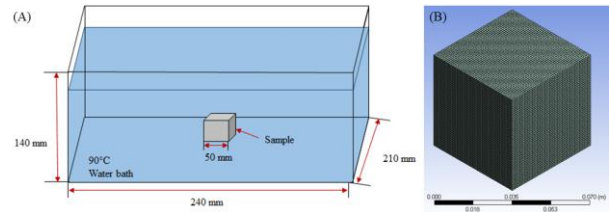


Figure 1: (a) The illustration of cooking of surimi paste in the water bath and (b) the 3-D geometrical model of the surimi block at 3 mm mesh size.

Transient 3D CFD simulation was performed with all side heating (wall temperature was set as $T_{wall} = 90$ °C). Initially surimi paste was at rest with uniform temperature of 18 ± 1.0 °C (based on the experiments). The hot water temperature (90 ± 0.5 °C) was remained constant. Calculations were performed on an Intel® Xeon® CPU E5-2690, 2.6 GHz PC (Intel Corporation, Santa Clara, CA, USA) with 256 Gbyte RAM running a Windows 10 64-bit edition (Microsoft, Redmond, WA, USA). The surimi paste was considered as non-Newtonian fluid, but it is considered as a semi-solid because of its high viscosity (Park 2013) and no applied shear stress. The properties of surimi paste (thermal conductivity, specific heat and density) was applied based on three different models.

- Model A - Constant value of each property at 30 °C

In model A, the thermal properties of surimi paste (thermal conductivity, specific heat and density) during simulation were constant values measured at 30 °C.

- Model B – the mean values of each thermal property during heating with consideration the phase transition were used for the simulation

Based on Lee and Yoon (2016), the mean values from the temperature penetration curves with consideration for the phase transition were used for Model B. A logistic model (Augusto et al., 2012).

$$f(t) = T_{max} / (1 + a \cdot e^{-b \cdot t}) \quad (5a)$$

where T_{max} = a constant value related to the equilibrium temperature; a = the constant; b = increase rate constant (s⁻¹); t = time (s). The mean temperature of each sample were calculated using eq. (5b) as follows”

$$\text{Mean temperature} = 1 / (b - a) \int_a^b f(t) dt \quad (5b)$$

where $f(t)$ = temperature function of time. The temperature function was estimated using a logistic equation. The R² values of all logistic equations used in this study were higher than 0.99 (data were not shown). The sol-gel phase transition of surimi paste was considered based on the gelation temperature (40-50 °C) of surimi paste. The temperature was divided into three regions as follows: (1) lower than gelation temperature

(< 40 °C), (2) during gelation (40-50 °C), and (3) temperature higher than gelation temperature (> 50 °C). The thermal properties at the different mean values reflecting both phase transition and dimensions were used for the computer simulation.

- Model C – temperature-dependent functions of each property were coupled with the heat transfer model for the simulation.

The empirical models to predict the temperature-dependent properties (thermal conductivity, specific heat and density) of surimi were developed and used for the heat transfer simulations.

2.5. Calculation the heat transfer coefficient h

An average heat transfer coefficient, h , used in this study was estimated using dimensionless numbers. The film temperature was used to evaluate all the fluid properties (Hong et al. 2014):

$$T_f = \frac{T_w + T_s}{2} \quad (6)$$

where T_f = film temperature (°C); T_w = the water bath temperature (°C); T_s = the surface temperature of sample (°C);. T_w was 90.0 °C, and T_s (18 °C) was the sample temperature before applying the heat treatment.

As the volume of the surimi samples ($1.25 \times 10^2 \text{ cm}^3$) is very small compared to that of the water bath ($1.083 \times 10^4 \text{ cm}^3$), the geometry governing the forced convection from the fluid is assumed to be an immersed horizontal plate (Geankoplis 2003). For an immersed horizontal plate geometry, Reynold number (N_{Re}), Prandtl number (N_{Pr}), the Nusselt number (N_{Nu}), and the h value for the fluid around the sample were expressed by following equations, respectively:

$$N_{Re} = \frac{Lvp}{\mu} \quad (7)$$

$$N_{Pr} = \frac{C_p \mu}{k} \quad (8)$$

for the laminar region,

$$N_{Nu} = 0.664 N_{Re,L}^{1/2} N_{Pr}^{1/3} \quad (9a)$$

for the turbulent region,

$$N_{Nu} = 0.0296 N_{Re,L}^{4/5} N_{Pr}^{1/3} \quad (9b)$$

$$h = \frac{N_{Nu} k}{L} \quad (10)$$

where ρ is the density, μ is the viscosity, v is the velocity, L is the average length of the longest side of the sample, C_p is the specific heat, and k is the thermal conductivity. Physical properties of water at the T_f are $\rho = 986.42 \text{ kg/m}^3$, $\mu = 6.63 \times 10^{-4} \text{ Pa}\cdot\text{s}$, $C_p = 4178.65 \text{ J kg}^{-1} \text{ }^\circ\text{C}^{-1}$, and $k = 0.65 \text{ W m}^{-1} \text{ }^\circ\text{C}^{-1}$.

2.6. Evaluation of the validity of the simulation results

The transient temperature profiles resulted from the numerical simulation during the thermal treatment could be evaluated by comparing the experimental data. But, applying statistical analysis is a useful way to evaluate the validity of the simulation results. Generally, the validity of modeling results is evaluated with the root mean square error (RMSE).

RMSE was given by the following equation:

$$\text{RMSE} = \sqrt{\frac{1}{N} \cdot \sum_{i=1}^N (T - T_{\text{simulation}})^2} \quad (11)$$

The temperature measured at geometric center of surimi paste during thermal treatment and those from the simulation were used to calculate the RMSE.

2.7. Statistical analysis

The results were presented as the average and standard deviation (SD) of each experiment conducted at least in duplicate and evaluated using SPSS Statistics 22 (SPSS Inc., Chicago, IL, USA). Analysis of variance (ANOVA) with Duncan test was used to determine statistical significance ($p < 0.05$). Stepwise multiple regression tool in SPSS Statistics 22 was used for developing and analyzing the empirical models. At each step of stepwise multiple regression, a predictor were enter or removed based on partial F -tests. F -to-enter and F -to-remove were 0.05 and 0.10, respectively.

3. RESULTS AND DISCUSSIONS

3.1. Density

The density of AP surimi paste at various moisture (76 to 84 %) and salt (0 to 3 %) contents at different temperatures are listed in Table 1. The density of AP surimi paste significantly decreased ($p < 0.05$) with increasing moisture and temperature at the same level of salt. The heat induced gelation or setting led to an increase in volume of the sample. The density changes of surimi paste is mainly due to the spatial arrangement of the native protein chains during the heat treatment (Ziegler and Acton 1984). More disordered arrangement of myofibrillar molecules in surimi paste caused the volume changes and eventually the volume of surimi paste increased after the heat induced gelation. Since the density of water in the surimi paste is lower than that of other components, mainly protein, the density of surimi paste decreased as the moisture content increased (AbuDagga and Kolbe 1997). The density of Pacific whiting (PW) surimi with different moisture contents (74 to 84%) and temperature (30, 60, and 90 °C) were in line with the results observed in the present study (AbuDagga and Kolbe 1997).

At a low temperature, for example 20 or 30 °C, the density of paste increased for all moisture content as the

salt content increased, except 3% of salt at 84% of moisture content (Table 1). The increase of density might be because the addition of salt solubilizes more proteins and it causes the interaction between dissolved protein molecules in the paste. However, as the moisture content increased, the increment of density became smaller. That might be because the relative amount of protein in the paste on which the salt influences is smaller as the moisture content increases. It is an interesting observation that at a high temperature, such as 90 °C, the density decreased for all moisture content as the salt concentration increased. The temperature dependence of

the density at varied salt content is in agreement with the previous study in that the changes in density of surimi (threadfin bream) at a high salt content (3%) was larger at high temperature (90 °C) (Kok and Park 2006). A multiple linear regression model for the density of AP surimi paste as a function of temperature (T), moisture (M) content, and salt contents (S) was suitably fitted from the experimental data ($R^2 = 0.92$) as follows:

$$\rho = 1450.20 - 0.47 T - 4.23 M + 5.40 S - 0.90TS \quad (12)$$

Table 1: Density (ρ) of Alaska pollock surimi paste (kg/m^3).

T (°C)	76 M* (%)			80 M (%)			84 M (%)		
	0 S** (%)	1.5 S (%)	3 S (%)	0 S (%)	1.5 S (%)	3 S (%)	0 S (%)	1.5 S (%)	3 S (%)
20	1118.74±1.0 ^{a***, c****, a*****}	1125.95±1.3 ^{a, B, a}	1131.01±0.9 ^{a, A, a}	1101.12±0.8 ^{a, C, b}	1111.13±1.0 ^{a, B, b}	1116.06±1.1 ^{a, A, b}	1091.86±1.0 ^{a, B, c}	1099.58±0.9 ^{a, A, c}	1099.21±1.0 ^{a, A, c}
30	1114.96±0.7 ^{b, B, a}	1121.47±1.9 ^{b, A, a}	1120.86±0.5 ^{b, A, a}	1093.22±0.6 ^{b, B, b}	1106.13±0.8 ^{b, A, b}	1107.35±0.7 ^{b, A, b}	1088.04±0.8 ^{b, B, c}	1091.91±0.8 ^{b, A, c}	1086.00±0.4 ^{b, C, c}
60	1089.13±0.5 ^{d, C, a}	1097.9±0.3 ^{d, d, A, a}	1094.07±0.4 ^{c, B, a}	1070.09±0.2 ^{c, B, b}	1079.26±0.1 ^{c, A, b}	1079.15±0.4 ^{c, A, b}	1064.34±0.9 ^{c, B, c}	1065.65±0.1 ^{c, A, c}	1055.98±0.8 ^{c, C, c}
90	1092.36±0.9 ^{c, B, a}	1099.81±0.7 ^{c, A, a}	1090.24±0.7 ^{d, C, a}	1068.27±0.7 ^{d, B, b}	1072.50±0.9 ^{d, A, b}	1061.52±1.1 ^{d, C, b}	1056.99±0.8 ^{d, A, c}	1049.13±0.4 ^{d, B, c}	1010.03±0.2 ^{d, C, c}

*M: moisture content

**S: salt content, ±Standard deviations (%)

*** Different superscript small letters denote significant differences ($p < 0.05$) in each row at the same moisture content.

3.2. Specific heat

Table 2: Specific heat (C_p) of Alaska pollock surimi paste ($\text{J} \cdot \text{kg}^{-1} \cdot \text{°C}^{-1}$).

T (°C)	76 M* (%)			80 M (%)			84 M (%)		
	0 S** (%)	1.5 S (%)	3 S (%)	0 S (%)	1.5 S (%)	3 S (%)	0 S (%)	1.5 S (%)	3 S (%)
25	3500.63±2.2 ^{h***, A****, c*****}	3495.31±3.6 ^{h, A, c}	3483.17±3.9 ^{h, B, b}	3540.78±1.6 ^{h, A, b}	3532.97±2.5 ^{g, B, b}	3478.24±1.8 ^{g, C, b}	3603.73±1.7 ^{h, A, a}	3549.68±1.4 ^{h, C, a}	3556.16±2.2 ^{h, B, a}
30	3608.38±2.7 ^{g, A, b}	3524.52±3.5 ^{g, C, c}	3594.92±2.7 ^{f, B, a}	3587.58±2.4 ^{g, A, c}	3532.27±2.3 ^{g, B, b}	3517.00±2.3 ^{f, C, c}	3677.16±3.4 ^{g, A, a}	3656.62±2.4 ^{g, B, a}	3584.94±2.0 ^{g, C, b}
40	3703.23±2.6 ^{f, A, c}	3604.78±2.5 ^{f, B, c}	3572.19±1.6 ^{g, C, c}	3722.81±1.8 ^{e, A, b}	3618.56±1.6 ^{f, C, b}	3670.74±1.6 ^{d, B, b}	3740.35±2.9 ^{f, A, a}	3690.94±1.9 ^{f, B, a}	3691.75±1.7 ^{f, B, a}
50	3743.54±2.5 ^{d, A, b}	3643.27±1.0 ^{e, B, c}	3631.28±2.4 ^{e, C, c}	3718.52±0.8 ^{f, A, c}	3654.67±2.1 ^{e, C, b}	3661.34±2.1 ^{e, B, b}	3799.51±2.0 ^{e, A, a}	3741.82±1.9 ^{e, B, a}	3709.17±1.8 ^{e, C, a}
60	3737.52±2.0 ^{e, A, c}	3710.98±1.1 ^{d, B, c}	3672.80±2.0 ^{d, C, c}	3813.51±0.4 ^{d, A, b}	3756.22±1.8 ^{d, C, b}	3765.44±2.2 ^{c, B, b}	3899.92±1.1 ^{d, A, a}	3871.97±3.1 ^{d, B, a}	3865.60±2.2 ^{d, C, a}
70	3831.50±1.6 ^{c, B, c}	3850.56±1.7 ^{c, A, c}	3829.54±2.6 ^{c, B, b}	3930.79±1.7 ^{c, A, b}	3925.97±1.5 ^{c, B, a}	3763.42±2.4 ^{c, C, c}	3965.09±1.6 ^{c, A, a}	3918.37±1.1 ^{c, B, b}	3963.84±3.0 ^{c, A, a}
80	3906.92±1.0 ^{h, B, c}	3898.33±2.1 ^{h, C, c}	4028.03±2.1 ^{h, A, b}	4135.02±2.3 ^{h, A, a}	3953.50±2.3 ^{h, C, b}	4021.38±1.0 ^{h, B, c}	4114.61±2.7 ^{h, A, b}	4008.26±3.5 ^{h, B, a}	4106.07±3.1 ^{h, B, a}
90	4022.12±2.3 ^{a, B, c}	3976.58±3.1 ^{c, C, c}	4072.55±3.9 ^{a, A, c}	4154.02±2.8 ^{a, A, b}	4032.64±3.6 ^{a, B, b}	4152.46±2.5 ^{a, A, b}	4184.68±2.9 ^{a, B, a}	4184.55±0.7 ^{a, B, a}	4232.51±2.2 ^{a, A, a}

*M: moisture content

**S: salt content, ±Standard deviations (%)

*** Different superscript small letters denote significant differences ($p < 0.05$) in each row at the same moisture content.

**** Different superscript capital letters denote significant differences ($p < 0.05$) in each column at the same moisture content.

***** Different superscript small letters denote significant differences ($p < 0.05$) at different moisture content.

The specific heat of AP surimi paste with different moisture and salt contents was measured at different temperature (Table 2). Generally, the specific heat of a solid is highly dependent on temperature (Engel and Reid 2006). The specific heat with 76, 80, and 84% moisture contents with 1.5% salt content increased from 3495.31 to 3976.58, 3532.97 to 4032.64, and 3549.68 to 4184.55 J·kg⁻¹·C⁻¹, respectively, during heating (25 to 90 °C).

Increasing the moisture content significantly increased the specific heat of AP surimi ($p < 0.05$). Due to the high specific heat of water, the higher specific heat was observed at the higher moisture contents in food (Sopade and LeGrys 1991, Noel and Ring 1992, Taiwo et al. 1996). As salt content increased, the specific heat slightly decreased at lower temperatures (25-60 °C) (Table 2). According to Solomon et al. (2002), the hydrogen bonds that form between water molecules can store heat as potential energy of vibration in water. However, when salt is added to water, the sodium chloride ions interact with the water molecules, which results in the reduction of specific heat. But, the interaction might be decreased in the range of gelation temperature as the heat-induced gelation occur. Thus, the effect of salt on the specific heat

of AP surimi paste can be explained by interacting the sodium chloride ions with the water and protein molecules. Interestingly, the specific heat of AP and PW surimi pastes showed the same order of magnitude, although they are originated from different species. The specific heat of PW surimi paste at 80% moisture content was varied from 3542 to 4033 J·kg⁻¹·C⁻¹ over the temperature range of 25–90 °C (AbuDagga and Kolbe 1997).

A linear model for the specific heat of AP surimi paste as a function of temperature (T) and moisture (M) content, and salt contents (S) was fitted based on the experimental data:

$$C_p = 2208.48 + 8.71 T + 13.93 M - 14.13 S \quad (13)$$

Although the linear regression did not accommodate the denaturation peaks where the denaturation and gelation occur (Lee and Yoon 2016), it has a good overall fit with an R² of 0.97, and could be considered a workable model to support the heat transfer governing equation.

3.3. Thermal conductivity

Table 3: Thermal conductivity (k) of Alaska pollock surimi paste (W·m⁻¹·°C⁻¹).

T (°C)	76 M* (%)			80 M (%)			84 M (%)		
	0 S** (%)	1.5 S (%)	3 S (%)	0 S (%)	1.5 S (%)	3 S (%)	0 S (%)	1.5 S (%)	3 S (%)
25	0.544±0.00 3 ^{g****} , B****, c*****	0.549±0.00 3 ^g , A, b	0.549±0.00 4 ^g , A, b	0.565±0.00 3 ^g , A, a	0.544±0.00 2 ^h , B, b	0.545±0.00 3 ^f , C, b	0.556±0.00 3 ^g , A, b	0.561±0.00 3 ^h , A, a	0.557±0.00 3 ^h , A, a
30	0.544±0.00 3 ^g , B, c	0.558±0.00 4 ^f , A, b	0.559±0.00 3 ^f , A, b	0.561±0.00 3 ^g , B, b	0.569±0.00 2 ^g , A, a	0.548±0.00 4 ^f , C, c	0.578±0.00 3 ^f , A, a	0.568±0.00 3 ^g , B, a	0.573±0.00 3 ^g , AB, a
40	0.576±0.00 3 ^f , A, b	0.546±0.00 3 ^g , B, b	0.570±0.00 5 ^e , A, b	0.581±0.00 4 ^f , B, b	0.588±0.00 2 ^f , A, a	0.584±0.00 4 ^e , AB, a	0.594±0.00 3 ^e , A, a	0.588±0.00 3 ^f , A, a	0.590±0.00 2 ^f , A, a
50	0.584±0.00 3 ^e , A, c	0.566±0.00 3 ^e , C, b	0.572±0.00 2 ^e , B, c	0.606±0.00 3 ^e , A, a	0.595±0.00 3 ^e , B, a	0.585±0.00 4 ^e , C, b	0.594±0.00 3 ^e , B, b	0.593±0.00 1 ^e , B, a	0.609±0.00 4 ^e , A, a
60	0.594±0.00 3 ^d , A, c	0.589±0.00 4 ^d , A, c	0.594±0.00 3 ^d , A, c	0.615±0.00 2 ^d , AB, b	0.619±0.00 3 ^d , A, b	0.611±0.00 3 ^d , B, b	0.649±0.00 4 ^d , A, a	0.647±0.00 3 ^d , A, a	0.643±0.00 3 ^d , A, a
70	0.630±0.00 4 ^c , B, c	0.646±0.00 4 ^c , A, b	0.646±0.00 2 ^c , A, b	0.645±0.00 4 ^c , A, b	0.628±0.00 3 ^c , B, c	0.641±0.00 3 ^c , A, b	0.682±0.00 2 ^c , A, a	0.671±0.00 3 ^c , B, a	0.667±0.00 4 ^c , B, a
80	0.703±0.00 5 ^b , A, c	0.683±0.00 4 ^b , B, c	0.671±0.00 4 ^b , C, c	0.712±0.00 5 ^b , B, b	0.699±0.00 2 ^b , C, b	0.718±0.00 4 ^b , A, b	0.761±0.00 4 ^b , A, a	0.750±0.00 4 ^b , B, a	0.745±0.00 4 ^b , B, a
90	0.743±0.00 4 ^a , A, c	0.746±0.00 5 ^a , A, c	0.750±0.00 4 ^a , A, c	0.772±0.00 5 ^a , A, b	0.767±0.00 5 ^a , A, b	0.775±0.00 4 ^a , A, b	0.808±0.00 2 ^a , A, a	0.791±0.00 3 ^a , B, a	0.805±0.00 5 ^a , A, a

*M: moisture content

**S: salt content, ±Standard deviations (%)

*** Different superscript small letters denote significant differences ($p < 0.05$) in each row at the same moisture content.

**** Different superscript capital letters denote significant differences ($p < 0.05$) in each column at the same moisture content.

***** Different superscript small letters denote significant differences ($p < 0.05$) at different moisture content.

The thermal conductivity of AP surimi paste with different salt and moisture contents was measured at different temperature (Table 3). Thermal conductivity was significantly dependent on the temperature as well as compositions in food. Especially for surimi paste, the

moisture content in the paste is a major variable for the changes of thermal conductivity during heating. Compared to the moisture content in the surimi paste, the salt content showed no significant influence on the thermal conductivity. This result is in agreement with

other studies on blending of salt with meat (Zhang et al. 2007, Marcotte et al. 2008) and the surimi paste prepared with pacific whiting (AbuDagga and Kolbe 1997). Zhang et al. (2007) also reported that the level of added salt had no effect ($p < 0.05$) on the measured the thermal conductivity of the meat blends. Similarly, the thermal conductivity of PW (80% w.b.) ranged from 0.536 to 0.683 $\text{W}\cdot\text{m}^{-1}\cdot\text{C}^{-1}$ over the temperature range of 25 to 80 °C (AbuDagga and Kolbe 1997). The temperature dependence of thermal conductivity of surimi paste is in line with previous studies on the thermal conductivity behavior of other muscle foods (Marcotte et al. 2008). To develop an empirical model for thermal conductivity of AP surimi, a stepwise multiple regression was conducted. This process is continued only if additional variables show a statistical significance to the regression equation. The empirical model can be written as:

$$k = 0.34 + 4.57 \times 10^{-5} T^2 + 3.67 \times 10^{-5} M^2 - 2.46 \times 10^{-5} TM \quad (14)$$

As shown in eqn. 15, salt content was removed from the empirical model by the stepwise regression. The model with second degree terms of both temperature and moisture content satisfactorily predicted thermal conductivity of AP with an R^2 of 0.98. Our study concluded that the changes in thermal conductivity was highly dependent on the moisture content than salt content within our experimental range (Table 3).

The contour plots of thermal diffusivity of surimi paste during heating from 30 °C to 90 °C showed a strong moisture content dependence compared to salt content (Fig. 2.). As expected, the thermal diffusivity of AP surimi paste significantly increased with increasing temperature and moisture content while the salt content did not affect significantly the thermal diffusivity values. Thus, more comprehensive understanding of heat transfer of surimi paste during thermal processing could be obtained by analyzing the thermal diffusivity. The temperature and moisture dependency of thermal diffusivity of AP surimi paste is in agreement with previous studies on the thermal diffusivity behavior of other foods (Tansakul and Chaisawang 2006, Yang et al. 2002).

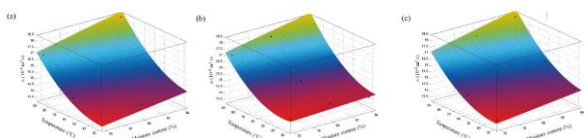


Figure 2: Surface plots of the thermal diffusivity (a) of AP surimi paste at (a) 0, (b) 1.5 and (c) 3% salt content.

3.4. Comparison of simulated and experimental temperature profiles of AP surimi pastes

The effect of the mesh size in the simulation geometry on the simulation of transient temperature profile of AP surimi paste during thermal processing was examined by comparing RMSE estimated at 80% moisture content and 1.5% salt content (Fig. 3).

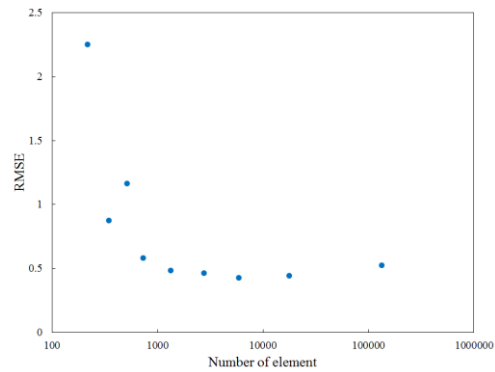


Figure 3: The RMSE result of AP surimi at 80% moisture content and 1.5% salt content at different number of element.

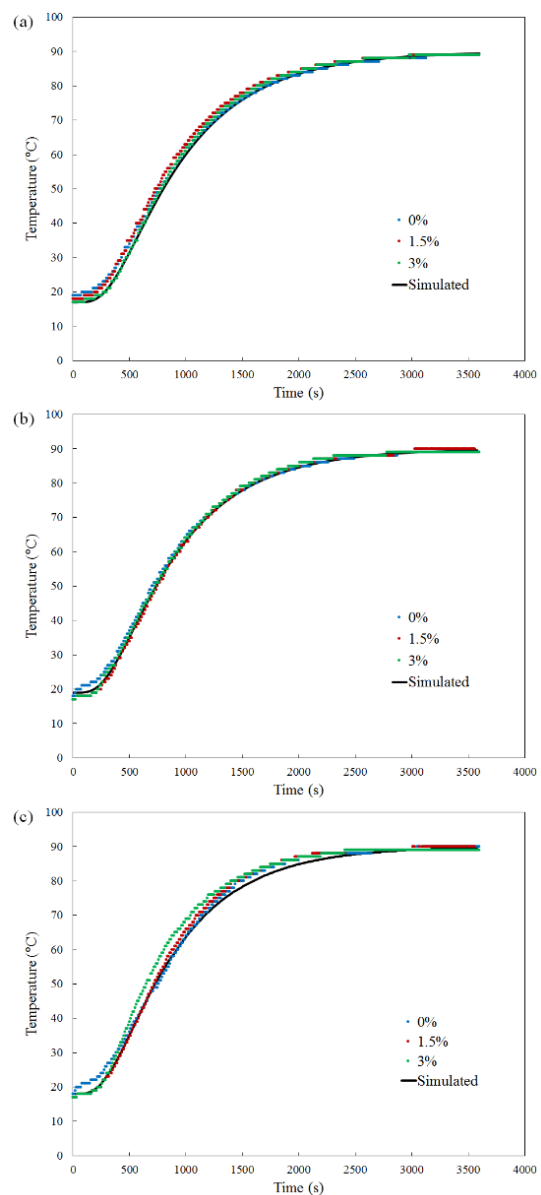


Figure 4: Temperature profiles of surimi pastes between measurement and CFD predictions (1.5% salt) for constant temperature (90 °C) water bath heating at (a) 76, (b) 80 and (c) 84% moisture content.

As the mesh size decreased from 10 mm to 1 mm, the number of element increased from 125 to 125000. At the lowest number of element, RMSE value was 2.26 and RMSE values were decreased as number of element increased. But, there was no significant differences in the range from 5 mm to 1 mm mesh size. As excess high mesh quality is inefficient for calculation time and the 3 mm mesh size (4913 elements) showed the lowest RMSE value in the range examined, the 3mm mesh size were used for the further analysis.

The transient temperature profiles at the center of the geometry from experiment and simulation were shown in Fig. 4. Since the salt content did not influence the thermal properties significantly, only 1.5 % of salt content was used for the validation. The transient temperature profiles at the center of the geometry from experiment and simulation were shown in Fig. 4. Since the salt content did not influence the thermal properties significantly, only 1.5 % of salt content was used for the validation. During convection heating using a water bath, the surimi sample with 76 % moisture with 1.5 % salt reached at the temperature of heating medium at 2990s, while the surimi samples with 80 and 84 % moisture took 2850 and 2420s, respectively. The sample with higher moisture content had a higher heating rate because it has a higher thermal conductivity (AbuDagga and Kolbe 1997). Because the specific heat also increases with moisture content, the high moisture content cannot increase the heating rate as much as the heat conductivity

increased (AbuDagga and Kolbe 2000). Similarly, at 0 and 3% of salt contents, the surimi samples with 76, 80, and 84 of moisture contents reached at the heating medium temperature at 3140, 2880, and 2650s and 2980, 2780, and 2410s respectively.

To validate the use of the empirical models of temperature dependence of thermal properties for simulation model, the simulation models with constant values of properties measured at 30 °C (model A) and the simulation models with properties considering the sol-gel phase transition region (model B) were also evaluated. The RMSE values of each simulation calculated using eq. (11) is summarized in Table 4 and also the temperature distributions obtained from the model A, B and C at 84% moisture content and 1.5% salt contents were represented in Fig. 5. Since the thermal properties measured at 30 °C were the lowest value during heating, the temperatures in the transient temperature profile were lower than the actual values. Additionally, the RMSE of model A showed the highest RMSE among the three models. The RMSE values from the model A ranged from 1.87 to 2.32 °C. For the model B, the mean temperature for three temperature regions (15-40 °C, 40-50 °C and 50-90 °C) were 26.79 °C (0-580s), 45.22 °C (580-770s) and 82.06 °C (770-3600s), respectively. With consideration for the sol-gel phase transition, the RMSE of model B (1.01 to 1.58 °C) showed lower than that of Model A (1.87 to 2.32 °C).

Table 4: Root mean square error (RMSE) of simulation and averaged experiment temperature profiles after convection heating.

	76 M*			80 M			84 M		
	Model A***	Model B****	Model C*****	Model A	Model B	Model C	Model A	Model B	Model C
0 S**	2.04	1.11	0.67	2.21	1.24	0.59	2.01	1.58	0.87
1.5 S	2.21	1.28	0.83	1.87	1.01	0.43	2.21	1.16	0.69
3 S	2.32	1.48	1.22	2.14	1.32	0.98	2.74	1.05	1.11

*M: moisture content (%).

**S: salt content (%).

***Model A: Simulation model with constant value of thermal properties at 30 °C.

****Model B: Simulation model with consideration the phase transition.

*****Model C: Simulation model with temperature-dependent functions of thermal properties.

The transient temperature profile obtained from the model B showed higher than those of actual values. It might be due to the average thermal properties were mainly estimated from the high temperature region that is the temperature above the sol-gel transition temperature. The mean thermal properties estimated in the high temperature region dominated the heat transfer simulation and such high value of thermal properties in the simulation resulted in the high temperature profile. The RMSE of the model C (0.43 to 1.22 °C) showed the lowest values. This demonstrated that the temperature dependent thermal property functions needs to be coupled with the heat transfer model to predict an accurate transient temperature profile of surimi paste

during heating. The slowest heating zone evaluated different simulation models (A, B, and C) were shown in Fig. 5. The simulation results clearly demonstrated that the model A and B will cause a lack of heating and an overheating, respectively. The slowest heating zone of product have to be provide adequate heat treatment to ensure that the detrimental effect of microorganisms inactivated while preventing the degradation of food quality and its nutritive properties from excessive heating. Therefore, simulation model should be developed as accurate as possible. The thermal properties of AP surimi and the simulation method applied in this study may be useful in design of processing equipment, in process calculations of heating and cooling rates or

times, and in calculating the process energy requirements, and also in the development of new processing techniques for surimi seafood products (Belibagli et al. 2003).

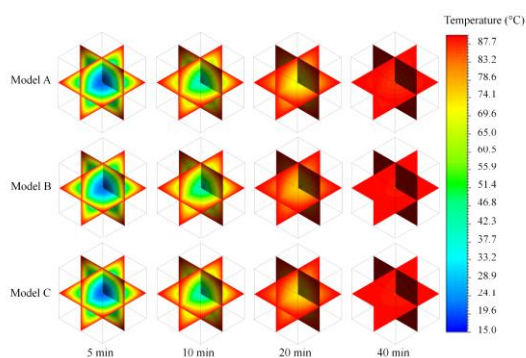


Figure 5: Estimation of the temperature distribution of the AP surimi at 84% moisture content and 1.5 % salt content during convective heating at 90 °C.

4. CONCLUSIONS

Density, specific heat, and thermal conductivity of AP surimi paste at varied moisture and salt contents have been measured and modelled in the temperature range 20-90°C. The density of AP surimi paste significantly decreased ($p < 0.05$) with increasing moisture content and temperature, and the density was slightly dependent on salt content. Specific heat and thermal conductivity increased with an increase in moisture content and temperature. Contrary to the expectations, the proportion of salt did not have any significant effect on the thermal conductivity. Thermal conductivity was most suitably fitted with a quadratic equation with an R^2 value of 0.98. The empirical models adequately predicted the thermal properties of AP surimi up on the moisture and salt content and the temperature. It was an interesting observation that the thermal properties of AP surimi were close to those of Pacific whiting surimi within our experimental range. It implies that the mixing two different species might be possible in the commercial processing with minimum effort of adjusting the existing process conditions. These models made of empirical measurements were validated by applying the thermal property models for the simulation. The RMSE values for the simulation model with empirical model ranged from 0.43 °C to 1.22 °C in AP surimi pastes while the RMSE values for the simulation model with constant value of each property at 30 °C (model A) and the simulation model with consideration for the sol-gel phase transition (model B) ranged from 1.87 °C to 2.32 °C and 1.01 to 1.58 °C, respectively. Simulated temperature profile of model C was found to be in good agreement with experimental temperature profile. Therefore, the simulation models with the empirical models of thermal properties can be used to identify cold point locations and can be used by food product developers for optimizing food composition and process design.

ACKNOWLEDGMENTS

This study has been worked with the support of a research grant of Kangwon National University in 2016.

REFERENCES

- AbuDagga Y., Kolbe E., 1997. Thermophysical properties of surimi paste at cooking temperature. *Journal of Food Engineering*, 32(3), 325-337.
- Abudagga Y., Kolbe E., 2000. Analysis of heat transfer in surimi paste heated by conventional and ohmic means. *Journal of Aquatic Food Product Technology*, 9(2), 43-54.
- Anadharamakrishnan C., 2003. Computational Fluid Dynamics (CFD): Applications for the food industry. *Indian Food Industry*, 22(6), 62-68.
- Augusto P.E., Soares B., Chiu M.C., Goncalves L.A., 2012. Modelling the effect of temperature on the lipid solid fat content (SFC). *Food Research International*, 45(1), 132-135.
- Belibagli K.B., Speers R.A., Paulson A.T., 2003. Thermophysical properties of silver hake and mackerel surimi at cooking temperatures. *Journal of Food Engineering*, 60(4), 439-448.
- Fontana A.J., Varith J., Ikediala J., Reyes J., Wacker B., 1999. Thermal properties of selected food using a dual needle heat-pulse sensor. In: ASAE Meeting Presentation.
- Fukushima H., Okazaki E., Fukuda Y., Watabe S., 2007. Rheological properties of selected fish paste at selected temperature pertaining to shaping of surimi-based products. *Journal of Food Engineering*, 81(2), 492-499.
- Geankoplis C.J., 2003. Transport processes and separation process principles: (includes unit operations) (4th ed.). Upper Saddle River, NJ, USA: Prentice Hall Press, 1056.
- Guennegues P., Morrissey M.T., 2005. Surimi resources. In: Park J.W., ed. *Surimi and surimi seafood* (2nd ed.). Boca Raton, FL, USA: CRC Press, 3-32.
- Hong Y.K., Uhm J.T., Yoon W.B., 2014. Using Numerical Analysis to Develop and Evaluate the Method of High Temperature Sous-Vide to Soften Carrot Texture in Different-Sized Packages. *Journal of Food Science*, 79(4), 546-561.
- Karunakar B., Mishra S.K., Bandyopadhyay S., 1998. Specific heat and thermal conductivity of shrimp meat. *Journal of Food Engineering*, 37(3), 345-351.
- Kok T.N., Park J.W., 2006. Elucidating factors affecting floatation of fish ball. *Journal of Food Science*, 71(6), 297-302.
- Lee M.G., Yoon W.B., 2016. Developing an effective method to determine the heat transfer model in fish myofibrillar protein paste with computer simulation considering the phase transition on various dimensions. *International Journal of Food Engineering*, 12(9), 889-900.
- Mahapatra A.K., Mi S.L., Isang E.M., 2013. Effect of moisture content on thermal properties of cowpea

- flours. *Agricultural Engineering International: CIGR Journal*, 15(2), 251-255.
- Marcotte M., Taherian A.R., Karimi Y., 2008. Thermophysical properties of processed meat and poultry products. *Journal of Food Engineering*, 88(3), 315-322.
- Mariani V.C., Lina A.G.B., Coelho L.S., 2008. Apparent thermal diffusivity estimation of the banana during drying using inverse method. *Journal of Food Engineering*, 85(4), 569-579.
- Mohan V.P.C., Talukdar P., 2010. Three dimensional numerical modeling of simultaneous heat and moisture transfer in a moist object subjected to convective drying. *International Journal of Heat and Mass Transfer*, 53(21-22), 4638-4650.
- Noel T.R., Ring S.G., 1992. A study of the heat capacity of starch/water mixtures. *Carbohydrate Research*, 227, 203-213.
- Norton T., Sun D.W., 2006. Computational fluid dynamics (CFD)—an effective and efficient design and analysis tool for the food industry: a review. *Trends in Food Science & Technology*, 17(11), 600-620.
- Park J.W., 2013. *Surimi and surimi seafood* (3rd ed.). Boca Raton, FL, USA: CRC Press.
- Pitchai K., Chen J., Birla S., Gonzalez R., Jones D., Subbiah J., 2014. A microwave heat transfer model for a rotating multi-component meal in a domestic oven: development and validation. *Journal of Food Engineering*, 128, 60-71.
- Scott G., Richardson P., 1997. The application of computational fluid dynamics in the food industry. *Trends in Food Science & Technology*, 8(4), 119-124.
- Solomon E.P., Berg L.R., Martin D.W., 2002. *Biology* (6th ed.). Belmont, CA, USA: Thomson Brooks/Cole.
- Sopade P.A., LeGrys G.A., 1991. Specific heat capacity of starch-sucrose systems. *Food Control*, 2(1), 50-52.
- Tabilo-Munizaga G., Barbosa-Cánovas G.V., 2004. Color and textural parameters of pressured and heat-treated surimi gels as affected by potato starch and egg white. *Food Research International*, 37(8), 767-775.
- Taiwo K.A., Akanbi C.T., Ajibola O.O., 1996. Thermal properties of ground and hydrated cowpea. *Journal of Food Engineering*, 29(3), 249-256.
- Tansakul A., Chaisawng P., 2006. Thermophysical properties of coconut milk. *Journal of Food Engineering*, 73(3), 276-280.
- Unklesbay N., Unklesbay K., Clarke A.D., 1999. Thermal properties of restructured beef snack sticks throughout smokehouse processing. *LWT-Food Science and Technology*, 32(8), 527-534.
- Yang W., Sokhansani S., Tang J., Winter P., 2002. Determination of thermal conductivity, specific heat and thermal diffusivity of borage seeds. *Biosystems Engineering*, 82(2), 169-176.
- Yongsawatdigul J., Park J.W., Kolbe E., 1995. Electrical conductivity of Pacific whiting surimi paste during ohmic heating. *Journal of Food Science*, 60(5), 922-925.
- Zhang L., Lyng J.G., Brunton N.P., 2007. The effect of fat, water and salt on thermal and dielectric properties of meat batter and its temperature following microwave or radio frequency heating. *Journal of Food Engineering*, 80(1), 142-151.
- Ziegler G.R., Acton J.C., 1984. Mechanisms of gel formation by proteins of muscle tissue. *Food Technology*, 38, 77-82.

AUTHORS BIOGRAPHY

Hyeon Woo Park is a second-year graduate student in Food Science and Biotechnology at Kangwon National University (KNU) in South Korea. He received his Bachelor's Degree in Food Science and Biotechnology from the Kangwon National University in 2015. His research interests include process optimization and new process design, surimi and surimi seafood processing and numerical and CFD simulation.

Dr. Park is a professor of Oregon State University since 1992. He was elected as IFT Fellow in 2007, which is the most prestigious recognition as a food scientist. He published 136 referred journal articles, 41 book chapters, and 3 patents. He offered over 100 invited speeches. Having devoted his entire professional career to fish protein (surimi) research and outstanding outreach in technology transfer, Dr. Jae Park has distinguished himself as an internationally renowned scientist in surimi research, education, and technology transfer. He received numerous awards to recognize his accomplishment regionally, nationally and internationally. He was recognized by IntraFish as 100 most powerful seafood executives in 2012. His most recent recognition was the 2016 IFT Bor S Luh International Award in Chicago in July, 2016.

Dr. Yoon is a professor at Kangwon National University (KNU) since 2008. He has a B.S. and M.S. in Food Science and Technology, and M.E. in Mechanical Engineering, and a Ph.D. major in Biological Systems Engineering and minor in Chemical Engineering. Before joining KNU, he worked in a processed food industry (associate director in Food R&D Center, CJ CheilJedang, Seoul, S. Korea) and a flavor company (Asia-Pacific regional marketing manager and Seafood specialist, Firmenich-Asia, Singapore). He has been working on food process engineering, food rheology and seafood processing for more than 13 years. His research interest includes gelation characterization of proteins and hydrocolloids, drying and powdering, high viscous fluid mechanics, heat and mass transfer during food processing, least cost formulation development, and computational fluid dynamics. He has so far published more than 80 articles in highly regarded journals in the field of food process engineering.

EFFECT OF INULIN IN JERUSALEM ARTICHOKE (*HELIANTHUS TUBEROSUS* L.) FLOUR ON THE VISCOELASTIC BEHAVIOR OF COOKIE DOUGH AND QUALITY OF COOKIES

YOUN JU LEE^(a), OK-HWAN LEE^(b), WON BYONG YOON^(c)

^{(a),(b),(c)} Department of Food Science and Biotechnology, College of Agricultural and Life Science, Kangwon National University, Chuncheon, Kangwondo, 200-701, S. Korea

^(a)skiee13468@nate.com, ^(b)loh99@kangwon.ac.kr, ^(c)wbyoon@kangwon.ac.kr

ABSTRACT

The aim of this research was to investigate the effect of inulin in Jerusalem artichoke on developing a gluten-free bakery product. Jerusalem artichoke flour (JF) was used as a substitute for wheat flour to enhance texture, functional and nutritional properties. The cookie dough with JF showed more elastic behavior due to a higher water holding capacity and fat absorption capacity compared with wheat flour and potato flour. The inulin influenced the properties of flour and also contributed to changes in the properties of the dough and cookies. The cookies made from 100 % JF had 42.67 % inulin. As the addition of JF increased, the dough showed a cohesive structure and the cookies did not expand in either diameter or thickness. Hardness of cookie increased with JF increased. The color and antioxidant activities were improved by JF due to the acceleration of Maillard reaction by inulin during baking.

Keywords: Jerusalem artichoke, inulin, viscoelasticity, cookie development

1. INTRODUCTION

Jerusalem artichoke (*Helianthus tuberosus* L.) tuber is a kind of potato. It stores carbohydrates in the form of inulin instead of starch. Inulin is a non-digestible carbohydrate and present in many vegetables, fruits and cereals (Zahn et al. 2010; Bach et al. 2012; Rinaldoni et al. 2012). Previous studies have reported that inulin has anti-obesity and antioxidant activities (Niness 1999, Lee and Kang 2009). In addition, inulin is used for applications in the food industry and has been used in a variety of food products due to its technological and nutritional benefits (Meyer et al. 2011, Rinaldoni et al. 2012). Several studies have examined the feasibility of inulin as replacement for fat or sugar in dairy and bakery products. Appropriate methods to enhance the texture and sensory properties of cookies using inulin have been reported (Zoulias et al. 2002; Meyer et al. 2011; Rodríguez-García et al. 2012). Generally, gluten possesses a structure-forming ability that contributes to the overall appearance and crumb structure of many baked products. Some studies have reported that adding inulin to more than an optimum level resulted in a hard and brittle texture, mainly due to insufficient expansion after baking (Rodríguez-García et al. 2012).

To develop a gluten-free baking product, a replacement with similar physical characteristics in bakery products must be developed. Thus, the rheological properties of dough and the textural properties of baking products are the most important properties in developing a gluten-free baking product. The rheological properties of dough are generally determined by measuring the viscoelasticity using creep recovery, stress relaxation, and small amplitude oscillatory shear test. Many small strain measurements have been conducted to evaluate the effect of ingredients and the processing conditions on the viscoelastic properties of cookie doughs (Bhattacharya 2010; Šeremešić et al. 2013; Pedersen et al. 2014; Raymundo et al. 2014; Filipčev et al. 2015; Sarabhai and Prabhasankar. 2015; Petrović et al. 2015; Mancebo et al. 2016). However, the small deformation test showed a difficulty to find a relationship between the assessed parameters and the dough properties during processing, so that a large deformation tests are required for understanding the dough properties during processing. The stress relaxation test with a large deformation has been used to characterize the viscoelastic properties of dough (Rodríguez-Sandoval et al. 2009; Bhattacharya 2010). Generally, the stress relaxation data can be analyzed by various models such as Maxwell model (Mohsenin 1970) or Peleg model (Peleg and Normand 1983). A nonlinear three-parameter model was also applied to predict the stress relaxation behavior of chickpea dough (Yadav et al. 2006).

Several studies have investigated gluten-free products made with grain flours (Schober et al. 2003; Ellouze-Ghorbel et al. 2010; Gupta et al. 2011; Zucco et al. 2011; Torbica et al. 2012) other than wheat and have shown an improvement in texture, mouthfeel, flavor, and nutrition. Recently, several functional ingredients such as starches or fibers also have been used for the gluten-free cookie development (Šeremešić et al. 2013; Raymundo et al. 2014; Filipčev et al. 2015; Petrović et al. 2015; Mancebo et al. 2016). Overall analysis has indicated that cookies with acceptable physical characteristics and improved nutritional profiles could be produced with partial or complete replacement of wheat flour (Zucco et al. 2011). Rice flour and buckwheat flour were successfully incorporated into gluten-free, cereal-based products, resulting in cookies

with a pleasant flavor and acceptable sensory qualities (Torbica et al. 2012). In addition, wheat bran and whole barley flour could be used for enriching biscuit fiber content without undesirable changes to their textural and sensory properties (Ellouze-Ghorbel et al. 2010, Gupta et al. 2011).

As previous studies have indicated, Jerusalem artichoke flour (JF) could be a useful replacement for the development of a gluten-free bakery product, especially cookies, but the rheological properties of dough and the quality characteristics of cookies with JF should be investigated. The objectives of this study were to characterize the effect of inulin in JF on the structure formation on cookie dough, and the characteristics compared with dough and cookie containing potato flour (PF). Eventually, the physical and nutritional properties of cookies prepared with PF and JF were evaluated.

2. MATERIALS AND METHODS

2.1. Materials

All ingredients used in cookie production (i.e., wheat flour (WF), unsalted butter, sugar, common salt, sodium bicarbonate and potato (*Solanum tuberosum* L.) flour (PF) were supplied from a local market in Chuncheon, Korea. Jerusalem artichoke (*Helianthus tuberosus* L.) flour (JF) was purchased from the Sangol farm (Hoengseong-gun, Korea). JF and PF with particle sizes below 100 μm were used for making cookies.

2.2. Chemical composition analysis

The chemical characteristics of ash in WF, PF, and JF, were determined according to AOAC (2000) methods. The moisture content was measured with a moisture analyzer (MB45, Ohaus, New Jersey, USA).

Water Holding and Fat Absorption Capacity

The water holding capacity (WHC) was determined using the methods described by Chen et al. (1988) and Tang (2007) with some modifications. The fat absorption capacity (FAC) was measured according to the method of Lin et al. (1974). The WHC and FAC are expressed as g of water and fat per gram of the sample on a dry basis (Tang 2007). Triplicate samples were analyzed for each treatment.

2.3. Preparation of Dough and Cookies

The control cookies were formulated with 220 g WF, 75 g sugar, 75 g salt-free butter, 50 g egg, 2 g sodium bicarbonate, and 0.5 g common salt. The dough was shaped into cylindrical discs with 5 cm diameters and 0.5 cm thicknesses, then baked at 180 °C for 10 min. After cooling for 1 h, the cookies were packed and used for the evaluation of various chemical, textural characteristics. All controls were made with WF only.

2.4. Dough Rheology Measurement

2.4.1. Stress Relaxation test

The level of PF and JF in the dough samples for stress relaxation test was adjusted to 50 % and 100 % flour in dough. Stress relaxation tests were conducted with a

texture analyzer (CT3, Brookfield, Raynham, Massachusetts, USA). Dough samples (50 mm in diameter and 40 mm thickness) were prepared with a cylindrical cutter. The sample was compressed by 10 % for the small deformation and 60 % for the large deformation with a cylinder probe (TA25/1000) of 50 mm diameter. The crosshead speed was 3mm/s. This constant compressive strain was applied to the sample for 100 s.

For analyzing the data from the small deformation test, Maxwell model. The generalized Maxwell model with 2 elements was applied.

$$E(t) = E_1 \exp(-t/\lambda_1) + E_2 \exp(-t/\lambda_2) + E_e \quad (1)$$

where E is the spring modulus (s), λ is relaxation time of the Maxwell body and E_e is the lone spring modulus. The viscosity of element i (number of element) can be calculated according to following equation:

$$\eta_i = E_i \lambda_i \quad (2)$$

Peleg model (Peleg and Normand 1983) and a three-parameter nonlinear model (Yadav et al. 2006) were applied to analyze the stress relaxation data from the large deformation (60 %). In the Peleg model (Eqn. 3), the stress relaxation data was described as the stress normalized.

$$(\sigma_0 t)/(\sigma_0 - \sigma(t)) = k_1 + k_2 t \quad (3)$$

The three-parameter nonlinear model (Eqn. 4) proposed by Yadav et al. (2006) was also used to predict the force decay during relaxation.

$$F(t) = A \exp(-\alpha t) + F_e \quad (4)$$

where F_e is the residual force at equilibrium, A is equivalent to initial force (F_0) when t is zero. When t is large, $F(t) \rightarrow F_e$. α represents the rate of exponential decay (Yadav et al. 2006, Bhattacharya 2010). The curve fitting tool in Matlab® (The MathWorks, Inc., Natick, Massachusetts, USA) was used for analyzing all the models.

The goodness-of-fit the theoretical models were assessed by calculating and comparing the root mean square error (RMSE) values of the models using Eqn. 5:

$$\text{RMSE} = \sqrt{\frac{\sum_1^n [\text{Experimental value} - \text{Model value}]^2}{\text{Degree of freedom}}} \quad (5)$$

2.4.2. Dynamic Oscillatory Measurement

Dynamic oscillatory measurement was conducted with a dynamic rheometer (Discovery HR-3, TA instruments, New Castle, USA). The level of PF and JF in the dough samples for the rheological measurements were adjusted at 25% and 50%, respectively. The dough sample was loaded between the plates and the gap was adjusted to 3

mm. The measurement system consisting of parallel plate geometry (40 mm diameter). Frequency sweeps test was performed from 1 to 10 Hz at a strain 0.02 % to determine the storage modulus (G'), loss modulus (G'') and loss tangent ($\tan \delta$) as a function of frequency. The strain level was selected from the linear viscoelastic region (approximately 0.05%) after the stress sweep test (data are not shown). All measurements were conducted at 25 °C. All tests were triplicated.

2.5. Scanning Electron Microscopy (SEM)

The structures of the flour, dough and cookie samples were analyzed by variable pressure field emission scanning electron microscopy (VP-FESEM). The surface of flour, dough and cookies were observed under a SUPRA55V VP-FESEM (SUPRA55V, Carl Zeiss, Jena, Germany) at the Korean Basic Science Institute, Chuncheon. The samples of dough and flours (particle sizes below 100 μm) were dried at room temperature for 24 h and cookies were ground without drying.

2.6. Measurement of Inulin Content

The method used to measure the level of inulin in cookies was appropriately modified based on the spectrophotometric method (Lingyun et al. 2007, Saengkanuk et al. 2011). For the analysis of inulin, all cookie samples were made without sugar. Each sample was pounded and 5.56 g of the sample was extracted with 50 mL of water by sonication for 20 min at 68 °C. The extracted liquid was centrifuged at 4000 g for 20 min to remove suspended particles. The supernatant was diluted before determination. The inulin contents in cookies were calculated using the following equation:

$$\text{Inulin} = k(F_{\text{tot}} - F_f) \quad (6)$$

where k is a correction factor for the glucose portion of the inulin and for the water loss during hydrolysis, F_{tot} is the total fructose content, F_f is the free fructose content. In this study, the k value was 0.995 (Saengkanuk et al. 2011).

2.7. Spread Ratio of Cookies

To measure the physical characteristics of cookies, round-shaped cookies with 5 cm diameters and 0.5 cm thickness were made and baked at 180 °C for 10 min. Cookies were analyzed for diameter (D), thickness (T) and spread ratio (D/T) (Rajiv et al. 2011). The mean of six values is presented.

2.8. Color Measurement

The color of cookie surface was measured using a CIELAB colorimeter system (CM-600d, KONIKA MINOLTA, Tokyo, Japan) for L^* , a^* and b^* , respectively. The mean of 12 values and the standard deviation values were used for further analysis.

2.9. Hardness of Cookies

The hardness of cookies (5 cm diameter and 0.5 cm thickness) made with WF, PF and JF was measured using a texture analyzer (CT3-50 kg, Brookfield, Massachusetts, USA). The measuring devices and conditions were: a load cell of 50 kg, a 6 mm diameter stainless steel cylindrical probe (TA41), the travel distance 5 mm, and the trigger force at 50 g.

2.10. Ferric Reducing Antioxidant Power (FRAP) Activity

According to the method of Benzie and Strain (1996), samples were prepared using the same method as for measuring the total phenolic compounds. FRAP was measured using a spectrophotometer at 595 nm.

2.11. 1,1-Diphenyl-2-picryl-hydrazyl (DPPH) Scavenging Activity

The DPPH radical scavenging activity of the flours and cookies were measured according to the method of Brand-Williams et al. (1995). The absorbance of the mixture was read at 490 nm (Wootton-Beard et al. 2011) using a spectrophotometer. The DPPH radical scavenging activity was calculated as follows:

$$\text{DPPH scavenging activity (\%)} = \{1 - (\text{Abs}_{\text{sample}} - \text{Abs}_{\text{blank}})\} \times 100 \quad (7)$$

where $\text{Abs}_{\text{sample}}$ is the absorbance of the mixture, and $\text{Abs}_{\text{blank}}$ is the absorbance of the mixture without a sample.

2.12. Statistical Analysis

All experiments were conducted three times, and mean values are given as results. The significant differences between treatments were evaluated by a one-way ANOVA using MS-Excel 2013.

3. RESULTS

3.1. Physico-chemical Characteristics of Flours

The results of the evaluated physico-chemical characteristics of wheat flour (WF), potato flour (PF), and Jerusalem artichoke flour (JF) are shown in Table 1. The average moisture content of WF was the highest followed by JF and PF. The crude ash content of JF was significantly different from the other flours ($p < 0.05$). The water holding capacity (WHC) and fat absorption capacity (FAC) of JF showed a significantly higher than those of WF and PF ($p < 0.05$).

Table 1: Physico-Chemical Characteristics of Flours

Characteristics	Wheat flour	Potato flour	Jerusalem artichoke flour
Moisture (%)	13.1 \pm 0.3 ^a	6.4 \pm 0.2 ^b	10.8 \pm 0.3 ^c
Crude ash	2.0 \pm 0.0 ^a	2.1 \pm 0.1 ^a	2.5 \pm 0.0 ^b
Water-holding capacity	0.5 \pm 0.0 ^a	2.7 \pm 0.0 ^b	3.7 \pm 0.2 ^c

(g water/g dry weight)			
Fat absorption capacity (g fat/g dry weight)	0.6±0.0 ^a	0.7±0.0 ^b	1.1±0.0 ^c

*a-c Means followed by different superscripts within a row were significantly different at $p < 0.05$.

3.2. Dough Rheological Analysis

3.2.1. Stress Relaxation-Small Deformation

The generalized Maxwell (GM) model (Eqn. 1) were applied to characterize the stress relaxation behavior of doughs at a small deformation 10 %. The calculated constants for models are presented in Table 2. All of the stress relaxation data at small deformation were suitably fitted with both of models ($r^2 > 0.99$). The RMSE values of GM model for cookie doughs ranged 34.1 to 220.6.

In the generalized Maxwell model, the dough of 100 % JF had a larger elastic modulus (E_1 , E_2 and E_e) and viscosity (η_1 and η_2) than other doughs. The relaxation time (λ_1 and λ_2) also showed a higher value on the dough with JF.

3.2.2. Stress Relaxation-Large Deformation

Stress relaxation data at a large deformation (60 %) were analyzed by Peleg model (Eqn. 3) and nonlinear three parameter (NT) model (Eqn. 4). The k_1 and k_2 values were calculated from the Peleg model and the A , α and F_e were determined from the NT model (Table 3). The dough samples were suitably fitted with the Peleg model ($r^2 > 0.99$), but the NT model was fitted with r^2 ranging from 0.79 to 0.88. The RMSE values of Peleg model and NT model for cookie doughs ranged 10.4 to 17.6 and 0.6-3.9, respectively. In the Peleg model, the constants (i.e., k_1 and k_2) of the control sample were significantly lower than those of other samples. Meanwhile, the doughs of 100 % PF and 100 % JF did not show any significant differences on the k_1 value. In the NT model, the addition PF and JF significantly affected the model parameters, except α value. A value (equivalent to initial force) and F_e significantly increased as the amount of PF and JF increased.

Table 2: Constants calculated for Maxwell Model for describing Stress Relaxation of Doughs

	CON	PF50	PF 100	JF50	JF 100
E_1	31.1 ±1.2 ^a	27.8 ±1.4 ^b	29.6 ±0.4 ^c	43.7 ±3.0 ^d	41.5 ±0.4 ^d
E_2	130.1 ±2.1 ^a	119.7 ±3.1 ^b	140.4 ±1.3 ^c	159.6 ±12.2 ^d	150.6 ±9.2 ^d
λ_1	18.7 ±0.0 ^a	16.3 ±0.7 ^b	12.4 ±0.3 ^c	18.2 ±0.2 ^a	20.9 ±2.5 ^a
λ_2	0.6 ±0.0 ^{ab}	0.6 ±0.0 ^a	0.5 ±0.0 ^b	0.6 ±0.0 ^{ac}	0.7 ±0.1 ^d
E_e	11.8 ±1.2 ^a	21.0 ±0.2 ^b	30.8 ±1.7 ^c	42.4 ±4.0 ^d	67.4 ±4.6 ^e
η_1	581.5	454.5	366.8	788.7	867.5

	±24.6 ^a	±40.6 ^b	±3.3 ^c	±44.9 ^d	±111.1 ^d
η_2	74.3 ±2.6 ^a	67.3 ±2.3 ^b	72.1 ±1.1 ^a	97.3 ±6.6 ^d	105.2 ±16.8 ^d
RSME	34.1	51.4	63.1	71.2	220.6

*a-c Means followed by different superscripts within a row were significantly different at $p < 0.05$.

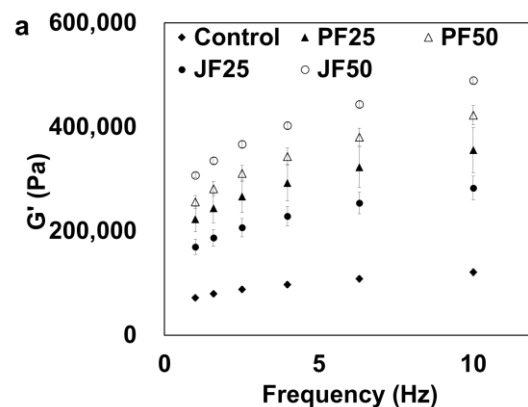
Table 3: Parameters calculated from the Peleg Model (PM) and the Nonlinear Three Parameters model (NT)

		CON	PF50	PF 100	JF50	JF 100
P M	k_1	1.1± 0.1 ^a	1.3± 0.1 ^b	2.0± 0.3 ^c	1.5± 0.0 ^d	2.0± 0.1 ^c
	k_2	1.1± 0.0 ^a	1.1± 0.0 ^b	1.2± 0.0 ^c	1.1± 0.0 ^d	1.2± 0.0 ^e
	RMSE	10.4	10.4	16.1	13.0	17.6
N T	A (N)	8.3± 0.8 ^a	14.2± 0.1 ^b	39.7± 2.9 ^c	26.2± 3.1 ^d	52.7± 5.2 ^e
	α (s ⁻¹)	0.3± 0.0 ^a	0.2± 0.0 ^b	0.2± 0.0 ^c	0.2± 0.0 ^b	0.2± 0.0 ^c
	F_e (N)	2.4± 0.3 ^a	6.0± 0.3 ^b	19.5± 0.8 ^c	10.8± 1.1 ^d	39.6± 3.1 ^e
	RMSE	0.6	1.0	2.5	1.9	3.9

*a-e Means followed by different superscripts within a row were significantly different at $p < 0.05$.

3.2.3. Dynamic Oscillatory Measurement

The mechanical spectra from the frequency sweep test on cookie doughs were shown in Fig. 1. The control dough had lower elastic modulus (G') and viscous modulus (G'') than other doughs. As the amount of PF and JF in dough increased, elastic (G') and viscous (G'') moduli increased significantly. The dough with 50 % JF showed the highest G' and G'' values. The $\tan \delta$ (G''/G') of dough with 50 % PF is higher than other doughs, but there was no difference in $\tan \delta$ between dough samples at 0 Hz, significantly, except dough with 25 % JF.



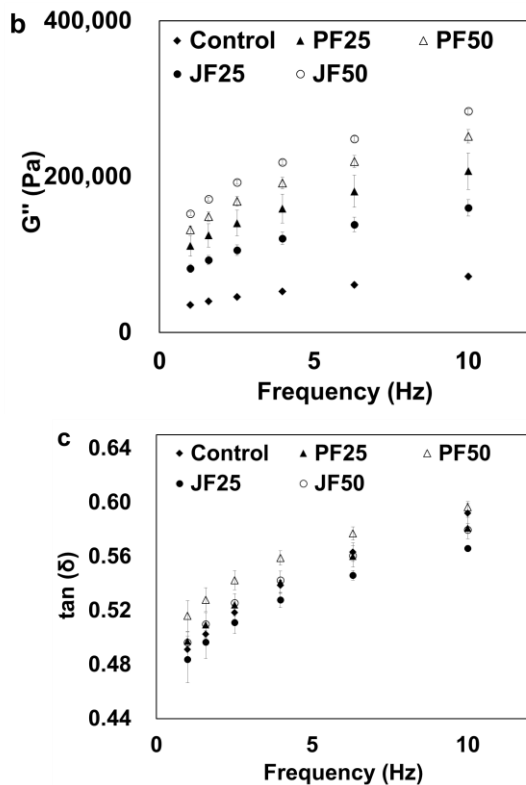


Figure 1: Mechanical Spectra of Dough Containing Different Flours

3.3. Microstructure of Flour, Dough and Cookie

Structural differences between WF, PF, and JF were clearly shown in Fig. 2. WF showed the starch granules with round shape. PF showed the smooth surface. Many small granules were observed in JF. The micrographs of dough and cookies with WF, PF, and JF are presented in Fig. 3. The dough with JF 50 % (Fig. 3c) showed a more cohesive structure than the control (Fig. 3a) and dough with PF 50 % (Fig. 3b). The surfaces of cookie with JF showed the deeper fractures (Fig. 3f).

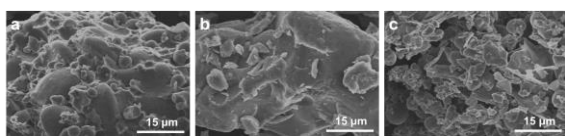


Figure 2: Scanning Electron Micrographs of Flours a) WF b) PF c) JF (Magnification: 2,000).

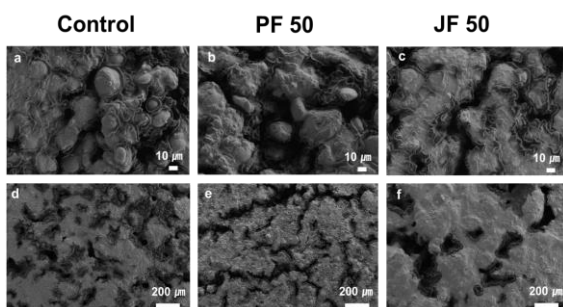


Figure 3: Scanning Electron Micrographs of Surface of Dough (a-c), Surface Fractures of Cookies (d-f).

Dough at magnification of 1,500, surface of fractures of cookies at magnification of 200.

3.4. Determination of Inulin Content in Cookies

The inulin content of cookies made with different amounts of JF was measured and calculated using Eqn. (6) (Table 4). The amount of inulin in the control sample was close to 0 %, and as the proportion of JF increased, the amount of inulin in the cookies increased. The inulin content in the cookies made from 100 % JF was 42.7 (± 1.7) %.

Table 4: Inulin Content of Cookies

	Content of sugar (dry wt. %)		
	Total fructose (F_{tot})	Free fructose (F_f)	Inulin
CON	0.0 \pm 0.8 ^a	0.3 \pm 0.0 ^a	-0.3 \pm 0.8 ^a
PF50	3.5 \pm 0.8 ^b	0.4 \pm 0.0 ^b	3.1 \pm 0.7 ^b
JF50	27.8 \pm 1.6 ^d	0.4 \pm 0.0 ^d	27.3 \pm 1.6 ^d
JF100	43.1 \pm 1.7 ^e	0.3 \pm 0.0 ^e	42.7 \pm 1.7 ^e

*a-e Means followed by different superscripts within a column were significantly different at $p < 0.05$.

3.5. Spread Ratio of Cookies

The spread ratios were measured by the ratio of the thickness to the diameter of cookies with 100 % WF, 50 and 100 % PF and JF (Table 5). The spread ratio of cookies with 50 % PF was not significantly different from that of the cookies with 100 % JF ($p < 0.05$). Cookies with PF and JF did not expand in either diameter or thickness. However, the spread ratio of cookies with only WF was lower because they expanded in both diameter and thickness.

Table 5: Spread Ratio of Cookies

	Cookie diameter (cm)	Cookie thickness (cm)	Diameter(D)/Thickness(T)
CON	5.3 \pm 0.1 ^a	1.1 \pm 0.1 ^a	5.0 \pm 0.5 ^a
PF50	5.2 \pm 0.1 ^b	1.0 \pm 0.1 ^b	5.1 \pm 0.6 ^b
PF100	5.0 \pm 0.0 ^c	0.8 \pm 0.1 ^c	6.1 \pm 0.6 ^c
JF50	5.0 \pm 0.0 ^d	0.7 \pm 0.0 ^d	6.7 \pm 0.4 ^d
JF100	5.0 \pm 0.1 ^{cd}	0.9 \pm 0.1 ^e	5.4 \pm 0.4 ^b

*a-e Means followed by different superscripts within a column were significantly different at $p < 0.05$.

3.6. Color Properties

The color on the surface of cookies was measured (Table 6). The images of cookie containing PF and JF are shown in Fig. 4. The lightness value (L^*) of cookies prepared with PF and JF decreased compared to the control cookie. As the amount of PF and JF increased, the a^* and b^* values increased. The a^* and b^* values showed higher values on the surface of the cookie with 100 % JF. All the color values did not show any significant differences between cookie with 100 % PF and 50 % JF.

Table 6: Color of Cookies made from Potato Flour (PF) and Jerusalem artichoke Flour (JF)

	L*	a*	b*
CON	84.4±1.4 ^a	1.8±0.6 ^a	27.1±0.9 ^a
PF50	73.2±3.2 ^b	6.8±2.0 ^b	32.3±2.1 ^b
PF100	63.0±1.1 ^c	13.2±0.7 ^c	38.9±0.4 ^c
JF50	63.1±4.0 ^c	13.6±1.5 ^c	38.8±0.5 ^c
JF100	57.7±3.2 ^d	15.1±0.9 ^d	39.1±1.0 ^c

*a-d Means followed by different superscripts within a column were significantly different at $p < 0.05$.



Figure 4: Cookies made from Wheat Flour (WF), Potato Flour (PF) and Jerusalem artichoke Flour (JF).

3.7. Texture Property of Cookies

The effect of the addition of JF on the hardness of cookie was measured (Table 7). As the amount of JF increased, the hardness of the cookie was increased. Between cookies with PF had no significant difference ($p < 0.05$).

3.8. Nutritional Properties of Flours and Cookies

Antioxidant activities in flours and cookies are shown in Table 7, respectively. DPPH radical scavenging activity and FRAP activity were used to evaluate the antioxidant activities of samples. Both DPPH and FRAP in samples with JF were significantly higher than for other flours. The antioxidant activities of cookies were lower than those of flours because other mixed ingredients, such as egg, butter, and sugar, have low antioxidant levels. The cookies with JF showed higher antioxidant activities than those with PF.

Table 7: Hardness of Cookies and Antioxidant Activities of Flour and Cookies

		Hardness (g)	DPPH radical scavenging activity (%)	FRAP activity (O.D. 595 nm)
Flour	WF	-	20.8 ± 1.7 ^a	0.1 ± 0.0 ^a
	PF	-	52.9 ± 2.2 ^b	0.1 ± 0.0 ^b
	JF	-	58.1 ± 1.3 ^c	0.1 ± 0.0 ^c
Cookie	CON	6204.2 ± 970.7 ^a	13.3 ± 2.4 ^d	0.1 ± 0.0 ^a
	PF50	3072.5 ± 348.1 ^b	35.9 ± 0.8 ^e	0.1 ± 0.0 ^b
	PF100	3338.3 ± 265.2 ^b	-	-
	JF50	7720.0 ± 330.0 ^c	51.1 ± 1.9 ^b	0.1 ± 0.0 ^d

JF100	13574.2 ± 495.6 ^d	55.4 ± 1.7 ^c	0.1 ± 0.0 ^c
-------	------------------------------	-------------------------	------------------------

*a-d Means followed by different superscripts within a column were significantly different at $p < 0.05$.

4. DISCUSSION

4.1. Flour Properties

The crude ash content of JF was higher than other flours because the major component of JF is inulin, a non-digestible carbohydrate (Rinaldoni et al. 2012). The WHC and FAC of flours are highly related to the compositions of flours. According to Raymundo et al. (2014), the amount of water-uptake increased as the level of fibers in flour increased. Generally, a large number of hydroxyl groups existing in the fiber structure allows more water interactions through hydrogen bonding (Ellouze-Ghorbel et al. 2010). In addition, the binding of oils depends on the surface availability of hydrophobic amino acids and other non-polar side chains of dietary fiber components (Benítez et al. 2013). This demonstrates that JF might be a good natural ingredient for cookies due to its high content of inulin (Zahn et al. 2010, Aravind et al. 2012).

4.2. Effect of JF on the Rheological Behavior of Dough

The rheological behaviors of dough samples were interpreted using the viscoelastic models. In the stress relaxation test at small deformation, the constants estimated from the generalized Maxwell model showed that elasticity and the viscosity of doughs were significantly different from the amount of PF and JF in doughs. The relaxation time (λ_1 and λ_2) of dough indicating the flexibility of dough is the useful parameter to determine how well the dough are applied to the processing. At a higher value of the relaxation time, the dough requires more time to reach to a new equilibrium status and it would be an inappropriate for dough handlings such as flatter and sheeting with a fast processing time (Bhattacharya 2010). The first term of the relaxation time (λ_1) showed no significant difference from that of the control dough. This implies that the addition of JF could be appropriate for the dough processing with slight modification of processing time.

The results from the stress relaxation test at large deformation were in accordance with those at small deformation. In the Peleg model, a high k_1 value shows a noticeable elastic behavior. The k_2 value indicates the degree of solidity and it varies from 1, for an ideal liquid, to infinity, for an ideal elastic solid where the stress does not relax at all (Peleg and Normand 1983, Fu et al. 2014). Thus, the dough with JF had more elastic characters than other doughs. In the NT model, the A value indicates the force at the beginning of relaxation test. Hence, the high A value requires a high resistive force which may not be a desirable condition for dough processing. Since the A values of dough with JF were higher than those of others, the processing ability such as flatter or sheeting of the dough with

JF was lower. The exponential decay (α) indicates the rate of decaying from the initial force to the residual force. The α values became lower as the amount of PF and JF in dough increased. Based on the model parameters, addition of JF appears to be less workable than the control.

The viscoelastic properties of dough have been studied using Maxwell or the Peleg model based on the stress relaxation data. Rodríguez-Sandoval et al. (2009) characterized the stress relaxation behavior of cassava dough with a model included two Maxwell elements with a residual spring in parallel and Peleg model. The dough properties were compared by the cooking time and methods, and the storage temperature. Bhattacharya (2010) also used both models to explain viscoelastic behavior of moth bean flour dough. The author performed the stress relaxation tests at low and large deformation and the 4 elements Maxwell model was chosen based on the r^2 value. In this study, Peleg model was less suitable to describe the rheological behavior of doughs affected by different moisture contents. The NT model proposed by Yadav et al. (2006) suitably described the effect of the moisture content in dough within 27 to 39 % on the rheological properties of dough. Bhattacharya (2010) also used the NT model to interpret the handling characteristics of moth bean flour dough with varied moisture contents in the range of 28 to 34 % and 40 to 46 %. The NT model was more suitable to describe the rheological behavior of doughs with high level of moisture content (Yadav et al. 2006, Bhattacharya 2010). The NT model parameters were sensitive particularly at low moisture content (25%) and higher strain level (75%). In our study, most of models suitably described the rheological behavior of doughs, but the NT model was not appropriate ($r^2=0.79-0.88$) than other models. This may be because our dough samples had a low level of moisture content (below 17 %).

Addition of JF into the cookie dough significantly influenced the dynamic rheological properties of the dough. According to the mechanical spectra, G' was higher than G'' ($\tan \delta < 1$) in the applied frequency range indicating solid elastic like behavior for all dough samples (Šeremešić et al. 2013; Sarabhai and Prabhasankar 2015). Both PF and JF increased the elastic properties, but adding JF more increased the elastic characters of dough. The inulin in JF might enhance to form network structures on cookie dough and increased the elasticity of dough. It implies that addition of JF may have a limitation to add in the dough although JF gives many benefits to the products. Recent studies on dough proposed the JF as a replacement of wheat flour because it influenced significantly the thermo-mechanical properties of dough. Addition of JF influenced positively the rheological properties of dough, bringing about its strengthening in concentration up to 10% of total amount of flour (Gedrovica and Karklina 2011).

The inulin in JF dramatically increased the water absorption properties of the cookie dough. High water

absorption properties increased the elastic behavior of dough (Petrović et al. 2015). This is in agreement with the high G' values observed from the dough with JF. Similarly, Raymundo et al. (2014) reported that the G' values of biscuit dough increased by adding the Psyllium flour as fiber abundant ingredient. The higher fiber content of Psyllium flour related to increasing G' values of the dough because of its strong water absorption ability, the possibility of establishment of interactions between other ingredients. Moreover, the structure of flour granules affects the dough characteristics. As shown in Fig. 3, the small granules aggregated in the dough with JF dough showed more complex structures which gives more possibility to interact with other ingredients. According to Schiedt et al. (2013), the interaction between starch and proteins in the dough increases the elastic nature of the dough. The small granules of JF observed in the microscopic image provides a visual evidence that the elastic behavior of the dough increased with the addition of JF.

Consequently, low deformation experiments can generate data to understand the behavior of dough and the aspects of structural features and large strain non-linear deformation data are suitable for practical aspects of cookie dough handling (Bhattacharya 2010).

4.3. Effect of JF on the Physical Properties of Cookie

A high content of inulin in cookies made from JF implies that the physical properties, such as structure, color, and texture, of dough and cookies with JF. Many studies have showed that the physical properties of cookies with inulin were very different from those of cookies with WF only. Inulin has been used as a replacement for sugar or fat in bakery products (Zoulias et al. 2002, Zahn et al. 2010). According to previous studies, the addition of inulin to baked goods plays an important role in the overall appearance and crumb structure of baked products by replacing wheat, sugar, and fat. In our study, the inulin in JF influenced the cookie hardness by forming a firm structure. Several studies on the effect of inulin on the physical and sensory properties of baked products have shown that those baked products that included inulin had hard and brittle characteristics (Zoulias et al. 2002; Zahn et al. 2010; Morris and Morris 2012). This is because the baked product, with a low concentration of gluten, was not able to expand properly after baking (Rodríguez-García et al. 2012). Other researchers have observed that inulin or fiber-based fat replacers increased crumb firmness (hardness) in muffins (Zahn et al. 2010).

The high WHC and FAC of JF, mainly due to the inulin in JF, highly influenced the micro structure of dough samples. The structure differences caused by inulin have been applied in the formation of new structures to replace fat or sugar in baked products (Zoulias et al. 2002, Zahn et al. 2010). As the gluten content decreased, the structure became cohesive, and eventually, some part of structure became cracked (Fig. 3f). Rosell et al. (2009) studied the structure of inulin and found that inulin is composed of granular particles with numerous

aggregates with modular shapes. Our results demonstrated that the addition of JF changed the internal structure of cookies to more compact (Fig. 3) and consequently the surface of cookies became more fractured (Fig. 4).

The spread ratios indicate the spread ability of dough during baking. It might be due to the changes in the use of free water in the cookie dough. Generally, adding an ingredient having higher water retention properties into wheat dough results in aggregates with increased competitive capacity for the limited free water present in cookie dough. Rapid partitioning of free water to these hydrophilic sites, occurring during dough mixing, results in a decreased solution of sugar, increased concentration of the solution and greater internal dough viscosity (Hooda and Jood 2005, Rajiv et al. 2011). Such partitioning of free water due to an ingredient having a high WHC would limit gluten and starch hydration during mixing and baking, resulting in a less developed structure. Thus, adding JF or PF, which have higher WHC, holds more free water than dough made with only WF, consequently lowering the spread ability of cookie dough during baking. A similar behavior was found in the sponge cake process, where the height of a sponge cake with inulin was lower than one without inulin (Rodríguez-García et al. 2012). Moreover, the amount of free water in the dough was reduced by adding JF, so that it caused an insufficient hydration of proteins and their conversion into a suitably developed gluten network. Thus, the protein matrix interacted with the starch granules may not be changed during cooking (Raymundo et al. 2014).

4.4. Effect of JF on the Cookie Characteristics by Maillard reaction

The formation of color and flavor in the crust of all bakery products during baking is the result of the Maillard reaction of caramelization. The Maillard reaction involves condensation of amino groups and reducing sugars that result in the formation of intermediate chemical compounds that ultimately polymerize to form brown pigments (Isleroglu et al. 2012).

The level of inulin in cookies with JF might accelerate the chemical reactions involved in the surface color of cookies. The surface color of cookies is an important quality associated with flavor, texture, and appearance characteristics that are important to consumers and is often used as an indicator of baking completion. During baking, the fructan chains of inulin in JF were degraded, leading to the formation of new low-molecular weight products on the crusty surface, and eventually, the Maillard reaction of the crust of baked goods could be accelerated (Poinot et al. 2010). Similar results have been reported by Sharma and Gujral (2014) where a slight increase in non-enzymatic browning upon baking was observed as the proportion of barley flour increased. In our study, the changes in color and degree of browning showed a positive influence from the addition

of JF and demonstrated that JF can be used to improve the consumer acceptance of flavor and color.

The high antioxidant activities in samples with JF might be associated with a higher degree Maillard reaction due to the inulin. Many previous studies have had similar results. Bressa et al. (1996) reported that antioxidant activities in butter cookies could be increased by producing a brown compound using the Maillard reaction. According to Zeng et al. (2011), as heating time increased, DPPH radical scavenging increased because of the Maillard reaction with fructose in psicose-lysine and fructose-lysine model systems. Vhangani and Wyk (2013) also showed that the antioxidant activity associated with the Maillard reaction in the fructose-lysine model based on DPPH radical scavenging activity was increased with an increase in the reaction temperature and time. The antioxidant activities of cookies with JF were higher than those of the control cookies with only WF due to inulin in JF and to the degree of the Maillard reaction during baking. These results demonstrated that the addition of JF could enhance the nutritional characters of cookies.

5. CONCLUSIONS

Jerusalem artichoke flour (JF) presented better physico-chemical characteristics, adequate texture properties of dough and cookies and improved nutritional properties in compared with potato flour (PF). Notably, the inulin content in the cookies made from 100 % JF was 42.7 (± 1.7) %. Increasing the amount of JF in the dough enhanced the elastic properties of cookie dough. The inulin in JF mainly contributed to change the internal structures, and the structural changes due to the inulin were reflected in the stress relaxation and dynamic oscillatory data. The increase of water holding capacity and fat absorption capacity associated with the inulin in JF directly related to the rheological properties of dough. The cookies with JF showed the highest values of hardness. This might be due to the firm structure in the baked products associated with the inulin in JF. The internal structure, illustrated by the micrographs, showed the cohesive structure of dough and cookies with JF. JF also affects the appearance of the product and chemical changes. The cookies with JF had a suitable surface color. The Maillard reaction due to inulin content caused changes in the surface color of cookies. In addition, the antioxidant activities of cookies with JF were higher than those of the controls (with only WF) due to the inulin in JF being highly related to the degree of Maillard reaction during baking. Such comprehensive research can be used to develop cookies with JF for improved consumer acceptance of texture, flavor and color.

ACKNOWLEDGMENTS

This research was financially supported by the Ministry of Trade, Industry and Energy (MOTIE) and Korea Institute for Advancement of Technology (KIAT)

through the Promoting Regional specialized Industry (R0004761-1).

REFERENCES

- AOAC. 2000. Official methods of analysis 19th. Washington: Association of Official Analytical Chemists.
- Aravind N., Sissons M.J., Fellows C.M., Blazek J., Gilbert E.P., 2012. Effect of inulin soluble dietary fibre addition on technological, sensory, and structural properties of durum wheat spaghetti. *Food Chemistry*, 132 (2), 993–1002.
- Bach V., Kidmose U., Bjørn G.K., Edelenbos M., 2012. Effects of harvest time and variety on sensory quality and chemical composition of Jerusalem artichoke (*Helianthus tuberosus*) tubers. *Food Chemistry*, 133 (1), 82–89.
- Benítez V., Cantera S., Aguilera Y., Mollá E., Esteban R.M., Díaz M.F., Martín-Cabrejas, M.A., 2013. Impact of germination on starch, dietary fiber and physicochemical properties in non-conventional legumes. *Food Research International*, 50 (1), 64–69.
- Benzie I.F.F., Strain J.J. 1996. The ferric reducing ability of plasma (FRAP) as a measure of “Antioxidant Power”: The FRAP assay. *Analytical Biochemistry*, 239 (1), 70–76.
- Bhattacharya S., 2010. Stress relaxation behaviour of moth bean flour dough: Product characteristics and suitability of model. *Journal of Food Engineering*, 97 (4), 539–546.
- Brand-Williams W., Cuvelier M.E., Berset C., 1995. Use of a free radical method to evaluate antioxidant activity. *LWT-Food Science and Technology*, 28 (1), 25–30.
- Bressa F., Tesson N., Rosa M.D., Sensidoni A., Tubaro F., 1996. Antioxidant effect of maillard reaction products: Application to a butter cookie of a competition kinetics analysis. *Journal of Agricultural and Food Chemistry*, 44 (3), 692–695.
- Chen H., Rubenthaler G.L., Schanus E.G., 1988. Effect of apple fiber and cellulose on the physical properties of wheat flour. *Journal of Food Science*, 53 (1), 304–305.
- Ellouze-Ghorbel R., Kamoun A., Neifar M., Belguith S., Ayadi M.A., Kamoun A., Ellouze-Chaabouni S., 2010. Development of fiber-enriched biscuits formula by a mixture design. *Journal of Texture Studies*, 41 (4), 472–491.
- Filipčev B., Šimurina O., Hadnađev T.D., Jevtić-Mučibabić R., Filipović V., Lončar B., 2015. Effect of liquid (native) and dry molasses originating from sugar beet on physical and textural properties of gluten-free biscuit and biscuit dough. *Journal of Texture Studies*, 46 (5), 353–364.
- Fu J.T., Shiao S.Y., Chang R.C., 2014. Effect of calamondin fiber on rheological, antioxidative and sensory properties of dough and steamed bread. *Journal of Texture Studies*, 45 (5), 367–376.
- Gedrovica I., Karklina D., 2011. Influence of Jerusalem artichoke powder on dough rheological properties. In *Proceedings of the 6th Baltic Conference on Food Science and Technology*, pp. 5-6, May 5-6, Jelgava (Latvia, Europe)
- Gupta M., Bawa A.S., Abu-Ghannam N., 2011. Effect of barley flour and freeze-thaw cycles on textural nutritional and functional properties of cookies. *Food and Bioproducts Processing*, 89 (4), 520–527.
- Hooda S., Jood S., 2005. Organoleptic and nutritional evaluation of wheat biscuits supplemented with untreated and treated fenugreek flour. *Food Chemistry*, 90 (3), 427–435.
- Isleroglu H., Kemerli T., Sakin-Yilmazer M., Guven G., Ozdestan O., Uren A., Kaymak-Ertekin F., 2012. Effect of steam baking on acrylamide formation and browning kinetics of cookies. *Journal of Food Science*, 77 (10), 257–263.
- Lee E.H., Kang S.M., 2009. Effect of diet food containing Jerusalem artichoke's inulin, lotus leaf, and herb on weight and body fat of obesity university students. *Journal of Applied Biological Chemistry*, 52 (1), 8-14.
- Lin M.J.Y., Humbert E.S. Sosulski F.W., 1974. Certain functional properties of sunflower meal products. *Journal of Food Science*, 39 (2), 368-370.
- Lingyun W., Jianhua W., Xiaodong Z., Da T., Yalin Y., Chenggang C., Tianhua F., Fan, Z., 2007. Studies on the extracting technical conditions of inulin from Jerusalem artichoke tubers. *Journal of Food Engineering*, 79 (3), 1087–1093.
- Mancebo C.M., Rodriguez P., Gómez M., 2016. Assessing rice flour-starch-protein mixtures to produce gluten free sugar-snap cookies. *LWT - Food Science and Technology*, 67 (1), 127–132.
- Meyer D., Bayarri S., Tárrega A., Costell E., 2011. Inulin as texture modifier in dairy products. *Food Hydrocolloids*, 25 (8), 1881–1890.
- Mickley H.S., Sherwood T.K., Reed C.E., 1957. *Applied Mathematics in Chemical Engineering*. McGraw-Hill Book Co., New York, NY.
- Morris C., Morris G.A., 2012. The effect of inulin and fructo-oligosaccharide supplementation on the textural, rheological and sensory properties of bread and their role in weight management: A review. *Food Chemistry*, 133 (2), 237–248.
- Niness K.R., 1999. Inulin and oligofructose: what are they? *The Journal of Nutrition*, 129 (7), 1402S–1406S.
- Pedersen L., Kaack K., Bergsøe M.N., Adler-Nissen J., 2004. Rheological properties of biscuit dough from different cultivars, and relationship to baking characteristics. *Journal of Cereal Science*, 39 (1), 37–46.
- Peleg M., Normand, M.D., 1983. Comparison of two methods for stress relaxation data presentation of solid foods. *Rheologica Acta*, 22 (1), 108–113.
- Peressini D., Sensidoni A., 2009. Effect of soluble dietary fibre addition on rheological and

- breadmaking properties of wheat doughs. *Journal of Cereal Science*, 49 (2), 190–201.
- Petrović J., Fišteš A., Rakić D., Pajin B., Lončarević I., Šubarić D., 2015. Effect of defatted wheat germ content and its particle size on the rheological and textural properties of the cookie dough. *Journal of Texture Studies*, 46 (5), 374–384.
- Poinot P., Arvisenet G., Grua-Priol J., Fillonneau C., Le-Bail A., Prost C., 2010. Influence of inulin on bread: Kinetics and physico-chemical indicators of the formation of volatile compounds during baking. *Food Chemistry*, 119 (4), 1474–1484.
- Rajiv J., Lobo S., Lakshmi A.J., Rao G.V., 2012. Influence of green gram flour (*phaseolus aureus*) on the rheology, microstructure and quality of cookies. *Journal of Texture Studies*, 43 (5), 350–360.
- Raymundo A., Fradinho P., Nunes M.C., 2014. Effect of Psyllium fibre content on the textural and rheological characteristics of biscuit and biscuit dough. *Bioactive Carbohydrates and Dietary Fibre*, 3 (2), 96–105.
- Rinaldoni A.N., Campderrós M.E., Padilla A.P., 2012. Physico-chemical and sensory properties of yogurt from ultrafiltered soy milk concentrate added with inulin. *LWT-Food Science and Technology*, 45 (2), 142–147.
- Rodríguez-García J., Puig A., Salvador A., Hernando, I., 2012. Optimization of a sponge cake formulation with inulin as fat replacer: Structure, physicochemical, and sensory properties. *Journal of Food Science*, 77 (2), C189–C197.
- Rodríguez-Sandoval E., Fernández-Quintero A., Cuvelier G., 2009. Stress relaxation of reconstituted cassava dough. *LWT-Food Science and Technology*, 42 (1), 202–206.
- Rosell C.M., Santos E., Collar C., 2009. Physico-chemical properties of commercial fibres from different sources: A comparative approach. *Food Research International*, 42 (1), 176–184.
- Saengkanuk A., Nuchadomrong S., Jogloy S., Patanothai A., Srijaranai S., 2011. A simplified spectrophotometric method for the determination of inulin in Jerusalem artichoke (*Helianthus tuberosus* L.) tubers. *European Food Research and Technology*, 233 (4), 609–616.
- Sarabhai, S., Prabhasankar P., 2014. Influence of whey protein concentrate and potato starch on rheological properties and baking performance of Indian water chestnut flour based gluten free cookie dough. *LWT-Food Science and Technology*, 63 (2), 1301–1308.
- Schiedt B., Baumann A., Conde-Petit B., Vilgis T.A., 2013. Short- and long-range interactions governing the viscoelastic properties during wheat dough and model dough development. *Journal of Texture Studies*, 44 (4), 317–332.
- Schober T.J., O'Brien C.M., McCarthy D., Darnedde A., Arendt E.K., 2003. Influence of gluten-free flour mixes and fat powders on the quality of gluten-free biscuits. *European Food Research and Technology*, 216 (5), 369–376.
- Šeremesic M.M., Dokić L., Nikolić I., Radosavljević M., Simović D.Š., 2013. Rheological and textural properties of short (cookie) dough made with two types of resistant starch. *Journal of Texture Studies*, 44 (2), 115–123.
- Sharma P., Gujral H.S., 2014. Antioxidant potential of wheat flour chapattis as affected by incorporating barley flour. *LWT - Food Science and Technology*, 56 (1), 118–123.
- Tang C.H., 2007. Functional properties and in vitro digestibility of buckwheat protein products: Influence of processing. *Journal of Food Engineering*, 82 (4), 568–576.
- Torbica A., Hadnađev M., Hadnađev T.D., 2012. Rice and buckwheat flour characterisation and its relation to cookie quality. *Food Research International*, 48 (1), 277–283.
- Vhangani L.N., Wyk J.V., 2013. Antioxidant activity of Maillard reaction products (MRPs) derived from fructose-lysine and ribose-lysine model systems. *Food Chemistry*, 137 (1–4), 92–98.
- Wootton-Beard P.C., Moran A., Ryan L., 2011. Stability of the total antioxidant capacity and total polyphenol content of 23 commercially available vegetable juices before and after in vitro digestion measured by FRAP, DPPH, ABTS and Folin-Ciocalteu methods. *Food Research International*, 44 (1), 217–224.
- Yadav N., Roopa B.S., Bhattacharya S., 2006. Viscoelasticity of a simulated polymer and comparison with chickpea flour doughs. *Journal of Food Process Engineering*, 29 (3), 234–252.
- Zahn S., Pepke F., Rohm H., 2010. Effect of inulin as a fat replacer on texture and sensory properties of muffins. *International Journal of Food Science and Technology*, 45 (12), 2531–2537.
- Zeng Y., Zhang X., Guan Y., Sun Y., 2011. Characteristics and antioxidant activity of maillard reaction products from psicose-lysine and fructose-lysine model systems. *Journal of Food Science*, 76 (3), 398–403.
- Zoulias E.I., Oreopoulou V., Kounalaki E., 2002. Effect of fat and sugar replacement on cookie properties. *Journal of the Science of Food and Agriculture*, 82 (14), 1637–1644.
- Zucco F., Borsuk Y., Arntfield, S.D., 2011. Physical and nutritional evaluation of wheat cookies supplemented with pulse flours of different particle sizes. *LWT-Food Science and Technology*, 44 (10), 2070–2076.

SUSTAINABLE DISTRIBUTION SYSTEM IN FOOD RETAIL SECTOR- A SIMULATION MODELLING APPROACH

Sameh M. Saad ^(a), Ramin Bahadori ^(b), Jishnu Ravisankar ^(c)

^{(a), (b), (c)} Department of Engineering and Mathematics,
Sheffield Hallam University, City campus Howard street Sheffield S1 1WB, UK

^(a)S.Saad@shu.ac.uk, ^(b)b2047010@my.shu.ac.uk, ^(c)b6001595@my.shu.ac.uk

ABSTRACT

Nowadays, sustainability has become one of the most important topics in supply chain management which is received more global attention. Within food retail supply chain, downstream distribution system has a significant effect on environmental performance. The aim of this research is to model sustainable distribution system in food retail supply chain through two variables; Greenfield service constraints and fleet types which enables practitioners to make decision about the optimal number and location of distribution facilities and optimal types of fleet to minimise the CO₂ emission and transportation cost, maximise responsiveness and determine the optimal number of required transportation asset to meet customers demand. Through understanding the mathematical equations governing the problem of CO₂ emission, transportation cost and transportation time; multiple scenarios through a hypothetical two-stage food supply chain are created and validated using Supply Chain GURU Software. Experimental factorial design and statistical techniques are used to generate and analyse the results.

Keywords: modelling and simulation, sustainable distribution system, food retail supply chain

1. INTRODUCTION

Nowadays, sustainable supply chain is motivating many of the industrialists to meet customers, stakeholders and government's expectation through three dimensions of sustainable development including economic, environmental and social (Seuring and Müller 2008). Implementation of sustainable supply chain management is not voluntary, but it is a necessary requirement (Carter and Rogers 2008). While, there are different interpretations of sustainability there is a basic concept among all interpretations which is triple approach of sustainability; economic, environmental and social (Elkington 1997). In sustainable supply chain, environmental, social and ethical criterion should be considered by all supply chain members from upstream stage to downstream stage (Lerberg Jorgensen and Steen Knudsen 2006). Initiative to achieve sustainability in supply chain can be done by undertaking strategies, tactics and operational planning which are resulted in making sustainable decisions in

network design, purchasing, freight transportation manufacturing and information technology (Allaoui et al. 2017).

Food industry is one such example for a dynamic type of environment where the expectation of customer's quality and availability of food is high. The awareness of retail firms in procuring green supply chain promotes high consciousness in delivering sustained food products to customers (Beske et al. 2014). The food supply chain can be distinguished from other kind of supply chains in terms of parties which are involved, features of process and product, and alternative redesign strategies (Van Der Vorst et al. 2009). Food supply chain includes vast variety of process centres like procurement and manufacturing companies, distributors, wholesale, retailers and food service firms deal with vegetable or animal-based products which each should acquire sustainability to develop long term relationship with the customers (Mattevi and Jones 2016). In terms of food products characteristics, seasonal production, quality constraints (e.g. degree and speed of decay), special condition requirements for transportation and storage, high demand frequency and etc. can be noted.

Within the field of food supply chains reducing the product waste which is caused by surplus food in each day, travelling distance of a product before it reaches to the target consumers and all greenhouse gas emissions related to the business processes in the supply chain network can make a green food supply chain (Van Der Vorst et al. 2009). In this research, the sustainability discussion focuses on the food distribution system design.

Distribution system consists of various activities which are differing according to the product and its market (Schary and Larsen 2001). Transportation is the basic link between each node in a supply chain and can be considered as the greatest pollution making factor in a logistics system. In a supply chain, distribution of product and the emission caused by transportation are the major environmental concern (Validi et al. 2014a). Matthews, Hendrickson, and Weber (2008) claimed that about 80% of CO₂ emission in a supply chain is the direct emission from transportation. Facility location, capacity of facility, the technologies used in the facilities and the transportation system provides a

framework on creating a strategic approach to implement a sustainable distribution system in a supply chain (Salem and Haouari 2016). Food industry is the biggest user of transportation which constantly increases pollution by GHG and congestion. In the traditional methodologies, the food market distribution is handled by transportation and storage of perishable food products which is not sufficient to execute a sustainable environment on today's distribution system (Aghazadeh 2004). A traditional distribution system is controlled by a series of independent enterprises which are making their own decisions about inventory and products (Scharly and Larsen 2001). These days, incorporating the environmental management principles into the operational decision-making process is the main challenge for the modern logistics system.

As part of global warming the green supply chain become a major trend for every organisation agenda and the government issues policies to fabricate supply chain sustainable. For the last couple of decades, there is research going on for location routing and fleet designing for reducing carbon foot-print from the network to implement sustainable supply chain (Lee et al. 2010). Location routing is done to optimise the product and vehicle movement based on the demand in the supply chain to deliver the product from primary stage to the end customers (Validi et al. 2014b). Optimum positioning the distribution centres will reduce the carbon foot-print throughout the system and also affect the financial and social aspect in a supply chain. There are different kinds of optimisation techniques adapted by the researchers to optimise the transportation system to achieve sustainable distribution system. For instance, Schwardt and Fischer (2009) developed a self-organised mapping technique to optimise vehicle routing problem. Marinakis et al. (2008) developed Honey Bees Mating algorithm to resolve location routing problem in distribution system. Bell and McMullen (2004) presented the Ant Colony Optimisation technique to analyse and optimise vehicle routing problems.

In the next section, sustainable distribution system through multiple scenarios is modelled for a hypothetical two stage supply chain involved in the distribution of food and beverage in the United Kingdom. To achieve the aim of this study, three methodologies are used; Greenfield analysis is used to identify the optimal number and location of facilities with different service constraints. Greenfield analysis can be useful for determining the location of a new facility in a regional configuration. In this method, the objective is to minimise the weighted total distance, where the demand of the customer is used as the weight. This method of analysis is quite frequently used in industries to determine the best location for a new and existing facility by which the location is indicated by latitude and longitude. This will be involved to optimise the travelling distance, travelling time, transportation routes etc. to consummate sustainability in food supply chain. Moreover, fleet route optimisation is used to

minimising empty kilometres through outbound shipment consolidation to optimise the delivery routes. In addition, results are generated and analysed by using experimental factorial design and statistical techniques (MANOVA). Results obtained from these methodologies are shown in Section 3. Section 4 presents the optimisation of fleet type selection. The last part of this paper gives the overall conclusion of this study.

2. SUSTAINABLE DISTRIBUTION SYSTEM MODELLING THROUGH HYPOTHETICAL TWO-STAGE FOOD SUPPLY CHAIN

A large British food and beverage company wanted to determine the best number and location for DC facilities as well as optimal type and number of required fleet to meet customers demand for its national operations with multi objective approach; minimise the CO₂ emission and transportation cost and maximise responsiveness. The company has 10% market share and serves 350 stores around the country (see Figure 1). In this case, the demand is considered to be 10% of the population of the city/town of stores location with respect to (Census, 2011).

There are two types of fleet available at the company; rigid 7.5 tonne and rigid 17 tonne with following attributes as shown in table 1.

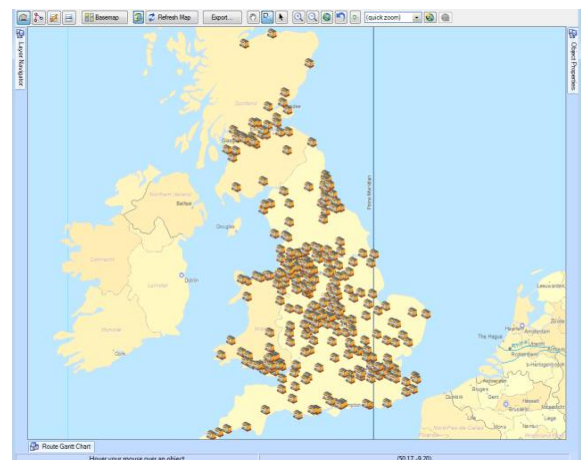


Figure 1: Supply Chain Guru Screen Shot of the Considered Stores

Table 1: Fleet Types Attributes

	Rigid 7.5 tonne	Rigid 17 tonne
CO ₂ rate	0.0005442 kg per km	0.0007273 kg per km
Average transportation cost	£2.1 per km	£2 per km
Tare weight	3500 kg	9000 kg
weight fill level	1000 kg	3000 kg
weight capacity	3000 kg	8000 kg
Velocity	90 km/h (56 mile/h)	90 km/h (56 mile/h)

To achieve the company operational objectives, three scenarios through two variables; Greenfield Service Constraints and fleet types are created and validated using Supply Chain GURU Simulation Software. Greenfield analysis is used to identify the optimal number and location of DC facilities with different service constraints which is 100% of customer served within max sourcing distance of 113 km (first scenario), 161 km (second scenario) and 209 km (third scenario). Moreover, fleet route optimisation is applied on each scenario to minimising empty kilometres through outbound shipment consolidation to optimise the delivery routes. The output data is used to investigate performance measures impact of the different fleet designs.

The following equations are used to calculate the CO₂ emission, transportation cost and transportation time.

$$CO_{2e} = (F_w + SH_w) \times R_{CO_{2e}} \times T_d \quad (1)$$

Where

CO_{2e}= CO₂ emission

F_w=Tare weight of fleet

SH_w= Weight of shipments on board

R_{CO_{2e}}= CO₂ emission rate

T_d= Travelled distance by fleet

$$T_C = T_d \times A_C \quad (2)$$

Where

T_C= Transportation cost

A_C= Average transportation cost per km

$$T_t = \frac{T_d}{F_v} \quad (3)$$

Where

T_t= Transportation time

F_v= Fleet velocity km/h

2.1. Experimental design

This section provides the design of experiments which allow us to find out the impact of the Greenfield service constraints and fleet type on the performance of distribution chain. Four performance measures (dependent factors) namely transportation cost, CO₂ emission, transportation time and number of required fleet are considered in this study.

After conducting pilot experiments, the two independent factors with their levels are identified and displayed in Table 2. Based on full factorial experimental design, a total of 46 experiments are required to gather enough data and to allow the authors to draw a valid conclusion from this study.

Table 2: Independent Factors with Their Levels

Factor	Level		
Greenfield Service Constraints	100% of Customer Served within 113 km	100% of Customer Served within 161 km	100% of Customer Served within 209 km
Fleet Type	Rigid 7.5 tonne		Rigid 17 tonne

3. RESULTS ANALYSIS AND DISCUSSION

A full statistical factorial MANOVA technique was used to analyse the results obtained from GURU Simulation Software at 95% confidence interval. Table 3 displays these results and the following can be concluded:

- Greenfield Service Constraints has significant relationship with transportation cost, CO₂ emission, transportation time and number of required fleet.
- Fleet Type has significant relationship with transportation cost, CO₂ emission, transportation time and number of required fleet.
- Interaction between Greenfield Service Constraints and Fleet Type show that there is a significant relationship with transportation cost and transportation time; however, it is appeared that both CO₂ emission and number of required fleet are not significantly affected.

Table 3: Full Factorial MANOVA Results

Dependent variables	Independent variables	F	P
Greenfield Service Constraints	Transportation costs	20.124	.000 < .05
	CO ₂ emission	23.507	.000 < .05
	Transportation time	20.439	.000 < .05
	Number of required fleet	7.129	.002 < .05
Fleet Type	Transportation costs	21.955	.000 < .05
	CO ₂ emission	4.230	.046 < .05
	Transportation time	20.320	.000 < .05
	Number of required fleet	16.068	.000 < .05
Greenfield Service Constraints * Fleet Type	Transportation costs	4.067	.025 < .05
	CO ₂ emission	.635	.535 > .05
	Transportation time	3.778	.031 < .05
	Number of required fleet	1.377	.264 > .05

3.1. Greenfield analysis and fleet route optimisation result

By applying Greenfield analysis, twelve, seven and four potential Greenfield DC facilities are determined within the best geographic locations which 100% of stores can be served within max sourcing distance of 113 km, 161 km and 209 km respectively.

GURU outputs which are obtained from fleet route optimisation through each scenario are presented as follows:

- First Scenario:** The results proved that by using rigid 7.5 tonne fleet, 922 units of transportation asset are required to meet stores demand and total CO₂ emission, transportation cost and transportation time are 258,667 kg, £200,471 and 1,061 hours respectively. However, rigid 17 tonne fleet has better rate in terms of total transportation cost and transportation time with £ 81,978 and 455 hours respectively except total CO₂ emission which is 381,525 kg. Moreover, just 351 units of transportation asset of rigid 17 tonne fleet are required to meet all the stores demand.
- Second Scenario:** The results showed in order to meet the stores demand in the case of rigid 7.5 tonne fleet t, 915 units of transportation asset are required resulting in the total CO₂ emission, transportation cost and transportation time are 411,825 kg, £318,994 and 1,688 hours respectively. Although, by using rigid 17 tonne fleet, 348 units of transportation asset are required to meet stores demand but this will result in total CO₂ emission, transportation cost and transportation time are 603,697 kg, £128,468 and 714 hours respectively.
- Third Scenario:** In terms of service constraint which 100% of customer served within max sourcing distance of 209 km, 910 units of transportation asset of rigid 7.5 tonne fleet are required for meeting the stores demand and total CO₂ emission, transportation cost and transportation time are 483,163 kg, £373,868 and 1,978 hours respectively. But by using 17 tonne fleet, 352 units of transportation asset are required to meet stores demand and total CO₂ emission, transportation cost and transportation time are 677,256 kg, £143,455 and 797 hours respectively.

As illustrates in figures 2 and 3, CO₂ emission, transportation cost and transportation time for both fleets have rising trends from the first scenario to the third scenario with Greenfield service constraints which 100% of customer served within max sourcing distance of 113km, 161km and 209 km respectively, while, number of required transportation asset to meet stores demand has almost stable trends. Therefore, Greenfield service constraint which 100% of customer served within max sourcing distance of 113 km is identified

as the optimum scenario to have the lowest CO₂ emission, transportation cost and transportation time.

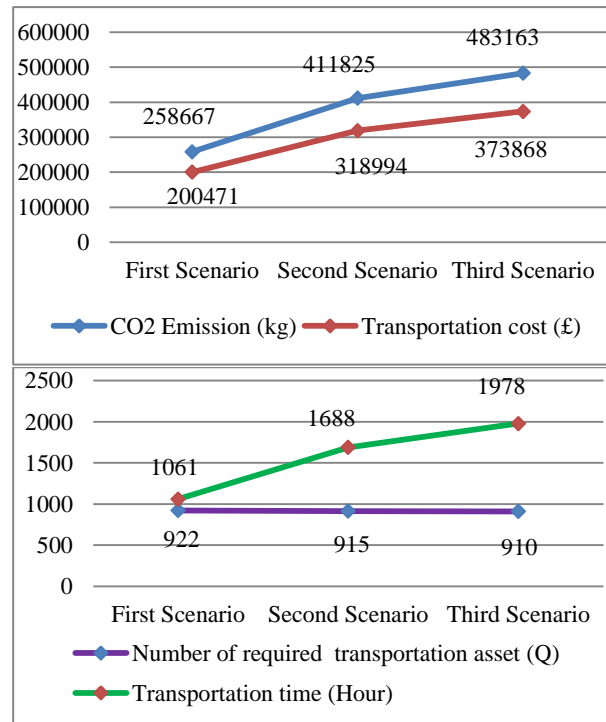


Figure 2: Performance Measures Trends from First Scenario to Second Scenario Based on Rigid 7.5 tonne Fleet

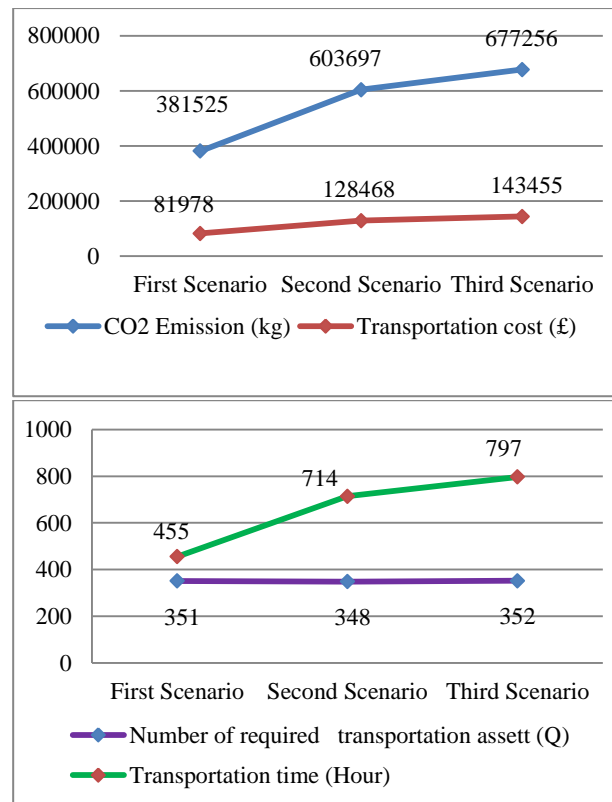


Figure 3: Performance Measures Trends from First Scenario to Second Scenario Based on Rigid 17 tonne Fleet

4. OPTIMISATION OF FLEET TYPE SELECTION

In accordance with obtained results in previous section, although, rigid 7.5 tonne fleet produced lower total CO₂ emission in comparison to rigid 17 tonne fleet, but it has more total transportation cost and transportation time. In this section, shuffling shipments among different fleet types are applied to determine the best balance among CO₂ emission, transportation cost and transportation time through Greenfield service constraint which 100% of customer served within max sourcing distance of 113 km which is identified as the optimum scenario. Thus, both fleet types are assigned among DC facilities, while, rigid 7.5 tonne fleet is specified as the first priority.

The results presented that 450 units of transportation asset of rigid 7.5 tonne fleet and 175 units of transportation asset of rigid 17 tonne fleet are required to meet stores demand and total CO₂ emission, transportation cost and transportation time are 330,109 kg, £146,715 and 789 hours respectively. Figure 4 displays the total CO₂ emission, transportation cost, transportation time and number of required transportation asset at different fleet designs; mix fleet design, rigid 7.5 tonne fleet and rigid 17 tonne fleet.

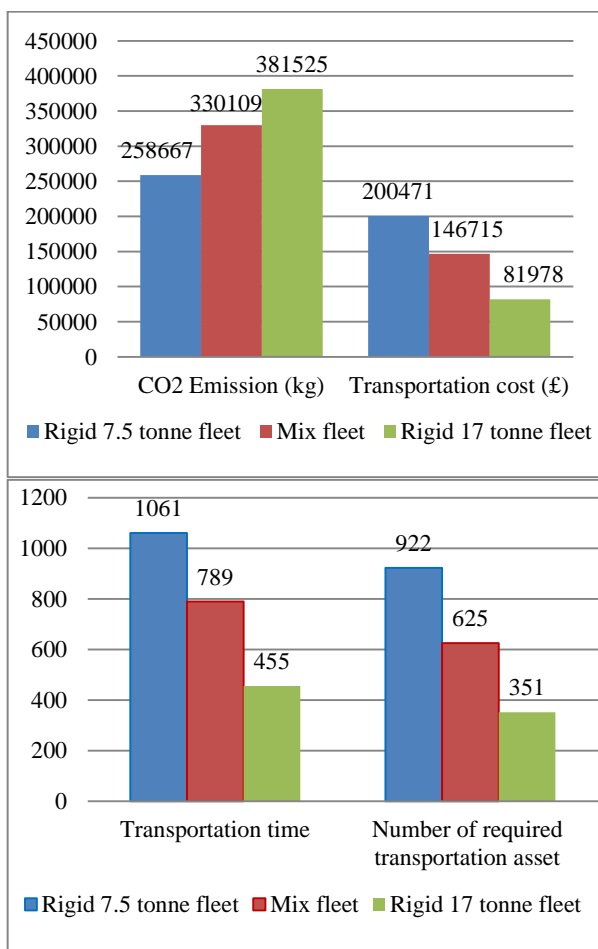


Figure 4: Total CO₂ Emission, Transportation Cost, Transportation Time and Number of Required Transportation Asset at Different Fleet Designs.

5. CONCLUSION

In this paper, sustainable distribution system in food retail supply chain is modelled to minimise the CO₂ emission and transportation cost, maximise the responsiveness and determine the optimal number of required transportation asset to meet customers demand through distribution chain.

Multiple scenarios through two variables; Greenfield service constraints and fleet types within a hypothetical two-stage food supply chain were developed and implemented and validated using Supply Chain GURU Software. Greenfield analysis was used to identify the optimal number and location of potential DC facilities with different service constraints. Moreover, fleet route optimisation was applied on each scenario to minimising empty kilometres through outbound shipment consolidation to optimise the delivery routes. The output data is used to investigate performance measures impact of the different fleet designs and results have been analysed and validated with a statistical techniques (MANOVA).

In order to have the best balance among the performance measures, shuffling shipments among different fleet types were applied through optimum scenario. Thus, both fleet types are assigned among DC facilities, while, rigid 7.5 tonne fleet is specified as first priority.

This work provides a systematic method through which practitioners should be able to decide upon the optimal number and location of distribution facilities as well as optimal types of fleet to minimise the CO₂ emission and transportation cost, maximise responsiveness and determine the optimal number of required transportation asset to meet customers demand through distribution chain.

REFERENCE

- Aghazadeh, S.M., 2004. Improving logistics operations across the food industry supply chain. *International journal of contemporary hospitality management*, 16(4), 263-268.
- Allaoui, H., Guo, Y., Choudhary, A. and Bloemhof, J., 2016. Sustainable Agro-Food Supply Chain Design Using Two-Stage Hybrid Multi-Objective Decision-Making Approach. *Computers & Operations Research*, 1-16.
- Bell, J.E. and McMullen, P.R., 2004. Ant colony optimization techniques for the vehicle routing problem. *Advanced engineering informatics*, 18(1), pp.41-48.
- Beske, P., Land, A. and Seuring, S., 2014. Sustainable supply chain management practices and dynamic capabilities in the food industry: A critical analysis of the literature. *International Journal of Production Economics*, 152, 131-143.
- Carter, C.R. and Rogers, D.S., 2008. A framework of sustainable supply chain management: moving toward new theory. *International journal of physical distribution & logistics management*, 38(5), 360-387.

- Elkington, J., 1997. Cannibals with forks. The triple bottom line of 21st century.
- Lee, J.H., Moon, I.K. and Park, J.H., 2010. Multi-level supply chain network design with routing. *International Journal of Production Research*, 48(13), pp.3957-3976.
- Lerberg Jorgensen, A. and Steen Knudsen, J., 2006. Sustainable competitiveness in global value chains: how do small Danish firms behave?. *Corporate Governance: The international journal of business in society*, 6(4), 449-462.
- Marinakakis, Y., Marinaki, M. and Matsatsinis, N., 2008, June. Honey bees mating optimization for the location routing problem. In *Engineering Management Conference, 2008. IEMC Europe 2008. IEEE International*, pp. 1-5. IEEE.
- Mattevi, M. and Jones, J.A., 2016. Traceability in the food supply chain: awareness and attitudes of UK small and medium-sized enterprises. *Food Control*, 64, 120-127.
- Matthews, H.S., Hendrickson, C.T. and Weber, C.L., 2008. The importance of carbon footprint estimation boundaries. *Environmental Science & Technology*, 42(16), 5839-5842.
- Salem, R.W. and Haouari, M., 2017. A simulation-optimisation approach for supply chain network design under supply and demand uncertainties. *International Journal of Production Research*, 55(7), 1845-1861.
- Schary, P.B. and Skjøtt-Larsen, T., 2001. *Managing the global supply chain*. Copenhagen, Denmark: Copenhagen Business School Press.
- Schwardt, M. and Fischer, K., 2009. Combined location-routing problems—a neural network approach. *Annals of Operations Research*, 167(1), 253-269.
- Seuring, S. and Müller, M., 2008. From a literature review to a conceptual framework for sustainable supply chain management. *Journal of cleaner production*, 16(15), 1699-1710.
- Van Der Vorst, J.G., Tromp, S.O. and Zee, D.J.V.D., 2009. Simulation modelling for food supply chain redesign; integrated decision making on product quality, sustainability and logistics. *International Journal of Production Research*, 47(23), 6611-6631.
- Validi, S., Bhattacharya, A. and Byrne, P.J., 2014a. A case analysis of a sustainable food supply chain distribution system—A multi-objective approach. *International Journal of Production Economics*, 152, 71-87.
- Validi, S., Bhattacharya, A. and Byrne, P.J., 2014b. Integrated low-carbon distribution system for the demand side of a product distribution supply chain: a DoE-guided MOPSO optimiser-based solution approach. *International Journal of Production Research*, 52(10), 3074-3096.

AUTHORS BIOGRAPHY

Professor Sameh M. Saad, BSc (Honours), MSc, PhD, PGCHE, CEng, MIET, MILT, FHEA, FCILT is the Professor of Enterprise Modelling and Management, Postgraduate Research Coordinator and MSc/MBA Course Leader, in the Department of Engineering, Faculty of Arts, Computing, Engineering and Sciences, Sheffield Hallam University, UK. His research interests and experience include fractal supply chain, modelling and simulation, design and analysis of manufacturing systems, production planning and control, reconfigurable manufacturing systems and next generation of manufacturing systems including fractal and biological manufacturing systems. He has published over 150 articles in various national and international academic journals and conferences, including keynote addresses and a book.

Ramin bahadori is a PhD candidate in the Department of Engineering, Sheffield Hallam University, UK. He received his BSc in Industrial Management from Persian Gulf University, IRAN and MSc degree in Logistics and Supply Chain Management from Sheffield Hallam University, UK in 2010 and 2014 respectively. His research interest is in the field of fractal supply chain, food supply chain sustainability, Co2 emission optimisation, modelling and simulation, logistics capabilities, inventory optimisation, logistics cost optimisation, information system, responsiveness optimisation, supply network integration, communication and collaboration within supply network, and multi-criteria decision-making fuzzy AHP.

Jishnu Ravisankar is an MSc student in the Sheffield Hallam University, UK. He received his B-Tech in Mechanical engineering from University of Kerala, India in 2010. He worked as an engineer in Automobile dealer service engineering sectors for over 2 years from 2012 to 2015 in India. From bachelors he got experience in mechanical model designing software. His field of interest is in sustainability approach in supply chain, logistics carbon emission optimization, logistics cost optimization, designing, modelling and simulation, application of lean approach in supply chain, inventory management and optimization, procurement and strategic approaches etc. He is also a member of Chartered Institute of Procurement and supply (CIPS).

DRYING PROCESS SIMULATION IN FOOD INDUSTRY USING LATTICE BOLTZMANN METHOD

Mohammad Mobarak ^{(a),(b)}, Mohamed Hussein ^(a), Antonio Delgado ^(a)

^(a) Institute of Fluid Mechanics, Friedrich-Alexander-Universität Erlangen-Nürnberg, 91058 Erlangen, Germany

^(b) Aerospace Department, Faculty of Engineering, Cairo University, Giza, Egypt

^(a) moharak.mohammad@fau.de

ABSTRACT

Drying Process thermodynamics has recently earned a significant interest in the research of food industry. Moisture release from the pasta-dough due to the external diffusive-convective heat transfer is investigated. From a process engineering point of view, such phase transition analysis can be used for process optimization. The objective of this study is the development of a lattice Boltzmann model in the particle scale, to solve the simultaneously coupled mass and heat transfer between the pasta-dough sample and the surrounding environment, also, the evaporation process across the boundaries is considered. Numerical simulations are held to deliver an insight into the heat and mass transfer processes, offering visualization and yet more understanding of the field variables. Simulation parameters are to be selected using the experimental data.

Keywords: Lattice Boltzmann Method, Drying Process, Phase Transition, Mass and Heat Transfer.

1. INTRODUCTION

Pasta are considered as one of the most common food around the world, originating from Italy in 1700 (Tammerman et al. 2006). Production quality of pasta, and in contrast production defects like crumbling during packaging, in-homogeneous, unevenness in size, cracks due to extra dehydration, all have always been a concern to producers (Mokhtar et al. 2011). So, Drying process is an interesting topic for the industry of pasta and noodles. The drying parameters; Drying Air speed, its temperature, and relative humidity all are questionable values for high production rate and quality. All those parameters are usually gained by experience, though, it's thought that if they are studied using the developed tool, it can enhance the efficiency and the time cost of this process. The work in this publication, is to develop this computational tool using single time relaxation Lattice Boltzmann Method (LBM) but for multiple physical parameters which are the flow field, temperature, and moisture concentration to simulate this complicated process. Noodles' Geometry was implemented into the code using the image processing of a binary stack of images from a high resolution μ CT Scanner. Finally, models from literature was used for the estimation of the thermo-physical properties of pasta-

dough and drying air which are essential for the estimation of the relaxation time for each physical distribution function in LBM. The work is distributed as following; problem definition including process conditions, and image extraction process, then the mathematical equations, distribution functions, and non-dimensional parameters used in the LBM solver, then the implemented thermo-physical models from literature based on correlations of semi-empirical data for pasta-dough, and gas mixture of humid air, finally the available results from the simulation tool.

2. MATERIALS AND METHODS

2.1. Material Definition

Random sample of band noodle (Figure 1) of size 190x137x150 mm was investigated inside the computational domain shown in Figure 2. As sample's distribution and orientation are highly random, the geometry extraction was an issue for the computational domain. So, it was suggested to be done using a high-resolution GE/Phoenix μ CT scanner. 3D model was built inside the solver by reading multiple binary Image scaffolds (Figure 3) extracted from the volume model (Figure 4), the final result is shown in Figure 5. Simple edge detection was also made to indicate the noodles' surface inside the simulation tool.

Initial conditions were set as 20 °C for the whole domain, and 0.3 moisture concentration for the noodles. Drying air inlet velocity, temperature and relative humidity were set to as 3m/s, 80 °C and 60% respectively.



Figure 1: Sample Band Noodles

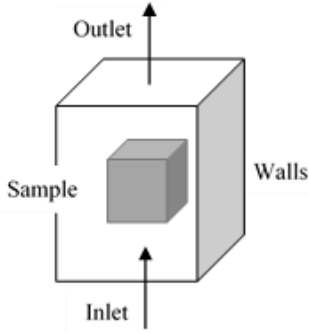


Figure 2: Computational Domain



Figure 3: Binary Image Scaffolds

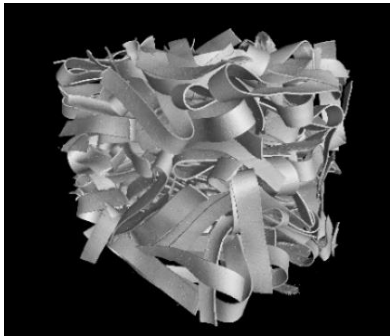


Figure 4: Volume File from the μ CT scanner

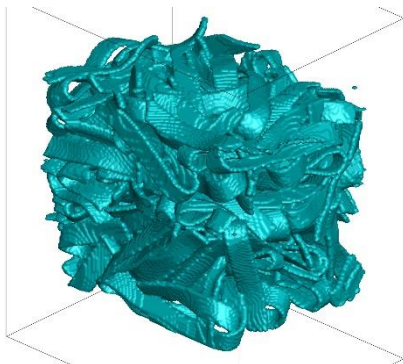


Figure 5: Exported Geometry from the code after processing and assembly of the images' stack

2.2. Lattice Boltzmann Method

Lattice Boltzmann Method has gained a lot of attention in the field of fluid mechanics, including Multi-phase flow, thermal flows, flow in complex and micro-scale media. This is due to the nature of the Boltzmann's

equation, which describes the motion and interaction of fluid particles in a microscopic level.

The lattice Boltzmann's Equation relates the particle distribution f per unit time to the propagation motion and collision (Hussein 2010).

$$\frac{\partial f}{\partial t} + u \cdot \nabla f = Q \quad (1)$$

Where u the particle velocity and Q is the collision operator.

The collision operator was approximated by (Koelman 1991), using the Bhatnagar-Gross-Krook (BGK) model as follows:

$$Q_i = -\frac{1}{\tau} [f_i - f_i^{(equ)}] \quad (2)$$

Where τ is the relaxation time toward the local equilibrium, and $f_i^{(equ)}$ is the Equilibrium distribution function (Equation 3) which is evaluated from the Maxwell-Boltzmann distribution (Succi 2001).

$$f_i^{equ} = w_i \rho \left[1 + 3 \frac{\hat{e}_i \cdot u}{c^2} + \frac{9}{2} \frac{(\hat{e}_i \cdot u)^2}{c^4} - \frac{3 u^2}{2 c^2} \right] \quad (3)$$

Where \hat{e}_i , w_i , c , and u are the discrete unit vectors, the weighting factor, the lattice speed $c = \frac{\Delta x}{\Delta t}$, and the macroscopic velocity respectively. The used lattice in this work would be the D3Q19 (Figure 6) & (Table 1).

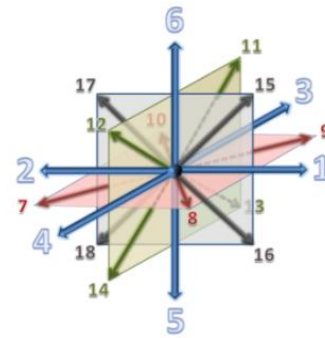


Figure 6: D3Q19 lattice model representing 19 velocity direction in 3D lattice (Hussein 2010)

Table 1: Weighting factors for each unit direction of the D3Q19 lattice

\hat{e}_i	w_i
0	1/3
1, 2, 3, 4, 5, 6	1/18
7, 8, ..., 18	1/36

The advection-diffusion equation for Concentration and Temperature can be written as follows:

$$\frac{\partial C}{\partial t} + u \cdot \nabla C = D \nabla^2 C \quad (4)$$

$$\frac{\partial T}{\partial t} + u \cdot \nabla T = \alpha \nabla^2 T \quad (5)$$

Where C , u , D , T , and α are the moisture concentration, macroscopic velocity updated from the flow field equation, mass diffusivity, temperature, and thermal diffusivity respectively.

The Advection-Diffusion mass and heat transfer were then modelled in LBM using the following three distribution functions: Moisture concentration, Temperature, and Density. So, the flow field has been solved across the noodles and coupled with the Moisture and Temperature fields.

The three LB Equations (LBE) used in this work are expressed as follows:

$$\frac{\partial \{f\}}{\partial t} + v \cdot \nabla \{f\} = \{Q\} \quad (6)$$

$$\{f\} = \begin{bmatrix} \rho \\ T \\ C \end{bmatrix}; \{Q\} = \begin{bmatrix} -\frac{1}{\tau_f} (f_i - f_i^{(equ)}) \\ -\frac{1}{\tau_T} (T_i - T_i^{(equ)}) \\ -\frac{1}{\tau_C} (C_i - C_i^{(equ)}) \end{bmatrix}$$

$$f_i^{equ} = w_i \rho \left[1 + 3 \frac{\hat{e}_i \cdot u}{c^2} + \frac{9}{2} \frac{(\hat{e}_i \cdot u)^2}{c^4} - \frac{3}{2} \frac{u^2}{c^2} \right] \quad (7)$$

$$T_i^{equ} = w_i T \left[1 + 3 \frac{\hat{e}_i \cdot u}{c^2} + \frac{9}{2} \frac{(\hat{e}_i \cdot u)^2}{c^4} - \frac{3}{2} \frac{u^2}{c^2} \right] \quad (8)$$

$$C_i^{equ} = w_i C \left[1 + 3 \frac{\hat{e}_i \cdot u}{c^2} + \frac{9}{2} \frac{(\hat{e}_i \cdot u)^2}{c^4} - \frac{3}{2} \frac{u^2}{c^2} \right] \quad (9)$$

Where ρ & u are evaluated from the zeroth and first moments of the density distribution function (Equation 10), while the macroscopic T and C are calculated from the zeroth moment of Temperature and Concentration distribution function respectively (Equation 11 & 12).

$$\rho = \sum_i f_i; \rho \hat{u} = \sum_i f_i \hat{e}_i \quad (10)$$

$$T = \sum_i T_i \quad (11)$$

$$C = \sum_i C_i \quad (12)$$

The relaxation time τ_f , τ_T , τ_C are related to the kinematic viscosity ν , thermal diffusivity α , mass diffusivity D respectively through the following relations (Wolf-Gladrow 2000):

$$\tau_f = 3\nu + \frac{1}{2} \quad (13)$$

$$\tau_T = 3\alpha + \frac{1}{2} \quad (14)$$

$$\tau_C = 3D + \frac{1}{2} \quad (15)$$

The kinematic viscosity, thermal and mass diffusivities are evaluated in the lattice units according to the following non-dimensional groups respectively (Hussein 2010):

$$Re = \frac{u_\infty \cdot l}{\nu} \quad (16)$$

$$Fo_T = \frac{\alpha \cdot t}{l^2}, Fo_C = \frac{D \cdot t}{l^2} \quad (17)$$

$$Bo_T = \frac{u_\infty \cdot l}{\alpha}, Bo_C = \frac{u_\infty \cdot l}{D} \quad (18)$$

Where the Reynold's, Fourier, and Bodenstein numbers are used to define the flow field across the noodles, both thermal and mass diffusivities inside the noodles' structure, and the ratio between momentum diffusivity to both thermal and mass diffusivities within the air domain between the noodles respectively. Given that u_∞ , l , and t are the inlet flow velocity, the characteristic length, and process time.

2.3. Thermo-Physical Properties

2.3.1. Pasta-Dough

In order to get an estimation for the LBM relaxation time to each distribution function, pasta-dough thermo-physical properties should be implemented using semi-empirical relationships from literature. Though, uncertainty in these models was already stated due to the difference in raw materials for each case and experiment, these different models can be easily replaced if any is later appeared in literature, also can be tuned easily according to the dough properties.

2.3.1.1. Thermal Conductivity

Pasta-dough thermal conductivity can be correlated with its temperature and moisture content through the

following four parameter model (Saravacos and Maroulis 2001):

$$k_d = \frac{\lambda_0}{1+x} \exp\left[-\frac{E_o}{R}\left(\frac{1}{T} - \frac{1}{T_{ref}}\right)\right] + \frac{\lambda_i x}{1+x} \exp\left[-\frac{E_i}{R}\left(\frac{1}{T} - \frac{1}{T_{ref}}\right)\right] \quad (19)$$

Where λ_0 , λ_i , E_o , E_i are dough material parameters given as 0.273 W/m K, 0.8 W/m K, 0.0 KJ/mol, 2.7 KJ/mol respectively, x is the water content on the dry basis, R is the universal gas constant ($8.314 \cdot 10^{-3} \frac{KJ}{mol \cdot K}$), $T[^\circ C]$ is the dough temperature, $T_{ref} = 60^\circ C$.

2.3.1.2. Heat Capacity

Heat Capacity can be computed by the weighted average of the dough main components as follows:

$$C_{d,Total} = \frac{x}{1+x} C_{water} + \frac{1}{1+x} C_{Solid} \quad (20)$$

$$C_{Solid} = y_{Starch} C_{Starch} + y_{Proteins} C_{Proteins} + y_{Fats} C_{Fats} \quad (21)$$

Where the specific heat of each component is given by (De Cindio et al. 1992) in $[\frac{J}{Kg \cdot K}]$ as:

$$C_{Starch} = 5.737(T+273) + 1328 \quad (22)$$

$$C_{Proteins} = 6.329(T+273) + 1465 \quad (23)$$

$$C_{Fats} = 2000 \quad (24)$$

Considering that y is the mass fraction of each component with respect to the solid basis, given as 0.84, 0.146, 0.014 for each of starch, proteins, fats respectively as given by (Tammerman et al. 2006), and T is the dough temperature in $[^\circ C]$.

2.3.1.3. Density

The dough density can be evaluated as (De Cindio et al. 1992):

$$\rho_d = (3.02 \cdot \frac{x}{1+x} + 6.46)^{-1} \cdot 10^4 \left[\frac{Kg}{m^3}\right] \quad (25)$$

2.3.1.4. Thermal Diffusivity

Thermal diffusivity is then calculated from its definition by:

$$\alpha_d = \frac{k_d}{\rho_d \cdot C_d} \left[\frac{m^2}{s}\right] \quad (26)$$

2.3.1.5. Mass Diffusivity

Water Mass diffusivity in dough can be evaluated using the semi-empirical model given by (Waananen and Okos 1996) as:

$$D_d = \left(1.2 \times 10^{-7} + \varepsilon \cdot \frac{8 \cdot 10^{-5}}{P}\right) \cdot \exp\left(-\frac{6.6 e^{-20x} + E_a}{R(T+273)}\right) \left[\frac{m^2}{s}\right] \quad (27)$$

Where ε is the porosity of the dough which is assumed to be 0.26 (Xiong et al. 1991), $T[^\circ C]$ is the dough temperature, E_a is the activation energy for diffusion of a free water molecule which is used as $22.6 \frac{KJ}{mol}$ (Waananen and Okos 1996), R is the universal gas constant ($8.314 \cdot 10^{-3} \frac{KJ}{mol \cdot K}$), and P is the dough pressure [KPa].

2.3.2. Humid Air

As for Pasta-dough, humid air thermo-physical properties should also be evaluated based on its Temperature and Humidity using analytical procedure from literature for the gas mixture properties of dry air and saturated water vapour.

2.3.2.1. Dynamic Viscosity

Dynamic viscosity of humid air can be calculated using the fitted function by (Durst et al. 1996):

$$\mu = [(A_1 + A_2(T+273)) + (B_1 + B_2(T+273))x_v + (C_1 + C_2(T+273))x_v^2] \times 10^{-6} \left[\frac{N \cdot s}{m^2}\right] \quad (28)$$

Where T is the air temperature expressed in $[^\circ C]$, while, the numerical coefficients can be given in Table 2, x_v here is the molar fraction of water vapour in air which can be easily related to the specific humidity ω by:

$$x_v = \frac{\omega M_a}{\omega M_a + M_v} \quad (29)$$

Where M_a and M_v are the molar mass of dry air and saturated water given by 28.97 and 18.01528 g/mole respectively.

Also, specific humidity can be related to the common Relative humidity ϕ through (Cengel and Boles 2002):

$$\omega = \frac{0.622 \phi P_g}{P - \phi P_g} \quad (30)$$

Where P and P_g are the total mixture pressure and the water saturation pressure at a given temperature respectively, the later can be evaluated by (Tammerman et al. 2006):

$$P_g = 610.78 \exp \left[17.2694 \frac{T}{(T + 238.3)} \right] [Pa] \quad (31)$$

Where T is the expressed in [$^{\circ}C$].

Table 2: Coefficients for the dynamic viscosity function

Coefficient	Value
A_1	6.0453459
A_2	0.042489943
B_1	-6.8323022
B_2	0.0059284286
C_1	-0.67799257
C_2	-0.011338714

2.3.2.2. Thermal Conductivity

Humid air thermal conductivity can be evaluated using the following expression for mixtures (Tsilingiris 2008; Reid et al. 1987):

$$k_{mixture} = \frac{(1-x_v)k_a}{(1-x_v) + x_v \Phi_{av}} + \frac{x_v k_v}{x_v + (1-x_v) \Phi_{va}} \quad (32)$$

Where k_a and k_v are the thermal conductivities of air and water vapour respectively, which can be fitted by a polynomial (Durst et al. 1996):

$$k_i = A_i + B_i (T + 273) + C_i (T + 273)^2 + D_i (T + 273)^3 \quad (33)$$

the coefficients A , B , C , and D are given in Table 3.

Also, Φ_{av} and Φ_{va} are an interaction parameters given by:

$$\Phi_{av} = \frac{\left[1 + \left(\frac{\mu_a}{\mu_v} \right)^{0.5} \cdot \left(\frac{M_v}{M_a} \right)^{0.25} \right]^2}{\left[8 \left(1 + \frac{M_a}{M_v} \right) \right]^{0.5}} \quad (34)$$

$$\Phi_{va} = \frac{\mu_v M_a}{\mu_a M_v} \Phi_{av} \quad (35)$$

Table 3: Coefficients for the thermal conductivity polynomial equation

Coefficient	Value	
	Dry Air	Water Vapour
A	$-0.56827429 \times 10^{-3}$	31.997566×10^{-3}
B	$0.10805198 \times 10^{-3}$	$-0.13308958 \times 10^{-3}$
C	$-7.3956858 \times 10^{-8}$	3.8160429×10^{-7}
D	$3.7302922 \times 10^{-11}$	-2.0×10^{-10}

Where μ_a and μ_v are the dynamic viscosity of dry air and saturated water vapour respectively, which can be calculated using Equation 28, where the output at $x = 0$ is corresponding to the dry air, while $x = 1$ is for the saturated water vapour.

2.3.2.3. Heat Capacity

Specific heat can be evaluated using the correlated polynomial function (Durst et al. 1996) which assumes a linear mixture of the gas values:

$$C_{mixture} = [A_a + B_a (T + 273) + C_a (T + 273)^2 + D_a (T + 273)^3] (1 - x_v) + [A_v + B_v (T + 273) + C_v (T + 273)^2 + D_v (T + 273)^3] x_v \quad (36)$$

Where T is expressed in [$^{\circ}C$], and the coefficients are given in Table 4.

Table 4: Coefficients for the heat capacity polynomial function

Coefficient	Value
A_a	1.0653697
B_a	$-4.4730851 \times 10^{-4}$
C_a	9.8719042×10^{-7}
D_a	$-4.6376809 \times 10^{-10}$
A_v	6.564117
B_v	$-2.6905819 \times 10^{-2}$
C_v	5.1820718×10^{-5}
D_v	$-3.2682964 \times 10^{-8}$

2.3.2.4. Density

Humid air density can be calculated from the gas equation of state (Durst et al. 1996):

$$\rho_{mixture} = \frac{1}{Z_F(T, x)} \frac{P_o}{RT} M_a \left[1 - x_v \left(1 - \frac{M_v}{M_a} \right) \right]$$

Where Z_F is the compressibility factor for the mixture i.e. The deviation correction of real gas from ideal gas behaviour, which can be expressed as:

$$Z_F = 1 + x_v \left[\frac{a + c(T + 273)}{1 + b(T + 273)} - 1 \right] \quad (37)$$

Where $a, b,$ and c are given as 1.00784, $-3.4299543 \times 10^{-3}$, and $-3.4396097 \times 10^{-3}$ respectively.

2.3.2.5. Thermal Diffusivity

Thermal diffusivity is again calculated from its definition by:

$$\alpha_{mixture} = \frac{k_{mixture}}{\rho_{mixture} \cdot C_{mixture}} \left[\frac{m^2}{s} \right] \quad (38)$$

Thermal diffusivity could also be directly read from the chart in the work by (Tsilingiris 2008) as a function of temperature and relative humidity.

2.3.2.6. Mass Diffusivity

The mass diffusion of water in air can be expressed using the correlation from (Perry and Green 1984; Migliori et al. 2004):

$$D_a = \frac{10^{-3} \cdot T_f^{1.75} \left(\frac{M_a + M_v}{M_a \cdot M_v} \right)^{0.5}}{P \left[(\sum \nu)_a^{1/3} + (\sum \nu)_b^{1/3} \right]^2} \left[\frac{m^2}{s} \right] \quad (39)$$

Where P is the Pressure in atm, T_f is the film temperature which can be set as the average between the temperature of the humid air and noodles' surface temperature, $(\sum \nu)_a$ and $(\sum \nu)_b$ are material parameters which are given for air and water as 20.1 and 12.7 respectively.

3. RESULTS

Flow field streamlines can be shown, as well as temperature and moisture distribution around, inside, at the surface of the noodles in Figure 6, 7, 8, 9, and 10.

Heat transfer by convection is highly effective with higher time constant than diffusion in humid air, which truly appears in the temperature contours around the noodles. The thermal diffusion inside the noodles is also much slower, that's already appeared from the thermal diffusivity of the noodles', which is lower than that of air by order of magnitude of ($\mathcal{O} \sim 10^{-2}$).

Average Temperature rise of the noodles during the process can be shown in Figure 11.

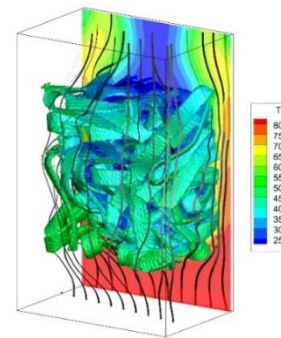


Figure 6: Flow streamlines with pasta's surface Temperature [$^{\circ}C$]

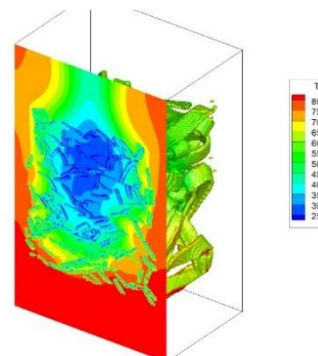


Figure 7: Temperature Distribution inside and around the pasta structure

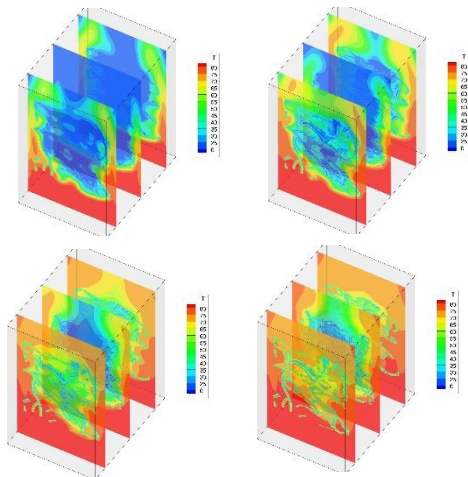


Figure 8: Sectional view for the Temperature Distribution with time inside and around the pasta structure

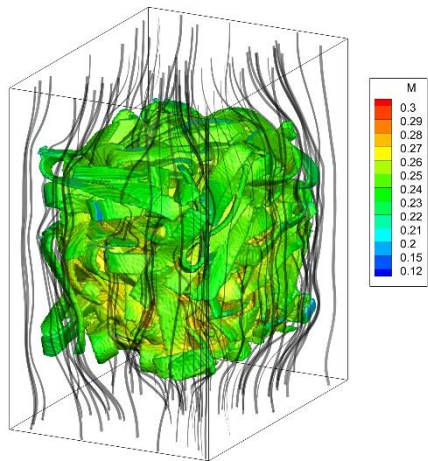


Figure 9: Flow streamlines with pasta's surface moisture concentration on dry basis

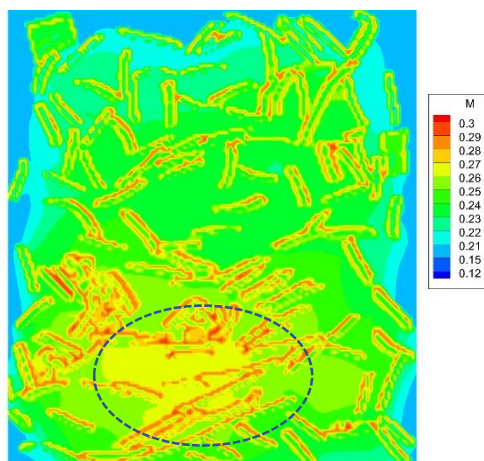


Figure 10: Sectional view for the Moisture Distribution inside and around the pasta structure

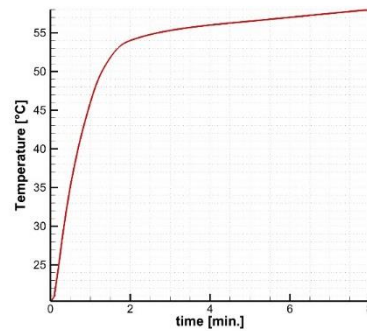


Figure 11: Average temperature of the Noodles with time

Temperature profile seems to be higher at the regions of high velocity profiles which is between the walls and noodles' assembly. Although velocity within noodles are much lower than the inlet, this's due to the noodles network which obstructs the flow field, delaying heat and mass transfer by convection, that explains why both the temperature and the moisture at the core of the noodles' network are lower and higher respectively.

Noodles surface temperature are always higher than its core, which is logical as the heat flux through the noodles surface are faster than the heat diffusion inside its structure (Figure 7 & 8), the inverse happens with the moisture, water evaporates from the surface, then diffuses inside the noodles from the core to the surface (Figure 10). Worth to mention, that the areas of higher noodle intensity reflect lower evaporation due to the limited air voids blocking the hot flux to propagate, thus inhibited drying region (see Figure 10 dotted region).

4. CONCLUSION AND FUTURE WORK

Drying process physics seems to be much complicated, also the estimation of the thermal and mass diffusive properties are not very straight forward. Though, the developed three distribution LBE appears to be a powerful way to analyse this complex phenomena. Results seems to be reasonable, flow field is dominating the transport phenomena of moisture and temperature. Although, further developments need to be done with the noodles' surface treatment, also a deeper insight is required for the parameters of the semi-empirical models used to exactly match the drying product.

ACKNOWLEDGMENTS

This work has been supported by the FEI (Forschungskreis der Ernährungsindustrie), AiF (Arbeitsgemeinschaft industrieller Forschungsvereinigungen), and Ministry of Economics and Technology. AIF project number: 19018 N.

It's notable to mention that the μ CT scan wouldn't be done without the cooperation and help of the GeoZentrum Nordbayern, Faculty of Natural Sciences, Friedrich-Alexander University Erlangen-Nürnberg, we specially would like to thank Dipl.-Geol. Christian Schulbert for his valuable and professional support with the μ CT imaging session. Special thanks to M. Sc. Julian

Thünnesen ^(a) for his valuable help with data collection and cooperation with the μ CT scan.

REFERENCES

Cengel Y.A., Boles M.A., 2002. Thermodynamics: an engineering approach. Sea.

De Cindio B., Brancato, B., Saggese A., 1992. Modellazione del processo di essiccamento di Paste Alimentari. Università "Federico II" di Napoli, Final Report, IMI-PAVAN Project (italian language).

De Temmerman J., Verboven P., Nicolai B., Ramon H., 2007. Modelling of transient moisture concentration of semolina pasta during air drying. Journal of food engineering 80(3): pp.892-903.

Durst F., Noppenberger S., Still M., Venzke H., 1996. Influence of humidity on hot-wire measurements. Measurement Science and Technology 7(10): p.1517.

Hussein M.A., 2010. On the theoretical and numerical development of Lattice Boltzmann models for biotechnology and its applications. PhD. Technische Universität München, München.

Koelman, J.M.V.A., 1991. A simple lattice Boltzmann scheme for Navier-Stokes fluid flow. EPL (Europhysics Letters) 15(6): p.603.

Migliori M., Gabriele D., de Cindio B., Pollini C.M., 2005. Modelling of high quality pasta drying: mathematical model and validation. Journal of Food Engineering 69(4): pp.387-397.

Mokhtar A., Hussein M.A. and Becker, T., 2011. Monitoring pasta production line using automated imaging technique. Procedia Food Science, 1, pp.1173-1180.

Perry R.H., Green D.W., Maloney, J.O., 1984. Perry's Chemical Engineer's Handbook Chemical Engineer's Handbook. Mcgraw-hill.

Reid R.C., Prausnitz J.M., Poling B.E., 1987. The properties of gases and liquids. 4th. New York: McGraw.

Saravacos G.D., Maroulis Z.B., 2001. Transport properties of foods. CRC Press.

Succi S., 2001. The lattice Boltzmann equation: for fluid dynamics and beyond. Oxford university press.

Wolf-Gladrow D.A., 2004. Lattice-gas cellular automata and lattice Boltzmann models: an introduction. Springer.

Tsilingiris P.T., 2008. Thermophysical and transport properties of humid air at temperature range between 0 and 100 C. Energy Conversion and Management 49(5): pp.1098-1110.

Waananen K.M., Okos M.R., 1996. Effect of porosity on moisture diffusion during drying of pasta. Journal of Food Engineering 28(2): pp.121-137.

Xiong X., Narsimhan G., Okos M.R., 1992. Effect of composition and pore structure on binding energy and effective diffusivity of moisture in porous food. Journal of Food Engineering 15(3): pp.187-208.

ADVANCED APPROACHES TO SOLVING CRITICAL AND COMPLEX PRODUCTION SCHEDULING PROBLEMS

Marco Better^(a), James P. Kelly^(b), Manuel Laguna^(c), Ross Palmer^(d)

^{(a),(b),(d)} OptTek Systems, Inc., 2241 Seventeenth Street, Boulder, CO, 80302, USA

^(c) University of Colorado at Boulder, Leeds School of Business, CB419, Boulder, CO, 80309, USA

^(a)better@opttek.com, ^(b)kelly@opttek.com, ^(d)palmer@opttek.com
^(c)laguna@colorado.edu

ABSTRACT

For food manufacturing, processing and packaging companies whose processes exhibit high levels of complexity, creating optimal production schedules can provide a source of competitive advantage. For these companies, production costs often represent a significant portion of their total product cost, multiple products often share manufacturing infrastructure and resources, and production schedules are required on a timely basis. Our scheduling approach takes advantage of robust, custom optimization and simulation to satisfy this growing need in the food operations market.

We have developed a sophisticated production scheduling solution approach that combines mathematical programming, metaheuristic optimization, and simulation to craft optimal or near-optimal production schedules in a timely, reliable and effective manner. In this paper, we describe our approach in detail and provide computational results for a moderately-sized liquid food processing facility.

Keywords: production scheduling, parallel machines, simulation optimization, food processing, packaging

1. INTRODUCTION

Existing solution approaches for production process scheduling typically focus on two basic questions:

- When should a specific task be scheduled?
- What resources should be assigned to perform the task?

In many cases, these questions can be answered by applying simple, rule-based heuristics, such as sequencing tasks by earliest due date, or by the length of their

processing times. More complex rules can be used based on combining two or more simple rules into ratios or products, but the basic concept remains the same. Although appealing for their simplicity and intuitive nature (i.e., it is intuitive to order tasks based on when they are due), these methods usually produce inferior results because they tend to ignore other attributes of the tasks, such as penalties for tardiness, interactions with other tasks, availability of resources to perform all the work, changeover and setup times and costs, etc.

In more complex situations, optimization-based approaches can be used. These methods use mathematical programming techniques to find the optimal solution – an assignment of tasks or flows to a production line and a sequence of those tasks or flows – to maximize or minimize some metric, like throughput, makespan, or operating cost. The complexity of most real-world systems renders the application of exact optimization methods impractical, either because the time to obtain the optimal solution would be excessive, or because such systems are too complex to be mathematically formulated. In this case, what is needed is a combination of mathematical methods combined with heuristic solution techniques and, often, simulation modeling approaches.

We propose OptPro, a sophisticated production scheduling solution approach that goes beyond rule-based systems to enable optimal decision making through powerful algorithmic and analytical techniques. Our proposed approach meets a growing need from companies with complex planning, design and operational scheduling requirements. These companies are typically dissatisfied with their current scheduling capabilities, and are seeking

to develop a competitive advantage through optimal scheduling.

1.1. Optimized Production Scheduling

At a recent meeting, a process engineer for a food plant manufacturing design consultancy was discussing why he liked “greenfield” design problems (completely new design unencumbered by existing infrastructure). He found such problems to be “easy” because, as he said, “there is so much flexibility that many solutions will work.” On the surface, this sounds reasonable. But the problem with this perspective is that although it may be easy to find a solution that “works,” finding the best solution might be quite difficult. When the number of choices is large (the definition of flexibility), the number of possible different solutions can be enormous. Optimization is the preferred approach to find the best solution in these types of situations. In today’s competitive environment, it is unwise to settle for less than an optimal solution. This paper discusses how production scheduling optimization can produce the best possible outcomes for those operations where a good schedule may provide a competitive advantage.

Though the industries they come from are diverse, potential users of this approach usually share a common set of characteristics, including, but not limited to:

- Production costs represent a significant portion of the total cost of their product(s);
- Real-time, daily or weekly schedules need to be obtained quickly;
- Multiple products share common processing infrastructure and resources;
- The types and quantities of products to produce do not vary significantly from one period to the next;
- Construction of a new plant, or a plant expansion, is being planned.

1.2. Advanced Optimization Approaches

The production planning and production scheduling academic literature is very vast, and includes many pure optimization and hybrid optimization-based approaches to food production scheduling. Recent surveys (Jahangirian, et al. 2010) and (Smith 2003) identify more than 20 implementations involving discrete event simulation approaches, with more than a dozen others involving alternative types of simulation. Numerous other implementations involve mixed integer programming formulations (Wari and Zhu 2016) and metaheuristics

(Abakarov, et al. 2009). However, these implementations either make severe simplifications of the processes they are trying to represent, consider only portions of a complete process, or do not provide an integrated system capacity and job sequencing framework. We have developed a sophisticated production scheduling solution that utilizes mathematical programming, metaheuristic optimization techniques, and simulation to craft optimal or near-optimal system capacity designs and production schedules in a timely, reliable and effective manner.

Our approach is not designed for situations where using straight-forward rules such as FIFO or EDD would suffice. It is for those operations where multiple products compete for common resources, such as production infrastructure and materials; it is for those companies where a good production schedule can turn into a competitive advantage; it is for companies who seek to optimize and automate their plant design and production schedule, or to maximize the benefit derived from their operational processing decisions. In manufacturing settings, the approach enables optimal decision making by simultaneously optimizing scheduling, sequencing, line-assignment, capacity and layout decisions to meet forecasted customer demands.

In general, the approach simultaneously solves a set of optimization problems. Depending on the goal of the operation, multiple objective functions can be simultaneously addressed, such as:

- Maximizing throughput
- Maximizing equipment utilization
- Minimizing makespan or total processing time
- Minimizing operational costs and capital expenditures

Regardless of the objectives, the approach can also handle several physical and logical constraints that may come into play in a production schedule, such as:

- Maximum time to complete production
- Lower and upper bounds on the number of units – and/or capacity – of each equipment type (i.e., machines, tanks, pumps, jigs, etc.)
- Lower and upper bounds on the number of personnel required to operate the plant
- Changeover and setup times and costs related to how particular jobs are sequenced in the schedule (i.e., switching from high charge to low charge, switching from one flavor to a different flavor; preparing a batch for processing, etc.)
- Cost and budget constraints

We demonstrate the benefits of our proposed approach on a real-world food processing example, and discuss future work related to expansion of the methodology into other potential food processing operations.

2. PROBLEM DESCRIPTION, FORMULATIONS, AND HEURISTIC APPROACHES

More than an “off-the-shelf”, one-size-fits-all solution, OptPro is a custom *solution approach* to complex production and process scheduling situations. These complex situations arise in many types of industrial manufacturing settings, including pharmaceuticals, construction materials, automotive assembly, oil refinery, and food operations. In the latter, some of the more complex systems encountered relate to the processing of liquid foods. The reasons for the complexity of liquid foods processing operations are multiple, and include the following, to name a few:

1. These are continuous flow systems, where flow rates and line capacities are dynamic and depend on upstream and downstream constraints;
2. Flow of different product types occurs on shared resources (i.e., pipes, tanks, coolers, mixers, fillers, etc.) which usually require cleaning during changeovers; in many cases, changeover times and costs are dependent on the sequencing of flows, thus creating the need for a good sequencing algorithm;
3. Products often have short shelf-lives such that storage capacity and time, as either work-in-process or as finished goods, are limited. Therefore, there is a need to process raw materials as quickly as possible to minimize the probability of the product “standing around” in the different stages of the system;
4. Disruptions in operations usually involve stopping all upstream flows from the point of disruption, creating costly product losses and production delays.

For these reasons, an efficient schedule of the operation is critical to ensure the highest utilization rates for the plant equipment, while minimizing product losses and operating costs, and ensuring timely delivery of products to the retailers (e.g., grocery stores).

We are generally interested in optimizing three aspects of the operation. (1) the assignment of runs (product flows) to a line (i.e., a set of equipment units); (2) the sequencing of runs on each line; and, (3) the capacity of each line (i.e., the number of units and/or size per unit of each equipment

type). We first provide a solution approach to the first two aspects, and then focus on the third.

2.1. The Assignment and Sequencing Problem

The best way to approach these problems is to begin with customer demand. Expressing the problem in terms of the stock keeping units (SKUs) required by the customers provides a way to define meaningful units of flow throughout the process. Let’s illustrate this idea with a simple example. In this example, we will assume that production consists of a single step; i.e., we treat all steps in the process as a “black box”.

We have a production facility that faces daily demand for five products, each having a specific volume required. In addition, each product’s flow can be assigned to one of three available production lines, and production must be completed within 24 hours.

We can represent these SKUs as shown in Table 1.

Table 1: Daily SKU demand and production data

SKU ID	Daily Demand (lbs)	Feasible Lines	Maximum Rate (lbs/min)	Processing Time (min)
1	66,000	1, 2	150	440
2	27,000	1, 2	150	180
3	90,000	1, 2, 3	75	1,200
4	48,000	1, 2, 3	75	640
5	60,000	2, 3	75	800

Column 1 in Table 1 contains the SKU identifier; Column 2 shows daily demand for each product, in pounds, that must be produced by the end of the day; Column 3 contains all feasible assignments of each SKU to a specific production line (for example, SKU 1 can be processed on either Line 1 or Line 2 but not on Line 3; similarly, SKU 5 can be processed on either Line 2 or Line 3, but not on Line 1); Column 4 denotes the maximum production rate, in pounds per minute, of each SKU on the production line. Tables 2 and 3 contain data corresponding to changeovers. In Table 2, the cost factors related to product changeovers are given. These cost factors represent the cost required to clean the line and change settings in preparation for the next SKU. We assume that cleaning the line has a cost of 2, and changing a setting has a cost of 1. For example, if a line is running production of SKU 1, and needs to change to SKU 3, the cost factor is 1 because it requires a setting change only; however, if the inverse is true – that is, the line is running production of SKU 3 and needs to change to SKU 1 – then both, a settings change and a line cleaning are required, so the cost factor is 3 (see red-circled figures

in the table). In Table 3, we show the setup time, in minutes, required during a changeover from one SKU to another.

Table 2: Changeover cost factors

		TO				
		SKU	1	2	3	4
FROM	1	0	0	1	1	1
	2	2	0	1	2	3
	3	3	2	0	0	2
	4	3	3	2	0	2
	5	1	3	2	2	0

Table 3: Setup times

		TO				
		SKU	1	2	3	4
FROM	1	0	0	60	60	60
	2	120	0	60	120	180
	3	180	120	0	0	120
	4	180	180	120	0	120
	5	60	180	120	120	0

This simple example can be formulated as a mathematical optimization program. For simplicity, let's assume that our only objective is to minimize the operating cost of running the facility.

To solve the problem, we know the following:

- N = the number of SKUs to be scheduled;
- M = the number of lines available for production;
- c_{ij} = the cost associated to changing from SKU i to SKU j on a line (changeover cost);
- s_{ij} = the setup time required when changing from SKU i to SKU j on a line (setup time);
- p_i = the processing time for SKU i ;
- B = some large scalar, at least greater than the maximum allowable makespan.

We will set variable x_{ijk} equal to 1 if SKU i directly precedes SKU j on Line k , and equal to 0 otherwise. We will set variable t_j as the start time for SKU i . Assuming, for simplicity, that the only costs we need to worry about are changeover costs, we can express the objective function as:

$$\text{minimize } \sum_{i=1}^N \sum_{j=1}^N \sum_{k=1}^M c_{ij} x_{ijk} \quad (1)$$

The schedule is subject to the following constraints:

$$\sum_{i=0}^N \sum_{k=1}^M x_{ijk} = 1 \quad \forall j = 1, \dots, N \quad (2)$$

$$\sum_{\substack{i=0, \\ h \neq 1}}^N x_{ihk} - \sum_{\substack{j=0, \\ h \neq j}}^N x_{hjk} = 0 \quad \forall h = 1 \dots N, \\ \forall k = 1, \dots, M \quad (3)$$

$$\sum_{j=1}^N x_{0jk} \leq 1 \quad \forall k = 1, \dots, M \quad (4)$$

$$t_j \geq t_i + s_{ij} + p_i + \left(\sum_{k=1}^M x_{ijk} - 1 \right) B \quad \forall i, j \quad (5)$$

$$s_i \geq 0 \quad \forall i = 1, \dots, N \quad (6)$$

$$x_{ijk} \in \{0,1\} \quad \forall i, j = 0, \dots, N \quad \forall k = 1, \dots, M \quad (7)$$

Equation 1 is the objective function that will be minimized, and it computes the total changeover costs. Equation 2 ensures that every job is assigned to a line. Here, we only need to worry about feasible assignments. Equation 3 makes sure that if SKU i directly precedes SKU j , the opposite is not possible. In Equation 4 we make sure that if a job is assigned to a line, there is a SKU that occurs first in the sequence (i.e., it cannot be preceded by another SKU). Equation 5 computes the latest possible start time for SKU j , by making sure it is no later than the start time of SKU i , which directly precedes it, plus the processing time for SKU i , plus any setup time required when changing from SKU i to SKU j . Equation 6 ensures that no start time can be a negative value, and Equation 7 states that the sequencing variables x_{ijk} are binary.

This mathematical program can be solved to optimality as a mixed integer program. Given the data shown in Tables 1 and 2, the optimal solution is obtained when SKUs 1 and 2 are processed sequentially on Line 1, SKUs 3 and 4 are processed sequentially on line 2, and SKU 5 is processed on Line 3, producing a Total Cost = 0. The problem with this solution is that the makespan (total time to complete all jobs) is 1,840 minutes. This solution is shown in Figure 1.a. If we assume we must complete all jobs within a day's time, this solution is not acceptable.

We need to add a variable, which we will call C_{max} , to represent the maximum completion time of all jobs. Then, we denote C_i as the completion time for SKU i . We then add the following constraints to our mathematical program:

$$C_i = t_i + p_i \quad \forall i = 1, \dots, N \quad (8)$$

$$C_{max} \geq C_i \quad \forall i = 1, \dots, N \quad (9)$$

Finally, to guarantee that all production is completed within one day (1,440 minutes), we add a final constraint:

$$C_{max} \leq 1,440 \quad (10)$$

Solving this complete formulation results in the optimal solution shown in Figure 1.b., where Total Cost = 2, by sequencing SKUs 1, 2 and 4 on Line 1; SKU 3 on Line 2; and SKU 5 on Line 3. We now achieve a makespan of 1,380 minutes (on Line 1), but at a sacrifice in terms of cost due to the changeover required by switching production from SKU 2 to SKU 4 on Line 1. In the figure, the changeover is represented by the red bi-directional arrow.

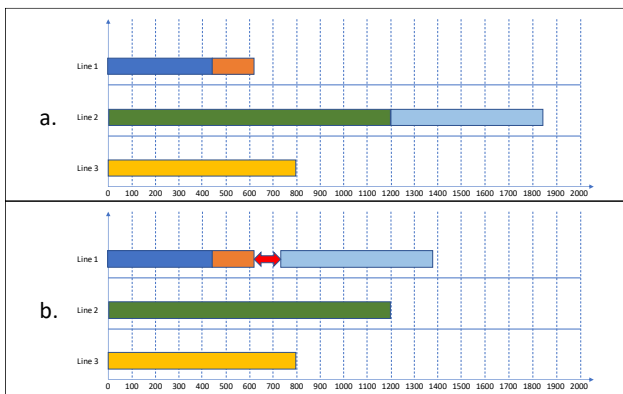


Figure 1. Optimal schedules

Implicit in the above formulation is that SKUs cannot be split, such that we can schedule part of a SKU on one line and the other part on another. Under some conditions, splitting SKUs might provide additional flexibility that may enable a reduced makespan, or the achievement of other desired goals, like maximizing equipment utilization. It is evident, however, that the formulation is applicable to SKU splits, by simply considering splits as additional SKUs. Thus, we can split each SKU into p equal-sized pieces, where each piece becomes a new SKU itself, and re-solve the problem.

The parallel machine scheduling problem with sequence-dependent costs and setups belongs to the class of NP-hard problems (Karp 1972), and solution times for even moderately sized such problems can be very large. When we consider splitting SKUs, we may quickly find ourselves with a very large scheduling problem in our hands. Let's consider, for example, that we split each of the five SKUs in our example into two equal pieces. Now we have a

11x11 matrix of sequencing variables on each line. With three splits, the new matrix will be of dimension 16x16x3. Thus, the number of variables and constraints will grow rapidly with respect to the number of splits (Xing and Zhang 2000). Many heuristic methods have been developed to solve this problem; see (Vilarinho and Santos 2010), for a good survey of proposed methods. We propose an approach that relies on a greedy procedure with randomized starts.

2.2. An Effective Metaheuristic

We shift our attention to problems where SKUs can be split into p equal pieces. We seek solutions that minimize completion time while maximizing equipment utilization (the reason will become apparent later, when we discuss capacity requirements). As stated above, even moderately-sized problems cannot be solved to optimality in reasonable time. Client requirements often make it necessary to obtain a good solution in a matter of minutes, hence the need to develop an efficient solution method.

A *metaheuristic* is a “problem-independent algorithmic framework that provides a set of guidelines or strategies to develop heuristic optimization algorithms.” (Glover and Sorensen, Metaheuristics 2013) As such, metaheuristic algorithms rely on heuristics, and are “designed specifically to find a solution that is good enough in a computing time that is small enough”. (Glover and Sorensen, Metaheuristics 2013) Thus, metaheuristics are employed in complex cases where exact methods cannot be applied, or where their application would be impractical. The production scheduling of SKUs on parallel lines is such a case. To find high-quality solutions to this problem in a reasonable time, we developed a metaheuristic algorithm, which combines a greedy construction heuristic with a randomized start procedure. We will now describe the method in detail.

To balance the solution in terms of completion time and equipment utilization, we use a compound objective function, as follows.

Let T denote the *tardiness* of a schedule, defined as a percentage; for example, if the required completion time is 1,440 minutes, and a solution has a makespan that runs over by 100 minutes, then $T = 100/1,440 = 6.94\%$.

Let U denote the average percent utilization rate of the equipment, such that $u_i = 1 - \frac{\text{idle time}}{\text{available time}}$ for equipment unit i . If this unit has been idle for 60 minutes, and it is available daily for 1,200 minutes from the time it starts production before it needs to shut down for maintenance,

then $u_i = 1 - \frac{60}{1,200} = 95\%$. Assuming we have Q units of equipment, then we compute U as

$$U = \frac{1}{Q} \sum_i u_i \text{ for } i = 1, \dots, Q$$

The method is designed to find the schedule that minimizes the function $w_1T - w_2U$, where w_1 and w_2 are weights assigned to each term, and $w_1 \gg w_2$. In other words, we consider the tardiness more critical than the utilization metric. In general terms, the method proceeds as follows:

- Step 1.** Construct an initial sequence and *Evaluate* the schedule
- Step 2.** Randomly order all SKUs into a list O
- Step 3.** Going down list O :
For SKU $i = 1$ to N
 - a. Consider every possible *insert* into the current sequence
 - b. *Evaluate insert*
 - c. Pick best improving *insert*
 - d. Move to next SKU
- Step 4.** At end of list O , if improving *insert* was found go back to Step 2; otherwise STOP

(*Evaluate* denotes a method where the current solution is evaluated in terms of the objective function. Depending on the complexity of the system, this might involve a simple computation or a more detailed simulation of the system.) This greedy method picks the best (improving) move at each step. We have defined a move as an *insert*. If we refer to Figure 2, a valid move is obtained by taking SKU 1 out of Line 2 and inserting it into Line 1, as shown. This particular insert creates the need for a setup (red two-way arrow) and a cleaning (black two-way arrow) on Line 1.

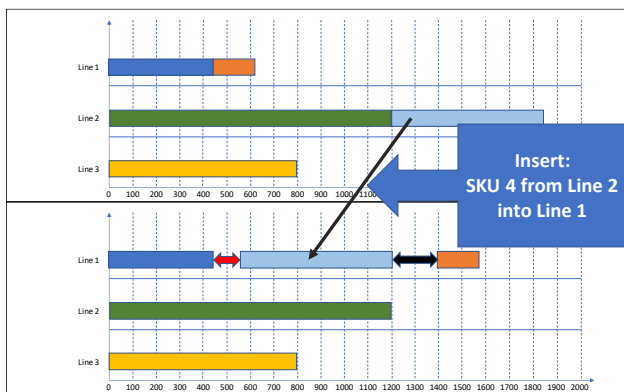


Figure 2. Example of an *insert* move

Moves in metaheuristic algorithms are common in what is typically called “local search” or “neighborhood search,” where immediate (local) neighbors of a solution are evaluated, by creating single-move changes. Local search methods tend to get “stuck” in suboptimal regions, so it is necessary to provide a way to explore more of the solution space. Based on principles from Tabu search (Glover 1989), we developed a method designed to escape suboptimal regions. To achieve that, we repeatedly run the method described above for a set number I of iterations, where Step 1 is randomized. In other words, we create a set I of random initial sequences, and apply Steps 2-4 to each. If I is large, there is a better chance that the method will converge to the optimal solution, but processing time will increase, so we need to pick I such that we can obtain a good solution in a maximum allotted time. Later, in Section 3, we discuss some computational results.

2.3. Optimizing System Capacity

So far, we have focused our attention on a method that optimizes the schedule for a given facility configuration. What happens when the facility is still in its design stages and has not been built yet? Process design engineers often call this a “greenfield” case because everything in it has yet to be defined.

In these cases, the typical approach is to design the facility first, and then – given the design – determine an optimal schedule. However, the decoupling of the design step from the scheduling step produces potentially suboptimal solutions, with unnecessary overestimation of capital expenditure and operating expense estimates. Consider, for example, a liquid flow system. You are considering building a plant in a new location. Your marketing department has provided you with estimated daily customer demand for the new facility. Given these estimates and your prior experience you decide that the design includes a need for four storage tanks of 100,000 liters each to handle work in process inventory. Then, you proceed to optimally schedule production given the design. With this approach, you failed to recognize that there is a schedule that does slightly worse in terms of total makespan, but only requires *three* storage tanks. In terms of the return on investment, this solution would have been highly superior.

Our approach handles the design step iteratively with the scheduling case. Each iteration consists of a system capacity optimization step followed by a production schedule optimization step, as shown in Figure 3.

The system capacity optimization step utilizes OptQuest®, a general-purpose metaheuristic optimizer developed by OptTek Systems, Inc. (www.opttek.com) OptQuest is a black box optimizer based on scatter search and tabu search methodologies (Laguna 2011), designed to provide an effective tool to optimize complex systems arising in industry.

In our context, OptQuest will suggest a set of input values that represent a facility configuration – i.e., number and capacity of storage tanks, number and capacity of coolers, number and capacity of mixers, number of machine operators, etc. OptQuest will then call upon the production scheduling optimization algorithm to evaluate the quality of the suggested configuration in terms of an objective function that is directly relevant to the system’s capacity. This process will continue in a loop until certain stopping conditions are met.

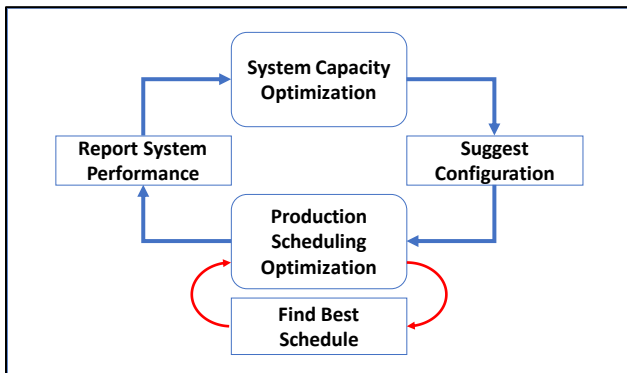


Figure 3. Capacity and schedule optimization procedure

2.4. Multi-objective optimization

In a greenfield case, it might be useful to craft an objective function that directly addresses the minimization of capital expenditures in addition to minimizing operating expenses and/or makespan. The coupling of both steps makes it possible to find an optimal schedule and, therefore, optimal performance for each design. Thus, we can make use of special features in OptQuest to obtain solutions that a decoupled approach would likely ignore.

For example, instead of enforcing a hard constraint on the allowed production time, we may penalize a solution that exceeds it. This enables us to obtain solutions where the savings in capital expenditures would greatly outweigh any costs associated with the excess processing time. In fact, we can simultaneously optimize the system with respect to two or more objectives that may be at odds with each other. For instance, we can seek a solution that produces a facility design and production schedule that minimizes capital

expenditures, while simultaneously minimizing makespan *and* operating costs. We call this “multi-objective optimization.”

Multi-objective optimization is very useful in many practical situations involving multiple conflicting objectives. (Deb 2014) In our example, for instance, it is desirable to minimize capital expenditures and to also minimize total production time (makespan). However, decreasing capital expenditures will generally result in longer production times. We would like to find a schedule that minimizes both objectives at once. Let us assume that the graph in Figure 4 represents the tradeoff between these two objectives. In the graph, the vertical y-axis represents the level of capital expenditures, and the horizontal x-axis, the total time required to finish a production run. As shown, production times are lowest when capital expenditures are quite high (it is important to note that after a certain point, increasing the capital expenditures will not have any effect on production time.) Initially, the curve is almost vertical, and capital expenditures can be reduced without a large increase in production time. After a certain point, however, the capacity of the system becomes progressively tighter, and the curve levels off. With such a complete description of the *trade space*, the production planning engineer can make an informed decision about how much immediate capital expenditures to trade for a decrease in total production time.

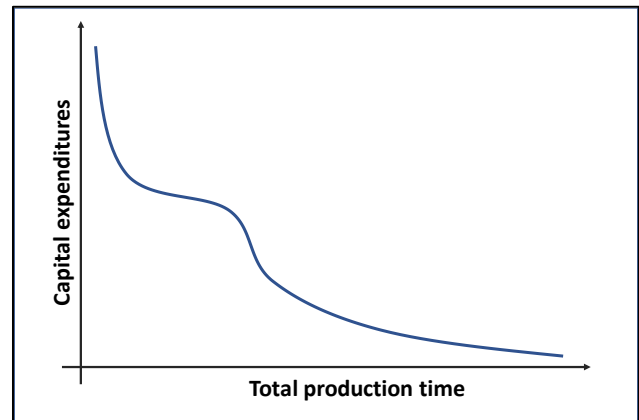


Figure 4. Pareto frontier

Our multi-objective optimization algorithms provide a complete picture of this multi-objective trade space, which we call the pattern frontier. Points on the frontier for which no improvement can be made to one objective without making another objective worse.

3. COMPUTATIONAL RESULTS

To test our method, we used a real-world case provided by a client. The case involves a small liquid food production facility with one separator, and six filling machines (a simplified schematic of the facility is provided in Figure 5.) Demand is specified by 17 SKUs of different product types and package sizes. In the plant, raw material reception occurs daily. Raw material storage tanks are directly filled by through pipes from the reception area. These are then pumped into the separator. After separation, the raw material is separated into a refined material we call “pulp,” and a waste byproduct. The byproduct is stored until it can be dispatched at the end of the day. Pulp is mixed with flavoring and stored until a filling machine is available. In the final step of the process, filling machines fill containers of a prespecified size with pulp of the appropriate flavor. A SKU is defined by the combination of flavored pulp and container size.

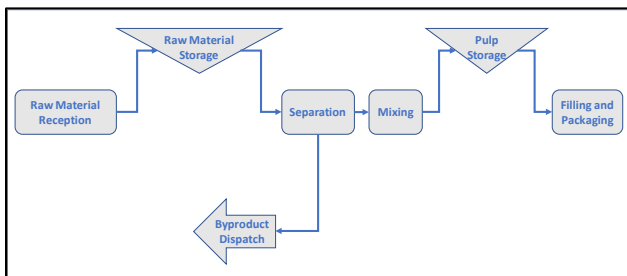


Figure 5. Liquid foods plant schematic

To evaluate the method, we conducted 8 distinct tests, and measured the time to completion and the quality of the solution in terms of makespan, equipment utilization, and capital expenditure (Capex) costs, where applicable. The tests and their respective results are described in Table 4.

Table 4. Evaluation tests

#	Type	Obj	Time	Mksp	Util	Capex
1	SA	<i>U</i>	7	99.1%	85%	N/A
2	SAE	<i>U</i>	15	99.1%	85%	N/A
3	SM	<i>M</i>	11	97.4%	95%	N/A
4	SME	<i>M</i>	9	97.4%	96%	N/A
5	CA	<i>C</i>	57	98.7%	84%	20%
6	CAE	<i>C</i>	82	98.8%	85%	20%
7	CM	<i>C, M</i>	45	97.6%	96%	41%
8	CME	<i>C, M</i>	55	97.6%	96%	52%

In Column 2 of Table 4, we label the type of test as follows:

- **S:** SSequence only → the plant configuration is given, such that the equipment quantities and capacities are fixed;
- **C:** Capacity → equipment quantities and capacities are variable, so the algorithm must find optimal settings;
- **A:** Average: → weekly production is averaged over 7 days, such that one-seventh of the weekly demand must be completed in each day;
- **M:** Makespan minimizing schedule → total weekly production must be completed as soon as possible;
- **E:** Expanded → the number of SKUs is doubled to 34, but the demand per SKU is halved, to test the flexibility of the algorithm to larger quantities of SKUs, but guaranteeing that a feasible schedule exists.

Thus, if Column 2 contains the abbreviation: “CAE,” it means that the test is of type “*Capacity, Average, Expanded*”. This means that the test involves a system capacity case, which requires optimizing both, plant capacity as well as the production schedule, for a daily average demand equal to one-seventh of the total weekly demand for each SKU, and the number of SKUs will be 34, but the demand for a SKU will be half that of the original SKU.

Column 3, shows the primary objective(s) of the test case. The objectives are abbreviated as follows: *U* = equipment utilization (maximized); *M* = makespan (minimized); *C* = capex (minimized). Time, in Column 4, reflects the computer run time – in seconds – to obtain the best solution. Columns 5 through 7 display the values of all applicable metrics of system performance, such as Makespan (in minutes per day for “Average” cases or per week for “Makespan-minimizing” cases), Utilization and Capex, respectively. These are all expressed as percentages. Thus, makespan is reported as a percentage of the maximum allowable production time (i.e., 1,440 minutes per day for tests involving an “Average” production requirement, and 10,080 minutes per week for tests involving a “Makespan-minimizing” production requirement. For the “Capacity” cases, we forced the system capacity optimization to stop after 500 iterations of the OptQuest algorithm.

As the results show, though simple, our method produces high-quality solutions in very short computational time. This makes the method well-qualified not only in strategic production design and planning situations, but in real-time, operational scheduling. It is also useful for purposes of re-optimizing a schedule in the event of a major disruption in production (e.g., a machine breakdown). This last case is

of critical interest in many settings, where the usual reaction is to continue with the planned schedule and “work around” the disruption, which often leads to increased operating costs and excess product waste. (Mordechai 2015) By enabling the schedule to be re-optimized in a matter of seconds the disruption and its estimated duration can be addressed directly in the new schedule – thus minimizing these negative effects – and production can resume immediately.

4. CONCLUSIONS

In this study, we have described an effective approach to optimize the capacity and production schedule of a specific type of manufacturing operation – liquid foods. However, our approach is highly flexible and can be applied in virtually any complex production process. For instance, the metaheuristic described in Section 2.2 can be further enhanced or modified to accommodate other situations, and different solution approaches can be applied to different systems based on particularities of each system.

REFERENCES

- Abakarov, A., Y. Sushkov, S. Almonacid, and R. Simpson. 2009. "Thermal processing optimization through a modified adaptive random search." *Journal of Food Engineering* 200-209.
- Deb, Kalyanmoy. 2014. "Multi-objective optimization." In *Search Methodologies*, by Edmund K Burke and Graham Kendall, 403-449. New York: Springer US.
- Glover, Fred. 1989. "Tabu Search - Part 1." *ORSA Journal on Computing* 1 (2): 190-206.
- Glover, Fred, and Kenneth Sorensen. 2013. "Metaheuristics." In *Encyclopedia of Operations Research and Management Science*, by Saul I. Gass and Michael C. Fu (eds), 960-970. New York: Springer US.
- Jahangirian, Mohsen, Tillal Eldabi, Aisha Naseer, Lampros K Stergioulas, and Terry Young. 2010. "Simulation in manufacturing and business: A review." *European Journal of Operational Research* 1-13.
- Karp, Richard M. 1972. "Reducibility among combinatorial problems." Edited by James W. Thatcher, Jean D. Bohlinger Raymond E. Miller. *Complexity of Computer Computations*. Yorktown Heights, NY: Springer US. 85-103.
- Laguna, Manuel. 2011. "OptQuest - Optimization of Complex Systems." *OptTek Systems, Inc.* 5 9. Accessed 5 23, 2017. <http://www.opttek.com>
- Mordechai, Yael. 2015. *Optimization and reoptimization in scheduling problems*. Masters Thesis, Haifa: Israel Institute of Technology.
- Smith, Jeffrey S. 2003. "Survey on the Use of Simulation for Manufacturing System Design and Operation." *Journal of Manufacturing Systems* 157-171.
- Vilarinho, Pedro M, and F Charrua Santos. 2010. "The problem of scheduling in parallel machines: a case study." *Proceedings of the World Congress on Engineering*. London, UK: WCE.
- Wari, Ezra, and Weihang Zhu. 2016. "Multi-week MILP scheduling for an ice cream processing facility." *Computers and Chemical Engineering* 141-156.
- Xing, Wengxun, and Jiawei Zhang. 2000. "Parallel machine scheduling with splitting jobs." *Discrete Applied Mathematics* 103 (2): 259-269.

DISCRETE EVENT SIMULATION OF A PIGMEAT PACKING PLANT

L.M. Plà-Aragonés^(a), A. Pagès-Bernaus^(b), E. Novoa-Tufet^(c), J. Mateo-Fornés^(d), P. Tarrafeta^(e), D. Mendioroz^(f), Lorea Pérez-Cánovas^(g), Sandy López-Nogales^(h)

^{(a), (b), (c), (d)}, University of Lleida, Jaume II, 69, 25001 Lleida, Spain.

^{(e), (f), (g), (h)} Carnicas Iruña-Velasco, 31160 Orcoyen, Spain.

^(a)impla@matematica.udl.cat, ^(b)adela.pages@matematica.udl.cat, ^(c)enotu@gmail.com, ^(d)jmateo@diei.udl.cat, ^(e)ptarra@gmail.com, ^(f)dmendioroz@carnicasiruna.com, ^(g)lorea@carnicasiruna.com, ^(h)slopez@carnicasiruna.com

ABSTRACT

This paper is presenting the development of a discrete event simulation model of a pig meat packing plant located in Navarre (Spain) as result of a research collaboration between the pig industry and the University of Lleida. The packing plant processes between 900 to 800 pigs a day and it is located apart of the slaughterhouse. The simulation model was developed to represent all the tasks performed in the plant. The development was incremental as the whole model is made of different sub-models focused in different products as for example ham, ribbon or sirloin. The collaborative work with the employees of the company was essential for the success in the model outcome. The main utility of the proposed model was to compare different processing alternatives for primary cuts and a better production planning of the tasks for a day.

Keywords: meat plant operation, production planning, discrete event simulation

1. INTRODUCTION

Simulation is recognized as the second most widely used technique in the field of operations management, the most popular being ‘Modelling’. Generally speaking, a simulation-based approach does not provide exact or optimal solutions to problems but it allows users analyzing the behavior of complex systems, performing what-if analysis and choosing correctly among different possible scenarios/solutions (Bruzzone and Longo (2013)). Its use as a tool to help in the design and operation of manufacturing systems has been transformed by the invention and evolution of the computer, which has supported the uptake of practical simulation tools and techniques. (Jahangirian et al. 2010). These complex, dynamic and stochastic systems involve large capital investments, making cheaper and easier to experiment and compare alternative management strategies with simulation models, instead of experimenting with the real system (Negahban and Smith 2014).

Different surveys of the current state of the art clearly reveals discrete event simulation has been applied to various sectors, such as manufacturing, services,

defense, healthcare, and public services (Jahangirian et al. 2010, Negahban and Smith 2014). In particular, different simulation models for manufacturing systems operation have been published (Negahban and Smith 2014) and few of them are related to the food industry as referred Bruzzone and Longo (2013). That is also the case for the pig industry where most specialized software programs focus on herd management tools developed and introduced for on-farm use and less for slaughtering and meat processing plants (Plà 2010). This means that there are management areas where decision tools are less developed in the pig sector. A surprising fact, taking into account that decisions at different levels are important for the pig industry viability and for meat packing plants in particular. Then, there is a growing need to address the complexities of the whole pig enterprise and the difficulties of dealing with different layers of decision-making within a system (Rodriguez et al. 2014). Maybe the simplicity required in getting the big decisions right and making correctly the major tactical adjustments for the risk averse primary sector (Pannell et al. 2000) are the reasons.

Consequently, scarce examples exist about meat packing processing plant models and even less for pigs. The more similar approach to the problem presented here is that of Bixby et al. (2006) who presented a set of LP models developed to schedule dynamically beef packing plants operations for a beef company. Proposed models were deterministic and developed ad hoc given the characteristics of this specific beef company with five different plants to coordinate.

In this paper, we are concerned with the modelling of the tasks performed in a pig meat packing plant processing pig carcasses and selling different products, i.e. meat cuts and by-products in fresh or frozen, to wholesalers and local butcheries. The analysis is focused first in valuing the cost-benefit of the different alternatives for a products’ family as the plant receives many local offers of different products they do not produce usually and they meet problems to assess a convenient sale price. Hence, the goal of the model is to facilitate the analysis of different production alternatives for a working day either to compare specifically a products’ family or globally to assess the daily

production plan (a sole meat plant simulation model with all ordered products integrated).

2. MATERIAL AND METHODS

The company “Carnicas Iruña Velasco SA” settled in Orcoyen (Navarre, Spain) provided the data, collaboration and support for this project. The framework was a collaborative project understood as a joint collaboration between University of Lleida and “Carnicas Iruña Velasco SA” (“Carnicas Iruña” for short) to improve the knowledge in this kind of processes. The meat packing plant is embedded in a pig supply chain (PSC) where different long term agreements with pig producers and abattoirs are settled to assure the procurement of carcasses (body of the animal eviscerated) to process.

Broadly speaking, the PSC includes organizations in charge of procurement, production, slaughtering, processing, distribution and marketing of pork, derived and by-products to the final consumers. Different PSC agents under one or more vertically integrated companies work together in a coordinated way for producing and fattening pigs transferred to abattoirs for eventual slaughtering. Resulting carcasses will then be processed in a meat packing plant to satisfy customer’s demand for different products either fresh, cured or manufactured. Retailers, supermarkets and butcheries work in the final stage of the chain, supplying pork products to customers (Rodriguez et al. 2014).

The processing capacity of the “Carnicas Iruña” plant range between 800 to 900 carcasses as maximum per day. Three trucks a day coming from two different abattoirs, sending each one approximately a half of the stock, serve the plant. The day before, abattoirs communicate the information of slaughtered animals to the plant and so, the meat packing plant can plan the production planning for the following day according to pending or already received orders. The plant has only one line operating at a speed of 150 or 120 carcasses per hour. Usually, operations in the plant are deployed around the cutting tree of the pig carcass and the means to perform the disaggregation in commercial cuts. In a first stage, primary cuts are produced leading to a second stage where each primary cut is processed and first commercial cuts obtained. These cuttings are done along a processing line with two sides, one devoted for each semi-carcass. Depending on the product, off-line cuts may be required involving additional personnel, variable workload and time. The objective for the plant is to extract the maximum value of the carcass performing a disaggregation plan leading to the right (best valuable) products.

The simulation model was implemented in ExtendSim (see Figure 1), an interactive simulation tool (Krahl 2013) with 2D animation capabilities. The ExtendSim simulation environment provides the tools for all level of modellers to create accurate, credible, and usable models in an efficient way. The selection of a proper simulation software can make a significant difference in how well simulation analyses support

managerial decision making. Thus, ExtendSim was chosen because it facilitated every phase of the simulation project, from creating, debugging, verifying, and validating the model, to the construction of a user interface. This way, developers and target users could collaborate in the conceptual development of the model and later in the analysis of the system. An ExtendSim model is created by adding blocks to a model worksheet, connecting them together, and entering the simulation data. Each block has its own functionality, dialog, help, icon, and connections. Each instance of a block in the model has its own data. The logical entity that moves through the system is referred to as an item. Items carry properties or attributes with them as they progress from one block to the next. Items are represented using data structures allowing large numbers to exist simultaneously within a model. An additional advantage for developers is the ExtendSim’s built-in, compiled language, ModL, to create reusable modelling blocks beyond the standard libraries provided by ExtendSim. All of this is done within a single, self-contained software program that does not require external interfaces, compilers, or code generators. Hierarchical help to organize the model. Hierarchical blocks are elements that can be added to the model in number equal or greater to one and they are very useful to make the model more readable. For instance, each primary cut or product can be encapsulated as a sub model into a hierarchical block.

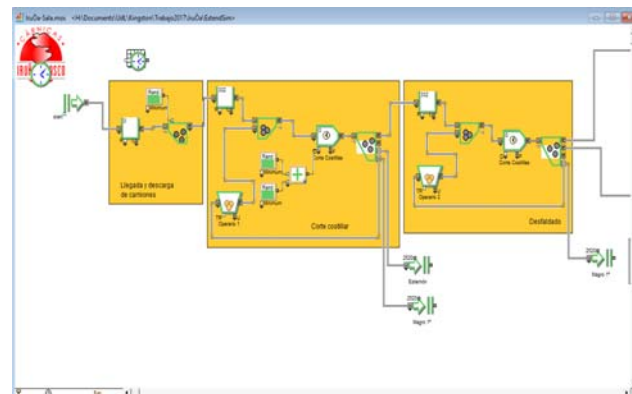


Figure 1: Overview of the model

3. BRIEF OVERVIEW OF THE SIMULATION MODEL

Based on the description of the process assisted by the employees of the company a conceptual model was developed. A first prototype was implemented according the first description. Later on, the conceptual proof was refined and the rationale of the model corroborated with different visits and inspections to the plant till the version was accepted by both parts.

The model represents carcasses as items that flow through the different blocks of the model. As the simulation progresses, initial items are split on other items as result of different activities: cutting operations. Then, an original cut can produce different sub cuts according to a pre-stated cut tree. In this sense, it is crucial the cutting tree with the representation and

product branch location of all the different cuts relevant for the Spanish market and corresponding products' family. In general, all products and by-products have a different commercial value and this can even vary from order to order. It is a task of the sales' department to agree the final value with clients when placing orders.

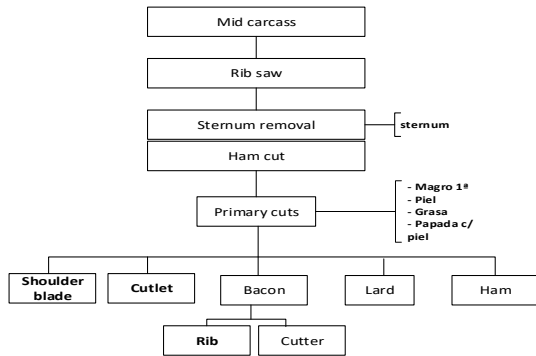


Figure 2: Primary cuts

The first part of the cutting tree produces primary cuts as shown in Figure 2. Before proceeding explicitly with primary cuts some preparation of the carcass is needed: to cut completely the carcass in two, to saw the rib for a later easier processing in the line with only knives, to remove the sternum and give a helping cut in the ham to ease its later separation from the rest of the mid carcass. As result, there are subproducts that can be obtained during this primary process like lean, skin, fat or dewlap with skin.

There are five primary cuts for each mid carcass (Figures 2) operated in one line. Once primary cuts are produced some of them can be marketed as such, like ham, lard or shoulder blade. However, it is more common to go on processing and getting additional and more elaborated/processed products. For instance, figure 3 represents the different products can be obtained from ham. First of all, a ham can be with skin or skinless. The latter is mainly used for York ham production. It is the result of removing skin, tail, ankle bone, foot, minor cuts of lean and fat to shape the ham. Further products are obtained with additional processing of the York ham: Ham 3D (boneless ham), Ham 4D (boneless and sinew removal), Ham 5D (like a leaner 4D) and Ham 6D (like a ham 5D without the aponeurosis). Ham with skin is the raw to produce cured ham products.

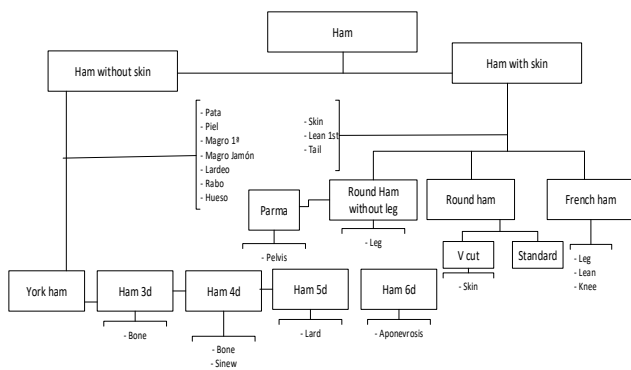


Figure 3: Ham cuts

Each cut information includes attributes as weight, lean, bone, fat and skin percent. If a meat cut can be processed further, each resulting cut is defined with the same attributes referred before. In order to consider different carcass composition a sampling by genotype (only Pietrain and Large White breeds are processed by Carnicas Iruña) and weight (three categories: low, regular, heavier) was performed considering normal distribution for weight attributes.

Table 1: Sample example

Low weight range			
#	Weight	Gender	%Lean
214	76.1	H	68.3
215	75.6	H	65.8
220	81.2	M	69.0
221	81.4	H	65.4
251	78.5	H	66.8
256	82.0	M	62.8
257	84.0	M	64.4
306	71.1	M	68.5
324	78.9	M	68.0
349	75.6	M	66.6

Table 1 shows an example of one sample of ten pietrain pigs of low weight category used to estimate the normal distribution for this genotype x weight category. Gender was not considered in the simulation. A t-test was performed over different samples to check no statistical differences to this measures between genders. Main results of the carcass composition for this sample is shown on table 2. Figures on table 2 are the base to randomly derive primary cut attributes. Similarly, each product family in the cut tree was sampled in similar terms to simulate them properly. It should be noted that several products or by-products come directly from the abattoir without no processing on plant like heads, blood or liver.

Table 2: Carcass composition for Pietrains of low range weight (total sample weight 784.4 kg)

Cut	Weight	Percent
Ham	255.2	32.4
Shoulder blade	110.3	14.0
Dewlap	24.9	3.2
Lard	47.5	6.0
Bacon	121.5	15.4
Cutlet	169.3	21.5
Skin	5.0	0.6
Lean 1st	0.6	0.1
Fat	0.25	0.0
Heads	42.6	5.4
Hands&feets	7.6	1.0
Sternum	2.9	0.4

4. RESULTS AND DISCUSSION

For verification purpose, the model was compared with analytical results (Kleijnen, 1995) running the model in a deterministic mode and later with the random capabilities for each category. The simulation model was not run with all possible parameters, only those compatible with the analytical model were set. Verification process was automatized by developing specific calculations keeping track of main variables for each meat cut as total meat weight and bone percent.

Later on, in order to validate the model and assess the suitability of the proposed simulation model a comparison was established between results performed without random variability of variables and correlations (i.e. adopting expectations for random parameters) and the same simulation model but taken into account full capabilities of the model to reflect real systems (i.e. generating random values for each random variable considered). Thus, a group of parameters satisfying the needs of both runs was set. This process was assisted by the personnel of “Carnicas Iruña” involved in this research. Results at this stage were also verified and discussed by the company giving their approval.

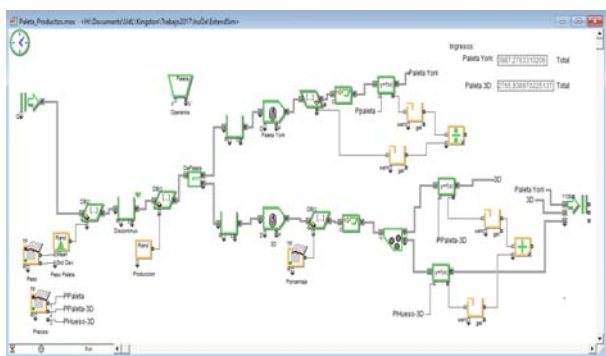


Figure 4: Comparison between incomes of two products: york ham and ham 3D (i.e. boneless)

The more interesting part of the model and the focus was the different sub models developed for each product (see e.g. Figure 4). For instance, ham. All the family products are those described in Figure 3 and also de subproducts associated to them (e.g lean, bone, skin, fat,...). However, in this example we limit our interest to two products: York ham and ham 3D. Figure 4 is shown the result of an instance comparing the two products mentioned according to the incomes generated. Hence, the manager of the plant can explore the range of prices for each product and subproduct involved that can make more interesting to produce one product or the other. In addition, he has a tool to get the shadow price for a product in case an interested customer request information about a specific product.

A real situation experienced by the meat plant was related to hams marketed in Spain and France. The plant has costumers from both countries and so the diversity of products make difficult sometimes to assess the commercial interest for the company to make one product or combine both demands. In addition, the value of the different costs affecting the manufacturing of one

cut or a different one is not always evident. Hence a cost-benefit analysis product by product was very appreciated by the company.

As every product and products' family were represented by a block, the link of all of them in a ExtendSim sheet allowed the representation of the full operation of the plant. It was necessary to add labor adjusting labor capacity with the number of employees available and to fix the production planning structure, i.e. the internal sequence to fulfill the incoming orders. Labor modeling out of the line was easy as these tasks were assigned to hired personnel paid per products regardless the time invested in the cutting.

5. CONCLUSION

The simulation model described here represents a practical approach for planning pig meat production under different carcass disaggregation plans. It is more flexible and accurate than deterministic or stationary approaches, essentially because it better captures the dynamics of the plant production and cutting operation process. The use of a visual simulation tool like ExtendSim is essential to interact with specialist during the development of the model. Moreover, different advantages are drawn respect to previously published models for similar purposes in other fields like a greater understanding of the system, the reduction of operating costs by a better control of products to serve and personnel, a risk reduction in failing to fulfill orders, lead time reduction, reduction of capital costs, and faster configuration changes in production planning. The simulation model considered only variations in carcass weight and breeds but can explore alternative products from the same primary cut.

ACKNOWLEDGMENTS

The authors are grateful to anonymous referees for their constructive comments, which helped us greatly improve the presentation of the article. L.M. Plà and A. Pagès are members of the excellence research group 2014-SGR151 and J. Mateo member of the excellence research group 2014-GR163, funded by the Generalitat de Catalunya (Spain).

REFERENCES

- Bixby, A.; B. Downs and M. Self, 2006. A Scheduling and Capable-to-Promise Application for Swift & Company. *Interfaces* 36(1):69-86.
- Bruzzone, A.G., Longo, F. (2013). An advanced modelling & simulation tool for investigating the behaviour of a manufacturing system in the hazelnuts industry sector. *International Journal of Food Engineering*, 9 (3): 241-257
- Jahangirian, M., Eldabi, T., Naseer, A., Stergioulas, L.K., Young, T. 2010. Simulation in manufacturing and business: A review. *European Journal of Operational Research*, 203: 1-13
- Kleijnen, J.H.P. 1995. Verification and validation of simulation models. *European Journal of Operational Research* 82: 145-162.

- Krahl, D. 2013. ExtendSim 9. In Proceedings of the 2013 Winter Simulation Conference, ed. R. Pasupathy, S.-H. Kim, A. Tolk, R. Hill, and M. E. Kuhl, 4065-4072. IEEE, Piscataway, NJ.
- Negahban, A., Smith, J.S. 2014. Simulation for manufacturing system design and operation: Literature review and analysis. *Journal of Manufacturing Systems*, 33(2): 241-261
- Panell, D.J., B. Malcom and R.S. Kingwell. 2000. Are we risking too much? Perspectives on risk in farm model-ing. *Agricultural Economics* 23: 69-78.
- Plà, L.M. 2010. DSS in Pig Production Systems. In: Basil Manos; Nikolaos Matsatsinis; Konstantinos Papparrizos; Jason Papatthanasiou (Eds), *DSS in Agriculture, Food and the Environment*. IGI-Global. New York 101-117.
- Rodriguez, S., L.M. Plà and J. Faulin. 2014. New opportunities in operations research to improve pork supply chain efficiency. *Annals of Operations Research*. 219: 5-23.

AUTHORS BIOGRAPHY

Lluís Miquel Plà-Aragonés is an associate professor in the Department of Mathematics at University of Lleida (UdL) and a Senior Researcher at the Agrotecnio Research Center. His research interests include operational research methods applied in agriculture and forest management, with special reference to simulation, dynamic programming, planning, Markov decision processes and production planning. Coordinator of the EURO-Working group (Operational Research in Agriculture and Forest management) <www.orafm.org> and head of the CYTED Latin-American network on Big Data and DSS in Agriculture <www.bigdssagro.udl.cat>. He is a member of EURO. His Web address is <www.udl.cat/usuaris/d4089492/>.

Adela Pagès-Bernaus is Senior Researcher in the Department of Mathematics at University of Lleida (UdL) and at the Agrotecnio Research Center. Her research interests include operational research methods applied in agriculture, with special reference to simulation, stochastic programming, simheuristics, planning and production planning.

Eva Novoa-Tufet is graduated student of the Department of Mathematics at University of Lleida (UdL). Her research interests include operational research methods applied in agriculture and economics with special reference to simulation.

Jordi Mateo-Fornés is a PhD student of the Department of Informatics and Industrial Engineering at University of Lleida (UdL). He is currently researching about different optimization methods and algorithms such as the benders decomposition, lagrangean relaxation and scenario analysis applied to real life problems. His research interests include operational research methods applied in agriculture and parallel computing, with

special reference to simulation, stochastic programming, scheduling and production planning.

Pedro Tarrafeta is the CEO of Carnicas Iruña-Velasco SA.

Daniel Mendioroz is the manager of Carnicas Iruña-Velasco SA in charge of the plant.

Lorea Pérez-Cànovas is the product manager of Carnicas Iruña-Velasco SA. She is in charge of inventory management and control. She is assisted by Sandy.

Sandy López-Nogales is the head of quality department at Carnicas Iruña-Velasco SA. She is in charge of sampling the products produced by the plant in accordance with carcasses procured and cuts demanded.

CFD MODEL VALIDATION OF A BAG FILTER FOR AIR FILTRATION IN A MILLING PLANT

Federico Solari^(a), Giorgia Tagliavini^(b), Roberto Montanari^(c), Eleonora Bottani^(d), Nicola Malagoli^(e), Mattia Armenzoni^(f)

^(b)Interdepartmental Center CIPACK, University of Parma – Parco Area delle Scienze 181/A, 43124 Parma (Italy)

^{(a),(c),(d),(e),(f)} Department of Engineering and Architecture, University of Parma – Parco Area delle Scienze 181/A, 43124 Parma (Italy)

^(a)federico.solari@unipr.it, ^(b)giorgia.tagliavini@unipr.it, ^(c)roberto.montanari@unipr.it, ^(d)eleonora.bottani@unipr.it,
^(e)nicola.malagoli@unipr.it, ^(f)mattia.armenzoni@unipr.it

ABSTRACT

Milling plants often adopt pneumatic conveying to transport grains or flour inside their pipes.

The most common conveyor is air, which must be cleaned from solid particulate in suspension, before being released into the atmosphere.

To ensure air depuration, a filtration system is installed at the end of the milling plant. Such systems typically consist of cyclones separators and bag filters.

This paper presents the design and the validation of a computational fluid dynamic model for a pilot plant reproducing the mentioned air filtration system.

The pilot plant, located inside a laboratory at the University of Parma, was equipped with sensors to collect velocity and pressure data.

The comparison between the experimental values and those from the fluid dynamic simulations made the model validation possible and thereby achieving a robust predictive approach for the design of air filtration systems.

Keywords: Computational Fluid-Dynamics, Air Filtration, Bag Filters, Milling Industry

1. INTRODUCTION

In milling plants, granular products are often moved thanks to pneumatic transport. Consequently, the air used as a conveyor must be filtered before being released back into the atmosphere.

Filtration consists in the separation of different phases by inserting a filter media along the fluid path. Such a technique employed in many areas: from automotive to food industry [Billings et al. (1970), Sutherland (2008)].

The separation between solid and gas/liquid phase is influenced by the particles size or the particle density. Cyclones separators have been the most common devices for removing dispersed particles from their carrying gases, thanks to their favorable balance of good separation efficiency and low cost of investment,

operation and maintenance. Moreover, cyclones are able to handle any combination of gas pressure, temperature and several particles types. Therefore, they are considered more simple, robust and reliable than other separation equipment.

All the factors described above are crucial to make cyclone separators key components in different sorts of industrial plants for gas filtration [Alexander (1949), Chen et al. (2007)].

For this reason, since the 19th century, experimental studies have been developed to investigate the flow characteristics inside cyclones for a better understanding of pressure drops and separation efficiency [Meier et al. (1998), Stendal (2013)].

Filters are classified according to their ability to remove particles of a specific size. Fabric is the most widely used filter material. It is made from natural or synthetic fibers and typically requires some kind of support to be used as filter medium [Le Goff et al. (1969), Sommerfeld (2000)].

Bag filters are a type of filter frequently used for liquid or gas filtration. In the latter case, the units are significantly larger and multiple installations are needed, because of high flow rates [Lo et al. (2009), Mehta et al. (1956), Yoa et al. (2001)]. These filters are long cylindrical fabric hoses, mounted on a cylindrical cage with holding rings along the filter length. The hose is upright, closed at the bottom, hanging from a plate with the aperture at the top fastened to a hole in the plate.

Cyclones can usually reach high separation efficiencies, but despite this, they fail to separate the finest particles; to overcome this limit, it is necessary to combine them with bag filters, especially when it comes to air depuration.

In the research described in this paper, a bag fabric filter was installed inside a cyclone separator. This particular solution combines the cyclone and the filter benefits to enhance the separation efficiency with low energy consumption. Furthermore, this solution not only

improves the system overall efficiency, but also allows positive effects on filters operating conditions, increasing their life cycle. Ultimately, dust emission levels into the atmosphere are kept within the limits prescribed by law regulations.

The objective of this work was to study the behavior of this combined filtering system at different operating conditions with the purpose to obtain a predictive fluid dynamic model for industrial design. This was possible due to computational fluid dynamics simulations validated with a targeted experimental campaign on a pilot plant.

2. EXPERIMENTAL APPROACH AND THEORETICAL ASPECTS

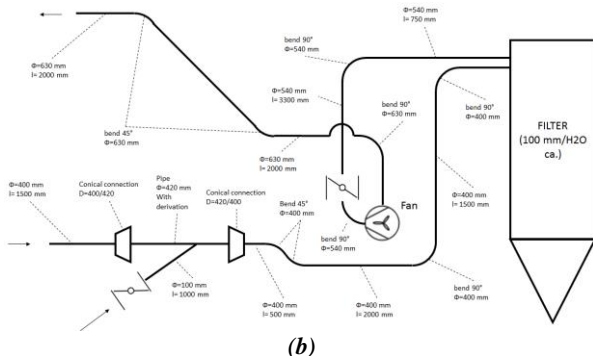
The experimental campaign was conducted on the pilot plant built up inside the Industrial Engineering laboratory of the University of Parma, reproducing the mill filtration system previously described.

It consists of a bag fabric filter with 31 hoses placed inside a cyclone separator.

As this filtration system is not connected to a real industrial plant, it needs to exploit the air from the external environment. To do so, a suction fan controlled by an inverter draws the air inside the system. After passing through the filter, the air is recirculated in the atmosphere (Figure 1).



(a)



(b)

Figure 1: Pilot plant (a) and its scheme (b).

Since ambient air was used, which is free from solid particulate, the data collection and the subsequent simulations focused only on the fluid dynamic aspects of the system, omitting the separation efficiency at this first stages.

2.1. Data acquisition and sensors description

The velocities inside the filter were collected thanks to a hot-wire anemometer and a Pitot tube flow meter, while the pressure drop was measured with a differential pressure sensor.

To test the correct functioning of the pilot, the airflow rates were estimated. Due to the evaluation complexity, the airflow rates acquired experimentally were compared to those from the fan operating curve at different inverter frequency values.

For velocity and pressure data acquisition, appropriate housings were created to insert the sensors probes at various points along the filter as well as along the inlet and outlet ducts.

In particular, the housings were placed on the filter in the following points (Figure 2):

- one at the bottom of the cyclone, to collect the velocities (green dot);
- four at the volute of the cyclone to evaluate the velocities (yellow dots);
- one at the inlet and one at the outlet section for pressure drop (red dots).

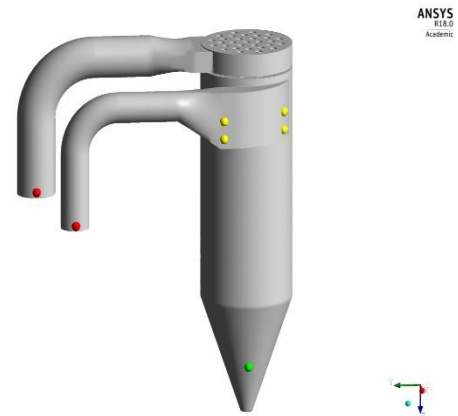


Figure 2: Sensor placement.

2.1.2. Hot-Wire Anemometer

A VelociCalc Air Velocity Meter 9565 Series was used. This instrument is commonly used to determine the air speed inside ventilation ducts.

It consists of a thermo-resistance, i.e. a resistor whose value is proportional to the temperature. This resistance is immersed in the tested flow. An electric current of known intensity keeps the resistance at a higher temperature compared to the fluid. The fluid cools the resistor proportionally to its velocity, allowing the data acquisition.

The advantages of this sensor are mainly associated to the reduced probe dimension. Hence, it allows to take measurements at various locations in the pipeline minimally affecting the fluid flow and ensuring a very quick response. Some drawbacks are related to calibration issues [VelociCalc Manual]. The main technical specifications are listed in Table 1.

Velocity (TA Probe)	
Range	0 to 50 m/s
Accuracy	±0.0015 m/s
Resolution	0.01 m/s
Temperature (TA Probe)	
Range	-10 to 60°C
Accuracy	±0.3°C
Resolution	0.1°C
Relative Humidity (TA Probe)	
Range	5 to 95% RH
Accuracy	±3% RH
Resolution	0.1% RH

Table 1: Hot-wire Anemometer technical specifications.

2.1.3. Pitot tube flow meter

The functioning of the Pitot tube grounds on the Bernoulli's equation (Equation 2).

$$p_{tot} = p_{st} + \frac{1}{2}\rho|v|^2 \quad (2)$$

$$v = \sqrt{\frac{2(p_{tot}-p_{st})}{\rho}} \quad (3)$$

The Pitot tube is a simple sensor but reliable sensor: a tube with at least two holes is inserted within the fluid flow. The holes are the pressure probes, located respectively tangentially and orthogonally to the flow. The first pressure probe measures the total pressure while the second one provides the static pressure. As the two separate channels converge towards a differential pressure gauge or a differential pressure transmitter, the dynamic pressure is calculated as the difference between the two detected pressures, which is proportional to the square of the fluid velocity (Equation 3).

The device used was a PCE PVM-620 Pitot tube, with the following technical specification (Table 2).

Pressure	±3735 Pa
Velocity	1.27 to 78.7 m/s
Resolution	1 Pa – 0.1 m/s
Accuracy	±1%

Table 2: PCE PVM-620 technical specifications.

2.1.4. Differential pressure sensor

The differential pressure sensor is an Endress Hauser Deltabar S PMD75, whose technical specifications are shown in Table 3.

Pressure	±10 mbar to ±40 bar
Temperature	-40 to +85°C
Output	4 to 20 mA
Accuracy	±0.035 %

Table 3: Deltabar S PMD75 technical specifications.

This sensor embodies process isolating diaphragms, which are deflected on both sides by the acting pressures. A filling oil transfers the pressure to a resistance bridge. The change in the bridge output voltage depends on the differential pressure, which can be measured and processed [Deltabar S PMD75 Manual] (Figure 4).

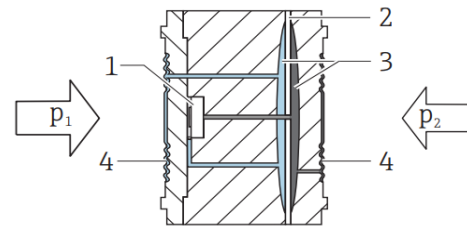


Figure 4: PMD75 measuring system: 1) measuring element, 2) middle diaphragm, 3) filling oil, 4) process isolating diaphragms.

2.2. Theoretical aspects of cyclone separators and filters

Cyclone separators draw the particles inside the fluid into a vortex, where inertia and gravitational forces act upon particles separation.

The fluid enters tangentially into the cylindrical chamber with a high rotational component. The flow descends rotating near the wall, until a certain location where the axial velocity component reverses itself, making the flow to ascend. The ascension proceeds near the cyclone axis [Cortés et al. (2007)].

As said above, it is helpful to understand how cyclones works but, in this case, their characteristic structure has not been strictly followed. The key function of the cyclone here, apart from separating the particulate, is to accelerate the flow towards the fabric filters, which are located in the central part where the vortex finder is usually located.

The basic principles of filtration can be traced back to those that regulate the general motion of fluids in porous media.

A porous medium is characterized by a partitioning of the total volume into solid matrix and pore space, with the latter being filled by the fluid.

The basic feature of this medium is porosity. The bulk porosity Π of a material is defined as the ratio of void volume V_v to body volume V_0 :

$$\Pi = V_v/V_0 \quad (4).$$

Since the remaining portion V_s of the total volume of the material is in the form of a solid matrix, then:

$$1 - \Pi = V_s/V_0 \quad (5)$$

Permeability (or gas permeability) is the property that gives a measure of the gas flow through a porous medium exposed to a pressure difference. The superficial velocity V of the fluid flow depends on permeability and pressure gradient in accordance with a Darcy's law.

At laminar flows, the inertia term in the Darcy's equation may be neglected and the equation takes the form that is widely used in the theory of filtration:

$$\frac{dp}{dx} = \frac{\mu}{K} \cdot v \quad (6)$$

where $K = 1/\alpha$ is the Darcy's permeability coefficient in $[m^2]$ and α is the permeability $[1/m^2]$.

The inertia term is instead needed in presence of turbulent flows: in this scenario, the equation becomes:

$$\frac{dp}{dx} = \frac{\mu}{K} \cdot v + \rho \cdot \frac{K_{loss}}{2} \cdot v^2 \quad (7)$$

where $\frac{K_{loss}}{2} = 0,043(1 - \alpha)^{-2,13}$ [ANSYS FLUENT 18 – Theory Guide].

The difference between Equation 6 and 7 is clarified in Figure 5.

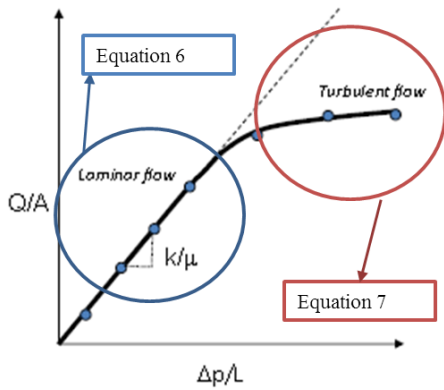
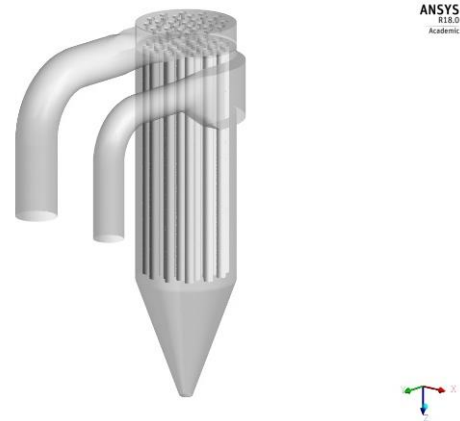


Figure 5: Difference between the Darcy's equations.

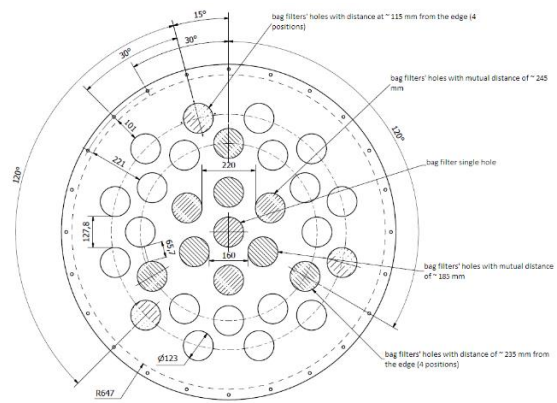
3. COMPUTATIONAL FLUID DYNAMICS MODEL

3.1. Geometry

The computational geometry reproduced the sizes of the bag filter in the pilot plant, with the details of the filter hoses positions (Figure 6).



(a)



(b)

Figure 6: Computational domain (a) and bag filters positions (b).

To obtain a fully developed flow, both the inlet and the outlet ducts were lengthened with the aim to avoid as much as possible the undeveloped flow disturbance. The dimension are shown in Table 4.

Cyclone total height	5308 mm
Cyclone diameter	1300 mm
Cyclone conical height	1550 mm
Cyclone conical min. diameter	168 mm
Bag filters height	3000 mm
Bag filters diameter	123 mm
Fabric filter hoses	31

Table 4: Domain sizes.

3.2. Volume discretization techniques

The domain was discretized with Ansys MESHING, based on the Finite Volume Method.

To be specific, a fine mesh was chosen in correspondence to the fabric filters to capture the velocities that cross the small gaps in-between them successfully.

Table 5 shows the mesh specifications and Figure 7 sketches the mesh structure.

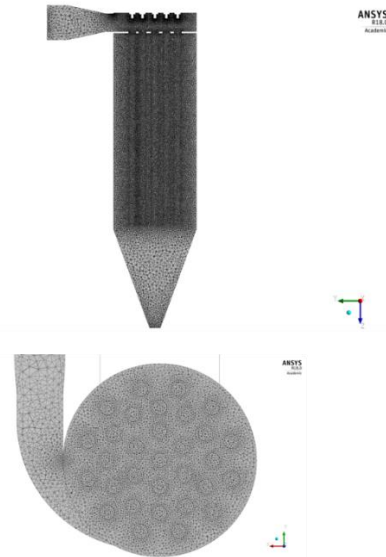


Figure 7: Computational domain.

Element Type	Tetrahedrons
Num. Elements	21499727
Num. Nodes	3673564
Max. Size	0.06 m
Curvature	10°
Edge Sizing	0.01 m
Growth Rate	1.1

Table 5: Mesh specifications.

3.3. Solver settings

Four simulations were carried out in Ansys FLUENT 17.0 in a steady-state condition, at the following inlet velocities: 15 m/s, 19 m/s, 22.5 m/s and 25 m/s. The atmospheric pressure was set at the outlet.

3.3.1. Turbulence model $k-\varepsilon$

To represent the fluid motion inside the filter accurately, the Realizable $k-\varepsilon$ turbulence model was chosen.

The $k-\varepsilon$ model is one of the most common turbulence models, although it just does not perform well in cases of large adverse pressure gradients. It is a two-equation model, which means it includes two extra transport equations to represent the turbulent properties of the flow. This allows a model to account for history effects like convection and diffusion of turbulent energy.

The first transport variable k is the turbulent kinetic energy. The second transport variable ε is the turbulent dissipation. The latter determines the scale of the turbulence, whereas the former, k , determines the energy in the turbulence.

As said before, the $k-\varepsilon$ model it is useful for free-shear layer flows with relatively small pressure gradients.

For the Realizable $k-\varepsilon$, the model transport equations are:

$$\underbrace{\rho U_i \frac{\partial k}{\partial x_i}}_{\text{Convection}} = \underbrace{\mu_t S^2}_{\text{Generation}} + \underbrace{\frac{\partial}{\partial x_i} \left(\alpha_k \mu_{\text{eff}} \frac{\partial k}{\partial x_i} \right)}_{\text{Diffusion}} - \underbrace{\rho \varepsilon}_{\text{Dissipation}} \quad (8)$$

for the kinetic energy and

$$\underbrace{\rho U_i \frac{\partial \varepsilon}{\partial x_i}}_{\text{Convection}} = \underbrace{C_{1\varepsilon} \left(\frac{\varepsilon}{k} \right) \mu_t S^2}_{\text{Generation}} + \underbrace{\frac{\partial}{\partial x_i} \left(\alpha_\varepsilon \mu_{\text{eff}} \frac{\partial \varepsilon}{\partial x_i} \right)}_{\text{Diffusion}} - \underbrace{C_{2\varepsilon} \rho \left(\frac{\varepsilon^2}{k} \right)}_{\text{Destruction}} - \underbrace{R}_{\text{Additional term related to mean strain \& turbulence quantities}} \quad (9)$$

for the dissipation rate. Both equations are written for steady, incompressible flow without body forces [ANSYS FLUENT 18 – Theory Guide].

3.3.2. Fabric filter characterization

For what concerns the representation of the filter, the porous jump option was activated in Ansys FLUENT using the parameters in Table 6.

Permeability	$6.72 \cdot 10^{-11} \text{ m}^2$
Thickness	0.0014 m
Pressure coefficient	0

Table 6: Porous jump parameters.

These values were calculated from the air permeability curve provided by the filter manufacturer (Figure 8), evaluating:

$$\frac{1}{\alpha} = \frac{\Delta p}{w \mu_{\text{air}} s} \quad (10)$$

where w is the flow rate in $[\text{l}/(\text{dm}^2\text{min})]$, Δp is the pressure drop introduced by the filter, μ_{air} is the air viscosity and s is the thickness of the filter surface.

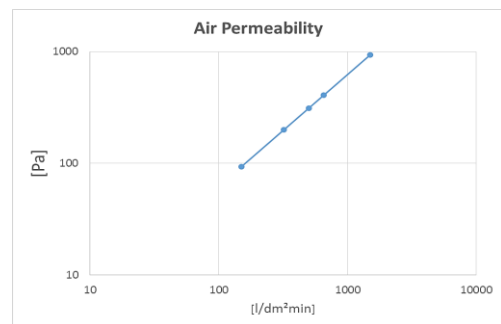


Figure 8: Air permeability curve.

Porous jump conditions are used to model a thin membrane that has a known velocity (pressure-drop) characteristics. It is essentially a 1D software simplification of the porous media model available for cell zones. Examples of uses for the porous jump condition include modeling pressure drops through screens and filters. This simpler model should be used whenever possible because it is more robust, yields better convergence and shortens the computational time.

The thin porous medium (porous jump) has a finite thickness over which the pressure change is defined as a combination of Darcy's law and an additional inertial loss term:

$$\Delta p = -\left(\frac{\mu}{\alpha} v + C_2 \frac{1}{2} \rho v^2\right) \Delta m \quad (11)$$

where μ is the laminar fluid viscosity [Pa·s], α is the permeability [m²], C_2 is the inertial pressure-jump coefficient [1/m], ρ is the fluid density [kg/m³], v is the velocity normal to the porous face [m/s] and Δm is the thickness of the medium [m] [ANSYS FLUENT 18 – Theory Guide].

4. RESULTS AND MODEL VALIDATION

The simulations were performed at 15 m/s, 19 m/s, 22.5 m/s and 25 m/s. The results showed a correct representation of the behavior of the bag filter, as it can be seen by observing the velocity contours in Figure 9.

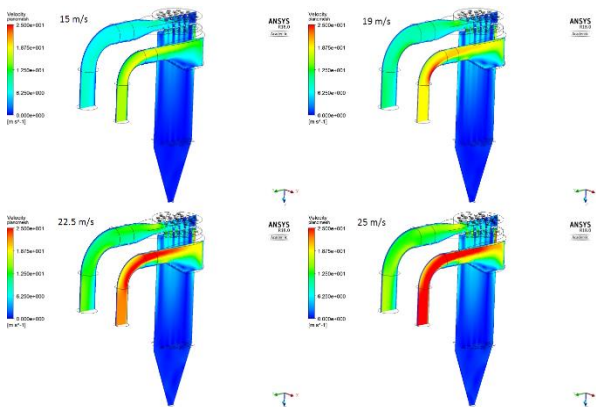


Figure 9: Inlet sensors positions.

Afterwards, the results were compared with the experimental data.

In particular, the comparison focused on inlet and bottom velocities together with the pressure drop.

4.1. Filter inlet velocities

The cyclone inlet velocities were evaluated at the four yellow points in Figure 2, whose detailed positions are shown in Figure 10.

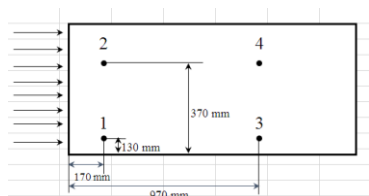


Figure 10: Inlet sensors positions.

The four positions have been chosen to capture the entire fluid flow accurately. The hot-wire anemometer was positioned at different distances from the external volute wall (Figure 11), 5 cm, 15 cm and 29 cm, and for each distance the maximum and the minimum velocity value was measured (Figure 11).

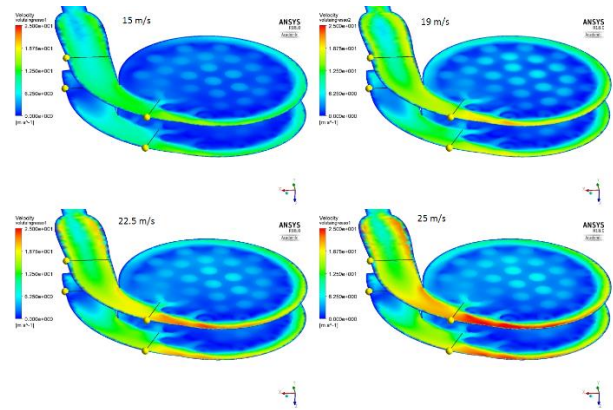


Figure 11: Inlet velocity magnitude contours and the collection points.

Table 7 lists the results obtained for each point at different depth. For the sake of brevity, only the values related to 15 m/s e 22.5 m/s are displayed.

	15 m/s							
	point 1		point 2		point 3		point 4	
	x [cm]	v [m/s]	x [cm]	v [m/s]	x [cm]	v [m/s]	x [cm]	v [m/s]
min	5	2.00	5	9.00	5	10.00	5	11.50
max		4.00		11.00		12.00		13.50
min	15	0.10	15	6.00	15	7.00	15	9.50
max		2.00		10.00		9.00		11.50
min	29	2.50	29	3.00	29	4.00	29	1.50
max		3.50		4.00		6.00		3.00
	22,5 m/s							
	point 1		point 2		point 3		point 4	
	x [cm]	v [m/s]	x [cm]	v [m/s]	x [cm]	v [m/s]	x [cm]	v [m/s]
min	5	3.00	5	15.00	5	15.00	5	17.50
max		5.50		17.00		18.00		20.00
min	15	0.01	15	10.00	15	10.00	15	14.00
max		2.00		12.00		14.00		17.00
min	29	4.00	29	4.00	29	5.00	29	4.50
max		6.00		5.50		8.00		7.00

Table 7: Cyclone inlet velocities at different inlet velocity.

The collected values showed a good correspondence with those returned from the simulations. The curves in Figure 12 and 13 are included, in fact, between the maximum and the minimum experimental value.

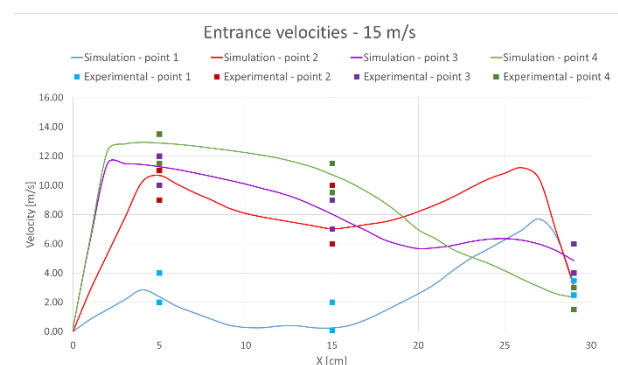


Figure 12: Volute velocities at 15 m/s. Comparison between experimental and simulations data.

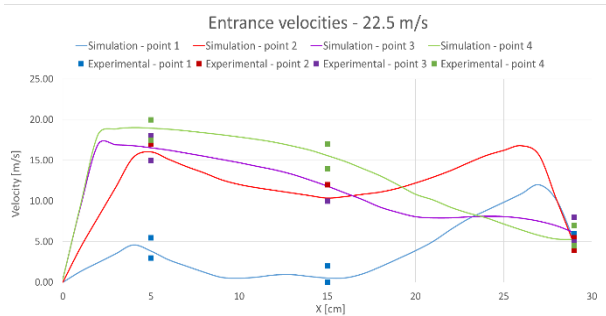


Figure 12: Volute velocities at 22.5 m/s. Comparison between experimental and simulations data.

Again, only the values at 15 m/s and 22.5 m/s are shown for simplicity purpose. As a result, the inlet distribution of velocity was successfully validated.

4.2. Bottom velocities

The next stage was the collection of the velocity data in the conical part of the filter, i.e. its bottom, in this case as well, these data were gained using the hot-wire anemometer at the point highlighted in Figure 14, which also shows the vertical velocity vectors.

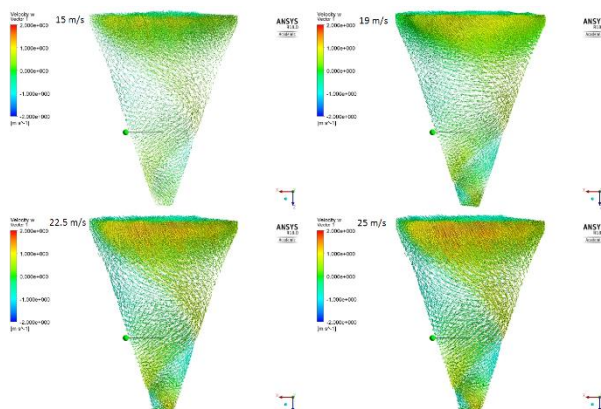


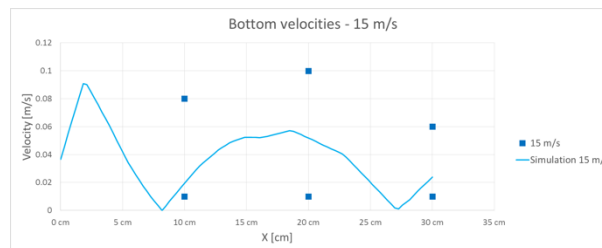
Figure 14: Bottom velocity vectors with the collection point.

Once again, the maximum and minimum velocity values were collected at different distances from the external wall and at each inlet velocity (Table 8).

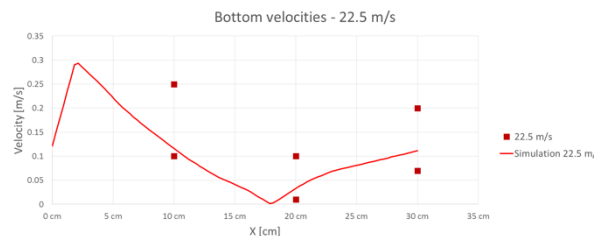
		Bottom velocities [m/s]		
		10 cm	20 cm	30 cm
15 m/s	min	0.01	0.01	0.01
	max	0.08	0.1	0.06
22.5 m/s	min	0.1	0.01	0.07
	max	0.25	0.1	0.2

Table 8: Cyclone bottom velocities at different inlet velocity.

Figure 15 illustrates the comparison between the experimental and the simulations values. It is clear that the maximum and minimum values include the curves extracted from the simulations, thus validating the model with respect to the bottom velocities.



(a)



(b)

Figure 15: Bottom velocities comparison at (a) 15 m/s and (b) 22.5 m/s.

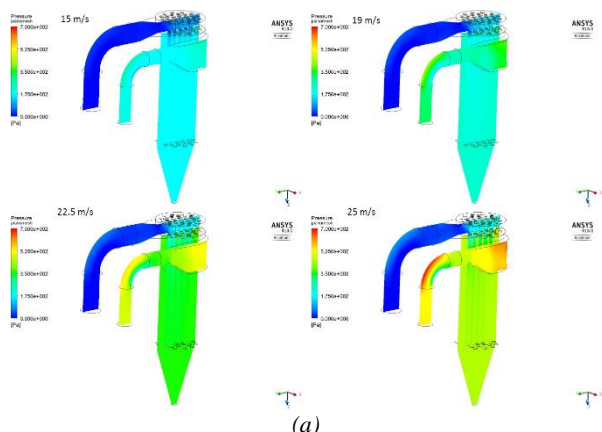
4.3. Pressure drop

The evaluation of the pressure drop was made thanks to the differential pressure sensor by measuring the inlet and the outlet pressure of the bag filter and then calculating the pressure drop as the difference between the previous two.

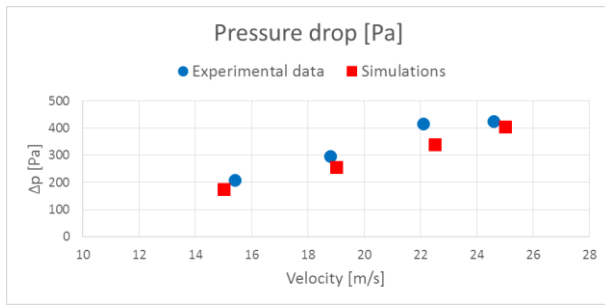
Table 9 illustrates the experimental pressure drops coupled with the velocities detected at the inlet duct with the Pitot tube sensor. In the same table, the computational results are collected to make the comparison easier.

Collected data		Simulated data	
Pitot velocity [m/s]	Δp [Pa]	Velocity [m/s]	Δp [Pa]
15.4	208	15	175
18.8	297	19	256
22.1	416	22.5	340
24.6	426	25	405

Table 9: Pressure drop values.



(a)



(b)

Figure 16: Pressure drop values (a) contours and (b) comparison.

As the chart in Figure 16 (b) shows, the pair of values from the sensors are very close to those from the simulations. This confirms that the one presented is a robust model for predicting the bag filter operating conditions, thus validating it once again.

5. CONCLUSIONS

The objective of this work was to study the behavior of a combined air filtration system consisting in a cyclone separator and a bag filter with 31 hoses.

The performance of such system was analyzed at different operating conditions with the purpose to obtain a predictive model for industrial design.

This was possible due to computational fluid dynamics simulations, which were validated with a dedicated experimental campaign on a pilot plant.

The first step of the study focused on the sensor placement, for the velocity and pressure data acquisition. The housings were created for the sensors probes along the filter as well as at the inlet and outlet ducts (Figure 2).

A hot-wire anemometer and a Pitot tube flow meter were used to measure the velocity data, while the pressure drop was collected using a differential pressure sensor.

To check the good response of the pilot plant, the airflow rates were acquired experimentally and compared with the ones from the fan operating curve at different inverter frequencies.

After the data acquisition, the 3D model of the bag filter was implemented. The model discretization inside Ansys MESHING considered the small gaps between the filter hoses, thus a fine mesh was created to capture the velocity field in those zones correctly.

Next, CFD simulations were carried out in a steady state, at the following inlet velocities: 15 m/s, 19 m/s, 22.5 m/s and 25 m/s.

The model validation was performed by comparing the simulations results with the data collected by the sensors, considering both the velocities (at the inlet and at the bottom) and the pressure drop inside the filter.

For the volute and the bottom velocities, a maximum and a minimum value was measured with a hot-wire anemometer. Thereafter, it was checked if the velocity curves from the simulation were included between the two experimental values.

The results of this comparison were satisfying, therefore the model could be validated from the velocity field point of view.

Regarding the pressure drop, a differential pressure sensor gauged the experimental data, in correspondence to the inlet velocities, collected with a Pitot tube. These pair of values were confronted with the ones from the simulations.

This comparison showed a good response of the computational model too, confirming its validation.

Finally, the project goal was achieved successfully and a predictive fluid dynamic model for the design of the filtration pilot plant was obtained.

Further developments will involve the analysis of the piping from the fluid dynamics point of view (velocities and pressure drop) and the model scale-up for the operating conditions simulation of the industrial plant.

REFERENCES

- Alexander, R. M. C. K., (1949). Fundamentals of Cyclone Design and Operation. Australian Institute of Minerals and Metallurgy, 152; 203 – 28.
- ANSYS FLUENT 18 – Theory Guide.
- ANSYS FLUENT 18 – User Guide.
- Billings, C. E., Wilder, J., (1970). Handbook of Fabric Filters Technology – Volume 1. GCA Corporation, Bedford, Massachusetts.
- Chen, J., Shi, M. (2007). A Universal Model to Calculate Cyclone Pressure Drop. Powder Technology, 171, 184 – 191.
- Cortés, C., Gil, A., (2007). Modeling the Gas and Particle Flow inside Cyclone Separators. Progress in Energy and Combustion Science, 33, 409 – 452.
- De Brito Dias, D., Mori, M., Martignoni, W. P., (1997). Study of Different Approaches for Modeling Cyclones Using CFD. University of Campinas, Campinas, SP, Brazil.
- Endress – Hauser Deltabar S PMD75 Manual.
- Hanakalic, K., (2004). Closure Models for Incompressible Turbulent Flows. Introduction to Turbulence Modeling. Von Karman Institute for Fluid Dynamics, 1 – 75.
- KIMO DEBIMO 400 Air Flow Measuring Blades Manual.
- Le Goff, P., Leclerc, D. M., Herzig, J. P., (1969). Flow Suspensions through Porous Media. Industrial and Engineering Chemistry.
- Lo, L. M., Chen, D. R., Pui, D. Y. H., (2009). Experimental Study of Pleated Fabric Cartidges in a Pulse – Jet Cleaned Dust Collector. Powder Technology, 197, 141 – 149.
- Mehta, N. C., Smith, J. M., Comings, E. W., (1956). Pressure Drop in Air – Solid Flow Systems. Fluid Mechanics in Chemical Engineering.
- Meier, H. F., Mori, M., (1998). Gas – Solid Flow in Cyclones: the Eulerian – Eulerian Approach. European Symposium on Computer Aided Process Engineering.

- Patankar, N. A., Joseph, D. D. Modeling and Numerical Simulation of Particulate Flows by the Eulerian – Lagrangian Approach. Department of Aerospace Engineering and Mechanics, Northwestern University, Evanston.
- Sommerfeld, F., (2000). Theoretical and Experimental Modelling of Particulate Flows. Von Karman Institute for Fluid Dynamics.
- Stendal, E. A. R. (2013). Multiphase Flows in Cyclone Separators. Department of Chemical Engineering, Gothenburg, Sweden.
- Sutherland, K., (2008). Filters and Filtration Handbook – 5th Edition. Elsevier Science.
- Ter Linden, A. J., (1949). Investigation into Cyclone Dust Collectors. Institute of Mechanical Engineering, 160; 233 – 51.
- VelociCalc Air Velocity Meter 9565 Series.
- Yoa, S. J., Cho, Y. S., Choi, Y. S., Baek, J. H., (2001). Characteristics of Electrostatic Cyclone/Bag Filter with Inlet Types (Lab and Pilot Scale). Korean Journal of Chemical Engineering, 18, 539 – 546.

AUTHORS BIOGRAPHY

Federico SOLARI is a PhD in Industrial Engineering at the University of Parma, from where he got a Master Degree in Food Industry Mechanical Engineering, discussing a thesis related to the design of a plant for the volatile compounds extraction. He achieved his PhD with a thesis entitled “Advanced approach to the design of industrial plants by means of computational fluid dynamics”. He attended several conferences related to food process, modelling and simulation. He published several papers on the same topics on international journal and conferences.

Giorgia TAGLIAVINI is a Research Assistant at the Department of Industrial Engineering at the University of Parma, where she graduated in Mechanical Engineering in March 2015. Her research activities focus mainly on CFD simulation of multiphase flows and non-Newtonian fluids, data analysis and modeling of Fluid Mechanics and Industrial Engineering processes.

Roberto MONTANARI is Full professor of Mechanical Plants at the University of Parma. He graduated (with distinction) in 1999 in Mechanical Engineering at the University of Parma. His research activities mainly concern equipment maintenance, power plants, food plants, logistics, supply chain management, supply chain modelling and simulation, inventory management. He has published his research in approx. 70 papers, which appear in qualified international journals and conferences. He acts, as a referee, for several scientific journals, is editorial board member of two international scientific journals and editor of a scientific journal.

Eleonora BOTTANI is Associate professor in Mechanical Industrial Plants at the Department of Engineering and Architecture of the University of Parma. She graduated (with distinction) in Industrial Engineering and Management in 2002, and got her Ph.D. in Industrial Engineering in 2006, both at the University of Parma. Her research activities concern logistics and supply chain management issues. She is author (or co-author) of more than 130 scientific papers, referee for more than 60 international journals, editorial board member of five scientific journals, Associate Editor for one of those journals, and editor-in-chief of a scientific journal.

Nicola MALAGOLI is a Research Assistant at the Department of Industrial Engineering at the University of Parma. He has a Master Degree in Food Industry Mechanical Engineering in October 2016. His research activities focus mainly on data analysis and food industry plants design.

Mattia ARMENZONI is a Research Assistant in Industrial Engineering at the University of Parma. He got a master degree in Food Industry Mechanical Engineering, discussing a thesis titled: "Advanced design of a static dryer for pasta with simulation tools". He attended several international conferences and published several papers related to food industry, modelling and simulation.

MARKET ANALYSIS OF DAIRY PRODUCTS PRODUCED IN THE PARMIGIANO-REGGIANO AREA

Rodolfo Mantione^(a), Giuseppe Vignali^(b)

^(a)CIPACK Interdepartmental Center, University of Parma, Parco Area delle Scienze 181/A, 43124 Parma (Italy)

^(b) Department of Engineering and Architecture, University of Parma, Parco Area delle Scienze 181/A, 43124 Parma (Italy)

^(a)rodolfo.mantione@gmail.com, ^(b)giuseppe.vignali@unipr.it

ABSTRACT

The present work aims to realize a market analysis related to a particular high quality dairy product category, such as Ricotta and Caciotta products, obtained by typical cows of the Parmesan Area. The purpose is to estimate the sales volumes for each product, considering the consumer interest on buying new product obtained with high quality standards, which therefore guarantee a superior genuineness, taste and chain control than market standards.

The market analysis was carried out on the "Parmigiano Reggiano" territory, taking into account some stores in the province of Mantova (south of Po River) and Parma, both supermarkets and discounts; Photographic surveys have also been carried out for this purpose.

For each product, we have noted all the informations reported on the label (ingredients, nutritional values, production plant, and price) and the size of the specific sales area for each brand. All the specific information were then tabulated and analysed.

Once this phase has been completed, a questionnaire has been set up for consumers of large distribution. Through this questionnaire, it is possible to understand the sales possibilities of each analyzed product, as well as their market placement potential and the average price range per kg at which consumers would be willing to buy them.

Keywords: market analysis, ricotta, caciotta, cheese, stores, survey

1. INTRODUCTION

The innovation represent, in the opinion of academics and executives, a fundamental prerequisite for the growth of society in today's competitive environment, as well as one of the key factors of long-term business success (Baker e Sinkula, 1999; Balkin Et al., 2000; Darroch e McNaughton, 2002; Lyon e Ferrier, 2002). In fact, innovative companies are able to respond to environmental challenges more quickly and better than non-innovative ones (Jimenez et al., 2008). Therefore, the organizations consider the innovation as an integral part of their business strategy. Therefore, organizations consider innovation as an integral part of their business strategy by offering products tailored to the needs of target customers to create a sustainable competitive advantage and stay above the rivalry (Calantone et al.,

1995; Damanpour e Gopalakrishnan, 2001; Scarborough e Zimmerer, 2002). In recent decades, a change has been observed from the model of technological innovation to market innovation, forcing companies to focus more on the quality product rather than on internal efficiency. In this way it is possible to quickly identify the needs of changing customers, to develop complex products to meet these needs, thus providing a higher level of support and customer service (Sheperd e Ahmed, 2000). In a world that dramatically change, where not only the demographic changes is altered, but where the impact of globalization result to be significant, the food industry is not an exception and must find its role in these revolutionary challenges (Vrontis and Altaluna, 2017).

In the food industry and in general in the manufacturing sector, the dairy industry is characterized by the high number of typologies and characteristics of "cheese". Cheese which is derived from milk transformation, has different features in relation to the times and methods of production, its intrinsic and specific characteristics, its consumption patterns, maturing degrees, the intensity of the bond with the lands of origin. The relationship with the territory is very strong: in the cheese chain, the territoriality of production and the originality of the raw material still represent a distinctive character, so as to make the territory a commercial value. The "product", belonging to a cheese family determines the added value, time of remuneration, packaging, supply and professional work. Of course, the same distribution channel, today crucial to the success of a product, is influenced by cheese type and vice versa (Freddi and De Angelis, 2015).

The cheese world market growth was largely due to the implementation of the World Trade Organization (WTO) international trade agreements, which facilitated the circulation of foodstuffs around the world. The dairy industry has also had repercussions, with increasing downward pressure on prices in the face of ever increasing quantities, similar to what has happened to other important products in the agri-food trade. In Italy, where cheese traditionally plays an important role both in production and consumption, the effect of the transformation of world trade has been very significant, leading to a reaction of domestic dairies and a quality repositioning of the industry, facilitated by the presence of Trademarks already widely known in the world (Ceccherini, 2016).

The growth in consumption and imports of dairy products in international markets is expected to continue in the coming years due to both economic development and the gradual urbanization of most populations currently residing in rural areas: industrialization / outsourcing of Economies that accompanies the increase in incomes result in a massive transfer of people from country to city, while accentuating the evolution of lifestyles and eating patterns. As a proof of this, according to the OECD (Organization for Economic Cooperation and Development) estimates, within ten years the consumption of cheeses will grow altogether (in quantity) by an amount of 17 % world-wide, with an increase that will reach 41% in Asian countries (Nomisma,2015).

The aim of the paper is to realize a market analysis related to a particular "high quality" dairy product category, such as Ricotta and Caciotta products. The remainder of the article is composed as follows. The second chapter describe the method, through photographic relief, to perform a market analysis on two dairy products (ricotta and caciotta). In the third chapter will be analysed all the information characterized the label of the product. Finally, section 4 concludes the work by summarizing the main results obtained.

2. MATERIALS AND METHODS

The market analysis of dairy products, and in particular of ricotta and caciotta products, was carried out in the territory of Parmigiano Reggiano. As shown in the following table, the study sites were altogether 10 of which 7 supermarkets and 3 discounts (Eurospin, Lidl and In's). For each supermarket, all the information on the label (ingredients, nutritional values, production plant and price) was taken into account through appropriate photographic surveys. Such information was then collected, tabulated and analyzed.

Table 1: Address of the ten supermarket

Supermarket	Address
FAMILA	Via Langhirano (PR)
ESSELUNGA	Via Sandro Pertini, 14 (PR)
SIGMA	Viale Antonio Gramsci, 9 (PR)
PANORAMA	Via Silvio Pellico, 20 (PR)
COOP	Via F. Mitterand, 1 Suzzara (MN)
CONAD	Via Venezia, 40/A (PR)
AFFARE	Via Donelli 4, Suzzara (MN)
EUROSPIN	Str. Langhirano, 150 (PR)
LIDL	Via Della Cooperazione, Gonzaga (MN)
IN'S	Str. Nazionale, 15/a Suzzara (MN)

In the context of the market analysis of high quality dairy products, namely ricotta and caciotta, two questionnaires were prepared to understand the possibilities of selling the products concerned, their market placement and the average price per kg to which consumers would be willing to buy them.

The questionnaire, which will be compiled by consumers, is listed in the Appendix A.

In the specific case of ricotta, the survey has set the following objectives:

1. Knowing consumer habits;
2. Understanding consumer perception of MAP (Modified atmosphere packaging);
3. Assess the interest of consumers in purchasing a new product created according to high quality standards;
4. Get an estimate of the value-added economic assessment of a quality product packaged in a protective atmosphere.

The questionnaire consists mainly of closed responses and 20 people will be interviewed in each of the 10 supermarkets so in total 200 people will be submitted in anonymous form.

After the photographic relief phase in the various supermarkets taken into account, all the information on the label has been reported in Excel. This work was done for both ricotta and caciotta. In the two Excel sheets, one for each product, tables were created showing the dimensions of the shelves used, the size of each brand in detail, the number of products per supermarket, price, nutritional values, place and manufacturing plant.

3. RESULTS AND DISCUSSION

3.1. Ricotta

The appendix B shows, for each supermarket, the space dedicated to each brand was quantified.

The average shelf space dedicated to the ricotta cheese amounts to 189.2 cm, the supermarket in which this product is most exhibited on shelves is "Esselunga" of Parma with a 22% share of ricotta brand "Esselunga". This brand represents the most exposed even among all the supermarkets under consideration.

As shown in table X, the supermarket in which the maximum number of brands is present is the "Rossetti Affair" of Suzzara (MN) with 17 different companies, against "Lidl" (Gonzaga, MN), where there is a only brand ("Marino") occupying 30 cm on shelves. The average is 9.2 brands per supermarket. In the 60% of retail stores analysed there are "Granarolo", "Santa Lucia" and "Vallelata" and in the 50% ones "Happened".

However, the average of supermarkets covered by a specific brand is only 15%. The "In's" (Suzzara, MN), "Eurospin" (PR) and "Lidl" (Gonzaga, MN) discounts have an average of 2 brands on the shelves while the other supermarkets have 13 different ricotta products; No brand is present in both discounts and supermarkets.

In the appendix C shows the prices of individual brands per supermarket expressed in € / kg. The product with the highest price, considering only ricotta with

cow's milk and not goat's one, is "Osella Farm" in Coop Supermarket (Suzzara, MN) with 10.47 € / kg.

The brand with the highest average price also considering products with goat's milk (Valsoia excluded) is "Bianca" with 16.98 € / kg while the products with the lowest one are "Valtenera", "Land" and "May Flower" with 2.2 € / kg.

The average price of all the brands under consideration is 6.58 € / kg.

The average selling price in each supermarket it is 6 € / kg; The highest price is 8 € / kg, while the lowest one is 4.2 € / kg in "In's" and Lidl discounts both located in province of Mantova. Particular attention is given to ricotta made in a protective atmosphere, i.e. "Caseificio Pini" sold at 5.72 € / kg, "Caseificio preziosa" at 6.90 € / kg, "Italiani" at 4.52 € / kg, Sabelli "at 5.30 € / kg," Sigma Ricotta "of goat's fresh milk at 12.45 € / kg.

Three of these ricotta products mentioned above are below the average total price (6.58 € / kg) while the one with the highest price is produced with goat's milk.

The average price among all packaged brands in MAP (Modified atmosphere packaging) is 6.98 € / kg or only 6% less than the total average price.

The ingredients indicated on the label were analysed. Considering all types of ricotta, i.e. those made in a protective atmosphere, those with goat's milk rather than cow's one, pasteurized and organic milk, it is possible to notice that some products differ significantly from others. The ingredients that are present in most brands are: pasteurized milk whey (7 brands), bovine milk (9), bovine milk / vaccine serum (28), cream of cow milk (9), cream Pasteurized milk (10), salt (45), acidity regulator (49), lactic acid (21) and citric acid (32). The acidity regulator is present in 85% of the brands being tested.

On the label are also shown, per 100g of product, the nutritional values for each brand.

The first is the energy value with an average value of 601.48 kcal: the maximum value is 844 kcal and the minimum one 256 kcal for the brands "Valsoia" and "Sigma goat" respectively.

Regarding the fat component, the average value is 11g, of which 7.54g of saturated fats. The maximum value is for "Sigma goat" with 23.5g (16.83g saturated fats), while "Malghette" has the minimum value with 5.5g of which 1.8g saturated fats. Carbohydrates, however, have a maximum value that amounts to 6.3 g associated to the brand "Fidel" with 5.4g of sugars. The minimum value amounts to 1.4g: 0.6 g of sugars for "Spegia". The average value is 3.43g, of which 3.10g related to sugar.

Proteins have an average value of 8.35g, a maximum value of 12.3g and a minimum value of 3.20g for "Spegia" and "Valsoia" respectively. Finally, for salt we find a maximum of 0.8g for "Sicilian Dairy" and a minimum value of 0.1g for "Spegia" with a total average value of 0.37g. Calcium and phosphorus measured in milligrams are indicated in some ricotta. Vitamin D is only present in the "Valsoia" brand in a smallest amount.

Finally, the Table 2 shows the number of brands served by a particular production plant. In some cases this information was unreadable as the label was damaged, or even such specifications were missed.

The most interesting thing is definitely the number of brands produced in one plant. In fact, in "Lat Bri" (Usmate Velate (MB)) 14 different brands are processed, followed by "Caseificio Pini" in Sanguinetto (VR), "Jacob Bustaffa" in Bagnolo San Vito (MN) and "Egidio Galbani spa" in Corteleona (PV) with 5 different types of ricotta.

Table 2: Number of brands served by a particular production facilities

Production facilities	Number of brands produced
Lat Bri	14
Caseificio del Cigno s.p.a.	1
Caseificio Villa	1
Caseificio Busti s.n.c.	1
Soc.Agr. Latte Beressanone	3
Biraghi s.p.a.	1
Giacobbe Bustaffa	5
Caseificio Pini	4
Caseificio Preziosa	1
Caseificio Elda	4
Fattorie Osella	1
Egidio Galbani s.p.a.	5
Sterilgarda s.p.a.	1
Francia Latticini s.p.a.	1
Sabelli s.p.a.	1
Latterie Venete s.p.a.	1
Soc. Argri. Cooperlat	1
Caseificio Matteassi Onelio srl	1
Fattorie Garofalo soc coop.	1

3.2. Caciotta

Referring to the size of a whole medium caciotta, for each supermarket analysed, the space dedicated to this cheese was evaluated by considering all the brands (Table 3).

On average, the size of shelves dedicated to caciotta is 55.7 cm. The "Famila" of Parma is the supermarket with less dedicated space (21 cm.), followed by "Esselunga" (22 cm.), while "L'affare Rossetto" in Suzzara (MN) has 117 cm. dedicated to the caciotta.

Analysing the spaces occupied by the different brands in the supermarkets considered in our study, "Valtenera" is the one with the largest space (60 cm- "IN'S" Suzzara, MN), while those with the smaller space are "Cusna" and "Sabelli", respectively in supermarkets "Esselunga" (PR) and "panorama" (PR), with 7 cm of dedicated space.

The following table shows all the brands (22) in the 10 supermarkets analysed.

Apart from being the supermarket with the largest space dedicated to caciotte, "Affare Rossetto" (Suzzara, MN) is also the supermarket with the most numbers of products, in particular 6 followed by "Coop" (Suzzara, MN) with 4 products. The last ones are "Famila" (PR) and "Sigma" (PR) supermarkets with just one caciotta. The average number of products is 2.7 brands per supermarket.

Table 3: Size of the shelves used for caciotta and the size of each brand in detail.

Store	Street	Length (cm)	Number of shelves	Height of shelves (cm)	Brand 1	Length (cm)	Brand 2	Length (cm)	Brand 3	Length (cm)	Brand 4	Length (cm)	Brand 5	Length (cm)	Brand 6	Length (cm)
AFFARE	Via Donelli 4, Suzzara (MN)	117cm	3	30	Bergader	15	Bucaneve	30	Buyerland	15	Roverella	30	Caciottina Cascina	12	Stella del Grappa	15
COOP	Via F. Mitterand, 1 Suzzara (MN)	71cm	3	30	Faggiola	12	Ceccardi	15	Belpaese	30	Monte cusna	12				
PANORAMA	Via Silvio Pellico, 20 (PR)	57cm	2	30	Bergader	30	Primi Pascoli	20	Sabelli	7						
CONAD	Via Venezia, 40/A (PR)	43cm	2	30	Fochi	14	Bosco Gerolo	15	Bacio di luna	14						
ESSELUNGA	Via Sandro Pertini, 14 (PR)	22cm	2	30	Cusna	7	Belpaese	15								
FAMILA	Via Langhirano (PR)	21m	1	30	Sabelli	21										
SIGMA	Viale Antonio Gramsci, 9 (PR)	15	1	30	Belpaese	15										
EUROSPIN	Str. Langhirano, 150 (PR)	45cm	2	30	Italiani	20	Steffel	25								
LIDL	Via Della Cooperazione, Gonzaga (MN)	28cm	2	30	Milbona	8	Merivio	20								
IN'S	Str. Nazionale, 15/a Suzzara (MN)	110cm	1	30	Valtenera	60	Caciotta in's	30	Piumetta	20						

Sales, price and quantity formats, depending on the brands and the supermarkets, change from the sale of whole caciotte to one-packed "monoportion". Obviously, this involves a change in sales price, so the price expressed in € / kg (Fig.1) was analyzed.

The average of caciotte made with cow's milk is 8.61 € / kg, while among the caciotte tested is 8.85 € / kg.

The brand with the highest average price is "Sabelli" sold at (13.25 € / kg), while "Belpaese" at "Sigma" (PR) has the highest price (15.9 € / kg), due to the fact that is not sold as a packaged product but served by the staff at the counter of fresh cheeses.

On the other hand, the brand with a lowest average price is "Steffel" at the "Eurospin" in Parma sold at 6.49 € / kg, followed by "Faggiola" at Coop (Suzzara, MN) and Valtenera at the "In's" discount Suzzara, (MN) at 6.5 € / Kg.

The caciotta with a variance between the highest price and the highest difference between the maximum and the minimum price is "Belpaese", as it is also sell in the counter of fresh cheeses while, with regard to the caciotte present only at the fridge, we have those of "Bergrader" and "Sabelli".

Particular attention is given to the caciotta packaged in protective atmosphere (MAP) "Buyerland" sold at 6.77 € / kg and "In's" at 6.9 € / kg. The average price of MAP products is 6.8 € / kg, which is 22% lower than the average of caciotte made only with cow's milk and 58% lower than the highest price, in particular if compared with "Belpaese" sold by "Sigma" (PR).

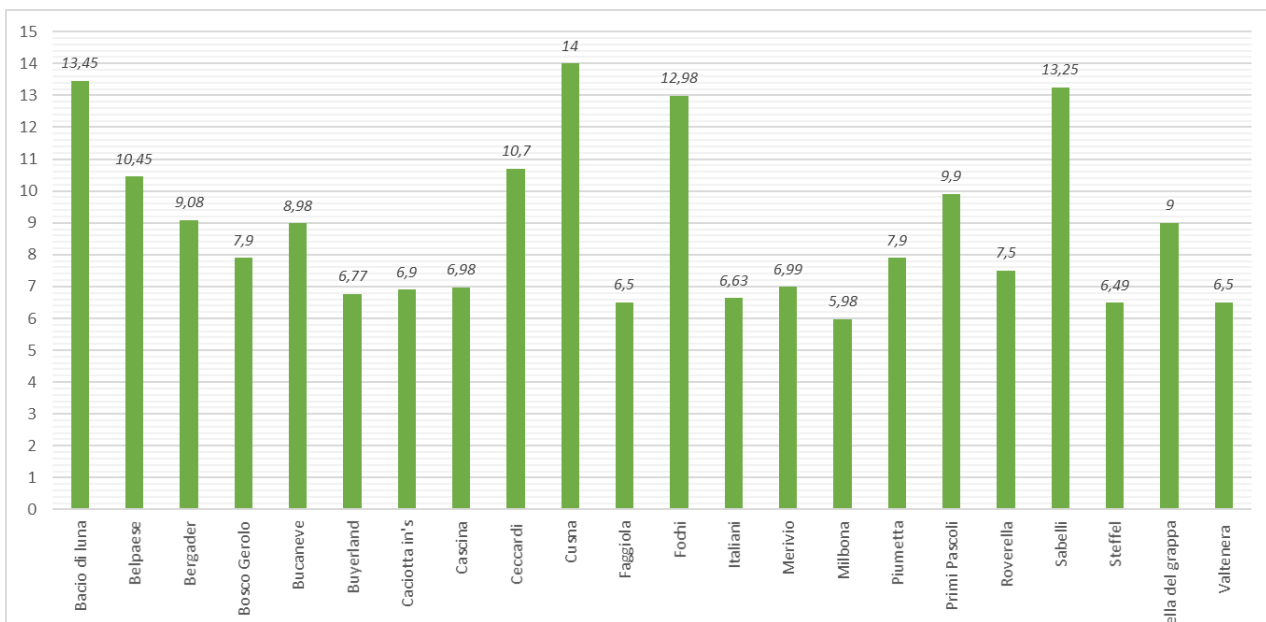


Figure 1: Average caciotta price for each brand

Table 4: The presence of a given ingredient for each brand

BRAND / INGREDIENTS	Biological pasteurized cow's milk	Pasteurized cow's milk	Cow's milk	Pasteurized sheep milk	Salt	Rennet	Ferments	Preservatives	Modified starch	Microbiological rennet	Lactic ferments	Penicillium candidum
Bacio di luna			x		x	x						
Belpaese			x		x	x			x			
Bergader			x		x	x						
Bosco Gerolo		x			x	x				x	x	
Bucaneve		x			x	x						x
Buyerland			x		x	x						
Caciotta in's			x		x	x						
Cascina		x			x	x					x	
Ceccardi		x			x	x						
Cusna		x		x	x	x		x				
Faggiola	x				x	x	x					
Fochi			x		x	x						
Italiani			x		x	x						
Merivio			x		x	x						
Milbona			x		x	x						x
Piumetta			x		x	x						
Primi Pascoli			x		x	x		x				x
Roverella			x		x	x	x					
Sabelli			x		x	x						
Steffel			x		x					x	x	
Stella del grappa			x		x	x						
Valtenera			x		x	x				x	x	
Competitive number for a particular product	1	5	16	1	22	21	2	2	1	3	6	1

In the above table lists the ingredients such as: milk type (cow or sheep), salt, rennet, preservatives, starch, lactic ferments and penicillium candidum.

The presence of salt and rennet (except the "Steffel" caciot) is a constant in all products. The type of milk used is always cow's milk, but in some brands it can be "pasteurized" or "biological", whereas only one case is added to sheep's milk (only for the brand "Cusna").

Lactic ferments are only present in 6 brands, such as "Valtenera", "Steffel", "Primi Pascoli", "Milbona", "Cascina" and "Bergader".

The only caciots packaged in MAP are "In's" and "Buyerland" and both have the same ingredients (salt, rennet and cow milk).

In the following table summarizes nutritional values for each brand by referring to 100g of product. Some brands, being sold in monoportion, have some unreadable data due to the ineffective state of the original

Table 5: Nutritional value for every 100 g of product

NUTRITIONAL VALUES IN A DETERMINED BRAND (for 100g)								
Number of brands	BRAND/ NUTRITIONAL VALUES	Energy(kcal)	Fat (g)		Carbs (g)		Protein (g)	Salt (g)
				of which saturated		of which sugars		
1	Bacio di luna*	/	/	/	/	/	/	/
2	Belpaese	1279	24	17	3	0,6	20	1,5
3	Bergader	1414	30	20,7	0,3	0,1	17,6	1,9
4	Bosco Gerolo	1416	28	20	0	0	22	0,63
5	Bucaneve	1383	25,94	16,83	0,95	0,68	23,3	1
6	Buyerland	1470	31	22	<0,1	< 0,1	19	1,3
7	Caciotta in's	1248	25	16,2	2	2	17	2,2
8	Cascina	1416	28	20	0	0	22	0,63
9	Ceccardi	1493	30	20	<0,5	0	22	0,8
10	Cusna	1510	30	20	<0,5	0	23	1,6
11	Faggiola	1493	29	20	1,7	1,7	23	0,9
12	Fochi	1210	24,96	16,73	1,8	1,38	18,3	0,99
13	Italiani	1550	31	22	1,7	0,8	22	0,96
14	Merivio	1364	25,7	17,9	1,3	0	23,3	1,47
15	Milbona	1242	23	15,4	1	1	22	1,6
16	Piumetta	1390	27	15	0	0	20	1,7
17	Primi Pascoli*	/	/	/	/	/	/	/
18	Roverella	1466	29,5	20,2	1,5	0,9	20,5	1,4
19	Sabelli	1524	29	20	2	2	24,5	2
20	Steffel	1414	30	20,7	0,3	0,1	17,5	1,9
21	Stella del grappa	1400	29	23	0,7	0,68	20	1,7
22	Valtenera	1414	30	20,7	0,3	0,1	17,5	1,9

* Packaged in monoportion and unreadable data

label being cut or torn. The analysis shows that the average energy of the caciotta is 1404.8 kcal, the highest is 1550 kcal (the "Italian" brand) and the lowest is 1210 kcal (brand "Fochi").

The "fat" is on average 28g of which 19g of saturated fat; The bands with the highest values are "Italians" and "Buyerland" with 31g of fat, of which 22g are saturated, whereas the one with the lowest is "Milbona" with 23g of fat, of which 15.4g saturated.

As for carbohydrates, the average value is 1.09g of which 0.63g of sugars. The maximum value is 3 of the "Belpaese" brand, which contains 0.63g of sugars while the minimum value is 0 in "Cusna" and "Piumetta" products.

The "Sabelli" caciotta has 24.5g of protein and represents the highest value among the brands taken into consideration, while with 17g the "In's" has the minimum value. The average protein quantity is 20.73g.

Finally, the average salt value is 1.4g; The "In's" cachet, packaged in a protective atmosphere, holds the maximum value with 2.2g, while the smaller quantity (0.63g) is contained in the "Bosco Gerolo" caciotta.

The transcription of the area and production site data for some brands was impossible, as the original labeling was unreadable due to ruined part of the label or of the packaging format of the caciotta itself, such as the monoportion.

On a total of 22 tabulated brands, five have German origins, while among the caciots of Italian origin, only those of "Ceccardi" and "Cusna" are produced in the same production site, in particular Gennaro Auricchio in Scandiano (RE).

Table 6: Production place and production facilities of caciotta

Number of brands	Brand	Production place	Production facilities
1	Bacio di luna*		
2	Belpaese	Giusaago (PV)	Galbani Egidio s.p.a
3	Bergader	Germania	Waging
4	Bosco Gerolo	Rivegnano (PC)	Cascina Bosco Geroldo s.r.l.
5	Bucaneve*		
6	Buyerland	Germania	Buyerland s.r.l
7	Caciotta in's	Pagazano (PG)	Arrigoni battista s.p.a
8	Cascina *		
9	Ceccardi	Scandiano (RE)	Gennato Auricchio s.p.a
10	Cusna	Scandiano (RE)	Gennato Auricchio s.p.a
11	Faggiola	Palazzuolo sul senio (FI)	Agricoop sac
12	Fochi	Parma	Fochi e tagliavini s.r.l.
13	Italiani	Cavaso del Tomba (TV)	Centro Veneto Formaggi s.r.l.
14	Merivio	Savignano (CN)	Peria s.n.c
15	Milbona	Germania	Meeder
16	Piumetta	Grigno (TN)	Cesaria Monti Trentini
17	Primi Pascoli	Noventa del Piave (VE)	Alimenta s.p.a
18	Roverella	Rovere Veronese	Lessini s.r.l.
19	Sabelli	Ascoli Picena	Sabelli s.p.a
20	Steffel	Germania	Bad Aibling
21	Stella del grappa*		
22	Valtenera	Germania	Bad Aibling

* Packaged in monoportion and unreadable data

4. CONCLUSIONS

The collected data show that dairy products and, in particular, ricotta and caciotta, regardless of where they are purchased, have very variable quality and packaging characteristics, probably depending on the geographical area of production.

From the extrapolated data it can be seen how ricotta is produced with different ingredients, packages and prices; In fact, for the price per Kg, it is noticed the passage from 2.2 € to over € 10 depending on the different origins of the milk (cow's milk rather than goat's one) but also according to the packaging (protective atmosphere). In addition, the average price per kg of ricotta is 6.10 €. An interesting data is about ricotta production: indeed, many brands are produced at the same plant (Usmate Velate (MB) excels with 14 different brands served.) The ricotta brand that appears to be present in most supermarkets with greater dedicated space is "Santa Lucia" with a price of 3.94 € / Kg for non-light cow's milk ricotta.

From the analysis carried out it is shown how the caciotta is produced and sold with different packaging and prices but with similar ingredients (except for milk differentiation); Indeed, for the price per Kg, it is possible to note the passage from € 5.8 to € 14, mainly based on the sales size (pre-packaged, bulk or full caciotta). The average price per kg of ricotta is 8.85 €. In addition, one of the interesting data is the sales size difference that is noticed by passing from the area of Parma, where monoportion prevails with low brand depth, to Suzzara (MN), where there are more than one full-size and more branded caciotte.

Probably this is due to the differentiation of customers according to the size and to the location of the city where the supermarket is present. Thanks to the compilation of the questionnaires, it will be possible to understand the possibilities of selling the products under review as well as their market placement and the medium-price at which consumers would be willing to buy them.

ACKNOWLEDGMENTS

Iniziativa realizzata nell'ambito del Programma regionale di sviluppo rurale 2014-2020 – Tipo di operazione 16.1.01 – Gruppi operativi del partenariato europeo per l'innovazione: "produttività e sostenibilità dell'agricoltura" – Focus Area 2A – Progetto "La bovina da latte nella zona del Parmigiano Reggiano: innovazione e tradizione per un allevamento sostenibile e per prodotti di qualità".

Initiative under the Regional Rural Development Program 2014-2020 - Type of operation 16.1.01 - Operations of the European Partnership for Innovation: "Productivity and sustainability of agriculture" – Focus Area 2A – Project " Milk beef in the Parmigiano Reggiano area: innovation and tradition for sustainable breeding and quality products".

REFERENCES

- Baker W.E. and Sinkula J.M. 1999. The synergistic effect of market orientation and learning orientation on organizational performance, *Journal of Academy of Marketing Science*, Vol. 27, No. 4, pp. 411-427.
- Balkin D.B., Markaman G.D. and Gómez-Mejía L.R. 2000. Is CEO pay in high-technology firms related to innovation, *Academy of Management Journal*, Vol. 43, No. 6, pp. 1118-1129.
- Calantone R.J., Vickery S.K. and Droge C. 1995. Business performance and strategic new product development activities: an empirical investigation, *Journal of Product Innovation Management*, Vol. 12, pp. 214-223.
- Damanpour F. and Gopalakrishnan S. 2001. The Dynamics of the Adoption of Product and Process Innovations in Organizations, *Journal of Management Studies*, Vol. 38, No. 1, pp. 45-65.
- Daniela Freddi and Gianluca De Angelis, 2015. L'industria casearia di Lombardia ed Emilia-Romagna nel contesto italiano – Struttura, caratteristiche e dinamiche evolutive. Editrice socialmente, Bologna.
- Darroch J. and McNaughton R. 2002. Examining the link between knowledge management practices and types of innovation, *Journal of Intellectual Capital*, Vol. 3, No. 3, pp. 210-222.
- Demetris Vrontis and Claudio Vignali 2001. "Dairy Milk in France – A marketing investigation of the situational environment", *British Food Journal*, Vol.10. Issue: 4, pp.291-296.
- Jimenez J., Valle R.S. and Espallardo M.H. 2008. Fostering innovation. The role of market orientation and organizational learning, *European Journal of innovation management*, Vol. 11 No. 3, pp. 389-412.
- Lyon D. and Ferrier W. 2002. Enhancing performance with product-market innovation: the influence of the top management team, *Journal of Managerial Issues*, Vol. 14, No. 14, pp. 452-469.

Nomisma – Società di Studi economici 2015. Relazione di accompagnamento alla proposta di piano produttivo del consorzio di tutela del formaggio Grano Padano DOP.

Paolo Ceccherini, 2016. Grano Padano e Parmigiano Reggiano – Dal mercato mondiale del formaggio al prodotto DOP, un comparto italiano di grande calore. Monte dei Paschi di Siena.

Scarborough N. and Zimmerer T. 2002. *Essentials of Entrepreneurship and Small Business Management*, Paperback.

Sheperd C. and Ahmed P.K. 2000. From product innovation to solutions innovation: a new paradigm for competitive advantage, *European Journal of Innovation Management*, Vol. 3, No. 2, pp. 100-106.

AUTHORS BIOGRAPHY

Rodolfo MANTIONE is a recent graduate at the University of Parma. After graduating from the food industry engineering in July 2013 at the University of Palermo in October 2016, he obtained a degree in Mechanical Engineering for the Food Industry at the University of Parma. His main fields of interest concern market analysis and food management.

Giuseppe VIGNALI is an Associate Professor at University of Parma. He graduated in 2004 in Mechanical Engineering at the University of Parma. In 2009, he received his PhD in Industrial Engineering at the same university, related to the analysis and optimization of food processes. Since August 2007, he worked as a Lecturer at the Department of Industrial Engineering of the University of Parma. His research activities concern food processing and packaging issues and safety/security of industrial plant. Results of his studies related to the above topics have been published in more than 90 scientific papers, some of which appear both in national and international journals, as well in national and international conferences.

APPENDIX A: Questionnaire for consumers.

PERSONAL DATA

1) Age

2) Are you?

- Male Female

3) Job

PURCHASE RICOTTA

1) How often do you buy ricotta?

- Never or almost never Daily
 Several times a week Several times a month

2) Where do you usually buy ricotta?

- Supermarket - Great distribution Market
 Farms (direct sales) GAS (Purchase groups)

3) Do you know the difference between the ricotta packaged in a protective atmosphere and in a traditional packaged?

- Yes No

4) Considering an average price of ricotta made in a protective atmosphere of 5.61 €/kg, how much is it willing to pay for buying a higher quality product?

- 0,50 €/kg 1,00 €/kg 1,50 €/kg
 2,00 €/kg 2,50 €/kg 3,00 €/kg

PURCHASE CACIOTTA

1) How often do you buy ricotta?

- Never or almost never Daily
 Several times a week Several times a month

2) Where do you usually buy ricotta?

- Supermarket - Great distribution Market
 Farms (direct sales) GAS (Purchase groups)

3) In which format do you usually buy the caciotta?

- Monoportion Unpackages (at the counter fresh) Caciotta entire

4) Do you know the difference between the ricotta packaged in a protective atmosphere and in a traditional packaged?

- Yes No

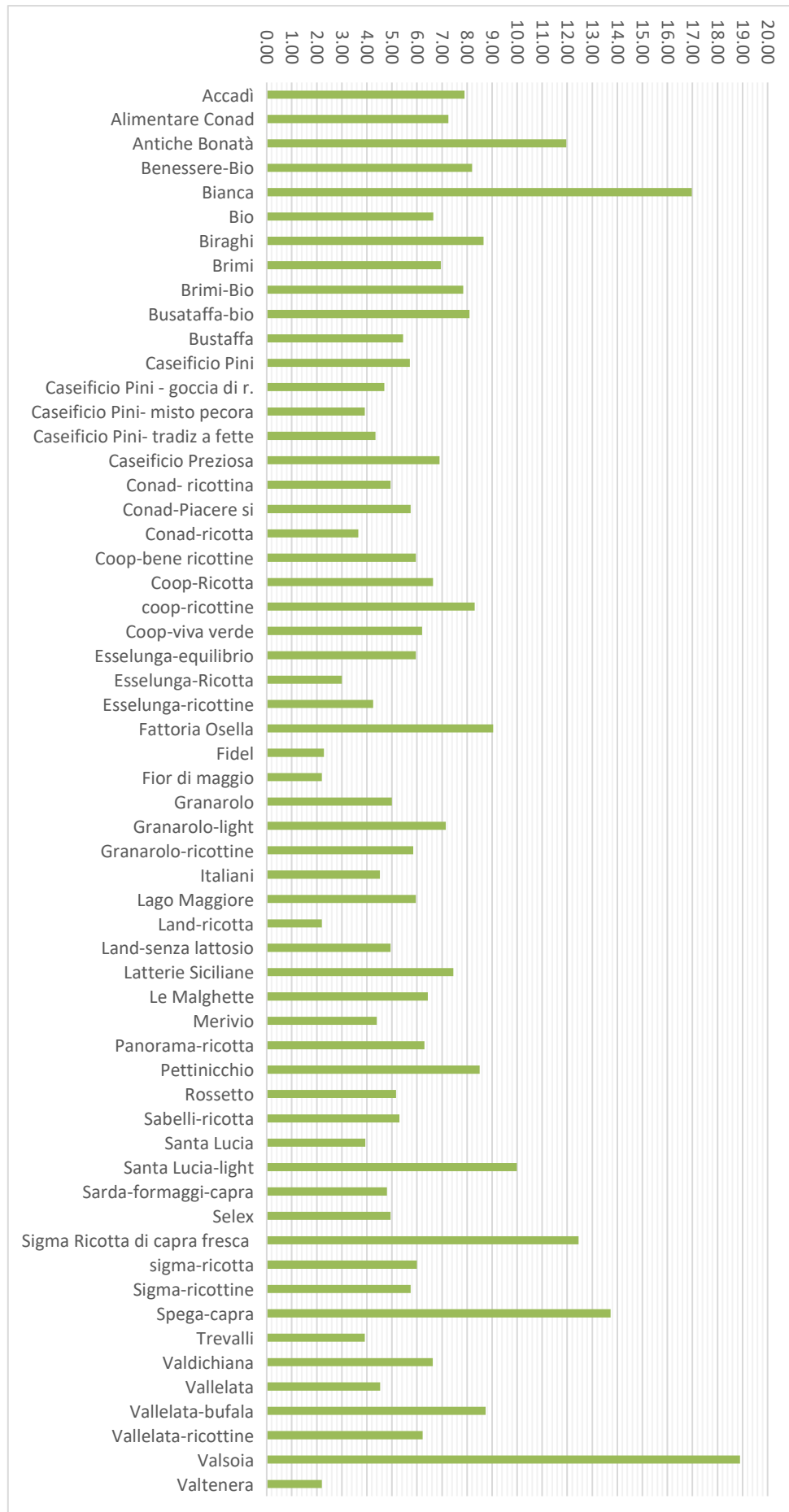
5) Considering an average price of 8.85 € / kg of caciotta, how much are you willing to pay for buying a superior quality product?

- 0,50 €/kg 1,00 €/kg 1,50 €/kg
 2,00 €/kg 2,50 €/kg 3,00 €/kg

APPENDIX B: Size of the shelves used for ricotta and the size of each brand in detail

Store	Street	Number of shelves (cm)	Height of shelves (cm)	Brand 1	Brand 2	Brand 3	Brand 4	Brand 5	Brand 6	Brand 7	Brand 8	Brand 9	Brand 10	Brand 11	Brand 12	Brand 13	Brand 14	Brand 15	Brand 16	Brand 17	
FAMILLA	Via Langhina no (PR)	80	6	Accad i	Brimi bio	Cas.Pi ma tete	Fattorie Osella	Grana rolo	Grana rolo	Le Ricotti	Santa Lucia	Selex	Spega	Vallelat a							
	Via Sandro Pertini 14 (GR)	200	3	Accad i	Antich Bont a	Bemes sere bio	Bianca	Essellu nga equili bio	Ricotti	Ricotti	Fidel	Pettinc chio	Santa Lucia	Valdich iana	Vallel ata	Vallel ata ricotti	Vallel ata Bufala	Grana rolo			
SIGMA	Viale Antonio Gramsci, 9 (PR)	140	3	Brimi bio	Grana rolo	Grana rolo ricotti	Santa Lucia	Santa Lucia light	Sigma capra	Sigma ricotta	Sigma ricottin e	Spega	Spega	Ricottin e Vallelat a							
	Via Sivo Pellico, 20 (PR)	60	4	ricotti	Lago Maggiore	Latteria Scilla	Panora ma	Sabelli	Santa Lucia light	Santa Lucia light	Vallel ata	Ricottin e Vallelat a	Valsoia								
COOP	Via F. Mitteran d. 1 Suzzara (MN)	100	7	Accad i	Bustaf abio	Coop bene	Coop ricotta	Coop ricotti ma	Coop viva verde	Fattori Osella	Fior di Maggio	Granar olio	Granar lo light	Santa Lucia	Sarda Formaggi	Spega	Vallel ata-ata-ricotti				
	Via Venezia, 40/A (PR)	100	4	Accad i	Conad almen tarti	Conad ricotta	Conad ricottin e	Conad piacer e sti	Cas.Pi Pini	Cas.Pi Peczo	Granar olio	Granar olio light	Granar olio	Santa Lucia	Vallelat a						
AFFARE	Via Donelli 4, Suzzara (MN)	220	3	Accad i	Briugh i	Brimi	Bustarf a	Caself Pini	Cas.Pi gocce di r.	Cas.Pi mi misto pecora	Cas.Pi ricottin e	Fattorie Osella	Granar olio	Granar lo light	Santa Lucia	Treva lli	Vallel ata	Vallel ata butali	Vallel ata ricotti	Ross etto	
	Sit. Langhina no, 150 (PR)	20	3	Italian i	Land	Land senza lattos															
LIDL	Via Della Cooperaz home, Gonzaga (MN)	30	1	Merivi o																	
	Sit. Nazionale, 15/a Suzzara (MN)	50	2	Bio	Valen era																

APPENDIX C: Average Ricotta price for each brand



AUTHORS' INDEX

Armenzoni	73
Bahadori	45
Better	59
Bottani	73
Delgado	51
Han	8
Hussein	51
Igwegbe	1
Kang	8
Kelly	59
Laguna	59
Lee M.-G.	25
Lee O.-H.	35
Lee Y.-J.	35
López-Nogales	68
Malagoli	73
Mantione	82
Mateo-Fornés	68
Mendiroiz	68
Mobarak	51
Montanari	73
Novoa-Tufet	68
Ogunniyi	1
Olaniyan	1
Oloye	1
Oyeniya	1
Pagès-Bernaus	68
Palmer	59
Park H. W.	8, 16, 25
Park J. W.	16, 25
Pérez-Cànovas	68
Plà-Aragones	68
Ravisankar	45
Saad	45
Solari	73
Tagliavini	73
Terrafeta	68
Vignali	82
Yoon	8, 16, 25, 35